TRANSCRIPTIONAL AND EPIGENETIC REGULATION OF HINDBRAIN DEVELOPMENT IN THE MOUSE

Inauguraldissertation

zur

Erlangung der Würde eines Doktors der Philosophie

vorgelegt der

Philosophisch-Naturwissenschaftlichen Fakultät

Der Universität Basel

von

Antonio Vitobello

von Barletta, Italien

Basel, 2015

Genehmigt von der Philosophisch-Naturwissenschaftlichen Fakultät

auf Antrag von

Prof. Dr. Filippo M. Rijli

Prof. Dr. Silvia Arber

Basel, den 17 September 2013

Prof. Dr. Jörg Schibler
(Dekan)

Table of Contents

Summary

During embryonic development, proper vertebrate body patterning is achieved through a series of highly regulated transcriptional mechanisms that result in a precise spatial and temporal control of specific master genes. Hox transcription factors play a crucial role in the specification of posterior positional identity, acting as part of a downstream regulatory network responding to Retinoic Acid (RA) activity. RALDH2 enzyme is solely responsible for embryonic RA synthesis until E8.5, and its mutation affects dramatically the development of different structures and organs such as heart, somites, pharyngeal arches, limb and neural tube (Niederreither et al., 1999). Yet, little is known about the molecular mechanisms involved in its regulation. Previous literature showed that Pbx mutant mice phenocopy most of the defects exhibit by *Raldh2*$^{-/-}$ mutant animals (Capellini et al., 2006; Manley et al., 2004; Stankunas et al., 2008). Moreover, Pbx proteins are well characterized Hox cofactors (reviewed in Moens and Selleri, 2006). In the first part of this work we investigate the role of Hox and Pbx transcription factors in the maintenance of RALDH2 expression. Using genetic tools and biochemical assays such as *in situ* hybridization, reporter gene analysis of RA activity, chromatin immunoprecipitation (ChIP), electrophoretic mobility shift assay (EMSA) and BAC recombineering we address this important question.

Furthermore, the generation of an early anterior boundary of RA activity, obtained through the complementary distribution of synthesizing and degrading enzymes, identifies a rostral embryonic domain devoid of *Hox* gene expression. Previously, it has been demonstrated that the maintenance of a Hox-negative domain is an essential condition required for the correct morphogenesis of vertebrate craniofacial structures (Couly et al., 1998; Creuzet et al., 2002). During early phases of neurogenesis, exogenous administration of RA or mutation of CYP degrading enzymes result in the anterior shift of *Hox* gene expression in the hindbrain and in the corresponding NCCs populating the pharyngeal regions (Hernandez et al., 2007; Mallo and Brändlin, 1997; Marshall et al., 1992; Mulder et al., 1998). These effects, associated with other RA-mediated molecular changes in the signalling epithelium of first pharyngeal arch, lead to impairment of craniofacial

development (Mallo and Brändlin, 1997; Vieux-Rochas et al., 2007). Later on, anterior *Hox* genes become unresponsive to RA signalling and its exogenous administration no longer affects head and pharyngeal patterning. These evidences suggest a possible role of epigenetic silencing mechanisms in the maintenance of transcriptional repression of *Hox* gene in the face. Takihara and colleagues (Takihara et al., 1997) show that *Phc1* disruption (the mouse homologue of the *Drosophila polyhomeotic* gene) leads to altered antero-posterior pattening and neural crest defects. Furthermore, Phc2 and Phc1 have been shown to act synergistically to establish a Polycomb-mediated repression of *Hox* genes (Isono et al, 2005). Although these works underscore the function PRC1 complex in the maintenance of transcriptional repression of *Hox* genes during antero-posterior specification, they do not account for the general function of Polycomb-mediated silencing in NCCs. Indeed, although a large majority of Polycomb targets are co-occupied by PRC2 and PCR1 complexes in ES cells, there is a substantial portion of target genes that show non-overlapping characteristics (Boyler et al., 2006; Ku et al., 2008). Moreover, a comprehensive analysis of craniofacial defects is missing, partly due to the early lethality of the analyzed mutant mice. In the second part of this work we address the genome-wide impact of cell-autonomous *Ezh2* mutation during craniofacial development in the mouse and we discuss the implications of our results in the context of collinear expression of *Hox* genes and their chromatin architecture inside the nucleus. Using ChIP coupled with high throughput sequencing (ChIP-seq) and RNA-seq data, we identify the epigenomic and transcriptomic features of defined rostro-caudal cranial NCC populations. This study deciphers the role of PCR2 during head and pharyngeal morphogenesis.

Finally, the present manuscript encompasses also two further research articles, result of the collaboration within the Prof. Rijli's group and with the Prof. Chiquet-Ehrismann's group at the FMI.

Abbreviations

(ANT-C) *Drosophila Antennapedia* complex

(BX-C) *Drosophila Bithorax* complex

(BMPs) Bone Morphogenetic Proteins

(ChIP) Chromatin Immmunoprecipitation

(Col2α1) Collagen type II α1

(CRABPs) Cellular-RA-Binding Proteins

(CRBPs) Cellular Retinol Binding Proteins

(CYPs) Cytochrome P450 enzymes

(DRs) Direct Repeats

(EMSA) Electrophoretic Mobility Shift Assay

(Ext) Extradenticle

(FGFs) Fibroblast Growth Factors

(GRNs) Gene Regulatory Networks

(GTFs) General Transcription Factors

(H3K27me3) Histone 3 Lysine 27 trimethylation

(HAT) Histone Acetyltransferase

(HDACs) Histone Deacetylases

(HMTs) Histone Methyltranferases

(HOM-C) *Drosophila* Homeotic gene complex

(Hth) Homothorax

(lncRNA) Long non-coding RNA

(NCCs) Neural Crest Cells

(NCoR) Nuclear Receptor Co-Repressor)

(Pc) Polycomb

(PcG) Polycomb group proteins

(PG1) *Hox* paralog group 1

(PG2) *Hox* paralog group 4

(PHD) Plant homeodomain finger

(PIC) Pre-initiation complex

(PolII) RNA polymerase II

(RA) Retinoic Acid

(Raldh2) Retinaldehyde dehydrogenase 2

(RARs) Retinoic Acid Receptors

(RBP) Retinol Binding Protein

(Raldhs) Retinaldehyde Dehydrogenases

(Rdh10) Retinol Dehydrogenase 10

(RXRs) Retinoid X Receptors

(SMRT) Silencing Mediator of Retinoic and Thyroid Hormone Receptor

(TALE) Three Aminoacid Loop Extention homeoproteins

(TF) Transcription Factor

(TFIID) Transcription Factor IID

(Trx) Trithorax

(TrxG) Trithorax group proteins

Chapter 1: Introduction

Body plan formation is achieved, during embryonic development, through a series of gene regulatory networks (GRNs) that act in response to cellular environmental cues and promote cell-specific differentiation and behavior. Transcriptional changes induced by environmental signals are then maintained over cell generations through tightly regulated epigenetic mechanisms (**Figure 1.1**). Genetic mutations or perturbations of the cellular environment, occurring during prenatal life, might affect specific cell function, survival or proliferation, resulting in tissue, organ and system dysfunction and eventually leading to death. Understanding the molecular mechanisms underlying the regulation of the developmental transcriptional pathways is important to shed light on the etiology of a broad spectrum of pathological conditions, from mental retardation to cancer.

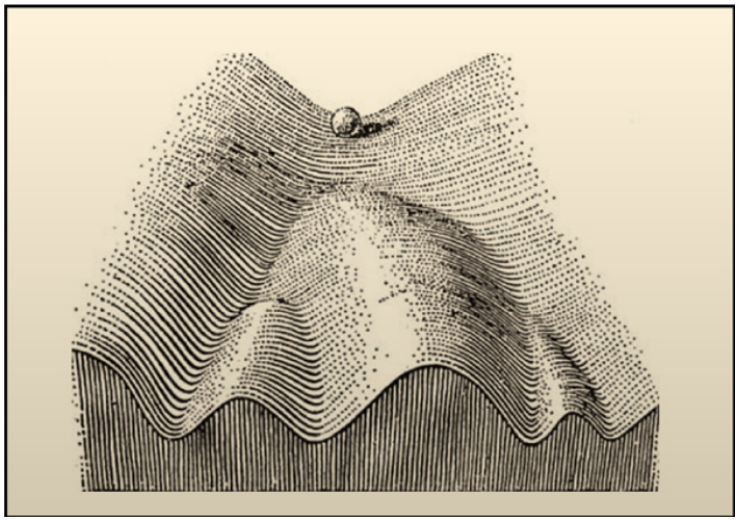

Figure 1.1. Waddington's classical epigenetic landscape. This drawing represents the process of cellular decision-making during differentiation (original image from Conrad Waddington, 1957).

During early embryonic development, the gastrulation process leads to the final positioning of the three germ layers (ectoderm, mesoderm and endoderm) that will give rise to all the organs and tissues that compose the organism. In parallel, the cells that compose these layers will acquire positional information according to their location along the rostro-caudal, dorso-ventral and left-right axes of the embryo. Morphogens are signalling molecules able to diffuse through the developing tissues and, according to their local concentrations, influence cell identity conveying positional information along the body axes. Although there are different mechanisms able to establish morphogen gradients, the most known are based on localized secretion, general spreading, and defined clearance/degradation. At the cellular level the gradient activates signaling effectors able to modulate the transcriptional state of target genes, which in turn, cross-regulate each other (**Figure 1.2**). By shaping the expression landscape of target cells, morphogens are able to induce spatio-temporal and cell-specific differentiation and behavior (Kicheva et al., 2012).

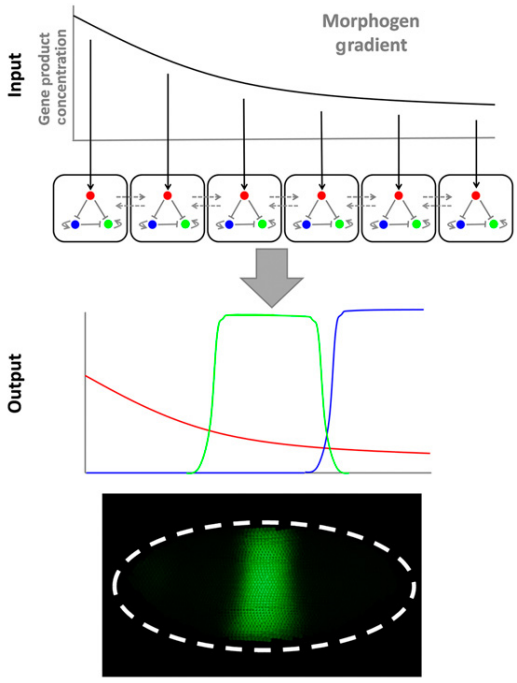

Figure 1.2. Positional information interpreted by a Gene Regulatory Network in response to a morphogen gradient. This spatial model consists of a one-dimensional row

of cells with the GRN repeated in each cell. The gene depicted in red responds to the local concentrations of a morphogen. Cells can signal to one another (dashed arrows) by means of diffusible gene products (Cotterell and Sharpe, 2010).

1.1. Hox genes: organization and early expression onset

In the embryo, key developmental proteins belonging to the homeodomain transcription factor family, shape the anterior-posterior neural tube through their differential and nested expression along the neuraxis. Otx and Emx define the most anterior part of the neural tube. Members of Pax, Gbx and En transcription factors define the midbrain/hindbrain boundary (Kiecker and Lumsden, 2005). Posteriorly, the rhombencephalic region is patterned by the expression of *Hox* transcription factors (Narita and Rijli, 2009), while *Cdx* transcriptin factors are co-expressed with *Hox* in the caudal part of the embryo (Young and Deschamps, 2009).

Described to confer segmental identity in *Drosophila*, *Hox* genes have conserved their function throughout evolution and also in vertebrates, in which they act as selector genes during the specification of metameric structures such somites and rhombomeres. *Hox* genes are organized in clusters. In *Drosophila* the Homeotic gene complex (HOM-C) is composed of eight genes organized in two groups: the *Antennapedia* compex (ANT-C), whose genes specify the identity of anterior segments (head to second thoracic segment), and the *Bithorax* complex (BX-C), whose genes specify the identity of posterior ones (third thoracic to abdomen). In mammals there are 39 *Hox* genes organized in four clusters (A to D) that have arisen through duplication and divergence, during the evolution, from a proto-*Hox* cluster (**Figure 1.3**). Their expression pattern along the embryonic antero-posterior axis and the onset of their activation follow their relative position (3'-to-5') along the chromosomes. These phenomena have been called respectively spatial (Lewis, 1978) and temporal collinearity (Izpisúa-Belmonte et al., 1991). Thetrefore, for example, *Hoxa1* and *Hoxb1*, which belong to the *Hox* paralog group 1 (PG1), are expressed before and reach more anterior expression boundaries than PG4 *Hox* members.

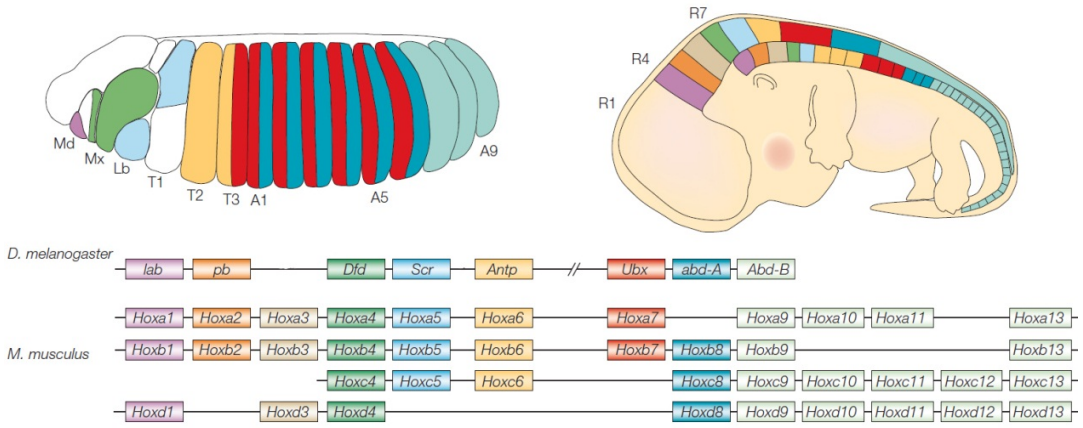

Figure 1.3. *Hox* expression and genomic organization. This image depicts the genomic organization and the expression patterns of *Hox* genes in fly and mouse embryos (from Pearson and al., 2005).

In *Drosophila*, activation of homeotic selector genes refines the antero-posterior pattern pre-imposed by the sequential expression of maternal genes *gap* and *pair-rule*. In amniotes, the molecular mechanisms leading to the temporal onset of their transcription are still elusive, although recent studies have indicated the role of regulatory regions located in the neighborhood regions outside the clusters (Tschopp et al., 2009). On the other hand, the events that cause their spatial distribution along the rostro-caudal axis have been well characterized. 3' *Hox* genes start to be expressed during gastrulation in the epiblast, in a salt-and-pepper manner, at the level of the presumptive paraxial mesoderm located bilaterally to the forming primitive streak (Forlani et al., 2003). At this stage, endodermal and mesodermal precursors located in the epiblast converge toward the streak where they undergo an epithelial-to-mesenchymal transition. These cells then ingress ventrally and migrate anteriorly and laterally to reach their final position. Moreover, as gastrulation proceeds, the primitive streak moves forward reaching its maximal extent. Then, activated 3' *Hox* gene expression spreads to all the paraxial progenitors located in the epiblast, all along the primitive steak. During their ingression through the streak, mesodermal and endodermal precursors enter into the presomitic mesoderm and maintain the *Hox* code acquired in the epiblast (Iimura and Pourquié, 2006).

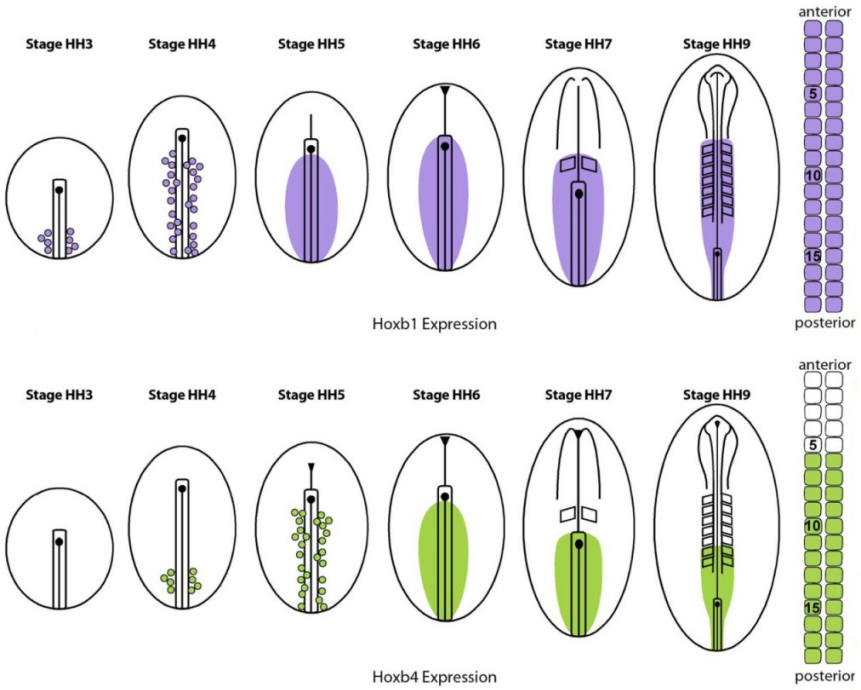

Figure 1.4. Onset and spreading of *Hox* activation in the chicken embryo. Temporal collinear *Hox* gene activation causes their spatial collinear expression in the chicken paraxial mesoderm (from Iimura et al., 2009).

Subsequently, the primitive streak and the node retract the notocord is laid down ahead while somites start to condense. Following the rule of the temporal collinearity, after a delay of few hours, subsets of more 5' *Hox* genes undergo the above mentioned activation steps. However, their anterior expression boundaries will be posteriorly shifted due to the regression of the primitive streak (**Figure 1.4**). *In vivo* overexpression experiments have shown that *Hox* genes are able to control the time the progenitors spend in the epiblast before they ingress through the streak. In this way, precursors that express more 5' *Hox* genes will spend longer time in the epiblast and will form more posterior somites compared to those expressing 3' genes. Therefore ,this mechanism links directly *Hox* code expression to spatial collinearity in the somites (Iimura and Pourquié, 2006).

1.2. Regulation of *Hox* gene expression in the hindbrain

Later on, *Hox* gene activation is induced in the neural tissue where they set their rostralmost boundaries of expression. At this developmental stage, the neural plate does not exhibit any of the morphological landmarks that will be present during the later phases of the central nervous system development. However, a subset of transcriptional factors, ligands and their cognate receptors start to be expressed in a nested manner along the antero-posterior axis of the neural tube, supplying the neural tissue with the first molecular hint of the future physical compartmentalization. Indeed, Hox proteins together with Krox20 and Kreisler transcription factors regulate the alternate expression of ephrin and Eph receptors along the antero-posterior axis in the rhombencephalon. The ephrin/Eph signaling acts as repulsive molecular mechanism that results in the subdivision of the hindbrain in seven distinct regions called rhombomeres. Inside each rhombomere, subpopulations of progenitors eventually form nuclei that will organize into circuits to regulate high physiological functions such as motor control, heart rate and respiration. This metameric organization impinges on the repetitive and stereotyped architecture of motor nerve exit and neural crest cell migration.

The nested expression of *Hox* genes in the hindbrain is driven by the modulation of *cis*-acting regulatory regions, whose activities are controlled in space and time through the integration of signalling pathways (e.g. Retinoic Acid (RA), Bone Morphogenetic Proteins (BMPs), Fibroblast Growth Factors (FGFs)), transcription factors (e.g. Krox20, Kreisler as well as AP-2, PBC and Meis family proteins) and epigenetic complexes (e.g. Polycomb, Trithorax).

1.2.1. Retinoic Acid Signalling

All-*trans* Retinoic Acid (RA), one of the active forms of Vitamin A, is a small lipophilic molecule that shows pleiotropic effects during embryonic development and adulthood, regulating several cellular mechanisms like proliferation, differentiation and apoptosis.

Perturbations of the RA signalling affect organogenesis, skeletal development and central nervous system patterning. Vitamin A cannot be synthesized by animals and should therefore be introduced into the organism through dietary supplementation. After ingestion it is bound to retinol binding protein (RBP) and transported through the plasma to cell surface receptors for uptake. Inside the cells, the amount of free Vitamin A available for a two-step conversion to RA is homeostatically regulated by the presence of cellular retinol-binding proteins (CRBPs). In the first step, the retinol dehydrogenase 10 (Rdh10) converts retinol to retinaldehyde. The second step is catalyzed by retinaldehyde dehydrogenases (Raldhs) that convert retinaldehyde to RA. Retinoic Acid, as lipophilic molecule, diffuses extracellularly and reaches target cells where it binds a subfamily of nuclear receptors, the Retinoic Acid Receptors (RARs), inducing transcriptional activation of downstream genes. At cellular level, retinoic acid forms complex with cellular-RA-binding proteins (CRABPs) that shuttles RA to its receptors. The amount of free RA depends on the presence of specific Retinoic Acid degrading enzymes belonging to the cytochrome P450 family (CYPs).

RARs form heterodimers with retinoid X receptors (RXRs) and bind to specific sequences of DNA called retinoic acid response elements (RAREs). RAREs are composed of two direct repeats (DRs) of a core hexameric motif PuG(G/T)TCA, usually separated by a spacer of five (DR5), two (DR2) or one (DR1) base pairs. In absence of the ligand, the apo-RAR/RXR heterodimers recruit a co-repressor complex (NCoR nuclear receptor co-repressor or SMRT silencing mediator of retinoic and thyroid hormone receptor) tethering histone deacetylases (HDACs), resulting in chromatin compaction and gene silencing. On the contrary, in presence of RA, the holo-RAR/RXR heterodimers undertake a conformational change that dislodges the co-repressor and recruits a co-activator complex belonging to the SRC/p160 family, which, in turn, interacts with chromatin modifying enzymes (p300/CBP, p/CAF, CARM1) and ATP-dependent chromatin remodelling complexes (SWI/SNF) (Flajollet et al., 2007). The histone acetyltranferase (HAT) activity mediated by the p300/CBP, p/CAF and SRC/p160, together with the nucleosome reposition/eviction activity mediated by the SWI/SNF complex induce decompaction of repressive chromatin and facilitate the positioning of the transcriptional machinery at the promoter of target genes (Bastien and Rochette-Egly, 2004). Indeed, after chromatin

remodelling, a transient ternary complex containing Mediator facilitates the dissociation of the co-activators and the positioning of the general transcription factors (GTFs) and RNA polymerase II (Pol II) into the pre-initiation complex (PIC) at the promoter regions.

Perturbations of RA signalling have teratogenic effects. Excess of RA, during embryonic development, causes severe defects in the hindbrain, limbs, heart, gut and many other organs (Durston et al., 1989; Marshall et al., 1992; Godsave et al., 1998). Vitamin A-deficiency (VAD) also induces defects, characterized by global reorganization of rhombomeric territories in the hindbrain: the anterior rhombomeres expand at the expenses of the posterior ones (r4-7) (Gale et al., 1999; White et al., 2000). The severity of these effects depends on the severity of the VAD (**Figure 1.5**).

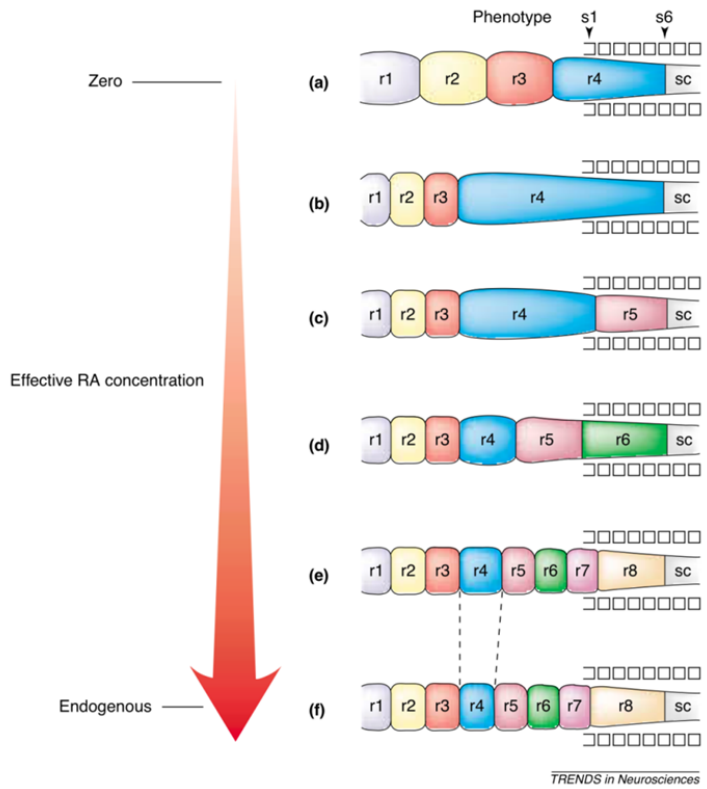

Figure 1.5. Hindbrain reorganization in response to RA signalling activity. VAD embryos show a variety of phenotypic hindbrain defects depending on the effective concentration of RA (from Gavalas, 2002).

RA acts as a morphogen during gastrulation. The RA morphogenetic gradient is established through the complementary distribution of synthesizing and degrading enzymes along the rostro-caudal axis of the embryo (Swindell et al., 1999). Raldh2 is the earliest synthesizing enzyme to be expressed. Initially, it is found in the primitive streak and mesodermal cells. Later on, it is expressed in somitic and lateral mesoderm (Niederreither et al., 1997). RALDH2 is solely responsible for embryonic RA synthesis until E8.5. *Raldh2*$^{-/-}$ mouse mutants die before mid-gestation due to defective heart morphogenesis. Moreover, they exhibit numerous abnormalities (Niederreither et al., 1999; Niederreither et al., 2001; Niederreither et al., 2000). Some of them can be rescued by transient maternal RA supplementation from E7.5 to E8.5-9.5 (e.g. Mic et al., 2002; Niederreither et al., 2003; reviewed in Rhinn and Dollé, 2012).

Once synthesized in the paraxial and somitic mesoderm RA diffuses extracellularly and reaches the surrounding tissues where it regulates the transcription of target genes. The RA degrading enzymes Cyp26a1, b1 and c1 exhibit combinatorial and dynamic expression patterns (White et al., 1997; Fujii et al., 1997; Hollemann et al., 1998; Swindell et al., 1999). In the hindbrain, their local activities modulate the RA signaling, resulting in rhombomere-specific control of RA signaling (Sirbu et al., 2005). Loss-of-function mutations of these genes show defects consistent with an increase in RA signaling (Hernandez et al., 2007; reviewed in White and Schilling, 2008).

1.2.2. Transcriptional networks

The molecular mechanisms that underlie hindbrain reorganization in response to perturbed RA signalling are mediated by deregulation of *Hox* genes (Marshall et al., 1994; Dupé et al., 1997, Gavalas et al., 1998) and their transcriptional networks. RAREs located within *cis*-regulatory regions of *Hoxa1* (Langston and Gudas, 1992; Frasch et al., 1995) and *Hoxb1* (Marshall et al., 1994; Langston et al., 1997), respond directly to RA and govern the early phases of spatial and temporal expression of these genes in the hindbrain and other tissues. Hoxa1 and Hoxb1 cooperate in the establishment of the rhombomere 4 (r4)

domain, which, in turn, exhibit a FGF signalling activity required for proper specification of posterior rhombomeric identities (Maves et al., 2002; Walshe et al., 2002). In *Hoxa1* mutants, rhombomere 3 expands posteriorly and the development of rhombomere 4 and 5 is severely affected (Dollé et al., 1993; Carpenter et al., 1993). This reorganization results in the absence of the abducens (VI cranial nerve), reduction of the facial (VII), absence of the spiral and vestibular ganglia (VIII) as well as reduction of glossopharyngeal (IX) and vagus (X) nerves (Mark et al., 1993). *Hoxa1*$^{-/-}$*/Hoxb1*$^{-/-}$ double mutants show a more severe phenotype, with r4-5 being dramatically affected or completely absent (Gavalas et al., 1998; Gavalas et al., 2001; Rossel and Capecchi, 1999; Studer et al., 1998). In wild-type animals, *Hoxa1* starts to be expressed in the epiblast and in the posterior primitive streak at the embryonic day 7.5 (E7.5). At E7.75, *Hoxa1* reaches its most anterior border of expression in the neuroepithelium, corresponding to the presumptive rhombomere 3 (Makki and Capecchi, 2010). Subsequently, its domain retracts to most posterior regions. This dynamic pattern of expression follows the spatial distribution of RA signalling in the developing embryo, which, at E7.75, reaches it maximal extension to the Cyp26a1 domain, corresponding to the r2/r3 boundary in the hindbrain. After that (E7.9), the anterior border of RA activity retracts towards the r4/r5 boundary because of the RA-mediated induction of Cyp26c1 in r4 (Sirbu et al., 2005). By E8.25, Cyp26b1 is expressed in r5, contributing to the local control of RA activity (Hernandez et al., 2007). Experiments carried in *Raldh2*$^{-/-}$ and in *Hoxa1 3'RARE* mouse mutants showed that the earliest temporal activation of *Hoxa1* in the epiblast and posterior primitive streak does not depend on RA activity (Dupé et al., 1997; Niederreither et al., 1999). On the other hand, the overall *Hoxa1* expression levels are reduced and a delay in the establishment of its anterior boundary in the presumptive hindbrain is observed. Similarly to *Hoxa1*, *Hoxb1* expression in the hindbrain depends on RA signalling. Between E7.5 and E8.0, *Hoxb1* reaches its maximal extension corresponding to the r4 presumptive region. In *Raldh2*$^{-/-}$ mutants and *RARα*$^{-/-}$*/RARγ*$^{-/-}$ double mutants, *Hoxb1* fails to establish its expression in r4 (Niederretiher et al., 1997; Wendling et al., 2001; Sirbu et al., 2005). In Cyp26a1$^{-/-}$ mutants, the expression of *Hoxb1* indicates an enlarged prospective r4 territory and misspecification of anterior regions (Abu-Abed et al., 2001). These effects are more drastic in *Cyp26a1*$^{-/-}$*/Cyp26c1*$^{-/-}$ double mutants (Uehara et

al., 2007). Furthermore, exogenous administration of RA leads to the ectopic expression of *Hoxb1* in the r2 territory (Mallo and Brändlin, 1997, Marshall et al., 1992).

Once RA has driven the initiation of *Hoxa1* and *Hoxb1* expression in the hindbrain, auto- and cross-regulatory interactions, together with the regulation mediated by other transcription factors, participate in the identification of rhombomeric regions. PBC and MEIS classes of Three Aminoacid Loop Extention (TALE) homeodomain proteins are well characterized Hox cofactors (reviewed in Moens and Selleri, 2006). Vertebrate PBC class comprises Pbx homoproteins, homologous to *Drosophila Extradenticle* (*Exd*), whereas the MEIS class includes vertebrate Meis and Prep homoproteins, homologous to *Drosophila Homothorax* (*Hth*). Hox regulatory elements often consist of Hox-Pbx bipartite motifs, frequently associated to nearby Meis/Prep binding sites that lead to the cooperative recruitment of tripartite Hox-Pbx-Meis/Prep complexes. Mutation of either Hox- or Pbx-binding element prevents reporter expression in transgenic mice (Ferretti et al., 2005; Maconochie et al., 1997; Pöpperl et al., 1995). Furthermore, vertebrate *Pbx* mutants exhibit phenotypic effects resembling those showed by *Hox* loss-of-function animals (Manley et al., 2004; Pöpperl et al., 2000; Selleri et al., 2001). More broadly, Hox and Pbx are thought to cooperate in the specification of rhombomeric identities posterior to r1 (McNulty et al., 2005; Waskiewicz et al., 2002). Between E8.0 and E8.5, the expression of *Hoxb1* becomes restricted to r4. A *cis*-regulatory region containing multiple binding sites for Hox proteins and their cofactors has been characterized to be responsible for r4 maintenance (Ferretti et al., 2005; Maconochie et al., 1997; Pöpperl et al., 1995). Indeed, Hoxa1, Hoxb1 and Hoxb2 have been shown to interact with members of Pbx and Meis families in order to maintain *Hoxb1* expression in r4 (Ferretti et al., 2005; Gavalas et al., 2003; Pöpperl et al., 1995; Studer et al., 1998). Furthermore, a different *Hoxb1 cis*-regulatory element containing a RARE and bound by the zinc-finger transcription factor Krox20 works as repressor in r3 and r5, to suppress its expression in surrounding regions (Studer et al., 1994). Krox20 starts to be expressed in the presumptive r3 region at E8.0 and then becomes expressed in the presumptive r5 region by E8.25 (Irving et al., 1996; Wilkinson et al., 1989). This transcription factor plays an important role in the regulation of *Hox* paralog group 2 (*Hoxa2*, *Hoxb2*) within its domain of expression (Maconochie et al., 2001; Sham et al., 1993).

Anteriorly, *Hoxa2* is the only *Hox* gene expressed in r2 and its regulation, driven through the activity of a *cis*-regulatory element located in its coding region, is important for the identity of this segment (Gavalas et al., 1997; Oury et al. 2006; Tümpel et al., 2008) (**Figure 1.6**).

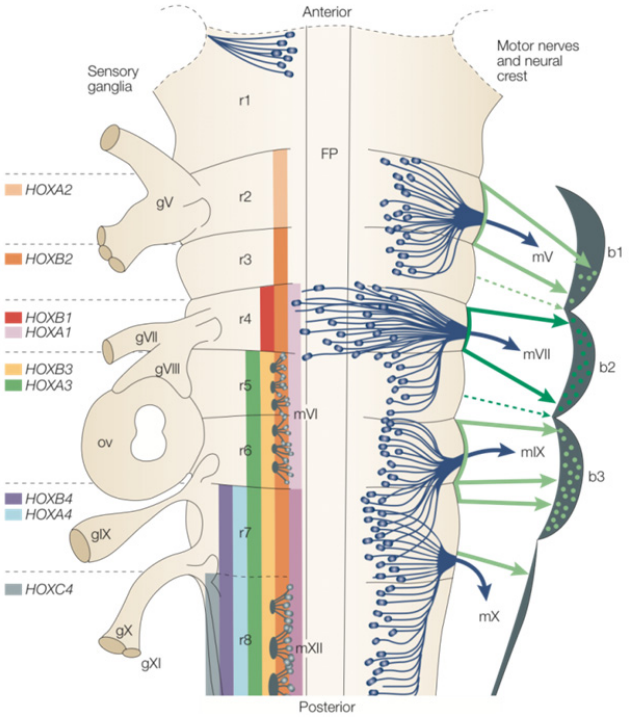

Figure 1.6. Segmental distribution of cranial nerves, neural crest cells and *Hox* gene expression. The nested expression of *Hox* genes along the hindbrain relies on RA responsiveness and gene regulatory networks, which, in turn, confer rhombomeric identity. Stereotyped architecture of motor nerve exit and neural crest cell migration are here depicted (from Kiecker and Lumsden, 2005).

The r5-6 domain is specified by the expression of the transcription factor Kreisler. In *kreisler*$^{-/-}$ mutants, r5 and r6 are lost and the otic vesicle, which normally lies adjacent to r5-6 is displaced laterally and develops into a cystic structure without an organized

vestibular apparatus or cochlea (McKay et al., 1994). This transcription factor is activated at E7.5 in the presumptive r5 region. Subsequently, its expression spreads also in the r6 region and stays activated until E9.0. Kreisler initiates the expression of *Hoxa3* and *Hoxb3*. Subsequently auto- and cross-regulatory interactions are respectively responsible for the maintenance of their expression (Manzanares et al., 1997, 1999, 2001).

Finally, between E8.5 and E9.5, also PG4 *Hox* genes reach their anterior boundary in the hindbrain (r6/7) driven by the sustained activity of the RA signalling (Folberg et al., 1997; Whiting et al., 1991) coming from the nearby somites (Gould et al., 1997). After RA-mediated initiation, the expression of these genes stars to regress toward posterior regions, while *Hoxb4* is maintained through mechanisms of auto- and cross-regulatory networks (Gould et al., 1997, 1998).

1.3. *Hox* genes and Neural Crest Cells

Hox gene expression does not affect only the patterning of the rhombomeric regions and respective cranial nerves, but influences also the positional identity and the differentiation potential of neural crest cells (NCCs).

The neural crest cells represent a transient migratory cell population specific to craniates and originating from the dorsal part of the developing neural tube. The ontogenesis of this cellular population requires a phase of induction, which involves the counteracting effects of several signalling pathways (e.g. BMP, FGF, Notch and Wnt). Then, they undergo an epithelial-to-mesenchymal transition, delaminate and acquire migratory properties to reach their target regions where they eventually differentiate into a variety of cell types such as neurons, glia and melanocytes. Unlike trunk NCCs, cranial cells show the unique capability to differentiate into mesenchymal derivatives such as cartilage, bone and connective tissue, substantially contributing to the craniofacial and pharyngeal structures that make up the vertebrate head (Gammill and Bronner-Fraser, 2003; Le Douarin and Kalcheim, 1999; Morales et al., 2005; Steventon et al., 2005) (**Figure 1.7**).

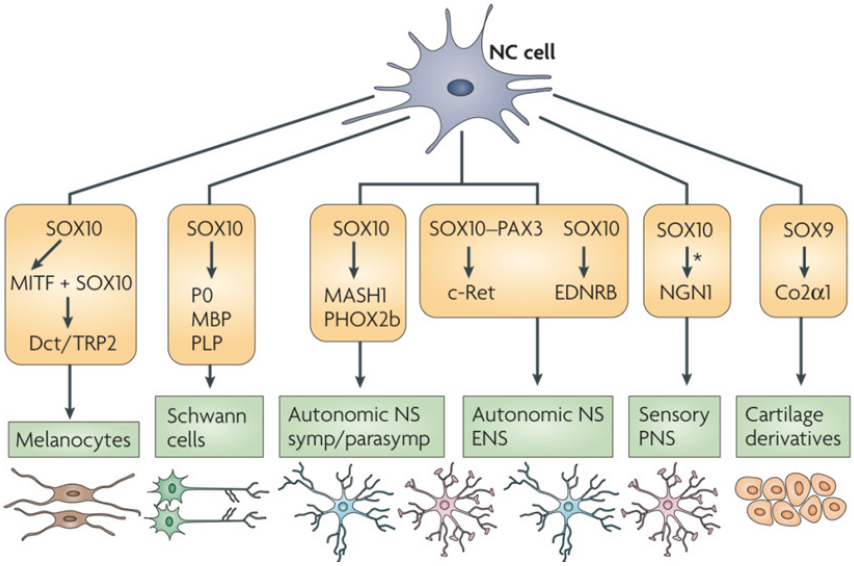

Figure 1.7. Sox transcription factors and cell fate potentials. Sox10 activity plays and important role in neural and melanocyte cell differentiation. Sox9 is required to proper differentiation of mesenchymal lineage (from Sauka-Spengler and Bronner-Fraser, 2008).

NCC differentiation is established through the instructive role of signalling molecules and transcription factors whose actions are spatially and temporally coordinated (reviewed in Sauka-Spengler and Bronner-Fraser, 2008). In particular, TGFβ signalling has been shown to promote mesenchymal lineage acquisition at the expenses of melanocyte and neural lineages, through *Sox10* repression in pre-migratory NCCs and activation of the early osteochondrocytic lineage marker *Sox9*, as well as *Runx2* and *osterix* (John et al., 2011; Sahar et al., 2005). Sustained expression of Sox9 in pre-migratory NCCs controls directly the expression of collagen type II α1 (Col2α1), a cartilage-specific gene (Lefebvre et al., 1997). Heterozygous loss of Sox9 function results in Campomelic Dysplasia, a lethal human disorder characterized by severe skeletal malformations and several craniofacial defects

(Spokony et al., 2002). In contrast, the neuronal and the melanocyte lineages require Sox10 activity (Potterf et al., 2001; Kim et al., 2003; Stolt et al., 2002; Lee et al., 2004).

Mesenchymal/skeletogenic neural crest cells exhibit different potentials according to their rostro-caudal origin along the neural tube. Rostral cranial NCCs give rise to the frontonasal skeleton and make important contributions to the membranous bones of the skull, whereas more posterior cranial NCCs fill the pharyngeal arches, where they form the cartilages and bones of the jaw, middle ear and neck (Couly et al., 1993; Köntges and Lumsden, 1996; Noden, 1983) (for reviews, see Gross and Hanken, 2008; McBratney-Owen et al., 2008; Santagati and Rijli, 2003). From their origin in the neural tube to their destination into the craniofacial and pharyngeal regions, cranial NCCs follow specific and stereotyped pathways of migration that are highly conserved amongst vertebrate species. NCCs originating from the diencephalon and anterior mesencephalon migrate into the frontonasal process (FNP), whereas NCCs coming from the posterior mesencephalon and the hindbrain colonize the pharyngeal arches (PAs). NCCs colonizing PAs migrate into three segmentally restricted streams: NCCs from the posterior mesencephalon, r1 and r2 fill the first arch (PA1), which will give rise to the maxillary (Mx) and the mandibular (Md) processes, NCCs from r4 fill the second (hyoid) arch (PA2) and NCCs from r6, r7 and r8 colonize the third and the fourth pharyngeal arches (PA3 and PA4) (Birgbauer et al., 1995; Kulesa and Fraser, 2000; Lumsden et al., 1991; Sechrist et al., 1993; Serbedzija et al., 1992). Few cells originating from odd-numbered rhombomeres migrate both rostrally and caudally, joining the adjacent even-numbered rhombomeric streams (Lumsden et al., 1991; Sechrist et al., 1993).

Molecularly, the transcriptional identity of NCCs is different from their antero-posterior origin. Forebrain NCCs colonizing the frontonasal region and midbrain NCCs colonizing the maxillary process of PA1 express the homeodomain transcription factor Otx2 (Kuratani et al., 1997). Accordingly, Otx2 haplo-insufficiency mainly affects the development of frontonasal and maxillary elements with no structural anomalies observed in rhombencephalic NCC derived structures (Matsuo et al., 1995). At hindbrain level, the AP positional identity of the NCCs is established by the same molecular mechanisms

controlling segmentation and AP patterning of the rhombomeres from which they delaminate; namely, by the nested and combinatorial expression of *Hox* genes (Lumsden et al., 1996). This Hox transcriptional code is transposed to the NCCs while they migrate out from the hindbrain, thus providing them an early AP molecular regionalisation and patterning information (Hunt et al., 1991). However, the *Hox* code of the neural tube is not strictly reproduced in the migrating NCCs (Hunt et al., 1991). For example, *Hoxa2* expression in the neural tube has its anterior limit at the r1/r2 boundary, but the NCCs arising from r2 and migrating into the first arch are devoid of *Hox* gene expression (Krumlauf, et al., 1993; Prince et al., 1994). As *Hoxa2* is the most anterior expressed *Hox* gene, its absence in r2 derived NCCs leads to an important molecular difference among cranial NCCs. Indeed, NCCs contributing to the FNP and the first arch do not express *Hox* genes, whereas NCCs contributing to the second and more posterior arches express various combinations of *Hox* genes, thus providing each arch with distinct regional identities along the AP axis.

The importance of *Hox* genes in determining the AP identity of the pharyngeal arches first became evident with the targeted mutagenesis of *Hoxa2* in the mouse. As a result of *Hoxa2* inactivation, the skeletal elements originating from the second arch were homeotically transformed into a duplicated set of Md-like elements with reverse polarity (Gendron-Maguire et al., 1993; Rijli et al., 1993). A similar outcome has been described following the inactivation of *Hoxa2* in *Xenopus* (Baltzinger et al., 2005) and of *Hoxa2*/*Hoxb2* in zebrafish (Hunter and Prince, 2002), thus underlying a conserved role for paralog group 2 *Hox* (PG2) genes in establishing second arch identity. However, some differences exist among vertebrate species, concerning the relative involvement of *Hoxb2* in patterning the second arch skeletal elements. Indeed, whereas zebrafish *Hoxa2* interacts genetically with its paralog *Hoxb2* (Hunter and Prince, 2002), this latter is dispensable in mouse and *Xenopus* (Baltzinger et al., 2005; Barrow and Capecchi, 1996; Davenne et al., 1999). This might be explained by the early downregulation of *Hoxb2* expression in the mouse and *Xenopus* post-migratory NCCs (Hunt et al., 1991; Baltzinger et al., 2005), which does not occur in zebrafish (Hunter and Prince, 2002). However, despite these regulatory differences, the outcome of *Hoxa2* or *Hoxa2/Hoxb2* inactivation indicates that *Hox* PG2 genes, that are the only *Hox* genes expressed in the second pharyngeal arch, superimpose a

second-arch-specific mode of development on a *Hox*-negative ground (default) patterning program, shared by the mandibular process of the first arch and the second arch (Rijli et al., 1993). Such a hypothesis has been confirmed by complementary gain-of-function experiments, where ectopic expression of *Hoxa2* in the first arch of chick and frog (Grammatopoulos et al., 2000; Pasqualetti et al., 2000) or of *Hoxa2/Hoxb2* in zebrafish (Hunter and Prince, 2002) led to the development of second arch-like structures in the place of Md derivatives. Hence, it appears that PG2 *Hox* genes act as selector genes for second arch development. However, their inactivation do not affect arches posterior to the second (Baltzinger et al., 2005; Gendron-Maguire et al., 1993; Hunter and Prince, 2002; Rijli et al., 1993), where PG3 and *Hoxd4* genes are expressed (Minoux et al., 2009).

It has been shown that deleting the entire *Hoxa* cluster in mouse NCCs, not only leads to the second arch homeotic transformation induced by the absence of *Hoxa2* but also results in partial homeotic transformation of third and fourth arch derivatives into morphologies characteristic of *Hox*-negative Md-derived structures (Minoux et al., 2009). Hence, it appears that all pharyngeal arches are patterned on the top of the same *Hox*-negative ground (default) state, which corresponds to the genetic program of the NCCs colonizing the mandibular process. On this common ground patterning program, the *Hox* code specifies each pharyngeal arch with a unique AP identity, resulting in the formation of arch-specific skeletal elements.

Ectopic expression of *Hoxa2* in *Hox*-negative NCCs, not only induces Md into PA2 homeotic transformation, but also severely impairs jaws and craniofacial development (Creuzet et al., 2002); a phenotype also observed by ectopic expression of *Hoxa3* or *Hoxb4* in chick (**Figure 1.8**). These experiments indicate that *Hox* genes repression in PA1 and more anterior NCCs is an essential condition for proper jaw and craniofacial morphogenesis (Couly et al., 1998; Creuzet et al., 2002). The elucidation of the molecular mechanism(s) involved in *Hox* gene cluster repression in the first arch will be of particular interest in the future and will be crucial for understanding jaw development and evolution.

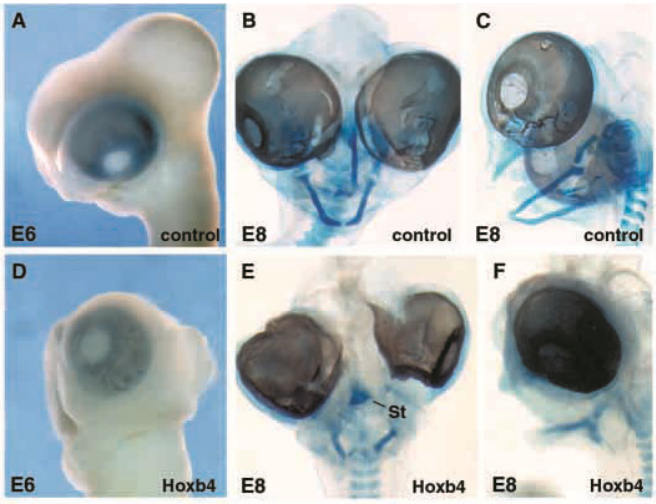

Figure 1.8. Phenotypic effects of ectopic *Hox* gene expression in chick embryo. Overexpression of Hoxb4 in NCCs leads to severe impairment of craniofacial structures (from Creuzet et al, 2002).

1.4. Epigenetic control of the collinear expression of *Hox* genes

In respect to the collinear expression of homeotic genes in *Drosophlila,* Welcome Bender and colleagues (Peifer et al., 1988), suggested the "open-for-business" model, speculating that each cell located within a segment selects, early in development, which regulatory elements are available for temporal and cell-specific transcriptional control of each gene (Akam et al., 1988). Subsequently, the same model was proposed as a possible mechanism explaining the temporal and spatial collinear Hoxd cluster expression during vertebrate limb development (Dollé et al., 1989). Nowadays, the term "open-for-business" has been replaced by "open chromatin" (Kmita and Duboule, 2003), yet the underlying concept of locus-related mechanisms implicated in the regulation of *Hox* genes remains almost unchanged (**Figure 1.9**).

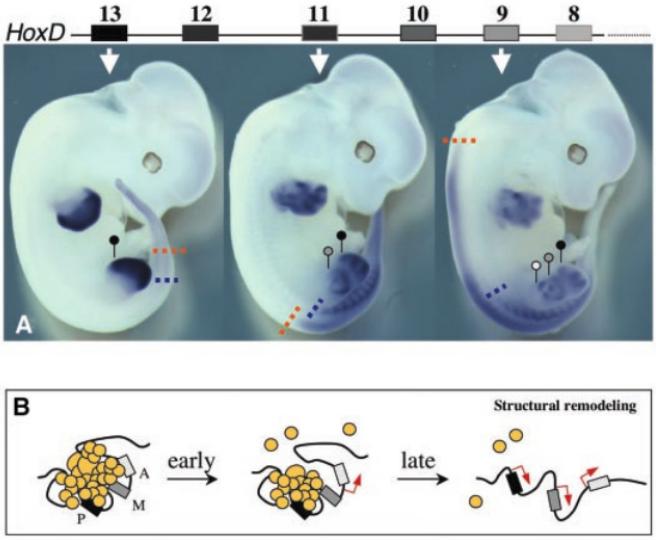

Figure 1.9. Model of collinear transcriptional activation along a *Hox* cluster. (A) Nested expression of *Hox* genes in developing mouse trunk and limbs. (B) Progressive chromatin remodeling as possible mechanism explaining the differential availability for transcription within the *Hox* clusters (from Kmita and Duboule, 2003).

In the nucleus, DNA is associated with histonic and non-histonic proteins, which confer structural, spatial and regulatory organization to the resulting polymer called chromatin. Local properties of the chromatin like compaction, folding, histone variants, post-translational modification and positioning interfere with the transcription factor (TF) accessibility to the cognate responsive elements located within regulatory regions. Consequently, chromatin organization modulates the ability of TF to regulate target genes (Spitz and Furlong, 2012).

In mouse, the observation that the RA-responding *Hoxb1-lacZ* transgene faithfully mimicking the endogenous gene (Marshall et al., 1994) did not exhibit the sensitivity of *Hoxb1* to precocious activation after exogenous RA treatment, lead to the idea that the

polarity, in initial activation of *Hoxb* genes, reflects a greater availability of 3′*Hox* genes for transcription, suggesting a pre-existing (susceptibility to) opening of the chromatin structure at the 3′ extremity of the cluster (Roelen et al., 2002). Recently, with the advent of genomic-scale techniques allowing the investigation of chromatin state on multiple loci in parallel, accumulating evidences are shedding light on the role of multiple epigenetic complexes in the regulation of *Hox* cluster expression during temporal and spatial collinearity *in vivo* (Bantignies et al., 2011; Soshnikova and Duboule, 2009).

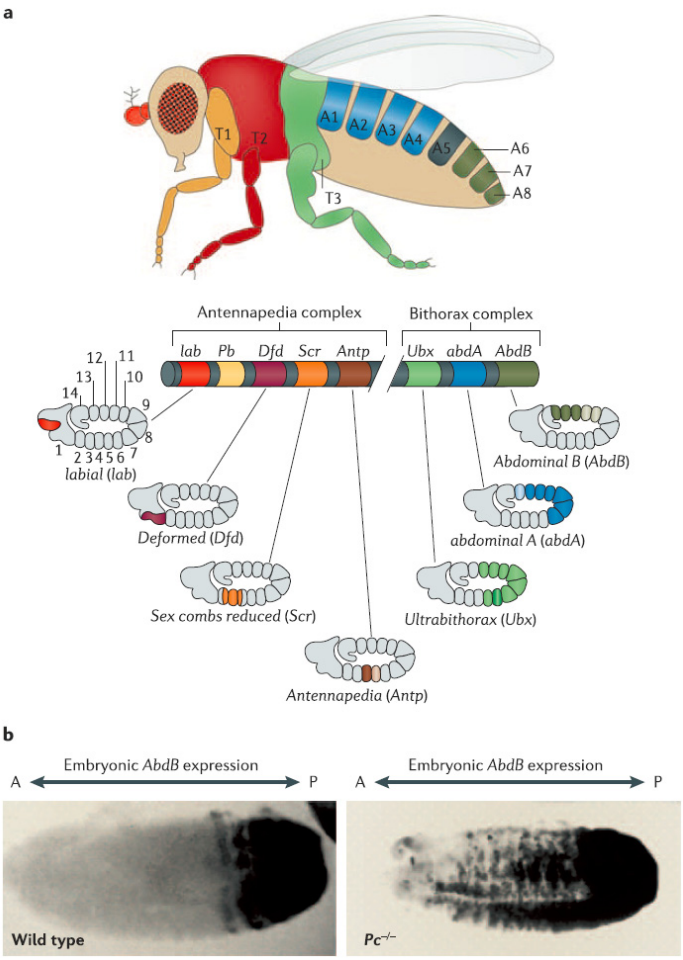

Figure 1.10. Expression of homeotic genes in *Drosophila* embryo and effect of Polycomb mutation. Normal antero-posterior distribution of homeotic gene expression is perturbed in *Polycomb* mutant embryos. Anterior derepression of *AbdB* gene is depicted in the figure (from Sparmann and van Lohuizen, 2006; original image from Moazed and O'Farrel, 1992).

What are the evidences indicating an involvement of epigenetic factors in the regulation of *Hox* collinearity *in vivo*? In *Drosophila*, a two-step process achieves spatial restriction of homeotic genes. During the first step (**initiation**), transcription factors regulate the transcriptional state of homeotic gene in sets of embryonic primordial. In the second (**maintenance**), molecular mechanisms ensure, over cell generations, the conservation of the silent/active state even in the absence of the factors that promoted the initiation (Müller et al., 1995). Genetic approaches identified, in *Drosophila*, a group of negative regulators, the *Polycomb* group (*PcG*) proteins (Lewis, 1978; Struhl, 1981; Jürgens, 1985), which are essential for maintaining spatial restrictions of homeotic gene expression (Moazed and O'Farrel, 1992) (**Figure 1.10**). On the other hand, Trithorax group (TrxG) proteins function as active regulators and are required to maintain correct level of Antennapedia and Bithorax complex expression (Ingham, 1985). PcG and TrxG, as part of the regulatory mechanisms maintaining the transcriptional memory of the cell, contribute to the regulation of a myriad of target genes through post-translational histone modification and, ultimately, by modifying chromatin state (Schuettengruber et al., 2009; Schwartz et al., 2006).

TrxG proteins act in the context of heterogenous multimeric complexes, which can be divided into three classes, based on their molecular function: histone methyltransferases, ATP-dependent chromatin remodelers and other histone modifiers (Schuettengruber et al., 2011). Of particular interest, the first class includes SET domain-containing factors that can trimethylate Lysine 4 of histone H3 (H3K4me3) a hallmark for gene activation. In mammals, MLL1 and MLL2, two HMTs homologous to Trithorax, exert their function within COMPASS-like complexes and interact, via their N-terminal domain, with the tumor suppressor Menin. Loss of Menin leaves little H3K4 methylation at *Hox* loci and almost no transcription of *Hox* genes suggesting its crucial role in the targeting MLL1/MLL2-containing COMPASS-like complexes to the *Hox* clusters (reviewed in Smith et al., 2011). Promoters enriched in H3K4me3 would then stimulate the pre-initiation complex (PIC) assembly by recruiting the plant homeodomain finger (PHD) of the transcription

factor IID (TFIID), resulting in the transcriptional activation of targeted genes (Lauberth et al., 2013).

As TrxG complexes, Polycomb proteins act within multimeric complexes named Polycomb repressive complex (PRC) 1 and 2. PRC2 core complex contains four core subunits: EED, SUZ12, RbAp 48/46 and Ezh2/1, the SET domain-containing HMTs that trimethylate Lysine 27 of histone H3 (H3K27me3). H3K27me3 is a hallmark associated to transcriptional repression. Although it is still unclear whether this epigenetic mark represents the cause or a consequence of the repressive state, there are some evidences that indicate multiple roles played by H3K27me3 in the transcriptional silencing. In fact, its enrichment at promoters would impair Pol II recruitment/elongation at target genes (Chen et al., 2012; Chopra et al., 2011). Primarily, H3K27me3 acts as scaffold for PRC1 recruitment, which, in turn, ubiquitynates Lysine 119 of histone H2A and leads to chromatin compaction (Francis et al., 2004; Wang et al., 2004) (**Figure 1.11**).

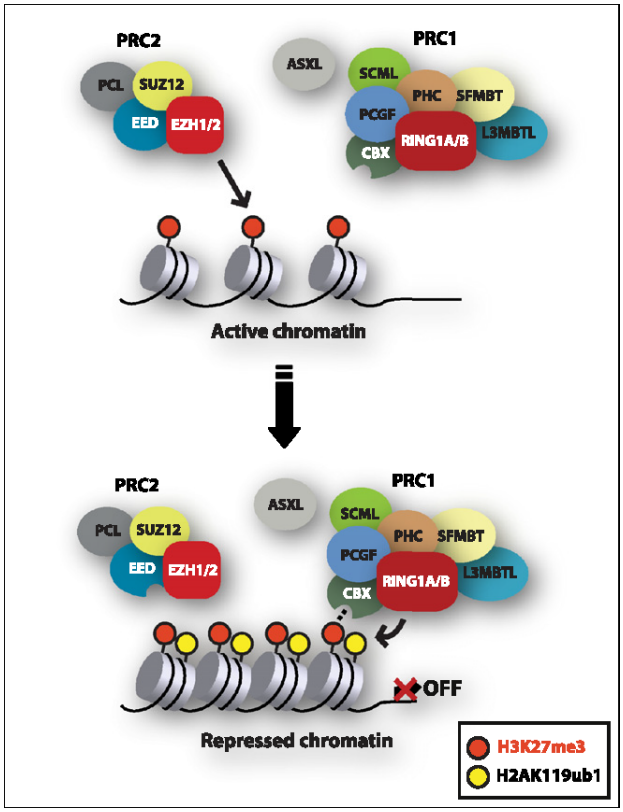

Figure 1.11. Canonical recruitment of the PRC1 complex via PRC2-mediated H3K27 methylation. PRC2 complex is recruited to chromatin, the histone methyltransferase EZH1/2 catalyzes the trimethylation of the lysine 27 of histone H3 (H3K27me3). Subsequent recruitment of the PRC1 complex occurs in part through affinity binding of the chromodomain of the CBX subunit to the H3K27me3 covalent mark. The PRC1 RING1 E3 ligase then monoubiquitylates the lysine 119 of histone H2A (H2AK119ub1 (from Sauvageau and Sauvageau., 2010).

Inside the nucleus, PcG proteins are not homogenously distributed, but are rather localized in discrete foci called Polycomb bodies (Saurin et al., 1998; Dietzel et al., 1999). During the last years, new effort has been put to address the functional role of these subnuclear compartments as well as to investigate their distribution, composition and dynamics (Cheutin and Cavalli, 2012). Furthermore, other PRC1 complexes have been recently identified, which exhibit H3K27me3-independent mechanisms of chromatin targeting (Gao et al., 2012; Morey et al., 2013; Tavares et al., 2012). A third complex named PhoRC has been characterized in *Drosophila* (homologous to YY1 in mammals), which show the ability to bind methylated histones and also DNA in a sequence-specific manner (Sparmann and van Lohuizen, 2006).

In *Drosophila*, Trithorax- and Polycomb-group complexes bind DNA sequences called TrxG response elements (TREs) and Polycomb response elements (PREs) respectively. These elements contain overlapping groups of binding motifs for transcription factors like Daf1, Gaf and Zeste, which are able to address PcGs and TrxGs to the target genomic sequences and perpetuate the transcriptional state of controlled loci (Ringrose and Paro, 2007). In 2011, Giacomo Cavalli and colleagues (Bantignies et al., 2011) demonstrated that Antennapedia and Bithorax complexes, located on the same chromosome arm and separated by 10 Mb of DNA, colocalize within Polycomb bodies in tissue where they are corepressed (embryonic head). Furthermore, this configuration is still maintained in posterior tissues where homeotic genes are active, but in this case, the active gene escapes from this restriction and localize outside the PcG body. Importantly, this colocalization

depends on the integrity of PRE elements located within the BX-C cluster and also on the PcG proteins that mediate long-range interaction between PRE elements and repressed promoters (**Figure 1.12**).

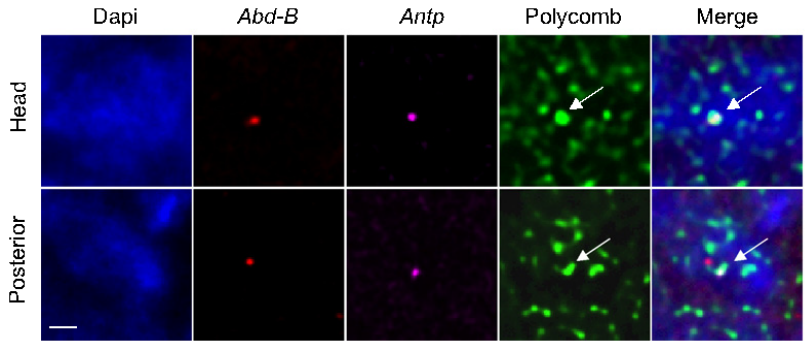

Figure 1.12. Homeotic complex "kissing" in *Drosophila* tissues. In the anterior tissue Abd-B and Antp colocalize within the same PcG body. In posterior tissue Abd-B is active and gets relocated outside the PcG body (from Bantignies et al., 2011).

What is the configuration of *Hox* cluster in vertebrates? As body plan complexity has increased during evolution, PcG and TrxG complexes have been co-opted and integrated in different hierarchies in order to regulate in space and time new cell-specific gene functions. Despite their conserved functions, the mechanisms adopted for the recruitment of these epigenetic complexes to their target sites have diverged between flies and mammals. To date, no TRE sequences have been identified in mammals, and only few PREs have been characterized in mouse (Mishra et al. 2007; Sing et al., 2009; Woo et al., 2010; Woo et al., 2013). Although, this situation might be interpreted as result of an incomplete characterization of PRE/TRE elements in higher vertebrates, some evidences suggest the adoption of different strategies to localize PcG and TrxG complexes to their target loci. For example, long non-coding RNAs (lncRNAs) such as *HOTAIR* and *HOTTIP* have been implicated in the regulation of target *Hox* genes through the interaction with PRC2 and MLL respectively (Rinn et al., 2007; Wang et al., 2011).

Because of the divergent epigenetic mechanisms that address PcG and TrxG proteins to their target genes and the different nature of spatial collinearity between flies and vertebrates, it is difficult to predict the outcome of the *Hox* cluster configuration in higher animals. Denis Duboule and colleagues (Noordermeer et al., 2011; Soshnikova and Duboule, 2009) revisited the idea of open and closed chromatin in terms of PcG- and TrxG-mediated epigenetic modifications during temporal and spatial collinear activation of the *Hox* clusters. The results of their research lead to the observation that transcriptionally repressed genes colocalize within an inactive compartment matching the presence of H3K27me3. Moreover, during collinear activation, the *Hox* genes located in 3' position get relocated to an active compartment marked with H3K4me3 (**Figure 1.13**), in keeping with the idea of a progressive 3' to 5' transcriptional competence of the clusters.

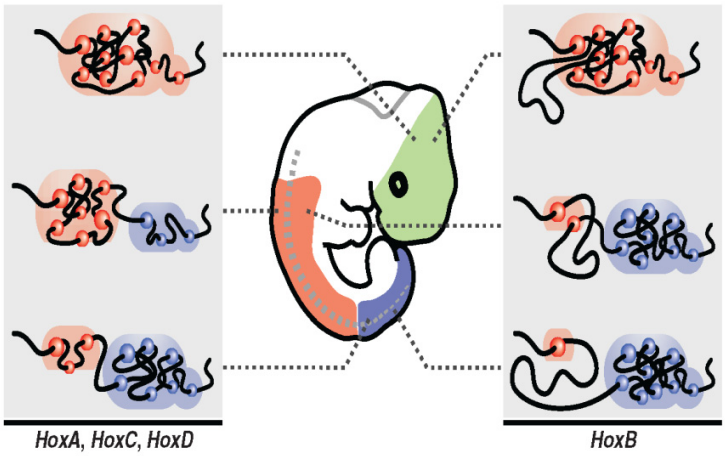

Figure 1.13. Active and repressive *Hox* cluster compartments in mouse embryo. Sequential activation of *Hox* genes along the rostro-caudal axis in the mouse leads to relocalization from a repressive compartment (red) to an active one (blue) (from Noordermeer et al., 2011).

Taken together, these results indicate the presence of evolutionary conserved epigenetic mechanisms that are responsible for the regulation of the collinear expression of *Hox* genes. These mechanisms go beyond the general idea of transcriptional regulation

based on transcription factor availability/*cis*-regulatory element responsiveness, and imply the usage of higher order 3D- chromatin organization modules called compartments.

1.5. Rationale of the work

Retinoic acid (RA) plays important roles during embryonic development, regulating key cellular processes such as migration, proliferation and differentiation. Furthermore, one of its well-known functions is to regulate the expression of *Hox* genes in the neuroepithelium, which, in turn, are responsible for the segmental identity of rhombomeric territories at the level of the developing hindbrain. RA acts as a morphogen during gastrulation. The RA morphogenetic gradient is established through the complementary distribution of synthesizing and degrading enzymes along the rostro-caudal axis of the embryo. In particular, Raldh2 is the earliest synthesizing enzyme to be expressed in somitic and pre-somitic mesoderm. Moreover, it is solely responsible for embryonic RA synthesis until E8.5. Although several studies addressed it function during early embryonic development, the molecular mechanisms responsible for its expression are still unknown. In the first part of this work we address the transcriptional network responsible for Raldh2 maintenance in the early developing embryo. Our findings, reported in the Chapter 2 of the present manuscript, demonstrate how retinoic signalling pathway could have been evolutionary co-opted for vertebrate patterning and integrated into the *Hox* positional system. The result of this research led to the discovery of a retinoic acid-mediated feedforward regulatory loop that puts in register the spatial collinear expression of *Hox* genes in the paraxial mesoderm with their expression in the neural tube (Vitobello et al., 2011).

Furthermore, several lines of evidence indicate that if on the one hand, the expression of *Hox* genes is crucial for the proper development of the rhombencephalic region, on the other hand their repression in the most anterior part of the embryo represents a prerequisite that allowed the evolution of an increasingly complex craniofacial architecture in the vertebrate lineage. In fact, most of the bones and cartilages that make-up the vertebrate face originate from *Hox*-negative cranial neural crest cells (cNCCs), a transient cell population originating from the dorsal part of the developing neural tube.

These cells undergo epithelial-to-mesenchymal transition and migrate in order to reach their target regions where they proliferate and differentiate into a variety of cell types. Experiments performed in the avian embryo demonstrated that the ectopic expression on *Hox* genes in this region leads to a severe impairment of craniofacial development. To date, the mechanisms responsible for the maintenance of the repressive state of *Hox* genes in the anterior part of the embryo remain elusive. Recent studies revisit the transcriptional state of *Hox* genes in terms of permissive and repressive chromatin domains, suggesting a possible role of epigenetic factors in the regulation of their expression. In the second part of the present manuscript we start to address the functional role of Ezh2, the catalytic component of the Polycomb repressive complex 2, during mouse craniofacial development. Our results, reported in this manuscript (Chapter 3), provide with new insight into the understanding of the spatial collinearity in vertebrates, the phenomenon that links the distribution of *Hox* gene expression along the rostro-caudal embryonic axis with their relative position within the clusters. Moreover, taking advantage from genetic tools that allowed us to isolate different rostro-caudal populations of *Hox*-negative and *Hox*-positive cranial neural crest cells (cNCCs) we investigate the role of Ezh2 in the cell fate maintenance.

Finally, the present manuscript encompasses also two further research articles, result of the collaboration within the Prof. Rijli's group (reported in Chapter 4) and with the Prof. Chiquet-Ehrismann's group at the FMI (reported in Chapter 5).

Chapter 2: Research Article

2.1. "Hox and Pbx Factors Control Retinoic Acid Synthesis during Hindbrain Segmentation"

During the evolution, the transcriptional events that lead to the initiation of Hox gene expression in the vertebrate hindbrain became under the control of Retinoic acid (RA), a lipophilic molecule able to regulate pleiotropic processes during embryonic development. Produced in the paraxial mesoderm through the activity of Raldh2, RA acts as a morphogen and regulates the transcriptional landscapes of target tissues by modulating the activity of responsive genes. However, the molecular events leading to proper expression of Raldh2 during embryonic development are still elusive. Starting from the observation that Pbx1/Pbx2 mutant mice exhibit most of the developmental defects caused by *Raldh2* knockout animals we explored the hypothesis that Pbx and their partners Hox transcription factors could be part of the transcriptional network ensuring appropriate RA signaling to the developing hindbrain. In this paper we identified a feed-forward mechanism that explains how retinoic signaling pathway could have been evolutionary co-opted for vertebrate patterning and integrated into the *Hox* positional system.

Author contribution statement: Experimentally, I collected the biological samples and performed the *in situ* hybridizations, β-galactosidase staining, *in ovo* electroporations and Xenopus injections. I contributed to the study design, analysis and interpretation of the results, preparation of manuscript and figures.

2.2. Main article

Developmental Cell
Article

Hox and Pbx Factors Control Retinoic Acid Synthesis during Hindbrain Segmentation

Antonio Vitobello,[1,5] Elisabetta Ferretti,[2,5] Xavier Lampe,[1,4] Nathalie Vilain,[1] Sebastien Ducret,[1] Michela Ori,[3] Jean-François Spetz,[1] Licia Selleri,[2,*] and Filippo M. Rijli[1,*]
[1]Friedrich Miescher Institute for Biomedical Research, Maulbeerstrasse 66, 4058 Basel, Switzerland
[2]Department of Cell and Developmental Biology, Weill Medical College of Cornell University, 1300 York Avenue, New York, NY 10021, USA
[3]Laboratory of Cell and Developmental Biology, Department of Biology, University of Pisa, via Abetone e Brennero 4, 56127 Pisa, Italy
[4]Present address: Laboratory of Cancer Epigenetics, Free University of Brussels, Faculty of Medecine, 1070 Brussels, Belgium
[5]These authors contributed equally to this work
*Correspondence: lis2008@med.cornell.edu (L.S.), filippo.rijli@fmi.ch (F.M.R.)
DOI 10.1016/j.devcel.2011.03.011

SUMMARY

In vertebrate embryos, retinoic acid (RA) synthesized in the mesoderm by *Raldh2* emanates to the hindbrain neuroepithelium, where it induces anteroposterior (AP)-restricted *Hox* expression patterns and rhombomere segmentation. However, how appropriate spatiotemporal RA activity is generated in the hindbrain is poorly understood. By analyzing *Pbx1/Pbx2* and *Hoxa1/Pbx1* null mice, we found that *Raldh2* is itself under the transcriptional control of these factors and that the resulting RA-deficient phenotypes can be partially rescued by exogenous RA. Hoxa1-Pbx1/2-Meis2 directly binds a specific regulatory element that is required to maintain normal *Raldh2* expression levels in vivo. Mesoderm-specific *Xhoxa1* and *Xpbx1b* knockdowns in *Xenopus* embryos also result in *Xraldh2* downregulation and hindbrain defects similar to mouse mutants, demonstrating conservation of this Hox-Pbx-dependent regulatory pathway. These findings reveal a feed-forward mechanism linking Hox-Pbx-dependent RA synthesis during early axial patterning with the establishment of spatially restricted Hox-Pbx activity in the developing hindbrain.

INTRODUCTION

Retinoic acid (RA), the acidic form of vitamin A, is essential for normal development and organogenesis of the vertebrate embryo. In the early mouse embryo, RA is mainly produced by the biosynthetic enzyme Raldh2 in presomitic mesoderm (PSM), paraxial mesoderm, and lateral plate mesoderm (LPM), from which it emanates to the developing central nervous system (Duester, 2008; Niederreither et al., 1999). In turn, RA binds to nuclear receptors and directly activates target gene expression (Forman and Evans, 1995; Lohnes et al., 1993; Mark et al., 2009). RA acts as a diffusible morphogen forming a posterior-to-anterior activity gradient required for normal rostrocaudal patterning of the spinal cord and hindbrain neuroepithelial segments, or rhombomeres (r) (Glover et al., 2006; Kiecker and Lumsden, 2005; Maden, 2007; Marshall et al., 1992; Niederreither et al., 2000). Rhombomere identity and patterning is mediated by the transcription factors of the *Hox* gene family, whose activation in the neuroepithelium is directly under RA control (Glover et al., 2006). *Hox* expression domains are further refined in specific rhombomeres by local RA degradation regulated by the cytochrome p450 family 26 (Cyp26) enzymes (Hernandez et al., 2007; Sirbu et al., 2005; White et al., 2007). Maintaining normal levels of RA is crucial because retinoid excess and deficiency have teratogenic effects, including abnormal hindbrain segmentation and patterning. An outstanding question is how the synthesis of RA is regulated to provide appropriate retinoid levels along the rostrocaudal axis of the developing hindbrain and achieve normal segmentation. However, little is known about how the expression of *Raldh2* is coordinated at the transcriptional level to generate appropriate retinoid levels and activate nested *Hox* gene expression domains with specific rostral boundaries in the developing hindbrain.

In this study, we found that *Raldh2* mesodermal expression is itself under the direct transcriptional control of Hox, Pbx, and Meis factors in vivo. In *Pbx1/Pbx2* null mice, *Raldh2* levels are not properly maintained, resulting in progressive reduction of endogenous retinoid activity. In *Hoxa1/Pbx1*-deficient embryos, *Raldh2* is also significantly downregulated at early somite stage, resulting in caudal shift of hindbrain RA activity and an RA-deficient rhombomere phenotype that is partially rescued by exogenous RA administration. *Xhoxa1* and *Xpbx1* mesoderm-specific knockdowns in *Xenopus* embryos also resulted in *Raldh2* downregulation and induced hindbrain patterning defects similar to those of mouse compound mutants. By chromatin immunoprecipitation (ChIP) in mouse embryos, we identified a specific *Raldh2* enhancer containing a Hox-Pbx bipartite element bound by a Hoxa1-Pbx1/2-Meis2 complex and required to maintain normal expression levels in the context of the endogenous *Raldh2* promoter. In the *Raldh2*-negative (*Raldh2*$^{-}$) head of early stage embryos this enhancer is selectively bound by Suz12, a member of the Polycomb Repressive Complex 2 (PRC2), correlating with an enrichment of the H3K27me3 mark associated with facultative heterochromatin. These findings reveal a molecular feed-forward mechanism linking Hox-Pbx-dependent RA synthesis in mesoderm with the establishment of Hox-Pbx neuroepithelial activity during hindbrain segmentation.

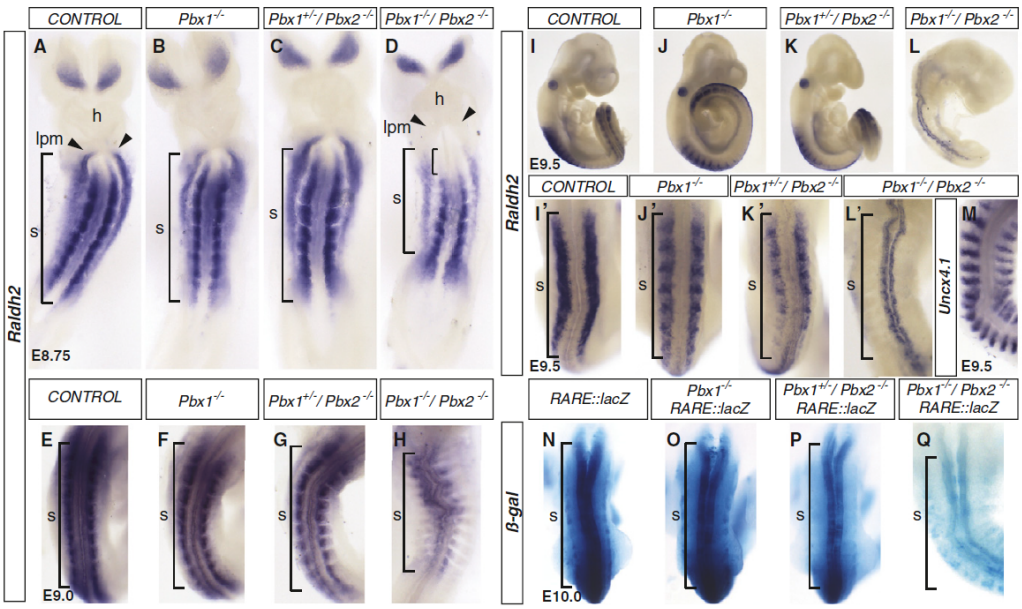

Figure 1. *Pbx1* and *Pbx2* Are Required for Maintenance of Mesodermal *Raldh2* Expression and Retinoid Activity

(A–L') Whole-mount in situ hybridization showing *Raldh2* expression in control (A, E, I, and I'), $Pbx1^{-/-}$ (B, F, J, and J'), $Pbx1^{+/-}/Pbx2^{-/-}$ (C, G, K, and K'), and $Pbx1^{-/-}/Pbx2^{-/-}$ (D, H, L, and L') embryos at E8.75 (A–D), E9.0 (E–H), and E9.5 (I–L and I'–L').

(M) Normal *Uncx4.1* expression in E9.5 $Pbx1^{-/-}/Pbx2^{-/-}$ mutants.

(N–Q) β-gal staining of E10.0 *RARE::lacZ* (N), $Pbx1^{-/-}$;*RARE::lacZ* (O), $Pbx1^{+/-}/Pbx2^{-/-}$;*RARE::lacZ* (P), and $Pbx1^{-/-}/Pbx2^{-/-}$;*RARE::lacZ* (Q). h, heart; lpm, lateral plate mesoderm; s, somites.

See also Figure S1.

RESULTS

Pbx1/2-Dependent Maintenance of *Raldh2* Expression and Retinoid Activity

Pbx genes encode three-amino-acid loop extension (TALE) class homeodomain (HD) transcription factors that form heteroligomeric complexes with a subset of Hox and Meis/Prep HD proteins and regulate a variety of developmental processes (Mann and Chan, 1996; Moens and Selleri, 2006). Compound $Pbx1^{-/-}/Pbx2^{-/-}$ (referred to as *Pbx1/2* null) embryos exhibit multiple organogenesis defects and eventually die by E10.5 (Capellini et al., 2006). Specifically, *Pbx1/2* null mutants display abnormal turning, shortened bodies, abnormal development of forebrain and limb buds, a dilated heart, hypoplastic posterior branchial arches, and somite/vertebral patterning defects (Capellini et al., 2008; Selleri et al., 2001; Stankunas et al., 2008). These developmental defects are markedly similar to those described for *Raldh2* deficient mouse embryos (Niederreither et al., 1999). Thus, the *Pbx1/2* null mutant pleiotropic phenotype may be partly due to reduced endogenous retinoid levels.

To test this hypothesis, we first investigated *Raldh2* expression in *Pbx1/2* null embryos. In E7.75 single and *Pbx1/2* null mutants, *Raldh2* spatial distribution and expression levels did not appear to be significantly altered, as compared to wild-type controls (see Figure S1 available online). In contrast, at E8.75 *Raldh2* transcript levels were significantly decreased in *Pbx1/2* null embryos; moreover, *Raldh2* expression was selectively absent from the LPM just posterior to the cardiac field and the anterior-most somites of the mutants (Figure 1D). By E9.0-E10.0, *Raldh2* expression was strongly downregulated in the somitic mesoderm (Figures 1H, 1L, and 1L'). Accordingly, endogenous retinoid activity was severely depleted in *Pbx1/2* null mutants mated to *RARE::lacZ* reporter mice (Rossant et al., 1991) (*Pbx1/2;RARE::lacZ*) (Figure 1Q). A progressive reduction of *Raldh2* expression and *RARE::lacZ* reporter β-gal activity was already evident in single $Pbx1^{-/-}$ as well as compound $Pbx1^{-/-}/Pbx2^{+/-}$ and $Pbx2^{-/-}/Pbx1^{+/-}$, though not in $Pbx2^{-/-}$ single mutants (Figures 1O and 1P and data not shown). Notably, treatment of *Pbx1/2* null embryos with exogenous RA (10 mg/kg) at E8.5 partially rescued the mutant phenotype and yielded embryos with normal turning (3/9; 33%) (Figure S1), suggesting that at least part of Pbx1/2 function is mediated through the control of RA production. These data strongly point to a synergistic genetic interaction between *Pbx1* and *Pbx2* for temporal maintenance of *Raldh2* transcriptional levels and control of endogenous retinoid signaling, with a main requirement for *Pbx1*.

Developmental Cell
Hox-Pbx-Dependent Raldh2 Regulation

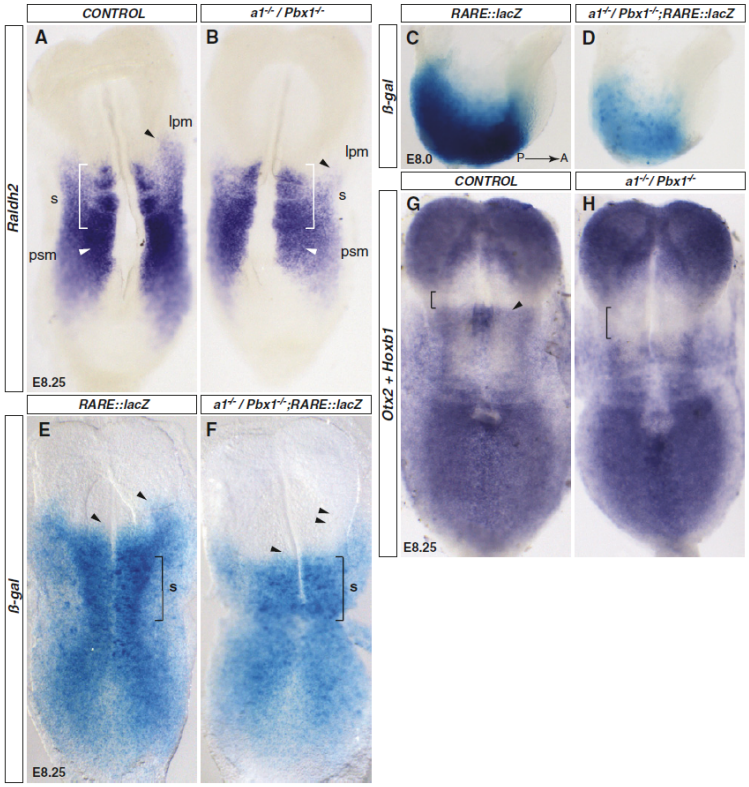

Figure 2. *Hoxa1*- and *Pbx1*-Dependent Regulation of Mesodermal *Raldh2* Expression and Retinoid Activity Boundary in the Early Hindbrain
(A and B) Whole-mount in situ hybridization shows *Raldh2* expression in E8.25 control (A) and $Hoxa1^{-/-}/Pbx1^{-/-}$ (B) embryos (ventral view).
(C–F) β-gal staining of *RARE::lacZ* (C and E) and $Hoxa1^{-/-}/Pbx1^{-/-}$;*RARE::lacZ* (D and F) embryos at E8.0 (C and D) and E8.25 (E and F).
(G and H) Double in situ hybridization for *Otx2* and *Hoxb1* in E8.25 control (G) and $Hoxa1^{-/-}/Pbx1^{-/-}$ (H). lpm, lateral plate mesoderm; psm, pre-somitic mesoderm; s, somites.

Hoxa1/Pbx1-Dependent Regulation of *Raldh2* Expression and Retinoid Activity

Pbx factors are essential DNA-binding partners of Hox transcription factors (Mann and Chan, 1996; Moens and Selleri, 2006; Popperl et al., 2000; Remacle et al., 2004). *Hoxa1* is activated in the posterior primitive streak and, in turn, in presomitic, somitic, and lateral plate mesoderm (Deschamps and van Nes, 2005; Murphy and Hill, 1991). RA-mediated activation of *Hoxa1* in the overlying neuroectoderm is induced through a 3′ retinoic acid responsive enhancer (3′RARE) (Dupe et al., 1997). Under RA response, the *Hoxa1* expression domain spreads up into the presumptive r3 territory and subsequently sets its border at the r3/r4 boundary, providing the earliest sign of molecular segmentation in the mouse hindbrain (Makki and Capecchi, 2010). *Hoxa1* inactivation resulted in hindbrain segmentation and rhombomere patterning defects (Carpenter et al., 1993; Mark et al., 1993) that resemble vitamin A partial deficiency phenotypes. *Hoxa1* mesodermal expression in the early embryo precedes *Raldh2* activation (Murphy and Hill, 1991; Niederreither and Dolle, 2008). Thus, Pbx factors may cooperate with Hoxa1 in mesoderm to regulate the early phase of *Raldh2* expression, and, in turn, the early availability of retinoids diffusing into the developing hindbrain prior to segmentation.

To test this hypothesis, we analyzed *Raldh2* expression in compound $Hoxa1^{-/-}/Pbx1^{-/-}$ (referred to as *Hoxa1/Pbx1* null) mutants. Several 3′ *Hox* genes are sequentially activated in a temporally collinear manner in the posterior end of the embryo (Deschamps and van Nes, 2005; Soshnikova and Duboule, 2009), thus resulting in potential functional redundancy for the regulation of *Raldh2* levels. Thus, we focused on early somitogenesis stages, when the lack of *Hoxa1* and its cofactor *Pbx1* may be expected to have a major functional impact. In E8.0–E8.25 (3–4 somite stage) *Hoxa1/Pbx1* null embryos, *Raldh2* transcript levels were significantly lower than in controls, specifically in PSM and somitic mesoderm (Figures 2A and 2B). Moreover, the rostral *Raldh2* expression domain in LPM, just posterior to

the heart field and adjacent to the presumptive hindbrain, was selectively downregulated (arrowhead, Figure 2B).

We next analyzed endogenous retinoid activity in *Hoxa1/Pbx1;RARE::lacZ* null mutants by β-gal staining. At 0–2 somite stage, β-gal activity was severely downregulated in *Hoxa1/Pbx1* null embryos (Figure 2D). By the 3–4 somite stage, the overall β-gal staining levels were still significantly lower than in controls (Figures 2E and 2F). Moreover, the rostral LPM domain of retinoid activity diffusing into the heart field was either missing or severely reduced (double arrowheads), in agreement with *Raldh2* in situ hybridization results (compare Figures 2B and 2F). Notably, the anterior boundary of β-gal staining in the presumptive hindbrain was posteriorly shifted in *Hoxa1/Pbx1* null mutants, as compared to controls (single arrowhead, Figures 2E and 2F). These data revealed that *Hoxa1* and *Pbx1* genetically interact in regulating early mesodermal *Raldh2* expression and setting the RA activity boundary in the presumptive hindbrain neuroepithelium.

RA-Deficient Hindbrain Phenotype of *Hoxa1/Pbx1* Null Mutants

We next analyzed the hindbrain segmentation pattern in *Hoxa1/Pbx1* null embryos (Figures 3A–3N). In *Pbx1* null mutants, the *Hoxb1*$^+$ r4 territory was normally positioned (Figure 3C). In contrast, *Hoxa1* inactivation results in a smaller and slightly caudally displaced *Hoxb1*$^+$ r4 (Figure 3B) (Barrow et al., 2000; Carpenter et al., 1993; Mark et al., 1993) because of an early requirement of *Hoxa1* for *Hoxb1* transcription in presumptive r4 (Di Rocco et al., 2001). Late *Hoxb1* expression in r4 is instead maintained by an autoregulatory mechanism (Ferretti et al., 2005; Popperl et al., 1995). *Hoxb1* is also a direct RA target through specific RAREs (Marshall et al., 1992, 1994; Studer et al., 1994, 1998). RA emanating from the mesoderm is required to position the anterior limit of *Hoxb1* expression at the r3/r4 border and to repress *Hoxb1* in r3 and r5 (Marshall et al., 1994; Studer et al., 1994, 1998).

In E8.25 *Hoxa1/Pbx1* null mutants, the *Hoxb1* expression border in presumptive hindbrains retreated caudally (compare *Otx2* and *Hoxb1* expression domains; Figure 2H), whereas the remainder of its expression domain appeared normal. At E9.0, the *Hoxb1* expression domain was shifted posteriorly beyond the otocyst, lacked sharp anterior and posterior borders, and was larger in *Hoxa1/Pbx1* than *Hoxa1* null mutants (r4*, compare Figures 3B and 3D). In keeping with the marked posterior shift of r4, r4-derived *Hoxa2*$^+$ neural crest cells (NCC) migrated caudally to the otic vesicle, rather than rostrally (Figures 3I′ and 3J′). A posterior shift of r3, which abnormally faced the otocyst, and lack of r5 were also observed, as assessed with the r3/r5- and r5/r6-specific markers *Krox20* and *Kreisler*, respectively (Figures 3K–3N; note that the r3-specific *Krox20*$^+$ expression domain is severely downregulated). Lastly, *Hoxa1/Pbx1* null mutants displayed a prominent posterior expansion of r2, as assessed with a *Hoxa2* probe, that was not present in either single *Hoxa1* or *Pbx1* null embryos (Figures 3I and 3J).

In summary, in the hindbrain of *Hoxa1/Pbx1*, though not single, null mutants we observed a posterior displacement of anterior rhombomere identities at the expense of the r5-r6 territory, similar to the phenotype observed in partial RA-deficiency, as posterior rhombomeres require higher RA signaling than rostral ones to be positioned and specified (Dupe and Lumsden, 2001; Gavalas, 2002; Niederreither et al., 2000). In this respect, the early reduction of mesodermal *Raldh2* expression and hindbrain RA activity in *Hoxa1/Pbx1* null embryos (Figure 2) strongly predicts that at least part of the above hindbrain phenotype may result from partial RA deficiency induced by early roles of *Hoxa1* and *Pbx1* in mesoderm, distinct from their later roles in neuroepithelium.

Mesoderm-Specific *Xhoxa1* and *Xpbx1b* Knockdown Results in *Xraldh2* Downregulation and an RA-Deficient Phenotype in *Xenopus* Embryo Hindbrain

To test Hox-Pbx-dependent conservation of *Raldh2* regulation across species, we used a mesoderm-specific morpholino (MO)-mediated knockdown approach in *Xenopus* embryos. We took advantage of the established fate map of individual blastomeres of the *Xenopus* embryo (Hirose and Jacobson, 1979; Moody, 1987; Moody and Kline, 1990) and injected antisense MOs against *Xpbx1b* (Maeda et al., 2002) and/or *Xhoxa1* (McNulty et al., 2005) selectively in the left V2.2 blastomere of the 16-cell stage embryo and compared to the uninjected side as internal control. The V2.2 blastomere and its progeny largely contribute to somitic mesoderm and LPM, though not, or only marginally, to hindbrain and nervous system (Hirose and Jacobson, 1979; Moody, 1987; Moody and Kline, 1990). To further screen for injected embryos devoid of morphant cells in the nervous system, we coinjected MOs in V2.2 with mRNAs for Red Fluorescent Protein (RFP) and nuclear lacZ (Figure 4). Embryos were sorted at the late neurula stage (stage 17–18) for the distribution of RFP fluorescence (n = 634 ; Figures 4A–4D) by selecting only those displaying significant unilateral RFP expression in paraxial mesoderm and LPM, but not in nervous system, as confirmed on tissue sections (e.g., Figure 4D). Moreover, a subset of the selected embryos was additionally stained by salmon-gal prior to further processing for in situ hybridization (n = 61/634), and consistently confirmed the lack of injected cells in the nervous system (Figure 4J and data not shown).

At stage 17–18, *Xraldh2* is mainly expressed in presomitic and somitic mesoderm, and LPM in the middle part of the trunk (Chen et al., 2001). Although embryos injected with *control* MO did not display molecular changes (n = 68; Figure S2; Figure 4E), the majority of embryos injected with a *Xpbx1b* MO in the mesoderm displayed a reduction of *Xraldh2* expression (n = 92/128; 72%) that ranged from significant (n = 80/128; 63%) to severe in some cases (n = 12/128; 9%) (Figure S2; data not shown; see also Figures 4F and 4G). Such variability is likely due to mosaicism of MO distribution inherent to the knockdown approach and/or to potential functional redundancy with other Pbx factors. At any rate, these findings underscored an important role of *Xpbx1b* in maintaining normal *Xraldh2* levels in the mesoderm, similarly to mouse (Figure 1).

We then investigated the potential impact of mesodermal knockdown of *Xpbx1b* on hindbrain patterning. We predicted that the variable impairment of *Xraldh2* expression could result in a range of RA-deficient rhombomere phenotypes. In situ hybridization with *Xkrox20* of *Xpbx1b* MO-injected embryos (n = 135) revealed rhombomere abnormalities that ranged from r5 reduction to absence in some cases (n = 74/135; 55%; data not shown; see also Figures 4F and 4G). A fraction of the injected

Developmental Cell
Hox-Pbx-Dependent Raldh2 Regulation

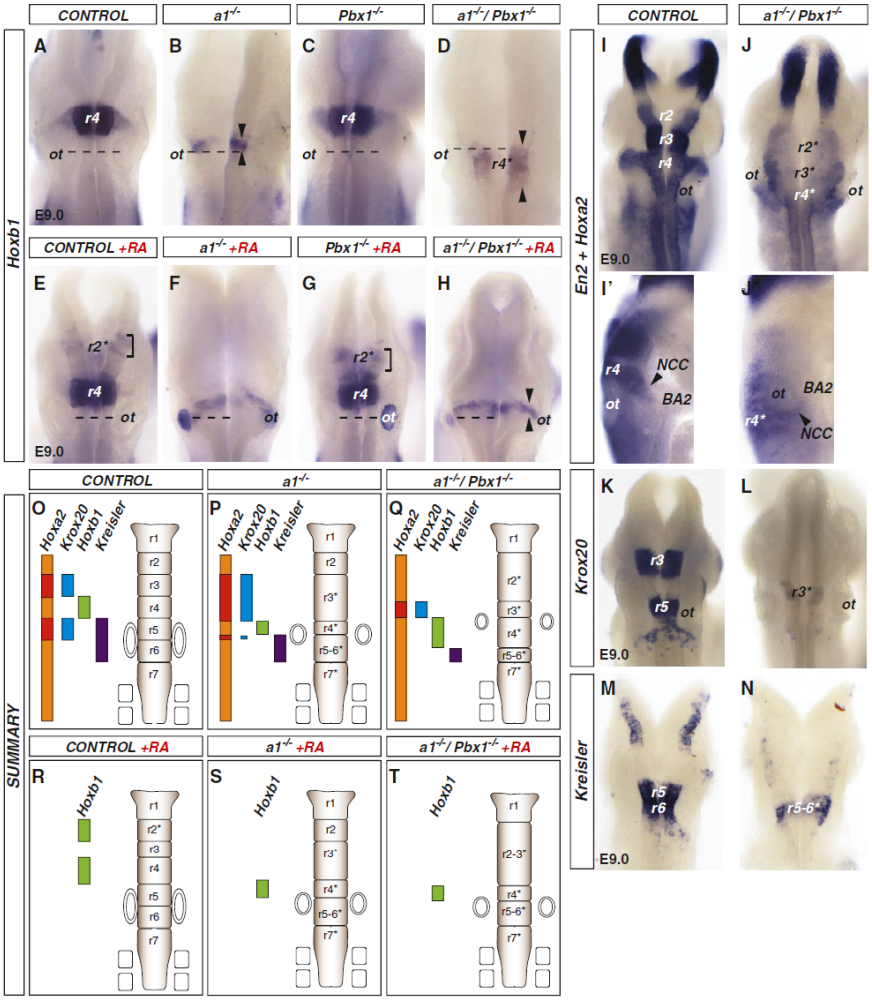

Figure 3. Retinoic Acid-Deficient Phenotype of *Hoxa1/Pbx1* Mutant Hindbrain and Rescue by Exogenous RA

(A–H) Whole-mount in situ hybridization for *Hoxb1* in E9.0-untreated (A–D) and RA-treated (E–H) control (A and E), *Hoxa1*$^{-/-}$ (B and F), *Pbx1*$^{-/-}$ (C and G), and *Hoxa1*$^{-/-}$/*Pbx1*$^{-/-}$ (D and H) embryos.

(I–J') *Hoxa2* and *En2* expression in E9.0 control (I and I') and *Hoxa1*$^{-/-}$/*Pbx1*$^{-/-}$ (J and J') embryos.

(K–N) *Krox20* and *Kreisler* expression in E9.0 control (K and M) and *Hoxa1*$^{-/-}$/*Pbx1*$^{-/-}$ (L and N) embryos.

(O–T) Summary diagrams illustrating the *Hoxa1/Pbx1* mutant RA-deficient phenotype and its RA-mediated rescue. BA2, second branchial arch; NCC, neural crest cells; ot, otic vesicle; r, rhombomere; RA, retinoic acid.

embryos (n = 14/135; 10%) additionally displayed a one-rhombomere posterior shift of r3 and r5 (data not shown; see also Figures 4H–4J), indicating a more severe RA deficiency. Direct correlation between the extent of *Xraldh2* reduction and the severity of the observed hindbrain defects was demonstrated by simultaneous in situ hybridization with *Xraldh2* and *Xkrox20* of an additional set of *Xpbx1b* MO-injected embryos (n = 100; Figures 4F and 4G; see also Figure 4K for a mosaic plot of the distribution of hindbrain phenotypes versus *Xraldh2* expression levels). In summary, *Xpbx1b* selective knockdown in mesoderm has a direct impact on *Xraldh2* expression and induces hindbrain abnormalities that are expected features of partial RA deficiency.

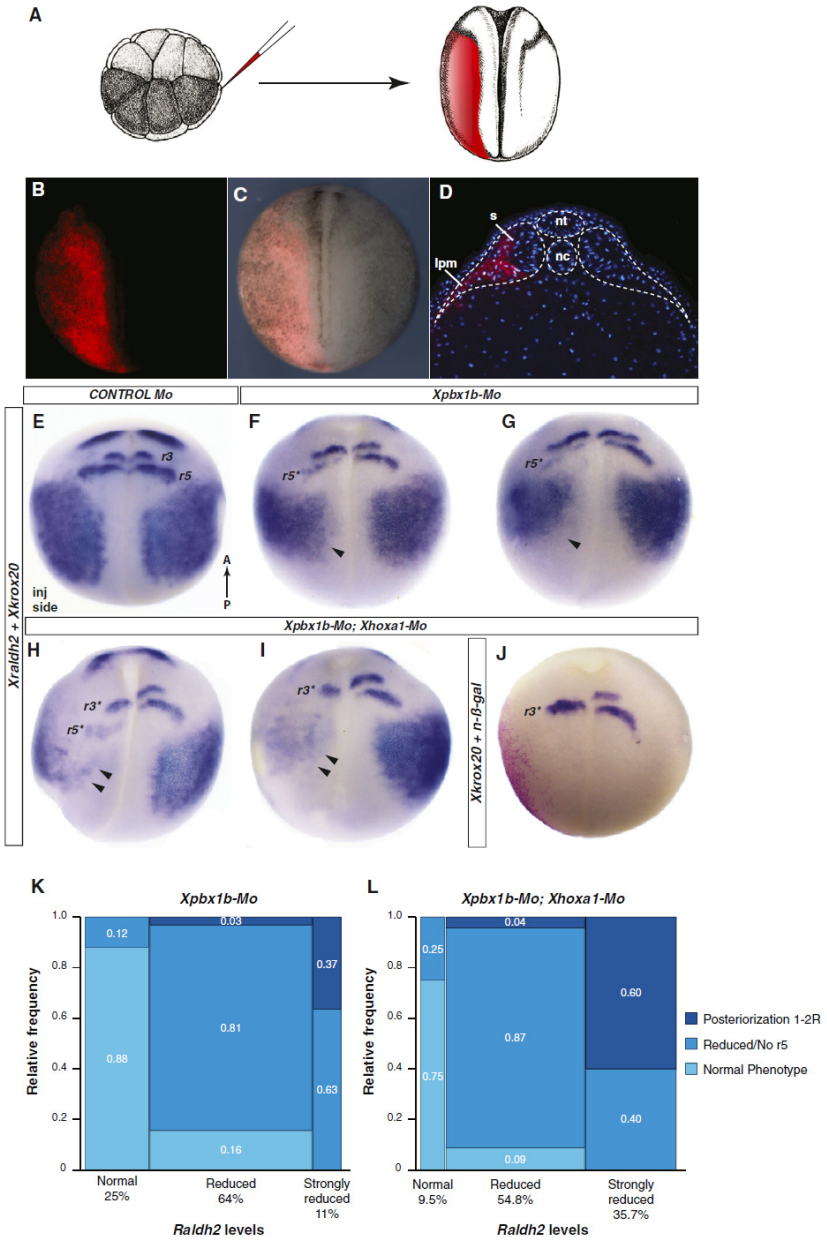

Figure 4. Mesoderm-Specific *Xpbx1* and *Xhoxa1* Knockdown in *Xenopus* Embryos

(A) Diagram of marginal zone V2.2 *Xenopus* blastomere injection at 16-cell stage, and fate of injected blastomere in stage 17 neurula.

(B) Whole-mount detection of RFP in left V2.2 blastomere-injected embryo.

Developmental Cell
Hox-Pbx-Dependent Raldh2 Regulation

We next asked whether *Xpbx1b* could functionally synergize with *Xhoxa1* for mesodermal regulation of *Xraldh2*. A previously described *Xhoxa1* MO induced only subtle hindbrain defects when injected at the four-cell stage throughout the left side of the embryo, likely because of functional redundancy with other *Hox1* paralogs (McNulty et al., 2005). The injection of this *Xhoxa1* MO in mesoderm (n = 26) did not significantly alter *Xraldh2* expression or hindbrain patterning (n = 21/26; data not shown). A mild decrease of *Xraldh2* expression was scored in the remaining 5 of 26 injected embryos, as compared to the uninjected side, that was not, however, sufficient to induce hindbrain patterning defects (data not shown).

Coinjection of MOs against both *Xhoxa1* and *Xpbx1b* in mesoderm strongly enhanced the effects of the *Xpbx1b* knockdown (Figure S2; Figures 4H and 4I). Increasingly severe downregulation of *Xraldh2* expression was observed in the vast majority of coinjected embryos (n = 98/110; 89%; Figure S2; see also Figures 4H and 4I). Moreover, the fraction of embryos displaying a drastic *Xraldh2* reduction was notably increased (n = 46/110; 42%; Figure S2; see also Figures 4H and 4I), as compared to singly *Xpbx1b* MO-injected embryos. These findings reveal a synergistic role of *Xhoxa1/Xpbx1b* in *Xraldh2* regulation in *Xenopus* embryo mesoderm.

Accordingly, we scored more frequent and/or penetrant hindbrain abnormalities in *Xpbx1b/Xhoxa1* MO-coinjected embryos (n = 93) than in singly *Xpbx1b* or *Xhoxa1* MO-injected embryos. These phenotypes ranged from strong reduction/absence of r5 (n = 52/93; 56%) to a 1-2-rhombomere posterior shift of r3 with loss of r5 (n = 18/93; 19%), as assessed with the *Xkrox20* probe (data not shown; see also Figures 4H–4J). Importantly, the specimen in Figure 4J was additionally costained with salmon-gal to directly detect the injected cells (red cells), thus demonstrating that a strong hindbrain phenotype (e.g., a posterior shift of r3 with loss of r5 ; Figure 4J) can be induced by the selective injection of *Xpbx1b/Xhoxa1* MOs in mesoderm.

Direct correlation between the extent of *Xraldh2* reduction and the severity of the hindbrain phenotype was further demonstrated by simultaneous in situ hybridization with *Xraldh2* and *Xkrox20* of *Xpbx1b/Xhoxa1* MO-injected embryos (n = 42; Figures 4H and 4I). Comparison of the mosaic plots in Figures 4K and 4L allows us to directly assess the synergistic role of *Xpbx1b/Xhoxa1* and the impact of their knockdowns in mesoderm on *Xraldh2* expression and hindbrain phenotype, as compared to singly *Xpbx1b* MO-injected embryos.

In sum, our mesoderm-specific knockdown approach demonstrated the requirement for *Xpbx1b* to maintain normal levels of *Xraldh2*, and its synergistic functional interaction with *Xhoxa1*. It also demonstrated that selective downregulation of Pbx-Hox factors in the mesoderm, independently of their roles in neuroepithelium, is sufficient to induce abnormal hindbrain segmentation. Such hindbrain defects phenocopied the effects of RA-deficiency (Dupe and Lumsden, 2001; Gavalas, 2002), and were notably similar, at least in part, to those observed in *Hoxa1/Pbx1* null mice (Figure 3).

Rescue of Mouse *Hoxa1/Pbx1* Mutant Hindbrain by Exogenous RA Treatment

We then asked which features of the *Hoxa1/Pbx1* null mouse phenotype could be specifically ascribed to the mesodermal *Hoxa1/Pbx1*-dependent decrease of retinoid synthesis (Figure 2), as opposed to those resulting from a direct role of *Hoxa1* and *Pbx1* in hindbrain neuroepithelium. The administration to double mutants of a subteratogenic dose of exogenous RA (5 mg/kg at E8.0 [5RA-8]; Pasqualetti et al., 2001) may be expected to rescue the former, though not the latter, aspects of the *Hoxa1/Pbx1* null hindbrain phenotype.

Remarkably, 5RA-8 treatment of *Hoxa1/Pbx1* null mutants was sufficient to rescue the AP position of the r4 *Hoxb1*$^+$ domain and shift it beyond the rostral aspect of the otocyst (4/4; 100%) (Figures 3E–3H). Moreover, the *Hoxb1*$^+$ domain was caudally shortened in 5RA-8-treated E9.5 mutant embryos, as compared to untreated double mutants (Figure 3H), indicating partial rescue of RA-mediated repression, which normally restricts *Hoxb1* expression caudal to r4 (Studer et al., 1994), and of posterior rhombomere patterning. However, 5RA-8 treatment was not able to ectopically induce *Hoxb1* in r2 of single *Hoxa1* or *Hoxa1/Pbx1* null mutants (Figures 3F and 3H), unlike in wild-type or single *Pbx1* mutant embryos (Figures 3E and 3G), confirming that ectopic *Hoxb1* activation specifically requires *Hoxa1* function in the neuroepithelium (Zhang et al., 1994; Di Rocco et al., 2001).

Thus, the hindbrain analysis of RA-rescued *Hoxa1/Pbx1* mutants provided strong additional evidence that the changes in rhombomere rostrocaudal position in untreated mutants may in part result from the *Hoxa1/Pbx1*-dependent decrease of mesodermal RA synthesis (Figure 2), independently of *Hoxa1/Pbx1* role in neuroepithelium.

A Specific *Raldh2* Regulatory Element Is Bound In Vivo by a Hoxa1-Pbx1/2-Meis2 Complex

Hox overexpression in chicken micromass cultures indicated the potential for direct regulation of *Raldh2* (Kuss et al., 2009). Therefore, we sought to assess whether *Raldh2* transcription in early embryonic mesoderm is directly regulated by Hoxa1 and Pbx1/2 factors.

In silico analysis revealed four conserved regions—namely, E1 (334 bp), E2 (980 bp), E3 (514 bp), and E4 (938 bp)—located

(C) Merge of bright field and fluorescence pictures of the embryo in (B).
(D) Cross-section showing selective RFP labeling in somites (s) and lateral plate mesoderm (lpm).
(E–I) Whole-mount double in situ hybridization for *Xraldh2* and *Xkrox20* in control-MO (E), *Xpbx1b*-MO (F and G), and *Xpbx1b*-MO;*Xhoxa1*-MO (H and I) left V2.2 blastomere-injected embryos.
(J) Nuclear-salmon-gal staining (red cells) of *Xpbx1b*-MO;*Xhoxa1*-MO V2.2-injected embryos indicate morphant cell localization in mesoderm. *Xkrox20* expression shows r3* posteriorization and r5* loss on the injected side.
(K and L) Correlation between *Xraldh2* downregulation and hindbrain phenotype in *Xpbx1b*-MO and *Xpbx1b;Xhoxa1*-MO injected embryos (mosaic plots). Relative phenotype severity is color-coded. Phenotype frequencies (*y* axis) are compared to levels of *Raldh2* (*x* axis). Synergistic action of *Xpbx1b*-MO;*Xhoxa1*-Mo results in rising the frequencies of *Xraldh2* severe reduction or loss and hindbrain patterning defects. MO, morpholino; r, rhombomere; RFP, Red Fluorescent Protein.
See also Figure S2.

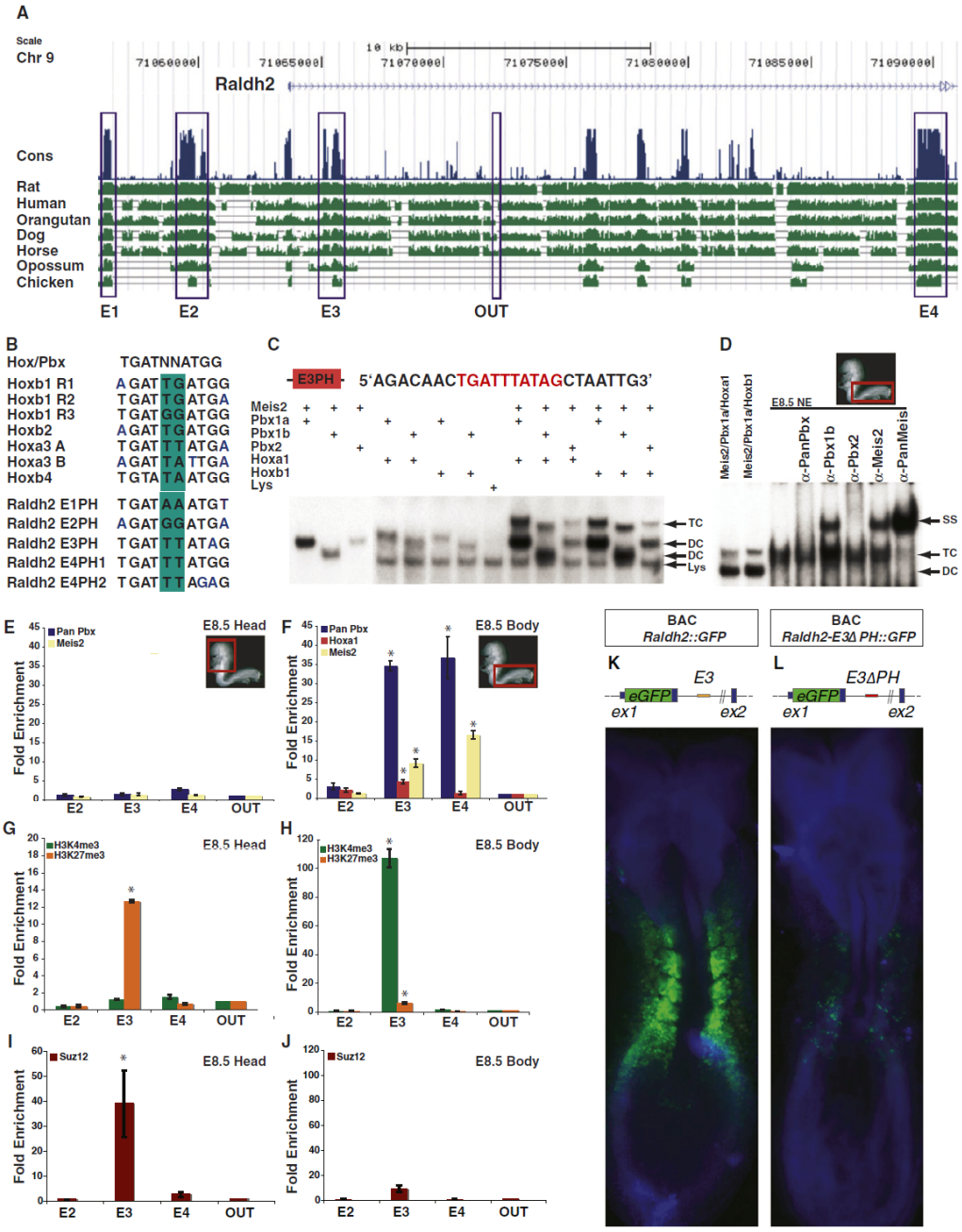
A
Scale
Chr 9
10 kb
71060000
71065000
71070000
71075000
71080000
71085000
71090000
Raldh2
Cons
Rat
Human
Orangutan
Dog
Horse
Opossum
Chicken
E1
E2
E3
OUT
E4
B
Hox/Pbx
TGATNNATGG
Hoxb1 R1 AGATTGATGG
Hoxb1 R2 TGATTGATGA
Hoxb1 R3 TGATGGATGG
Hoxb2 AGATTGATGG
Hoxa3 A TGATTTATGA
Hoxa3 B AGATTATTGA
Hoxb4 TGTATATGG
Raldh2 E1PH TGATAAATGT
Raldh2 E2PH AGATGGATGA
Raldh2 E3PH TGATTTATAG
Raldh2 E4PH1 TGATTTATGG
Raldh2 E4PH2 TGATTTAGAG
C
E3PH
5'AGACAACTGATTTATAGCTAATTG3'
Meis2
Pbx1a
Pbx1b
Pbx2
Hoxa1
Hoxb1
Lys
TC
DC
DC
Lys
D
Meis2/Pbx1a/Hoxa1
Meis2/Pbx1a/Hoxb1
E8.5 NE
α-PanPbx
α-Pbx1b
α-Pbx2
α-Meis2
α-PanMeis1
SS
TC
DC
E
Pan Pbx
Meis2
E8.5 Head
Fold Enrichment
E2
E3
E4
OUT
F
Pan Pbx
Hoxa1
Meis2
E8.5 Body
G
H3K4me3
H3K27me3
E8.5 Head
H
H3K4me3
H3K27me3
E8.5 Body
I
Suz12
E8.5 Head
J
Suz12
E8.5 Body
BAC
Raldh2::GFP
BAC
Raldh2-E3Δ PH::GFP
K
E3
eGFP
ex1
ex2
L
E3ΔPH
eGFP
ex1
ex2

Developmental Cell
Hox-Pbx-Dependent Raldh2 Regulation

upstream of the *Raldh2* transcription start site (E1 and E2) and in its first intron (E3 and E4), respectively (Figure 5A). Putative Pbx-Hox (PH) binding sites were identified in all such regions, whose sequences shared high conservation with previously described PH sites from Hox-Pbx target genes (Figure 5B; Figure S3). In vitro binding electrophoretic mobility shift assays (EMSAs) using different combinations of in vitro translated Hoxa1, Hoxb1, Pbx1a long isoform (Monica et al., 1991), Pbx1b short isoform (Monica et al., 1991), and Pbx2 proteins revealed that all PH sites could bind Pbx-Hox paralog group 1 (PG1) heterodimers (Figure 5C; Figure S3). Competition assays with cold wild-type or point-mutated oligonucleotides, or with specific antibodies against Pbx or Hox PG1 proteins, further demonstrated PH site specificity and Pbx-Hox requirement for in vitro binding (Figure S3).

Pbx-Hox binding and transcriptional activity can be enhanced by Prep or Meis proteins, which facilitate the formation of transcriptionally active ternary complexes on PH sites (Ferretti et al., 2000; Jacobs et al., 1999). Thus, we assessed the ability of Hox-Pbx-Meis/Prep ternary complexes to bind the *Raldh2* PH sites in vitro. Specific Hoxa1-Pbx1a(b)-Meis2 and Hoxb1-Pbx1a(b)-Meis2 ternary complexes formed only on the PH element within the E3 region (E3PH), though not on those in E1, E2, and E4 (Figure 5C; Figure S3). The establishment of a ternary, as opposed to multimeric, complex on the E3PH site was confirmed by using a combination of Pbx1a and Pbx1b, together with Hoxa1 (or Hoxb1) and Meis2 (Figure S3). Mutations in Hoxa1 DNA-binding or hexapeptide (Pbx-binding) domains disrupted the formation of the ternary complex, showing that complex assembly requires Hoxa1 binding to both Pbx1 and E3PH (Figure S3). Lastly, binding of nuclear extracts from posterior part of E8.5 embryos (inset, red box) to the E3PH oligonucleotide also resulted in the formation of a specific ternary complex containing Pbx, Meis2, and Hoxa1, that was super-shifted by specific antibody competition (Figure 5D and data not shown).

To assess whether Hoxa1, Pbx1, and their Meis2 cofactor could bind the E3PH site in vivo, we carried out chromatin immunoprecipitation (ChIP) on E8.5 mouse embryos. We compared the posterior "body" that includes the mesodermal *Raldh2*$^+$ domains (inset, Figure 5F) to the anterior "head" (inset, Figure 5E) that is *Raldh2*$^-$ at this stage. qPCR from "body" immunoprecipitated chromatin using anti-Pbx (pan-Pbx) and anti-Meis2 antibodies, demonstrated Pbx1 and Meis2 enrichment at *Raldh2* E3 and E4, though not E2 and E1, PH site-containing elements, respectively (Figure 5F and data not shown). ChIP with anti-Hoxa1 antibody demonstrated Hoxa1 enrichment only at *Raldh2* E3 (Figure 5F), supporting the in vitro data showing the formation of a ternary complex only on E3PH (Figure 4C; Figure S3; data not shown). In summary, despite the presence of multiple potential regulatory elements containing PH-binding sites at the *Raldh2* locus, the ChIP data in E8.5 embryos revealed in vivo selectivity for binding of all three Hoxa1, Pbx1/2, and Meis2 proteins only to E3 (Figure 5).

The E3 Pbx-Hox Element Is Necessary for In Vivo Transcriptional Regulation of *Raldh2*

The ChIP data revealed that in the "head" part of the embryo, Hoxa1, Pbx1/2, or Meis2 were not bound to any of the E1-E4 regions (Figure 5E; see below). This suggested that the E3 element accessibility may be related to the transcriptionally active or inactive state of *Raldh2*, which in turn may be determined by distinct epigenetic configurations of the chromatin in *Raldh2*$^+$ versus *Raldh2*$^-$ tissues at this specific locus.

We therefore analyzed the ChIP patterns of trimethylated histone H3 lysine 4 (H3K4me3) and trimethylated histone H3 lysine 27 (H3K27me3) at the *Raldh2* locus from E8.5 "body" and "head" embryonic regions, respectively (Figures 5G and 5H). H3K4me3 is catalyzed by trithorax-group (trxG) proteins and primarily associated with transcriptionally active chromatin regions at the start of transcription, whereas H3K27me3 is mainly catalyzed by Polycomb-group (PcG) proteins and associated with stable transcriptional repression (Ruthenburg et al., 2007). In ChIP qPCR assays from embryonic "bodies," we found a selective enrichment of H3K4me3 at the E3 element (Figure 5H and Figure 6E). Indeed, E3 is located proximal to (within about 1 kb of) the *Raldh2* transcription start site. In contrast, in chromatin obtained from "heads" the E3 element, though not E1, E2, or E4, was significantly enriched with H3K27me3 (Figure 5G, Figure 6E, and data not shown). This suggested that in tissues not actively expressing *Raldh2*, its transcription may be silenced by PcG activity. Accordingly, we found a strong enrichment of Suz12, a core PRC2 member (Pasini et al., 2004), at E3, though not at E1, E2, or E4 (Figure 5I and data not shown), correlating with the distribution of the H3K27me3 mark (compare Figures 5G and 5I). Moreover, Suz12 was not significantly enriched at E1–E4 in chromatin from *Raldh2*$^+$ "bodies" (Figure 5J), thus correlating with the transcriptionally active status of *Raldh2*.

Figure 5. In Vivo Direct Regulation of *Raldh2* by Hoxa1-Pbx1/2-Meis2

(A) Mouse *Raldh2* locus (chr9:71,055,462-71,092,461, UCSC Mouse Browser). Conservation plot across vertebrate species (green peaks); blue peaks indicate highest conservation. Blue boxes (E1, E2, E3, and E4) highlight conserved regions containing Pbx-Hox (PH) binding sites.

(B) Sequence comparison of PH elements from known targets and *Raldh2* E1PH, E2PH, E3PH, E4PH1, and E4PH2; blue letters indicate divergency from PH consensus, and variable bases are in green.

(C) In vitro binding EMSA with translated Pbx1a, Pbx1b, Pbx2, Meis2, Hoxa1, and Hoxb1 on the E3PH-containing oligonucleotide (red sequence).

(D) A ternary complex (TC) comigrating band binds to E3PH probe in nuclear extracts from E8.5 embryo posterior part (red box inset, E8.5 NE). Binding specificity is assessed using specific antibodies. Hoxa1(b1)/Pbx1a/Meis2 in vitro-translated proteins were used as molecular weight control of TC.

(E–J) In vivo chromatin immunoprecipitation (ChIP) from "head" (red box inset, E, G, and I) and "body" (red box inset, F, H, and J) of E8.5 embryos. Specific antibodies against Pbx, Meis2 (E and F), Hoxa1 (F), trimethylated histone H3 lysine 4 (H3K4me3), trimethylated histone H3 lysine 27 (H3K27me3) (G and H), and Suz12 (I and J) were used. In all ChIP assays, specificity was tested by nonspecific primers outside the conserved regions (OUT, in (A). Rabbit IgG is a control for amplification specificity. Fold enrichment over IgG is plotted. Bars represent mean ± SEM; *$p < 0.01$, t test. See also Figure S3.

(K and L) *eGFP* expression from transgenic E8.5 embryos carrying a *Raldh2* BAC construct (not in scale) recapitulates endogenous *Raldh2* expression pattern (K). Mutation of E3PH (E3ΔPH) in the *Raldh2* BAC causes *eGFP* downregulation (L). DC, dimeric complex; Lys, reticulocyte lysate endogenous binding activity; SS, supershifted band. See also Figure S4.

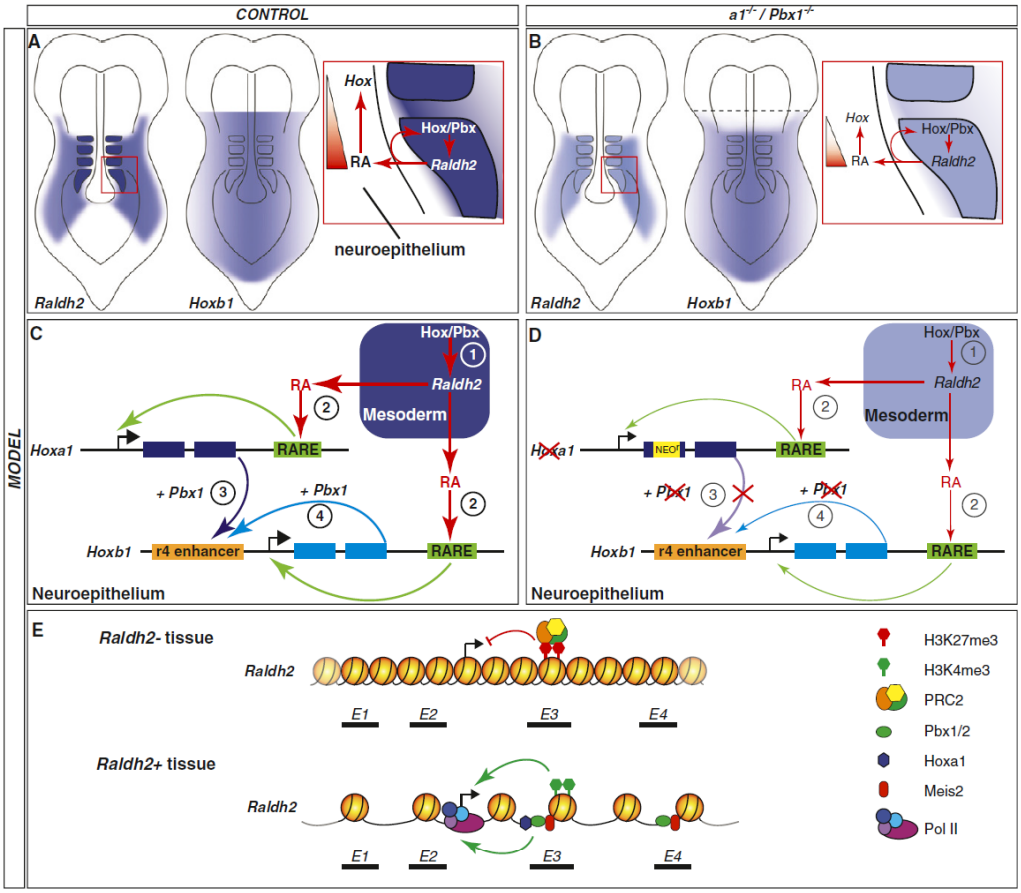

Figure 6. Transcriptional Feed-Forward Model of Pbx-Hox-Mediated *Raldh2* Mesodermal Regulation and Induction of *Hox* Expression in Early Hindbrain Neuroepithelium

(A) Pbx and Hox factors regulate *Raldh2* expression levels and maintenance in presomitic, somitic, and lateral plate mesoderm (red boxed inset) in early stage embryo. The resulting graded RA activity (red triangle) diffuses to neuroepithelium, drives *Hox* paralog group 1 activation, and sets their rostral boundary in the hindbrain. Retinoid signaling feedback on *Hox/Pbx* expression maintenance in mesoderm may also occur (e.g., Lohnes et al., 1994) (red curved arrow).

(B) In *Hoxa1/Pbx1* null embryos, *Raldh2* expression is lower in presomitic and somitic mesoderm (light blue) and absent from anterior lateral plate mesoderm. Decreased expression results in diminished RA activity (small triangle, inset) and posterior shift of *Hoxb1* anterior boundary in the neuroepithelium (dashed line indicates normal position, compare with A).

(C and D) RA- and Hox/Pbx-dependent regulation of *Hoxa1* and *Hoxb1* in presumptive hindbrain neuroepithelium and r4. Panels integrate known pathways of transcriptional regulation (e.g., Dupe et al., 1997; Popperl et al., 1995; Studer et al., 1998) with current findings. In (C), Pbx1/Hoxa1 mesodermal activity controls *Raldh2* expression levels and in turn the production of RA diffusing to the adjacent neuroepithelium (1). RA directly activates *Hoxa1* and *Hoxb1* in neuroepithelium up to r4 through retinoic acid response elements (RAREs) (2). In turn, Hoxa1/Pbx1- and Hoxb1/Pbx1-mediated cross- and auto-regulatory transcriptional mechanisms, respectively, maintain *Hoxb1* r4 expression levels (3 and 4). In (D), *Hoxa1/Pbx1* loss in mesoderm results in lower *Raldh2* expression levels, consequent lower RA activity (1), and reduced *Hoxb1* activation in neuroepithelium (2). Lack of Hoxa1 and Pbx1 in mutant neuroepithelium further impairs the establishment of normal levels of *Hoxb1* expression (3 and 4).

(E) In *Raldh2*-negative (*Raldh2*$^{-}$) tissue in the early embryo, the H3K27me3 mark on the *Raldh2* E3 enhancer and Suz12 binding reveal PcG-mediated repression (PRC2 presence at E3, but not at E1, E2, or E4, is depicted). In *Raldh2*-positive (*Raldh2*$^{+}$) tissue, the repressive mark at E3 is replaced by H3K4me3, associated with an active chromatin state. The locus is accessible for direct Pbx1/2, Hoxa1 and Meis2 binding and transcriptionally active. The binding of E4 by Pbx-Meis, though not Hoxa1, suggests the involvement of additional transcription factors, including Hox members from other paralog groups, in *Raldh2* regulation.

Developmental Cell
Hox-Pbx-Dependent Raldh2 Regulation

Next, we tested the potential of E3 to drive transcriptional activity in vivo and its dependence on the PH site. Coelectroporation in chick embryos of *Hoxa1* with *lacZ* constructs carrying either wild-type E3 (*E3::lacZ*) or E3 with a mutated PH site (*E3ΔPH::lacZ*) demonstrated Hoxa1-mediated E3 trans-activation in an in vivo heterologous system and the requirement for PH site integrity for such trans-activation (Figure S4). To investigate the spatial pattern driven by the *Raldh2* E3 enhancer in the mouse, we generated mouse transgenic embryos carrying the *E3::lacZ* construct (Figure S4). In E8.5 embryos, the reporter expression driven by the E3 element was spatially restricted to the posterior part of the embryo, similar to endogenous *Raldh2*. Reporter expression was detected in the PSM and strongly throughout the dorsoventral extent of the neural tube, up to a rostral border in the posterior hindbrain (Figure S4). Even though ectopic, as compared to the endogenous *Raldh2* expression pattern, the observed spatial domain of enhancer activity indicated that, in isolation from its surrounding genomic sequences, E3 behaves as a "*Hox*-regulated" enhancer driving spatially restricted AP expression. In transgenic mouse embryos carrying the PH mutated construct (*E3ΔPH::lacZ*), reporter expression in PSM and neural tube was almost abolished (Figure S4), thus demonstrating that E3 in vivo transcriptional activity is strictly dependent on PH site integrity.

To assess the role of the E3PH element within the intact *Raldh2* promoter, we made suitable constructs for transgenic mouse analysis by BAC (bacterial artificial chromosome) recombineering (Liu et al., 2003). We first generated a construct that carried the *eGFP* reporter in-frame to the *Raldh2* ATG translation start codon (BAC *Raldh2::eGFP*), containing a 160 kb DNA insert spanning the entire murine *Raldh2* locus, thus likely containing all the regulatory elements to achieve normal in vivo *Raldh2* transcriptional regulation. Indeed, when tested in transient transgenic assays in E8.5 (5–6 somite stage) mouse embryos, the BAC *Raldh2::eGFP* displayed an *eGFP* expression pattern faithfully reproducing endogenous *Raldh2* expression (n = 5/5; Figure 5K). We then mutated the E3PH element and generated the BAC *Raldh2-E3ΔPH::eGFP* construct. In E8.5 transgenic embryos, the E3ΔPH mutation resulted in severe *eGFP* downregulation (n = 5/7; Figure 5L; *eGFP* decrease, albeit less severe, was also observed in the two remaining embryos; data not shown).

In summary, these data demonstrate a fundamental role of the E3PH element in the context of the entire *Raldh2* promoter in maintaining normal *Raldh2* expression levels in the early embryo.

DISCUSSION

We demonstrate that Hoxa1 and Pbx1 synergistically regulate the levels of mesodermal *Raldh2* expression in the early embryo and, in turn, control endogenous RA levels available for normal hindbrain segmentation. This conclusion is supported by: (1) the decrease of *Raldh2* expression and endogenous RA activity observed in *Pbx1/2* and *Hoxa1/Pbx1* null embryos (Figure 2; model in Figures 6A and 6B); (2) the decrease of *Xraldh2* expression in frog embryos with mesoderm-specific knockdowns of *Xpbx1b* and *Xhoxa1/Xpbx1b* (Figure 4); (3) the induction of abnormal segmentation in frog embryo hindbrains following mesoderm-specific knockdown of *Xpbx1b* and *Xhoxa1/Xpbx1b*, independently of their roles in the neuroepithelium (Figure 4); (4) the posterior shift of endogenous RA activity in the hindbrain of *Hoxa1/Pbx1* null embryos (Figure 2; model in Figures 6A and 6B); (5) the partial rescue of *Hoxa1/Pbx1* null hindbrain phenotype by exogenous RA treatment (Figure 3); (6) the in vivo binding of the E3 *Raldh2* enhancer by Hoxa1/Pbx1(2)/Meis2 in E8.5 embryos (Figure 5); and (7) the demonstration of the E3PH element requirement for normal expression of *Raldh2* in vivo (Figure 5). Thus, *Hoxa1* and *Pbx1* are necessary in the mesoderm to generate sufficient levels of retinoids that, in turn, induce positionally appropriate gene activation in the early hindbrain neuroepithelium to begin normal segmentation.

Collinear *Hox* patterns are already established in mesoderm precursors before their ingression through the primitive streak (Deschamps and van Nes, 2005; Iimura and Pourquie, 2006), thus before *Raldh2* activation and independently of RA activity (Lloret-Vilaspasa et al., 2010). This early phase of *Hox* expression in turn controls ordered paraxial mesoderm ingression and its positioning along the AP axis (Iimura and Pourquie, 2006). Blocking RA activity only impairs the neuropithelial, though not the early mesodermal, *Hox* expression domains (Lloret-Vilaspasa et al., 2010). Feedback retinoid regulation of *Hox* expression maintenance in vertebral somite precursors may in turn take place at later stages (e.g., Lohnes et al., 1994). RA produced in the paraxial mesoderm is thought to act as a diffusible morphogen that patterns the hindbrain in a concentration-dependent manner by inducing spatially restricted *Hox* expression patterns in the overlying neuroepithelium. Based on our results, such "homeogenetic induction" (De Robertis et al., 1989) of *Hox* expression across germ layers may indeed be controlled by the *Hox* genes themselves through a feed-forward transcriptional mechanism that induces their own expression and sets their rostral boundary in the hindbrain neuroepithelium, through the direct control of mesodermal *Raldh2* expression and production of RA diffusing to the neuroectoderm (Figures 6A–6D). In this respect, *Hox* expression boundaries in mesoderm and hindbrain may not need to be in register, because of local control of retinoid levels and RA responsiveness along the hindbrain AP axis by degradation enzymes (e.g., Sirbu et al., 2005; Hernandez et al., 2007). Our current findings provide a conceptual framework to support such a model and reveal its potential importance for proper hindbrain segmentation.

Using a mesoderm-specific MO-mediated approach in *Xenopus* embryos, we showed that the functional knockdown of *Xhoxa1/Xpbx1b* in mesoderm results in decrease of *Xraldh2* expression. In turn, this correlates with a range of hindbrain segmentation defects, including posterior shift of rhombomere identities, a feature of partial RA deficiency. Notably, the hindbrain abnormalities observed in mesoderm MO-injected frog embryos phenocopied the hindbrain defects of *Hoxa1/Pbx1* null mutant mice, indicating that at least part of the mouse mutant hindbrain phenotype can be accounted for by the lack of *Hoxa1/Pbx1* in the mesoderm and its early effect on *Raldh2* downregulation. Previous work has shown that blocking *lzr(pbx4)/pbx2* or *pbx4/hox1* function in the zebrafish embryo results in extensive posterior expansion of r1 at the expense of more caudal rhombomere identities (Waskiewicz et al., 2002). It is tempting to speculate that such an extreme phenotype may also be partly contributed by a partial RA deficiency induced

Developmental Cell
Hox-Pbx-Dependent Raldh2 Regulation

by the lack of these factors in the mesoderm. Finally, although our results do not claim to rule out additional Hox-independent roles for Pbx factors, the synergistic effects of *Xhoxa1*/*Xpbx1b* knockdowns in the frog mesoderm, as well as the molecular and in vivo analyses of the mouse *Raldh2* locus demonstrate the functional impact of Hox-Pbx-mediated *Raldh2* regulation.

The above observations provide strong support for evolutionary conservation of this Hox-Pbx-dependent retinoid regulatory pathway. Moreover, by identifying Hox-Pbx factors as regulators of RA levels in the early vertebrate embryo, together with their known role as RA targets, these results help to better rationalize how the retinoid signaling pathway could have been evolutionary co-opted for vertebrate AP patterning and integrated into the *Hox* positional system. More broadly, given the pleiotropic and instructive functions of RA in vertebrate development (Duester, 2008; Niederreither and Dolle, 2008), including axial patterning, regional segmentation of the nervous system, regulation of early organogenesis, and differentiation of stem and progenitor cells, our results establish a mechanism for the transcriptional control of the synthesis of appropriate RA activity in the embryo.

EXPERIMENTAL PROCEDURES

Retinoic Acid Administration

Retinoic acid administration was performed as described elsewhere (Pasqualetti et al., 2001). Mice were mated for 2 hr. A vaginal plug at the end of the mating was scored as E0.0 +1 hr. Pregnant mice were treated at the following gestational stages: E8.0 +2 hr (*Hoxa1*/*Pbx1*) and E8.5 (*Pbx1*/*Pbx2*). Pregnant females were administered a final RA concentration of 5 mg/kg (*Hoxa1*/*Pbx1*) or 10 mg/kg (*Pbx1*/*Pbx2*) body weight by oral gavage.

In Situ Hybridization

Whole-mount mouse in situ hybridization (ISH) was performed as described elsewhere (Studer et al., 1998). Each probe was hybridized on at least three single or compound mutant embryos. As for frog ISH, Digoxigenin (DIG)-labeled antisense RNA probes were generated for *Xraldh2* and *Xkrox20*. Whole-mount ISH was performed as described elsewhere (Pasqualetti et al., 2000). After color development, embryos were post-fixed and bleached under fluorescent light to remove the pigment. For histological examination, whole-mount ISH processed embryos were embedded in a gelatin-albumin solution and then sectioned at 50 μm using a Leica VT1000S vibratome.

Mesoderm-Specific Morpholino Injections in *Xenopus* Embryos

Xenopus laevis embryos were obtained by hormone-induced laying and were staged according to Nieuwkoop and Faber (1956). Capped mRNAs were synthesized in vitro from template cDNAs: *Nuclear-β-galactosidase* (*n-β-gal*) and *Red Fluorescent Protein* (*RFP*, NotI/Sp6), using the SP6 mMESSAGE mMACHINE Kit (Ambion, catalog number AM1340). A morpholino antisense oligonucleotide (Gene Tools, LLC) was designed against the *Xpbx1b* mRNA (Gene Bank a.n. AF480430.1) complementary to −8 to +17 nucleotides: *Xpbx1b*-MO 5′- CTGGGCTGATCGTCCATTTCCAAGA-3′ (the ATG complementary sequence is underlined). A 5-base-mismatch *control*-MO was designed from the *Xpbx1b*-MO sequence (5′ CTGGcCTcATCGTCgATTTCg AAcA 3′, small caps indicate mismatched nucleotides) (Gene Tools, LLC). The *control* MO did not induce molecular alterations or patterning defects in injected embryos (n = 78; data not shown). The MO against the *Xhoxa1* mRNA was described elsewhere (McNulty et al., 2005). MOs (*Xpbx1b* 20ng/embryo, *Xhoxa1* 10 ng/embryo, *control*-MO 20-30 ng/embryo) or capped mRNAs (*RFP* and/or *n-β-gal*, 300 pg/embryo each) were injected into the marginal zone of V2.2 left blastomere of 16-cell stage embryos in 3% Ficoll-400 (Fluka, catalog number 46327) in 0.1× MMR. After injection, embryos were transferred in 0.1× MMR and incubated at 18°C until the desired developmental stage. The injected side was visualized by the RFP presence.

β-Galactosidase Staining

Mice carrying the *RARE::lacZ* reporter transgene (Rossant et al., 1991) (Jackson Laboratory) mated into the *Pbx1/2* or *Hoxa1*/*Pbx1* null backgrounds were used for endogenous retinoid detection by X-gal staining as described elsewhere (Rossant et al., 1991). *Xenopus* embryos injected with *Nuclear-β-galactosidase* (*n-β-gal*) *capped mRNA* were fixed and stained with salmon-gal substrate (BIOSYNTH AG, catalog number B-7200) before further processing for whole-mount ISH.

Constructs

A 514 bp fragment containing the E3 Pbx-Hox site was amplified by PCR from mouse genomic DNA. The amplicon was cloned into *pCRII-TOPO* plasmid (Invitrogen), generating the *pCR-E3* construct. A *SpeI-NotI* fragment of *pCR-E3* was subcloned into the *pBGZ40* plasmid (Itasaki et al., 1999) generating the *E3::lacZ* construct. *pCR-E3* was also used as template to obtain the pCR-*E3ΔPH* construct by PCR-mediated site-directed mutagenesis, replacing the Pbx-Hox binding site with a *SacII* site for diagnostic restriction. The *SpeI-NotI* fragment of pCR-*E3ΔPH* was subcloned into *pBGZ40* plasmid (*E3ΔPH::lacZ*).

In Ovo Electroporation

In ovo electroporation was performed as described elsewhere (Itasaki et al., 1999). Construct concentrations were as follows: 1.0 mg/ml for *E3::lacZ* reporter construct, *E3ΔPH::lacZ* and *pCMV::Hoxa1* expression vector, and 0.2 mg/ml *pCMV::eGFP* coinjected as positive control of electroporated cells. Embryos were harvested 24 hr after electroporation and processed for β-galactosidase staining.

Transient Mouse Transgenic Analysis

NotI-XhoI fragments containing either the *E3::lacZ* or its mutated version *E3ΔPH::lacZ* constructs were used for pronuclear injection. Embryos were harvested at E8.5 and X-gal staining was used for β-galactosidase activity detection. For coronal vibratome sectioning, stained embryos were fixed in 4% PFA overnight, rinsed in PBT, embedded in 3% agarose/PBS, and then cut. Nuclear fast red solution (Sigma) was used as counterstaining.

Generation of BAC Transgenic Mouse Embryos

The BAC clone RP24-159G6 (BACPAC Resources Center at Children's Hospital Oakland Research Institute, Oakland, CA), spanning from 23 kb upstream to 47 kb downstream the *Raldh2* locus, was used as template for bacterial recombineering (Lee et al., 2001). The plasmid pN21-eGFP-SV40 polyA was used to amplify an eGFP-frt-Kanamycin-frt cassette by using 70-mer primers containing 50 nt of homology surrounding the ATG codon of the *Raldh2* coding sequence. For the mutated construct, the plasmid pL452 (Liu et al., 2003) was used as template to amplify a LoxP-Kanamycin-LoxP cassette by using 70-mer primers containing 50 nt of homology surrounding the E3PH element. Following homologous recombination and resistance cassette removal, the E3PH element was replaced by a single LoxP site. Correct recombination and removal of resistance genes in the *Raldh2::eGFP* and *Raldh2-E3ΔPH::eGFP* BACs were tested by PCR, restriction enzyme digestion, and sequencing. Before microinjection, the modified BACs were linearized by PI-SceI digestion.

Chromatin Immunoprecipitation Assay

About 1600 E8.5 mouse embryos were manually dissected in posterior "body" and anterior "head" regions. Chromatin was prepared, and ChIP was performed as described elsewhere (Frank et al., 2001). Samples were immunoprecipitated overnight at 4°C with the following antibodies: Pbx1/2/3 (C20 sc888X, Santa Cruz), Meis2 (N17 sc10600, Santa Cruz), Hoxa1 (N20 sc17146X, Santa Cruz); Suz12 (ab12073, Abcam), H3K27me3 (9756, Cell Signaling Technology), H3K4me3 (9751, Cell Signaling Technology), and Rabbit IgG (Sigma). Conserved *Raldh2* fragment E1 to E4 containing the Hox-Pbx binding sites and control regions outside of the conserved regions (OUT) were amplified by real-time qPCR using specific primer pairs.

Electrophoretic Mobility Shift Assays

EMSAs were performed as described elsewhere (Ferretti et al., 2000) using nuclear extracts purified from E8.5 "body" embryonic region or in vitro

Developmental Cell
Hox-Pbx-Dependent Raldh2 Regulation

translated proteins. Labeled oligonucleotide probes contain the putative Hox-Pbx binding sites and their mutated forms within the distinct *Raldh2* conserved regions (E1 to E4). The antibodies used to assess DNA binding specificity are the same used for ChIP assay.

Sequence Conservation Analysis

Comparisons of mouse *Raldh2* genomic sequences to other vertebrates were performed using the UCSC algorithm (http://genome.ucsc.edu/).

Statistical Methods

Results are expressed as mean ± SEM from triplicate qPCRs. Student's t test was used when appropriate.

SUPPLEMENTAL INFORMATION

Supplemental Information includes four figures and Supplemental Experimental Procedures and can be found with this article online at doi:10.1016/j.devcel.2011.03.011.

ACKNOWLEDGMENTS

We thank L. Parra and C. Kratochwil for critical reading of the manuscript, C. Laumonnerie and M. Poulet for imaging and technical support, and M. Mallo for discussion. We also wish to thank P. Chambon, P. Dollé, R. Krumlauf, R. Rezsohazy, M. Cleary, P. McCaffery, T. Pieler, and N. Copeland for mouse lines, antibodies, probes, and reagents. E.F. was the recipient of Marie Curie Outgoing International Fellowship (MOIF-CT-2005-022003). X.L. was the recipient of a fellowship from the Fondation pour la Recherche Medicale. L.S. is an Irma T. Hirschl Scholar and recipient of grants from The Alice Bohmfalk Trust and The Frueauff Foundation, National Institutes of Health (grants 2R01HD043997-06, 1R01HD061403-01, and 3R21DE018031-02S1), and March of Dimes and Birth Defects Foundation (#6-FY03-071). Work in F.M.R.'s laboratory is supported by the Swiss National Science Foundation (CRSI33_127440), the Agence Nationale pour la Recherche (ANR07-BLAN0038), ARSEP, and the Novartis Research Foundation.

Received: September 21, 2010
Revised: February 7, 2011
Accepted: March 16, 2011
Published: April 18, 2011

REFERENCES

Barrow, J.R., Stadler, H.S., and Capecchi, M.R. (2000). Roles of Hoxa1 and Hoxa2 in patterning the early hindbrain of the mouse. Development *127*, 933–944.

Capellini, T.D., Di Giacomo, G., Salsi, V., Brendolan, A., Ferretti, E., Srivastava, D., Zappavigna, V., and Selleri, L. (2006). Pbx1/Pbx2 requirement for distal limb patterning is mediated by the hierarchical control of Hox gene spatial distribution and Shh expression. Development *133*, 2263–2273.

Capellini, T.D., Zewdu, R., Di Giacomo, G., Asciutti, S., Kugler, J.E., Di Gregorio, A., and Selleri, L. (2008). Pbx1/Pbx2 govern axial skeletal development by controlling Polycomb and Hox in mesoderm and Pax1/Pax9 in sclerotome. Dev. Biol. *321*, 500–514.

Carpenter, E.M., Goddard, J.M., Chisaka, O., Manley, N.R., and Capecchi, M.R. (1993). Loss of Hox-A1 (Hox-1.6) function results in the reorganization of the murine hindbrain. Development *118*, 1063–1075.

Chen, Y., Pollet, N., Niehrs, C., and Pieler, T. (2001). Increased XRALDH2 activity has a posteriorizing effect on the central nervous system of Xenopus embryos. Mech. Dev. *101*, 91–103.

De Robertis, E.M., Oliver, G., and Wright, C.V. (1989). Determination of axial polarity in the vertebrate embryo: homeodomain proteins and homeogenetic induction. Cell *57*, 189–191.

Deschamps, J., and van Nes, J. (2005). Developmental regulation of the Hox genes during axial morphogenesis in the mouse. Development *132*, 2931–2942.

Di Rocco, G., Gavalas, A., Popperl, H., Krumlauf, R., Mavilio, F., and Zappavigna, V. (2001). The recruitment of SOX/OCT complexes and the differential activity of HOXA1 and HOXB1 modulate the Hoxb1 auto-regulatory enhancer function. J. Biol. Chem. *276*, 20506–20515.

Duester, G. (2008). Retinoic acid synthesis and signaling during early organogenesis. Cell *134*, 921–931.

Dupe, V., and Lumsden, A. (2001). Hindbrain patterning involves graded responses to retinoic acid signalling. Development *128*, 2199–2208.

Dupe, V., Davenne, M., Brocard, J., Dolle, P., Mark, M., Dierich, A., Chambon, P., and Rijli, F.M. (1997). In vivo functional analysis of the Hoxa-1 3′ retinoic acid response element (3′RARE). Development *124*, 399–410.

Ferretti, E., Marshall, H., Popperl, H., Maconochie, M., Krumlauf, R., and Blasi, F. (2000). Segmental expression of Hoxb2 in r4 requires two separate sites that integrate cooperative interactions between Prep1, Pbx and Hox proteins. Development *127*, 155–166.

Ferretti, E., Cambronero, F., Tumpel, S., Longobardi, E., Wiedemann, L.M., Blasi, F., and Krumlauf, R. (2005). Hoxb1 enhancer and control of rhombomere 4 expression: complex interplay between PREP1-PBX1-HOXB1 binding sites. Mol. Cell. Biol. *25*, 8541–8552.

Forman, B.M., and Evans, R.M. (1995). Nuclear hormone receptors activate direct, inverted, and everted repeats. Ann. N Y Acad. Sci. *761*, 29–37.

Frank, S.R., Schroeder, M., Fernandez, P., Taubert, S., and Amati, B. (2001). Binding of c-Myc to chromatin mediates mitogen-induced acetylation of histone H4 and gene activation. Genes Dev. *15*, 2069–2082.

Gavalas, A. (2002). ArRAnging the hindbrain. Trends Neurosci. *25*, 61–64.

Glover, J.C., Renaud, J.S., and Rijli, F.M. (2006). Retinoic acid and hindbrain patterning. J. Neurobiol. *66*, 705–725.

Hernandez, R.E., Putzke, A.P., Myers, J.P., Margaretha, L., and Moens, C.B. (2007). Cyp26 enzymes generate the retinoic acid response pattern necessary for hindbrain development. Development *134*, 177–187.

Hirose, G., and Jacobson, M. (1979). Clonal organization of the central nervous system of the frog. I. Clones stemming from individual blastomeres of the 16-cell and earlier stages. Dev. Biol. *71*, 191–202.

Iimura, T., and Pourquie, O. (2006). Collinear activation of Hoxb genes during gastrulation is linked to mesoderm cell ingression. Nature *442*, 568–571.

Itasaki, N., Bel-Vialar, S., and Krumlauf, R. (1999). 'Shocking' developments in chick embryology: electroporation and in ovo gene expression. Nat. Cell Biol. *1*, E203–E207.

Jacobs, Y., Schnabel, C.A., and Cleary, M.L. (1999). Trimeric association of Hox and TALE homeodomain proteins mediates Hoxb2 hindbrain enhancer activity. Mol. Cell. Biol. *19*, 5134–5142.

Kiecker, C., and Lumsden, A. (2005). Compartments and their boundaries in vertebrate brain development. Nat. Rev. Neurosci. *6*, 553–564.

Kuss, P., Villavicencio-Lorini, P., Witte, F., Klose, J., Albrecht, A.N., Seemann, P., Hecht, J., and Mundlos, S. (2009). Mutant Hoxd13 induces extra digits in a mouse model of synpolydactyly directly and by decreasing retinoic acid synthesis. J. Clin. Invest. *119*, 146–156.

Lee, E.C., Yu, D., Martinez de Velasco, J., Tessarollo, L., Swing, D.A., Court, D.L., Jenkins, N.A., and Copeland, N.G. (2001). A highly efficient Escherichia coli-based chromosome engineering system adapted for recombinogenic targeting and subcloning of BAC DNA. Genomics *73*, 56–65.

Liu, P., Jenkins, N.A., and Copeland, N.G. (2003). A highly efficient recombineering-based method for generating conditional knockout mutations. Genome Res. *13*, 476–484.

Lloret-Vilaspasa, F., Jansen, H.J., de Roos, K., Chandraratna, R.A., Zile, M.H., Stern, C.D., and Durston, A.J. (2010). Retinoid signalling is required for information transfer from mesoderm to neuroectoderm during gastrulation. Int. J. Dev. Biol. *54*, 599–608.

Lohnes, D., Kastner, P., Dierich, A., Mark, M., LeMeur, M., and Chambon, P. (1993). Function of retinoic acid receptor gamma in the mouse. Cell *73*, 643–658.

Lohnes, D., Mark, M., Mendelsohn, C., Dolle, P., Dierich, A., Gorry, P., Gansmuller, A., and Chambon, P. (1994). Function of the retinoic acid

receptors (RARs) during development (I). Craniofacial and skeletal abnormalities in RAR double mutants. Development *120*, 2723–2748.

Maden, M. (2007). Retinoic acid in the development, regeneration and maintenance of the nervous system. Nat. Rev. Neurosci. *8*, 755–765.

Maeda, R., Ishimura, A., Mood, K., Park, E.K., Buchberg, A.M., and Daar, I.O. (2002). Xpbx1b and Xmeis1b play a collaborative role in hindbrain and neural crest gene expression in Xenopus embryos. Proc. Natl. Acad. Sci. USA *99*, 5448–5453.

Makki, N., and Capecchi, M.R. (2010). Hoxa1 lineage tracing indicates a direct role for Hoxa1 in the development of the inner ear, the heart, and the third rhombomere. Dev. Biol. *341*, 499–509.

Mann, R.S., and Chan, S.K. (1996). Extra specificity from extradenticle: the partnership between HOX and PBX/EXD homeodomain proteins. Trends Genet. *12*, 258–262.

Mark, M., Lufkin, T., Vonesch, J.L., Ruberte, E., Olivo, J.C., Dolle, P., Gorry, P., Lumsden, A., and Chambon, P. (1993). Two rhombomeres are altered in Hoxa-1 mutant mice. Development *119*, 319–338.

Mark, M., Ghyselinck, N.B., and Chambon, P. (2009). Function of retinoic acid receptors during embryonic development. Nucl. Recept. Signal *7*, e002.

Marshall, H., Nonchev, S., Sham, M.H., Muchamore, I., Lumsden, A., and Krumlauf, R. (1992). Retinoic acid alters hindbrain Hox code and induces transformation of rhombomeres 2/3 into a 4/5 identity. Nature *360*, 737–741.

Marshall, H., Studer, M., Popperl, H., Aparicio, S., Kuroiwa, A., Brenner, S., and Krumlauf, R. (1994). A conserved retinoic acid response element required for early expression of the homeobox gene Hoxb-1. Nature *370*, 567–571.

McNulty, C.L., Peres, J.N., Bardine, N., van den Akker, W.M., and Durston, A.J. (2005). Knockdown of the complete Hox paralogous group 1 leads to dramatic hindbrain and neural crest defects. Development *132*, 2861–2871.

Moens, C.B., and Selleri, L. (2006). Hox cofactors in vertebrate development. Dev. Biol. *291*, 193–206.

Monica, K., Galili, N., Nourse, J., Saltman, D., and Cleary, M.L. (1991). PBX2 and PBX3, new homeobox genes with extensive homology to the human proto-oncogene PBX1. Mol. Cell. Biol. *11*, 6149–6157.

Moody, S.A. (1987). Fates of the blastomeres of the 16-cell stage Xenopus embryo. Dev. Biol. *119*, 560–578.

Moody, S.A., and Kline, M.J. (1990). Segregation of fate during cleavage of frog (Xenopus laevis) blastomeres. Anat. Embryol. (Berl.) *182*, 347–362.

Murphy, P., and Hill, R.E. (1991). Expression of the mouse labial-like homeobox-containing genes, Hox 2.9 and Hox 1.6, during segmentation of the hindbrain. Development *111*, 61–74.

Niederreither, K., and Dolle, P. (2008). Retinoic acid in development: towards an integrated view. Nat. Rev. Genet. *9*, 541–553.

Niederreither, K., Subbarayan, V., Dolle, P., and Chambon, P. (1999). Embryonic retinoic acid synthesis is essential for early mouse post-implantation development. Nat. Genet. *21*, 444–448.

Niederreither, K., Vermot, J., Schuhbaur, B., Chambon, P., and Dolle, P. (2000). Retinoic acid synthesis and hindbrain patterning in the mouse embryo. Development *127*, 75–85.

Nieuwkoop, P.D., and Faber, J. (1956). Normal Table of *Xenopus laevis* (Daudin), a Systematical and Chronological Survey of the Development from the Fertilized Egg till the End of Metamorphosis (Amsterdam: North-Holland).

Pasini, D., Bracken, A.P., Jensen, M.R., Lazzerini Denchi, E., and Helin, K. (2004). Suz12 is essential for mouse development and for EZH2 histone methyltransferase activity. EMBO J. *23*, 4061–4071.

Pasqualetti, M., Ori, M., Nardi, I., and Rijli, F.M. (2000). Ectopic Hoxa2 induction after neural crest migration results in homeosis of jaw elements in *Xenopus*. Development *127*, 5367–5378.

Pasqualetti, M., Neun, R., Davenne, M., and Rijli, F.M. (2001). Retinoic acid rescues inner ear defects in Hoxa1 deficient mice. Nat. Genet. *29*, 34–39.

Popperl, H., Bienz, M., Studer, M., Chan, S.K., Aparicio, S., Brenner, S., Mann, R.S., and Krumlauf, R. (1995). Segmental expression of Hoxb-1 is controlled by a highly conserved autoregulatory loop dependent upon exd/pbx. Cell *81*, 1031–1042.

Popperl, H., Rikhof, H., Chang, H., Haffter, P., Kimmel, C.B., and Moens, C.B. (2000). lazarus is a novel pbx gene that globally mediates hox gene function in zebrafish. Mol. Cell *6*, 255–267.

Remacle, S., Abbas, L., De Backer, O., Pacico, N., Gavalas, A., Gofflot, F., Picard, J.J., and Rezsohazy, R. (2004). Loss of function but no gain of function caused by amino acid substitutions in the hexapeptide of Hoxa1 in vivo. Mol. Cell. Biol. *24*, 8567–8575.

Rossant, J., Zirngibl, R., Cado, D., Shago, M., and Giguere, V. (1991). Expression of a retinoic acid response element-hsplacZ transgene defines specific domains of transcriptional activity during mouse embryogenesis. Genes Dev. *5*, 1333–1344.

Ruthenburg, A.J., Li, H., Patel, D.J., and Allis, C.D. (2007). Multivalent engagement of chromatin modifications by linked binding modules. Nat. Rev. Mol. Cell Biol. *8*, 983–994.

Selleri, L., Depew, M.J., Jacobs, Y., Chanda, S.K., Tsang, K.Y., Cheah, K.S., Rubenstein, J.L., O'Gorman, S., and Cleary, M.L. (2001). Requirement for Pbx1 in skeletal patterning and programming chondrocyte proliferation and differentiation. Development *128*, 3543–3557.

Sirbu, I.O., Gresh, L., Barra, J., and Duester, G. (2005). Shifting boundaries of retinoic acid activity control hindbrain segmental gene expression. Development *132*, 2611–2622.

Soshnikova, N., and Duboule, D. (2009). Epigenetic temporal control of mouse Hox genes in vivo. Science *324*, 1320–1323.

Stankunas, K., Shang, C., Twu, K.Y., Kao, S.C., Jenkins, N.A., Copeland, N.G., Sanyal, M., Selleri, L., Cleary, M.L., and Chang, C.P. (2008). Pbx/Meis deficiencies demonstrate multigenetic origins of congenital heart disease. Circ. Res. *103*, 702–709.

Studer, M., Popperl, H., Marshall, H., Kuroiwa, A., and Krumlauf, R. (1994). Role of a conserved retinoic acid response element in rhombomere restriction of Hoxb-1. Science *265*, 1728–1732.

Studer, M., Gavalas, A., Marshall, H., Ariza-McNaughton, L., Rijli, F.M., Chambon, P., and Krumlauf, R. (1998). Genetic interactions between Hoxa1 and Hoxb1 reveal new roles in regulation of early hindbrain patterning. Development *125*, 1025–1036.

Waskiewicz, A.J., Rikhof, H.A., and Moens, C.B. (2002). Eliminating zebrafish pbx proteins reveals a hindbrain ground state. Dev. Cell *3*, 723–733.

White, R.J., Nie, Q., Lander, A.D., and Schilling, T.F. (2007). Complex regulation of cyp26a1 creates a robust retinoic acid gradient in the zebrafish embryo. PLoS Biol. *5*, e304.

Zhang, M., Kim, H.J., Marshall, H., Gendron-Maguire, M., Lucas, D.A., Baron, A., Gudas, L.J., Gridley, T., Krumlauf, R., and Grippo, J.F. (1994). Ectopic Hoxa-1 induces rhombomere transformation in mouse hindbrain. Development *120*, 2431–2442.

2.3. Supplemental Information

Developmental Cell, Volume *20*

Supplemental Information

Hox and Pbx Factors Control Retinoic Acid Synthesis during Hindbrain Segmentation

Antonio Vitobello, Elisabetta Ferretti, Xavier Lampe, Nathalie Vilain, Sebastien Ducret, Michela Ori, Jean-François Spetz, Licia Selleri, and Filippo M. Rijli

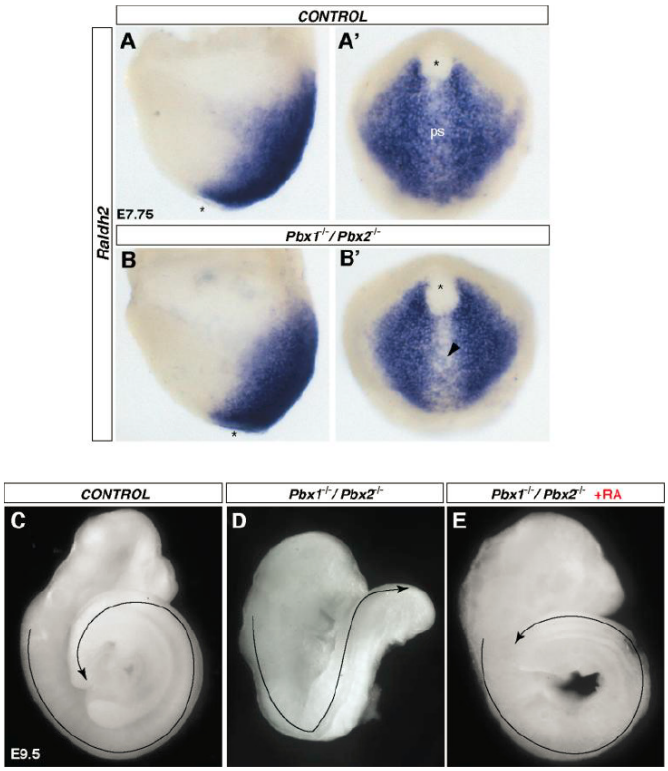

Figure S1. Early *Raldh2* Expression and Partial RA-Mediated Rescue in *Pbx1/Pbx2* Null Embryos, Related to Figure 1

(**A**-**B** and **A'**-**B'**) In control E7.5 embryos (**A**-**A'**), *Raldh2* is expressed in forming mesoderm (**A**, lateral view) and cells ingressing through the primitive streak (ps) (**A'**, ventral view) (asterisk, position of the node). In *Pbx1/Pbx2* null mutants (**B**-**B'**), lower *Raldh2* expression levels are detected in mesodermal cells that migrate through the primitive streak (**B'**, arrowhead).

(**C**-**E**) Partial morphological rescue by exogenous retinoic acid (RA) treatment in *Pbx1/Pbx2* null embryos. E9.5 control (**C**), *Pbx1/Pbx2* null (**D**), and RA-treated *Pbx1/Pbx2* null mutant (**E**) embryos. *Pbx1/Pbx2* null embryos show abnormal turning (**D**, curved arrow), that is rescued upon RA treatment and similar to control embryo (**E**, curved arrow, compare with **C**).

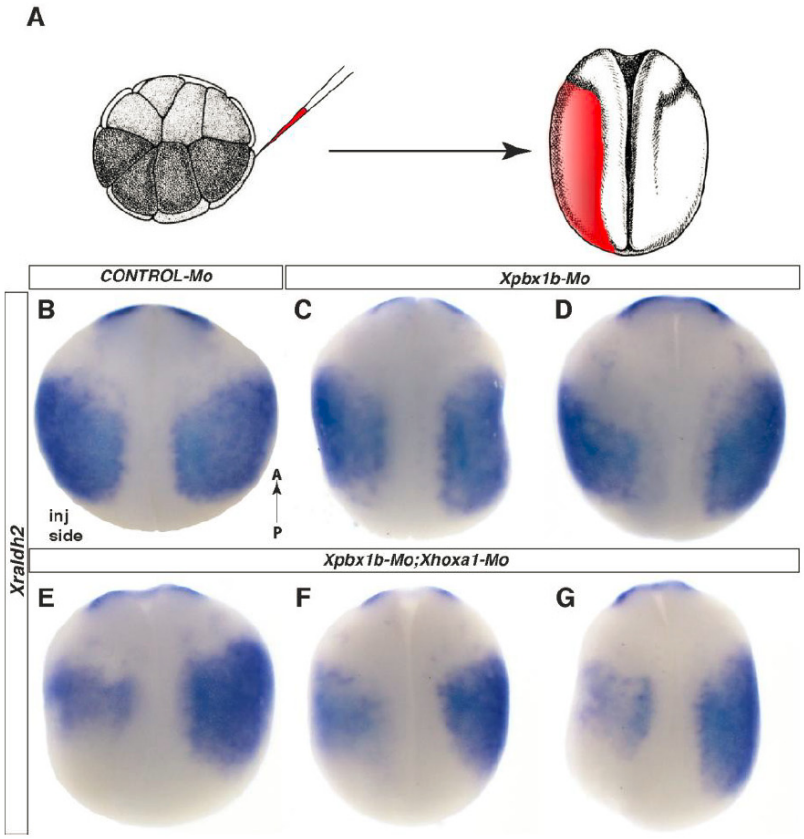

Figure S2. Mesoderm-Specific *Xpbx1* and *Xhoxa1* Knockdown Results in Downregulation of *Xraldh2* in Xenopus Embryos, Related to Figure 4

(A) Schematic illustration of the injection at the marginal zone of V2.2 *Xenopus* blastomere at the 16-cell stage. The fate of the progeny of the injected blastomere is depicted in a stage 17 neurula.

(B-G) *In situ* hybridization for *Xraldh2* in *control*-MO (**B**), *Xpbx1b*-MO (**C and D**), or *Xpbx1b*/*Xhoxa1*-MO (**E-G**) injected embryos. In (**B**), the injected side (left, inj side) is unaffected. In (**C and D**), the injected side show mild downregulation and narrowing of *Xraldh2* domain expression (compare with the controlateral uninjected side). In (**E-G**), different degrees of severe downregulation and narrowing of *Xraldh2* domain expression, demonstrating the synergistic role of *Xpbx1b* and *Xhoxa1* in Raldh2 mesodermal regulation.

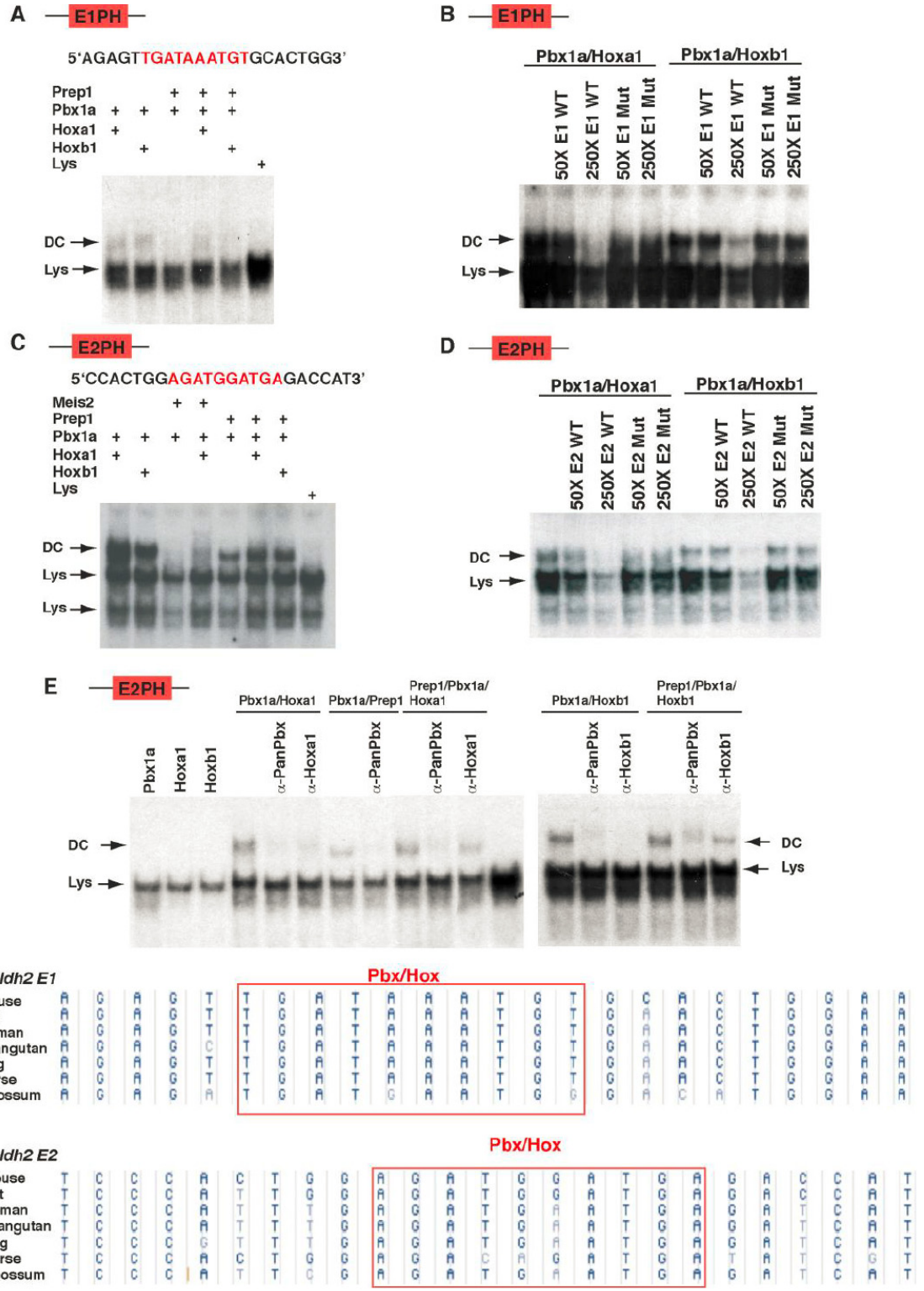
A
E1PH
5'AGAGTTGATAAATGTGCACTGG3'
Prep1
Pbx1a
Hoxa1
Hoxb1
Lys
DC
Lys
B
E1PH
Pbx1a/Hoxa1
Pbx1a/Hoxb1
50X E1 WT
250X E1 WT
50X E1 Mut
250X E1 Mut
DC
Lys
C
E2PH
5'CCACTGGAGATGGATGAGACCAT3'
Meis2
Prep1
Pbx1a
Hoxa1
Hoxb1
Lys
DC
Lys
Lys
D
E2PH
Pbx1a/Hoxa1
Pbx1a/Hoxb1
50X E2 WT
250X E2 WT
50X E2 Mut
250X E2 Mut
DC
Lys
E
E2PH
Pbx1a
Hoxa1
Hoxb1
Pbx1a/Hoxa1
α-PanPbx
α-Hoxa1
Pbx1a/Prep1
Prep1/Pbx1a/Hoxa1
Pbx1a/Hoxb1
α-Hoxb1
Prep1/Pbx1a/Hoxb1
DC
Lys
F
Raldh2 E1
Pbx/Hox
Mouse
Rat
Human
Orangutan
Dog
Horse
Opossum
G
Raldh2 E2
Pbx/Hox
Mouse
Rat
Human
Orangutan
Dog
Horse
Opossum

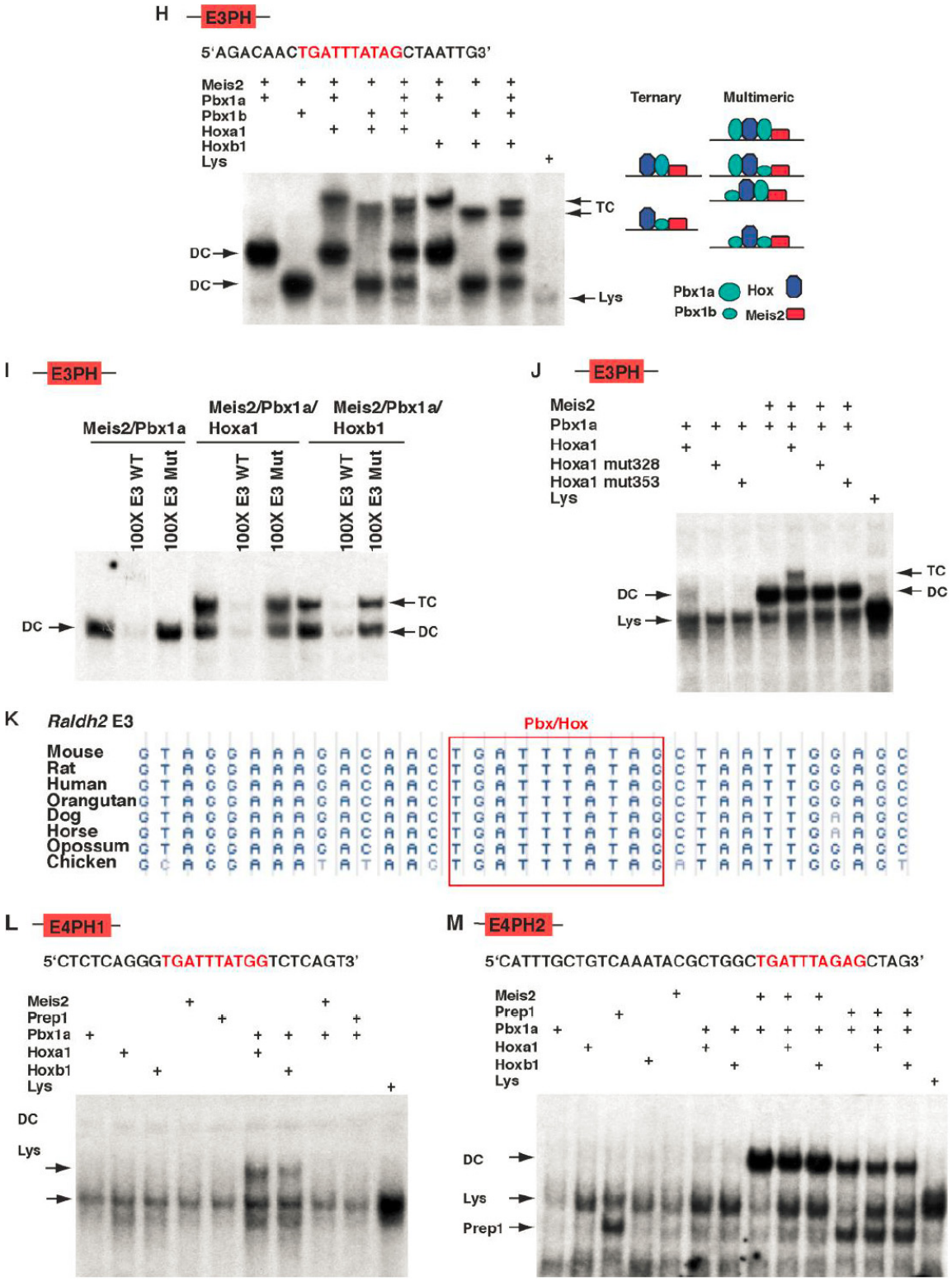
H
E3PH
5'AGACAACTGATTTATAGCTAATTG3'
Meis2
Pbx1a
Pbx1b
Hoxa1
Hoxb1
Lys
Ternary
Multimeric
TC
DC
DC
Lys
Pbx1a
Hox
Pbx1b
Meis2
I
E3PH
Meis2/Pbx1a
Meis2/Pbx1a/ Hoxa1
Meis2/Pbx1a/ Hoxb1
100X E3 WT
100X E3 Mut
100X E3 WT
100X E3 Mut
100X E3 WT
100X E3 Mut
DC
TC
DC
J
E3PH
Meis2
Pbx1a
Hoxa1
Hoxa1 mut328
Hoxa1 mut353
Lys
DC
Lys
TC
DC
K
Raldh2 E3
Pbx/Hox
Mouse
Rat
Human
Orangutan
Dog
Horse
Opossum
Chicken
L
E4PH1
5'CTCTCAGGGTGATTTATGGTCTCAGT3'
Meis2
Prep1
Pbx1a
Hoxa1
Hoxb1
Lys
DC
Lys
M
E4PH2
5'CATTTGCTGTCAAATACGCTGGCTGATTTAGAGCTAG3'
Meis2
Prep1
Pbx1a
Hoxa1
Hoxb1
Lys
DC
Lys
Prep1

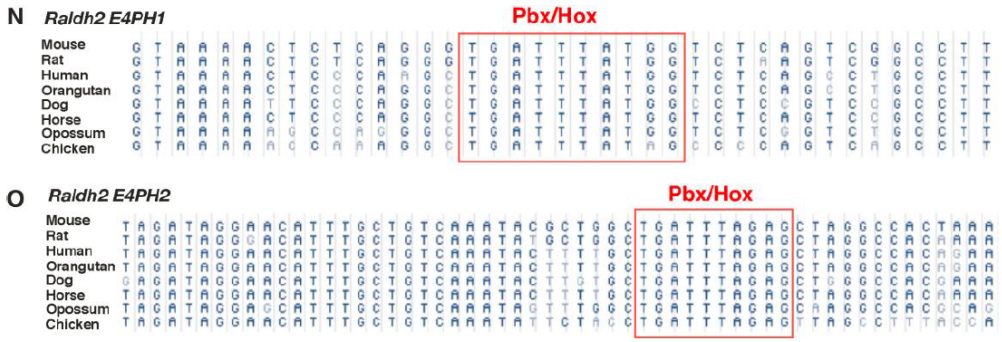

Figure S3. In Vitro Hox-Pbx-Meis Ternary Complex Formation on *Raldh2 E3PH* Element and of Hox-Pbx Dimeric Complex Formation on *Raldh2 E1PH*, *E2PH* and *E4PH* Elements, Related to Figure 5

(**A**) Hoxa1/Pbx1a and Hoxb1/Pbx1a in vitro translated proteins bind as dimeric complex (DC) to labeled *E1PH* oligonucleotide, though not Prep1/Pbx1a, with or without Hoxa1 or Hoxb1, in EMSA assay.

(**B**) Competition assay to assess binding specificity of Hoxa1/Pbx1a or Hoxb1/Pbx1a: 50 or 250 fold molar excess of unlabeled wild type (*E1*) or mutated (*E1 Mut*) was added to labeled *E1PH* and in vitro translated proteins.

(**C**) Hoxa1/Pbx1a, Hoxb1/Pbx1a, and Prep1/Pbx1a dimers bind to the labeled *E2PH* oligonucleotide, though not Meis2/Pbx1a.

(**D**) Competition assay to assess binding specificity of Hoxa1/Pbx1a or Hoxb1/Pbx1a: 50 or 250 fold molar excess of unlabeled wild type (*E2*) or mutated (*E2 Mut*) was added to labeled *E2PH* and in vitro translated proteins.

(**E**) Specific antibody competions show that the distinct dimeric complexes forming on *E2PH* oligonucleotide contain Prep1, Pbx1, Hoxa1, and Hoxb1.

(**F-G**) Sequence conservation of PH sites in *Raldh2 E1* and *E2* of different vertebrates.

(**H**) Hoxa1/Pbx1a(b)/Meis2 and Hoxb1/Pbx1a(b)/Meis2 in vitro translated proteins bind as ternary complex (TC) to labeled *E3PH* oligonucleotide in EMSA assay. Simultaneous use of Pbx1a and Pbx1b, two splice variants of Pbx1 with different molecular weight, allows to distinguish between ternary or multimeric complex (scheme of possible binding outcomes on the right). The protein composition of each binding reaction is shown on the top.

(**I**) Competition assay to assess binding specificity of Meis2/Pbx1a/Hoxa1 and Meis2/Pbx1a/Hoxb1: 100 fold molar excess of unlabeled wild type (*E3*) or mutated (*E3 Mut*) was added to labeled *E3PH* and in vitro translated proteins.

(J) Ternary complex formation requires wild type Hoxa1. TC does not form in the presence of two Hoxa1 mutant versions: mut328, mutated in the hexapeptide mediating Pbx binding, and mut353, mutated in the DNA-binding homeodomain.

(**K**) Sequence conservation in vertebrates of the *Raldh2 E3PH* element.

(L) Hoxa1/Pbx1a and Hoxb1/Pbx1a in vitro translated proteins bind as dimeric complex (DC) to labeled *E4PH1* oligonucleotide, though not Meis2/Pbx1a or Prep1/Pbx1a, in EMSA assay.

(**M**) Pbx1a/Meis2 and Pbx1a/Prep1 dimers bind labeled *E4PH2* oligonucleotide, though not Hoxa1/Pbx1a or Hoxb1/Pbx1a. Prep1 binding alone is also indicated (arrow).

(**N and O**) Sequence conservation in vertebrates of *Raldh2 E4PH1* (**N**) and *E4PH2* (**O**) elements, respectively. Lys, endogenous binding activity in reticulocyte lysate.

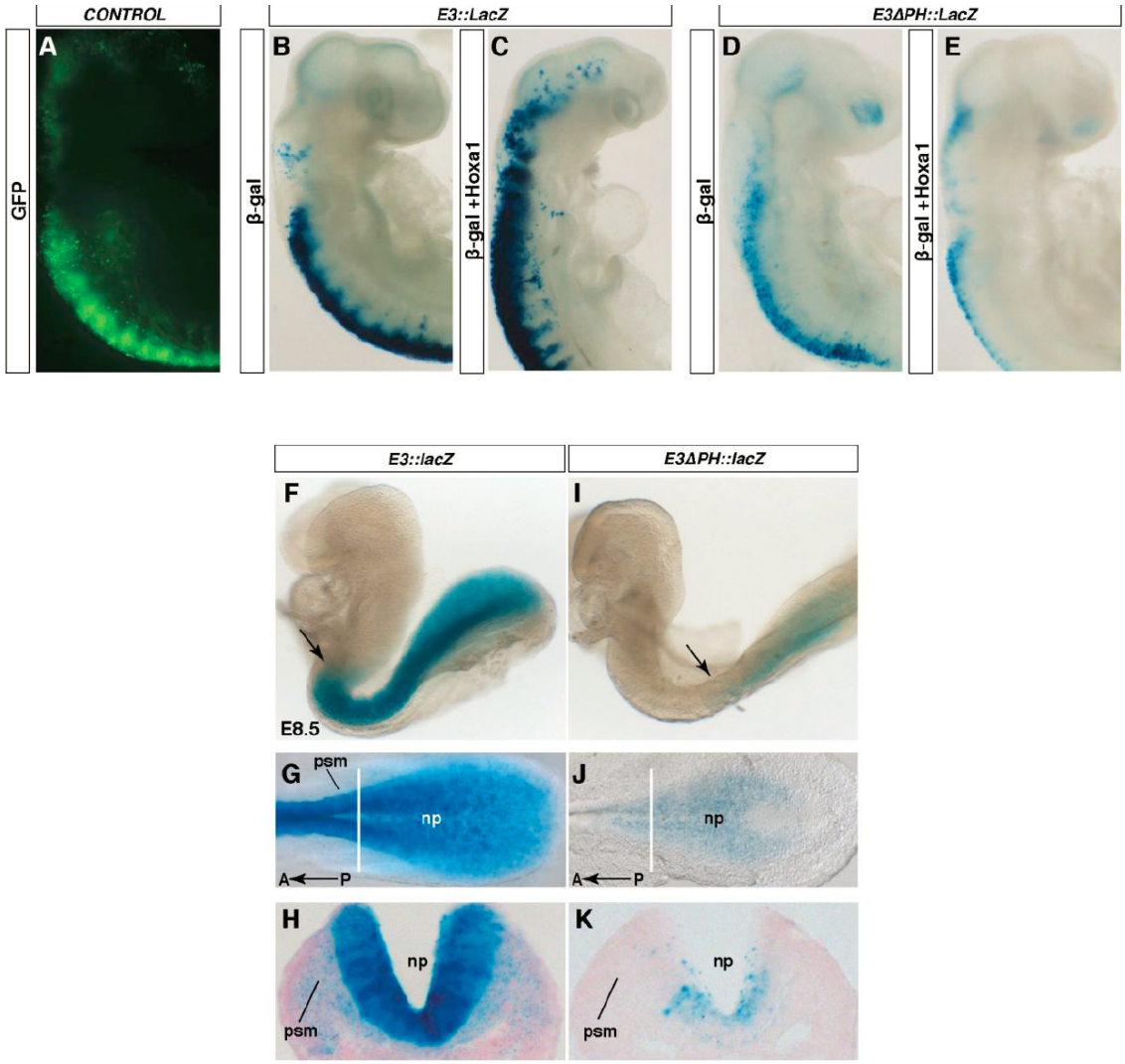

Figure S4. Trans-Activation in Chick Neural Tube and Transient Transgenic Mouse Assay of the *Raldh2 E3PH* Element, Related to Figure 5

(A-E) *In ovo* electroporation of chicken embryo neural tube with various constructs. **(A)** Representative control embryo electroporated with a *CMV::GFP* construct showing the spatial extent of GFP fluorescence.

(**B and C**) β-gal stainings of embryos co-electroporated with *E3::LacZ* and *CMV::GFP* (not shown) plasmids without (**B**) and with (**C**) *CMV::Hoxa1* construct, respectively. β-gal activity in (**C**) reveals a strong reporter up-regulation and ectopic trans-activation of *E3::LacZ* by Hoxa1.

(**D and E**) Mutation of Pbx-Hox site (*E3ΔPH::LacZ*) results in weaker activation of the reporter (**D**) and loss of responsiveness to Hoxa1 (**E**).

(F-K) *Raldh2 E3*-driven spatial activity in mouse. ß-gal stainings of E8.5 transient transgenic mouse embryos carrying the *Raldh2 E3::lacZ* reporter construct **(F-H)** or *E3ΔPH::lacZ* reporter construct **(I-K)**.

(F) Lateral view of whole-mount embryo showing spatial restriction of ß-gal staining with a rostral limit of transgene activity in the posterior hindbrain (arrow). **(G)** Posterior part of the embryo showing ß-gal activity in neural plate (np) and pre-somitic mesoderm (psm). White bar indicates the position of the cross-section in **H,** showing distribution of ß-gal staining in np and psm.
(I-K) ß-gal staining of E8.5 transient transgenic mouse embryos carrying the *Raldh2 E3ΔPH::lacZ* reporter construct, bearing a mutated Pbx-Hox binding site. PH site integrity within the *Raldh2 E3* enhancer is required to drive reporter expression in psm and partly in neural tube.

Supplemental Experimental Procedures

In Situ Hybridization

Briefly, mouse embryos were dissected, fixed in 4% paraformaldehyde (PFA) overnight, washed in PBT and dehydrated and stored at -20 °C in 100% methanol (Sigma). *Xenopus* embryos were collected, fixed in MEMFA for 2 hours, washed in PBT and dehydrated and stored at -20 °C in 100% ethanol (Sigma). Antisense riboprobes labeled with digoxigenin-11-dUTP or fluorescein-11-dUTP were used. Labeled probes were recognized by an antibody conjugated to alkaline phosphatase, and reactions were detected by NBT-BCIP reaction.

ß-Galactosidase Staining

Whole *RARE::lacZ* expressing transgenic embryos were dissected and fixed in 4% PFA at room temperature for 15 min. After three washes in PBT, embryos were put into the staining solution (1X PBS, 2 mM MgCl2, 5 mM K3Fe(CN)6, 5 mM K4Fe(CN)6, sodium deoxycholate 0.1%, NP-40 0.2%, and 1 mg/ml X-gal) at 37 °C for several hours. *Xenopus* embryos were fixed in MEMFA for 30 min and put into the staining solution (1X PBS, 2 mM MgCl2, 5 mM K3Fe(CN)6, 5 mM K4Fe(CN)6, 1 mg/ml salmon-gal) at 37 °C for 30 min.

Chromatin Immunoprecipitation Assay

About 1600 E8.5 wild type mouse embryos were manually dissected in posterior 'body' and anterior 'head' regions. Specimens were maintained in PBS+PMSF+AP (Complete Mini Roche) and kept on ice during dissection. After disrupting the tissues with a 20G-gauge syringe, crosslinking was performed with 1% Formaldehyde at RT and stopped by Glycine at final concentration of 0.125M. Chromatin preparations were sheared by sonication until reached an average length of 500-1000bp. Immunoprecipitation was performed by using Dynal magnetic beads (Invitrogen) prewashed with 5mg/ml BSA/PBS and 1mg/ml sonicated salmon sperm DNA. The eluted DNA was purified with QIAGEN PCR purification kit and resuspended in 30µl of TE.

For qPCR, sense oligos are indicated by "Fw" and antisense oligos indicated by "Rv":
Raldh2 OUT Fw: 5' GCCTAACCTGGCCTATTTCA3';
Radlh2 OUT Rv:5' GCAGGAAAGGATTTGTGACC3';
Raldh2 E2 Fw: 5'GTCCGTTAGAGTTTTCAGGA3';
Raldh2 E2 Rv: 5'GCTCTTGGGTTGTATGCAGAAT3';
Raldh2 E3 Fw: 5' TGGAAGCTCCT CCAATTCTC3';
Raldh2 E3 Rv: 5' CTCCGACATTAAAGGCTCCA3';
Raldh2 E4 Fw: 5' GCCTCAGCAACTTCTGGAAA3';
Raldh2 E4 Rv: 5' AGGCCGACTGAGA CCATAAA3'.

For quantitative ChIP, enrichment of specific DNA fragments was analyzed by real time qPCR using the ABI Prism 7000 thermocycler and QuantiTect SYBR Green PCR master mix (Quiagen). Immunoprecipitated DNA amounts were calculated from a standard curve of input DNA and normalized to rabbit IgG immunoprecipitations.

Electrophoretic Mobility Shift Assays

Oligonucleotide sequences (only sense strand is indicated).
E1PH: 5'AGAGTTGATAAATGTGCACTG3' ;
E2PH:5'CCACTGGAGATGGATGAGACCAT3';
E3PH:5'AGACAACTGATTTATAGCTAATTG3' ;
E4PH1:5'CTCTCAGGGTGATTTATGGTCTCAGT3' ;
E4PH2:5'ATTTGCTGTCAAATACGCTGGCTGATTTAGAGCTAG3';
E1Mut: 5'AGAGTTcgcAAcgGTGCATG3' ;
E2Mut:5'CCACTGGACGCGGCGTGAGACCAT3' ;
E3Mut:5'AGACAACTcgTTcgTAGCTAATTG3'.

Constructs

The E3 Pbx-Hox site was amplified by PCR from mouse genomic DNA using the following primers:
5'-CGTTTCTGAATTTTTGTTGCAT-3'(forward); 5'CTCCGACATTAAAGGCTCCA-3' (reverse).
For site-directed mutagenesis, pCR-E3 was used as a template and the following primers were used: 5'CTACCCCAGTAGGAAAGACAACTCCGCGGTAGCTAATTGGAGCC3' (forward);
5'GGCTCCAATTAGCTACCGCGGAGTTGTCTTTCCTACTGGGGTAG3' (reverse).

Generation of BAC Transgenic Mouse Embryos

The BAC containing the entire *Raldh2* locus (clone RP24-159G6 BACPAC Resources Center at Children's Hospital Oakland Research Institute, Oakland, CA, USA) was electroporated into the EL250 bacteria for modification by recombineering (Lee et al., 2001). To obtain the *Raldh2::eGFP* construct, bacteria were previously induced for recombineering at 42 °C and then electroporated with an eGFP-frt-Kanamycin-frt cassette amplified by PCR with primers containing 50 nucleotides of homology (indicated as caps) to the sequence upstream and downstream of the *Raldh2* ATG start codon :

Primers used for *Raldh2::eGFP* construct :
Forward : 5'CCAGCGAGATCGCCATGCCGGGCGAGGTGAAGGCCGACCCCGCCGC GCTCatggtgagcaagggcgagga3'
Reverse : 5'TACTTGATCTCGAGGTTGGGCGTGGGCGACGGCAGGAGCTGCAGCGA GGCtattccagaagtagtgagga3'.

Bacteria were subsequently arabinose-induced for Flpe expression in order to remove the Kanamycin cassette. To obtain the *Raldh2-E3ΔPH::eGFP* construct, the *Raldh2::eGFP* construct was electroporated into EL350 bacteria (Lee et al., 2001). These bacteria were subsequently induced at 42°C, as previously described, and were electroporated with a LoxP-Kanamycin-LoxP cassette amplified by PCR with primers containing 50 nucleotides of homology (indicated as caps) to the sequences surrounding the E3PH element.

Primers used for *Raldh2-E3ΔPH::eGFP* construct :
Forward primer : 5'-TTTCATTTGGAAGCTCCTCCAATTCTCCTTTTCTCTAGCCACC CCCTCTCagcccaattccgatcatattc-3'
Reverse primer : 5'-TGTTTTTCTTGGTAATAAGTGGGAAAGTGGATACTGGATAAAA GTCTTCAaactagtggatcccctcgag-3'

Finally, bacteria were arabinose-induced for Cre recombinase expression in order to remove the Kanamycin cassette. Correct recombination and excision of the resistance gene were validated by PCR, restriction enzyme digestion, and sequencing. Before microinjection, the modified BACs were linearized by PI-SceI digestion and dialysed. Constructs (0.8 ng/µl) were microinjected into pronuclei of (B6CF1 x C57Bl6) fertilized eggs.

Supplemental References

Lee, E.C., Yu, D., Martinez de Velasco, J., Tessarollo, L., Swing, D.A., Court, D.L., Jenkins, N.A., and Copeland, N.G. (2001). A highly efficient Escherichia coli-based chromosome engineering system adapted for recombinogenic targeting and subcloning of BAC DNA. Genomics *73*, 56-65.

Chapter 3: Manuscript in preparation

3.1 "Ezh2 maintains the Mesenchymal Potential and Positional Identity of Cranial Neural Crest Cells during Mouse Craniofacial Development"

A fundamental question during normal embryonic development is how the temporal and spatial collinear expression of *Hox* genes is achieved. Previous evidences pointed at the evolutionary significance to maintain *Hox* genes repressed in the rostral part of the embryo, which in turn allows normal development of vertebrate craniofacial skeleton and anterior brain. Recent discoveries shed light on the role of epigenetic complexes as key factors implicated in the remodeling and in the maintenance of the active and repressive transcriptional states of the chromatin, including at *Hox* clusters. Taking advantage from the cranial neural crest cell (cNCC) system, this unpublished work starts addressing the involvement of *Ezh2*, the catalytic component of the Polycomb repressive Complex (PRC) 2 which trimethylates lysine 27 of histone H3 (H3K27me3), in the maintenance of *Hox* gene repression during craniofacial development. This study is still under progress and not yet complete. However, it represents, to date, the advancement of our research. This draft contains the main findings and preliminary results.

Author contribution statement:
I contributed to the design of the study and the experiments. I contributed to the collection of the biological samples. I performed the ChIP assays and prepared the libraries for next-generation sequencing. I contributed to the interpretation of the results and to the writing of the draft, as well as to the preparation of the figures.

Ezh2 maintains the Mesenchymal Potential and Positional Identity of Cranial Neural Crest Cells during Mouse Craniofacial Development

Antonio Vitobello,[1,2,3*] Maryline Minoux,[1*] Claudius F. Kratochwil,[1,2] Alberto Loche,[1,2] Sebastien Ducret,[1] Nathalie Vilain,[1] Michael Stadler,[1] and Filippo M.Rijli[1†]

1 Friedrich Miescher Institute for Biomedical Research, Maulbeerstrasse 66, 4058 Basel, Switzerland

2 University of Basel

3 Current address: Novartis Institutes for Biomedical Research (NIBR), Basel, Switzerland

* These authors contributed equally to this work

† Correspondence: filippo.rijli@fmi.ch (F.M.R.)

3.2 Abstract

Background: A remarkable event taking place during vertebrate embryonic development is the temporal and spatial collinear activation of *Hox* genes. This process reflects the progressive propagation of permissive conditions that make available *Hox* genes for transcription according to their relative genomic positions within the clusters, from 3' to 5'. Previous studies indicated that this transcriptional competence acquisition involves the sequential relocation of each single *Hox* transcriptional unit from a repressive to an active chromatin compartment, which, in turn, correlates with the distribution of Polycomb- and Trithorax-mediated post-translational histone modifications respectively. In this study we address the functional role of Ezh2, the catalytic component of the Polycomb repressive complex 2 (PRC2) in the regulation of *Hox* transcriptional states during craniofacial development in the mouse. Cranial neural crest cells (cNCCs) are pluripotent cells that show the unique capability to differentiate into cartilages, bones and connective tissue. Although originating from the neural epithelium, these cells lose their neural potential contributing substantially to the formation of craniofacial and pharyngeal structures that make up the vertebrate head. This ability is interestingly dependent on the maintenance of a rostro-caudal migratory segregation of Hox-negative and Hox-positive cNCC pools which is considered to be the prerequisite that allowed the evolution of an increasingly complex craniofacial architecture in the vertebrate lineage. Yet, the transcriptional mechanisms

responsible for the restriction of the differentiation potential and the maintenance of the appropriate Hox code in cNCCs remain poorly understood.

Principal findings: By combining cell type-specific epigenomic and transcriptomic profiling, we characterized the molecular features of different rostro-caudal cranial NCC subsets. Genome-wide analysis revealed the presence of a common transcriptional and epigenetic ground-state from which each cell population diverges according to its antero-posterior pool of origin. Furthermore, we uncovered the role of Ezh2 as a crucial player in the maintenance of the rostro-caudal identity. Indeed, PRC2 activity is indispensable for the maintenance of the repressive state in the anterior *Hox*-negative domain. Moreover, in the *Hox*-positive domain, after the initial collinear activation of the clusters in pre-migratory cNCCs, Ezh2 re-establishes new repressive states in migratory and post-migratory cells in order to gain appropriate cell-specific *Hox* gene restrictions. Finally, our genome-wide analysis reveals that loss of Ezh2 activity results in a broad de-repression of the neurogenic potential, at the expenses of the mesenchymal differentiation program, indicating its involvement in the restriction of the cellular differentiation program.

Significance: Taken together these results unveil the pleiotropic functions of Ezh2 in the regulation of cellular identity during mouse craniofacial development by: i) maintaining the repressive state of *Hox* genes in the anterior part of the embryo; ii) re-establishing new silent domains within active 3' *Hox* clusters; iii) restricting the differentiation potential of mesenchymal NCCs.

3.3 Introduction

Morphogenesis of the craniofacial and pharyngeal regions involves the neural crest cells (NCCs), a vertebrate-specific transient cell population originating from different rostro-caudal compartments of the developing neural tube, which undergo epithelial-to-mesenchymal transition and gain migratory properties in order to reach their target regions where they proliferate and differentiate into a variety of cell types such as neurons, glia, melanocytes and smooth muscle. Moreover, in the cranial region, NCCs have the ability to differentiate into chondrocytes and osteoblasts, thus contributing to most of the

cartilages and bones of the skull, facial and pharyngeal skeletons (Santagati and Rijli, 2003; Minoux and Rijli, 2010).

Specification of NCC lineages has been shown to involve a set of signalling molecules and transcription factors whose actions are spatially and temporally coordinated (Dupin and Sommer, 2012). In parallel to the non-cell autonomous instructions affecting their lineage specification, NCCs exhibit also intrinsic molecular determinants limiting their differentiation potential according to their rostro-caudal distribution along the neuraxis. Indeed, at the level of the rhombencephalon, the positional identity of NCC pre-migratory progenitors is achieved through the nested and combinatorial expression of homeodomain (HD) transcription factors belonging to the *Hox* (homeobox) gene family. Hence, NCC subpopulations colonizing the different pharyngeal arches (PAs) express distinct combinations of *Hox* genes, providing each arch with a distinct AP molecular and positional identity (Trainor and Krumlauf, 2001; Santagati and Rijli, 2003; Minoux and Rijli, 2010). Paralog group 2 (PG2) *Hox* genes (*Hoxa2* and *Hoxb2*) are the only *Hox* genes expressed in post-migratory second PA (PA2) NCCs, whereas first PA (PA1) and more anterior NCCs are *Hox*-negative (Couly et al., 1998; Minoux et al., 2009). In vertebrates, *Hoxa2* inactivation (or in combination with *Hoxb2* loss-of-funtion in zebrafish) induces homeotic transformation of PA2 skeletal elements into a duplicated set of skeletal structures normally derived from PA1 mandibular process. *Hoxa2* ectopic expression in the anterior *Hox*-negative domain induces the reverse phenotype, i.e. the homeotic transformation of a subset of PA1 NCCs into a PA2-like identity (Baltzinger et al., 2005; Gendron-Maguireet al. , 1993; Grammatopoulos et al., 2000; Hunter and Prince, 2002; Minoux et al., 2013 submitted; Pasqualetti et al. 2000; Rijli et al., 1993; Santagati et al., 2005), indicating that PG2 *Hox* genes promote a PA2-like modality by modifying an underlying *Hox*-free ground (default) patterning program shared by mandibular and PA2-derived skeletogenic NCCs, though not by more anterior NCCs (Minoux et al., 2009; Minoux and Rijli, 2010; {Rijli, 1993). These observations infer the presence of common molecular characteristics shared by mandibular and PA2-populating NCCs, compared to those colonizing maxillary and fronto-nasal processes.

In addition, ectopic expression of *Hoxa2* in *Hox*-negative NCCs, severely impairs jaw and craniofacial development (Creuzet et al, 2002; Minoux et al., 2013 submitted). This

latter phenotype is observed also in *Hoxa3* or *Hoxb4* overexpressing chick embryos, thus indicating that, more broadly, *Hox* gene expression is incompatible with jaw and craniofacial development and that their repression in PA1 and more anterior NCCs is an essential condition to achieve proper morphogenesis(Couly et al., 1998; Creuzet et al., 2002). To date, the molecular mechanisms involved in *Hox* gene repression in anterior *Hox*-negative NCC remain elusive.

Recent evidences link the transcriptional activity of *Hox* genes to epigenetic factors regulating chromatin organization and function (Bantignies et al., 2011; Noordermeer et al., 2011; Soshnikova and Duboule, 2009). Inside the nucleus, transcriptionally active and repressed genes are thought to be located in distinct higher order chromatin compartments, whose functions correlate to Trithorax- and Polycomb-mediated histone modifications, respectively. Furthermore, previous studies indicated that *Phc1* full knockout mice (homologous to the *Drosophila polyhomeotic* gene) exhibit altered antero-posterior patterning and macroscopic neural crest defects (Takihara et al., 1997).

In the present work, we address the role of Ezh2, the catalytic component of the Polycomb repressive complex 2 (PRC2) which trimethylates Lysine 27 on histone H3 (H3K27me3) (Margueron and Reinberg, 2011). We used chromatin immunoprecipitation coupled with high throughput sequencing (ChIP-seq) and whole transcriptome sequencing (RNA-seq) assays, to identify, at genome-wide level, the epigenomic and transcriptomic features of distinct AP cranial subpopulations of control and *Ezh2*-mutant pre-migratory NCCs. We show that mesenchymal specification and positional identity in cranial NCCs are epigenetically maintained during early development. This study deciphers the role of PCR2 during head and pharyngeal morphogenesis.

3.4 Material and Methods

Mouse lines and embryonic tissues

Control reporter samples were dissected from E10.5 embryos, obtained from *ROSA26::RFP$^{f/f}$* pregnant mice crossed with *Wnt1::CRE$^{+/-}$* males. *Ezh2* mutant samples were dissected from E10.5 embryos, obtained from *ROSA26::RFP$^{f/f}$, Ezh2$^{f/f}$* pregnant mice crossed with *Wnt1::CRE$^{+/-}$; Ezh2$^{f/+}$* males. Our laboratory generated a conditional mouse line

overexpressing full-length *Hoxa2* cDNA under the control of *ROSA26* locus (*GT(ROSA)26Sor*$^{TM(Hox2a)f/+}$). Hoxa5 overexpressing fetuses were obtained by crossing *GT(ROSA)26Sor*$^{TM(Hoxa5)f/f}$ females with *Wnt1::CRE*$^{+/-}$ males.

In situ hybridization

In situ hybridization was performed as previously described (Santagati et al., 2005).

Sample preparation for next-generation sequencing

For RNA-seq experiments branchial arches were dissociated (trypsin 0.5%/EDTA at 37 °C for 10 minutes), rinsed (DMEM, 10% FBS), filtered and FACS-sorted. After sorting, 50,000 cells were pelleted by centrifugation for 5 minutes, 1000rpm at 4°C. PicoPure® Kit (KIT0204 Life Technologies) was used for RNA Isolation.

For ChIP-seq experiments, branchial arches were dissociated (trypsin 0.5%/EDTA at 37 °C for 10 minutes), rinsed (DMEM, 10% FBS), cross-linked with 1% formaldehyde for 10 minutes at room temperature and quenched with 125 mM glycine (Merck) for 5 minutes. Cells were pelleted by centrifugation for 10 minutes, 2000 rpm at 4°C and rinsed three times in ice-cold PBS and FACS-sorted. Cells where then rinsed in in ice-cold PBS containing PIC (Complete-EDTA free, Roche) and 20 mM sodiumbutyrate, pelleted and stored at -80°C until the amount of 500,000 cells per IP was achieved.

Chromatin immunoprecipitation (ChIP)

ChIP was performed as described previously (Dahl and Collas, 2008) with some modifications. Briefly, cells were thawed in ice and immediately lysed at 4°C by adding room-temperature equilibrated lysis buffer containing 50 mM Tris-HCl pH 8.0, 10 mM EDTA, 1% SDS (Fluka), PIC (Complete-EDTA free, Roche) and 20mM sodiumbutyrate. The samples were then snap-frozen in liquid-nitrogen and thawed at 4°C before sonication. The cell lysate was sonicated in a Diagenode Bioruptor to achieve a mean DNA fragment size of 250 bp. After clarification by centrifugation, the supernatants were diluted with RIPA buffer and incubated with anti-H3K4me2 (Millipore), anti-H3K27me3 (Millipore, 07-449) or anti H3K27ac (Millipore) coated protein A/G-magnetic bead complexes (Dynabeads Protein

A/G, Invitrogen 100.02D/04D) overnight at 4 °C. Ca. 500,000 cells were used for each IP. The next day, the beads were washed four times with RIPA buffer and once with TE buffer and the bead-bound complexes incubated with complete elution buffer (20 mM Tris-HCl pH 7.5, 5 mM EDTA, 50 mM NaCl, 1% SDS, 50 mg/mL proteinase K) at 68 °C for DNA elution, cross-link reversal and protein digestion. Finally, DNA from the immunoprecipitates was recovered by phenol-chloroform extraction and ethanol precipitation and processed for next generation sequencing.

Libraries were generated using the ChIP-seq DNA sample prep kit (Illumina, IP-102-1001). For sequencing, a single band of immunoprecipitated material was recovered from low-melting agarose gel, corresponding to the 300 bp size.

Genomic coordinates

The mouse genome assembly (GRCm38/mm10) was used as a basis for analyses. Annotation of RefSeq transcripts was obtained from the UCSC database. Genomic regions were defined as follows: promoter, sequences containing all bases within 1,000 bp of a RefSeq TSS; exon, non-promoter sequences that overlap with exons of RefSeq transcripts; and intron, non-promoter and non-exon sequences flanked by two exons of a single transcript. All other sites were defined as intergenic. A set of non-overlapping TSS regions (N = 17,012, 500 bp upstream and 200 bp downstream of the TSS) was generated using RefSeq TSSs.

Read filtering, alignment and weighting

Low-complexity reads were removed based on dinucleotide entropy (<1% of the reads). Reads were aligned to the mouse genome using Bowtie (version 0.9.9.1) with parameters -v 2 -a -m 100, which will find up to 100 best matches for each read with two or fewer mismatches. To track reads without genomic template (for example, exon-exon junctions), reads were also aligned to a databases containing known mouse sequences, tracking all best hits with no more than two mismatches. All quantifications were based on alignments weighted by the inverse of the number of query hits, ensuring that the total weight of a read did not exceed one.

Peak finding

Clusters of ChIP-Seq read alignments were identified using MACS (version 1.3.7.1) with a pool of alignments from all biological replicates and cellular stages (weights rounded to integers) and parameters set as: mfold = 8, gsize = 2700000000 and tsize = 36. Immunoprecipitation enrichment of resulting peak candidates was calculated, and peak candidates with enrichments less than twofold above background were removed.

Calculation of peak enrichments in genomic regions

Enrichment of peaks in genomic regions was calculated as the ratio of the observed over the expected number of peaks, where the observed number is the count of all peaks overlapping a region by more than half of their length and the expected number is the fraction of genomic bases in that region type multiplied by the total number of peaks.

Calculation of immunoprecipitation enrichment

Immunoprecipitation enrichment of a genomic region (TSS window or peak region) was calculated as $E = \log_2 ((n_{FG} / N_{FG} \times \min(N_{FG},N_{BG}) + p) / (n_{BG} / N_{BG} \times \min(N_{FG},N_{BG}) + p))$, where n_{FG} and n_{BG} are the summed weights of overlapping foreground and background (input chromatin) alignments, N_{FG} and N_{BG} are the total number of aligned reads in foreground and background samples, and p is a pseudocount constant used to regularize enrichments with low counts dominated by sampling noise.

Cut-offs for TSS-window enrichments were manually defined using scatter plots comparing biological replicates to separate correlated higher enrichments (positives) from the presumably negative and uncorrelated lower enrichments.

RNA-Seq data analysis

RNA from PA1-Mx, PA1-Md and PA2-Hy cells in three independent biological replicates each was used for cDNA preparation followed by sequencing on an Illumina HiSeq2000. Expression levels of RefSeq transcripts were calculated by $\log_2 (n / l \times \text{avg.}\_l + 1)$, where n is

the weighted sum of alignments to a RefSeq transcript scaled by the total number of reads in the sample, *l* is the length of the transcript and avg._*l* is the mean length of RefSeq transcripts. Expressed transcripts were defined based on the bimodal distribution of expression levels as transcripts with expression levels of at least 4.0 (log_2-transformed, length-normalized number of reads).

3.4 Results

3.4.1 Epigenomic organization and transcripton profiles of *Hox* gene clusters in mouse cranial NCC subpopulations

To identify the epigenetic and transcriptional features characterizing cranial NCCs according to their position along the embryonic antero-posterior axis, we focused our analysis on three defined NCC sub-populations at E10.5: namely, the *Hox*-negative NCCs of the PA1-derived maxillary (Mx) and mandibular (Md) processes, as well as the *Hox*-positive NCCs of PA2 (also called Hyoid (Hy) arch). In order to obtain pure populations of NCCs, we micro-dissected each of these prominences from embryos carrying the *Wnt1::Cre* and the *Rosa::RFP* conditional reporter alleles and we isolated NCCs by FACS sorting (Figure 1A, B). The *Wnt1* promoter drives Cre recombinase expression in NCC progenitors (Danielian et al., 1998), thus inducing RFP expression in NCC progenitors and their progeny. Our analysis showed that NCCs constitute nearly 80% of the total amount of cells that composed the pharyngeal arches at E10.5 (not shown).

We focused on cephalic NCCs destined to a mesenchymal (chondro/skeletogenic) fate. Indeed, i) based on NCC localization in the core of the pharyngeal arches, and ii) due to the fact that, already at E10.5, NCCs express chondrogenic markers such as *Col2a1* and *Sox9,* the NCC sub-populations collected in our experiments give most likely rise to chondrogenic and/or skeletogenic structures (Peters et al., 1999). Neurogenic NCCs are more proximal, localized into sensory ganglia, which were not included in our dissections.

We next processed these isolated NCC sub-populations for genome-wide transcriptional (RNA-seq) and epigenomic (ChIP-seq) characterization and the resulting data were integrated in order to correlate the transcriptional activity with the identified

epigenetic modifications. We examined histone modifications associated to Polycomb-mediated transcriptional repression (H3K27me3), to active/poised promoters and enhancers (Trithorax-mediated H3K4me2), and to active regulatory regions (H3K27ac). Our analysis revealed a high and selective enrichment of H3K27me3 at the level of the four *Hox* clusters compared to their flanking regions (Figure S1) in all the cNCC cell populations studied. However, a focused analysis on the epigenetic landscape at the level of *Hoxa* cluster showed that, specifically in PA2-derived cells, H3K4me2 and H3K27ac modifications are enriched at the expenses of H3K27me3 just at the level of the *Hoxa2* locus (Figure 1C). This distribution nicely correlates with the RNA expression profile that indicates a strong expression of Hoxa2 in the Hy sample, though not in samples from more anterior regions (Figure 1C). A quite similar pattern was found at the level of the *Hoxb* cluster in regard to *Hoxb2*, which is expressed at lower level in our cNCC samples (Figure S2). Such sharp windows of H3K27me3 depletion not only correlate with the unique expression of *Hoxa2* and *Hoxb2* genes in PA2 NCCs, but also suggest the presence of specific signals responsible for maintaining the expression of these selected *Hox* genes in second arch post-migratory NCCs. The specific lack of H3K27me3 enrichment observed in the E10.5 second arch NCC sub-population at the level of the *Hoxa2* and *Hoxb2* loci may therefore reflect the maintenance of an epigenetic configuration inherited from pre-migratory progenitors.

In vertebrates, *Hox* genes are expressed in space and time according to their physical position within their clusters; a process referred as spatio-temporal collinearity (Dolle and Duboule, 1989). This process is correlated with a progressive loss of H3K27me3 and a gain of H3K4me3 marks from the telomeric (3') extremity of the cluster to its opposite (5') end (Soshnikova and Duboule., 2009). The 3' most *Hox* paralogue group (PG) 1 genes, such as *Hoxa1* and *Hoxb1*, are the first genes expressed in rhombomere 4 (r4)-derived pre-migratory progenitors, i.e. the cells that give rise to the cNCCs populating PA2 (Gavalas et al., 1998; Makki and Capecchi, 2010; Murphy et al., 1991; Zhang et al., 1994). However, Hox PG1 genes are no longer expressed in post-migratory mesenchymal PA2 NCCs (Murphy and Hill, 1991; Hunt et al., 1991). Interestingly, we found an enrichment of H3K27me3 corresponding to *Hoxa1* and *Hoxb1* loci in this post-migratory NCC sub-population suggesting an active process responsible for *de novo* deposition of the H3K27me3

repressive mark following r4 NCC progenitor epithelial-mesenchymal transition (EMT) and migration into PA2 (Figs. 1 and S2).

3.4.2 Ezh2 is a key determinant of *Hox* gene repression in the anterior part of the head

Hox genes are not expressed in anterior head cranial NCCs. This specificity is conserved in the vertebrate lineage, from agnate to gnathostomes and is an absolute condition for the correct patterning of the fronto-nasal and first-arch derived skeletal structures (reviewed in Minoux and Rijli, 2010). Indeed, ectopic expression of *Hox* genes in chick *Hox*-free NCCs severely impairs jaw and craniofacial development (Couly et al., 1998; Creuzet et al., 2002). Similar defects are observed as a result of ectopic expression of *Hoxa2* and/or *Hoxa5* in mouse NCCs (Figure S3 and Minoux et al., 2013 submitted). The lack of *Hox* gene expression in the anterior *Hox*-free NCCs indicate that either absence of activators or presence of repressors, or both, are responsible for this condition.

The presence of high H3K27me3 levels (Figs. 1 and S1), strongly suggest a possible role of Polycomb for the acquisition and maintenance of a stably repressed chromatin configuration at *Hox* clusters. In order to test this hypothesis, we addressed the role of the PRC2 catalytic component *Ezh2* in during craniofacial development. We induced *Ezh2* deletion in NCCs progenitors before the onset of their migration by crossing mice carrying conditional (floxed) alleles of *Ezh2* (Shen et al., 2008) with *Wnt1::Cre* transgenic mice. At E10.5, *Wnt1::Cre;Ezh2*$^{flox/flox}$ conditional mutant embryos are indistinguishable from control embryos. However, craniofacial defects start appearing around E11.5, with the presence of a midline cleft at the level of the FNP (not shown). Analysis at E18.5 revealed that loss of *Ezh2* in NCCs results in a pronounced craniofacial phenotype characterised by absence of almost all NCC-derived bones, as shown by skeletal preparations (Figure 2).

To characterize the molecular mechanisms involved in the craniofacial and pharyngeal defects induced by *Ezh2* inactivation, we generated E10.5 *Wnt1::Cre;Ezh2*$^{flox/flox}$*;Rosa::RFP* mutant embryos. This approach allowed us to isolate the equivalent mutant subpopulations characterized in the previous analysis (PA1-derived Mx and Md proceses, as well as PA2-derived Hy NCCs) by FACS sorting and to use them for genome-wide transcriptional (RNA-seq) and epigenomic (ChIP-seq) analysis. For each of these prominences, comparable number of cells could be collected from E10.5

Wnt1::Cre;Ezh2$^{flox/flox}$;Rosa::RFP mutant embryos versus E10.5 *Wnt1::Cre;Ezh2$^{flox/flox}$* control embryos, supporting the absence of macroscopic defects in cell proliferation and/or apoptosis at this stage (not shown).

Loss of Ezh2 function would be expected to result preferentially in derepression (i.e. up-regulation) of gene expression. Accordingly, RNA-seq analysis revealed that, independently of the cranial NCC sub-population analysed, 9.3 % of genes display up-regulated expression, whereas only 0.7% were down-regulated in *Wnt1::Cre;Ezh2$^{flox/flox}$;Rosa::RFP* mutant NCCs compared to control *Wnt1::Cre;Ezh2$^{flox/flox}$* samples (Figure 3A). 90% of the genes however displayed unchanged expression, thus indicating that *Ezh2*-mediated regulation affects a relatively small percentage of the cranial NCCs genome (Figure 3A). Among the genes whose expression is mostly up-regulated as a result of *Ezh2* conditional inactivation, we found several *Hox* transcripts (Figure 3B and Figure S4) with a similar pattern of distribution between the three sub-populations analysed (Figure 3E and Figure S4). One exception concerns transcription 5' adjacent to *Hoxa2* and *Hoxb2* loci, as our RNA-seq analysis shows higher enrichment in Hy than in Md or Mx NCC sub-populations (Figure 3E). In particular, *in situ* hybridization confirms that *Hoxa3* expression is more up-regulated in Hy than in Md or Mx NCCs (Figures 3C,D), possibly suggesting a role of *Hoxa2* regulatory regions on the neighbour 5' locus. By carrying out H3K27me3 ChIP on mutant samples, we found that de-repression of *Hox* genes is associated, in all the sub-populations analysed, with the absence of this Ezh2-mediated epigenetic modification (Figure 3E and Figure S4).

In summary, these results support the notion that *Hox* genes are direct targets of Ehz2 and reveal that Ezh2 plays the major role, as compared to its paralogue *Ezh1*, in H3K27 methylation of the *Hox* clusters in cranial NCCs. Moreover, these data show that Ezh2 is involved in maintaining a collinear pattern of *Hox* expression in Hy *Hox* PG2^{+} NCCs and *Hox* repression in anterior head NCCs.

3.4.3 Ezh2 is crucial to maintain positional identity of distinct rostrocaudal NCC subpopulations

To characterize the molecular identity of E10.5 Mx, Md and Hy (PA2) NCC sub-populations, we performed a genome-wide analysis of their epigenetic and transcriptional

features. We found that only a few loci are differentially enriched/depleted in H3K27me3 (Figure 4A), H3K27ac (Figures 4B,C) or H3K4me2 (not shown) marks between Mx, Md and Hy samples. Among these, we found key regulators of cellular positional identity. Indeed, we show that *Hoxa2* is among the few genes that are the most selectively enriched in H3K27ac in PA2 cells (Figure 4D). Similarly, *Dlx5/6* and *Hand1/2*, known to be major determinants of PA1 (Md vs. Mx) dorsoventral identity (Beverdam et al., 2002; Depew et al., 2002; Sato et al., 2008) are among the subset of genes that show selective H3K27ac enrichment in the Md NCC sub-population compared to the other samples (Figure 4D). Altogether, these results emphasize the sub-population specific *in vivo* role of epigenetic regulation of the transcriptional states of key developmental genes.

In keeping with the epigenetic data, the transcriptional profiles show that control Mx, Md and Hy NCC sub-populations show high degree of correlation (Figure 4E). Interestingly, Md and Hy NCCs were more similar to each other than to the Mx sub-population (Figures 4E,F). In E10.5 Ezh2 mutant embryos, NCC sub-populations lost the molecular signatures that characterize their respective control samples (Figure 4F). Moreover, multi-dimensional analysis revealed that *Ezh2* deficient Md and Hy samples segregated together indicating that these sub-populations acquire the same transcriptional profile (Figure 4F). To investigate whether such a similar transcriptional molecular identity might result from intermingling of NCC subpopulations due to altered migratory behaviour, we performed *cellular retinoic acid-binding protein 1* (*Crabp1*) *in situ* hybridization on E9.5 control and *Wnt1::Cre;Ezh2*$^{flox/flox}$ mutant embryos (Figure S5 and not shown). No differences were observed in *Ezh2* deficient embryos, showing normal stream segregation of migrating NCCs from distinct rostrocaudal levels, similar to wild-type behaviour. Lastly, it is noteworthy that in *Ezh2* mutants the Mx sample transcription profile segregates distinctly from control Mx but also from *Ezh2* deficient Md and Hy NCC sub-populations (Figure 4F). Taken together, these data show that the *Ezh2* mutation has different effects on the three cranial NCC sub-populations. This might reflect their distinct rostrocaudal embryological origin. While the NCCs populating the Mx process derive from the mesencephalic region, NCCs colonizing Md and Hy colonizing cells are mostly of rhombencephalic origin (Kontges and Lumsden, 1996).

3.4.4 Ezh2 maintains the mesenchymal identity of cranial NCCs through repression of their neurogenic potential

To further investigate Ezh2 function in cranial NCC specification and identity, we next compared the delta-RNA-seq data, i.e. the genome-wide transcriptional differences between *Wnt1::Cre;Ezh2$^{flox/flox}$;Rosa::RFP* mutant versus *Wnt1::Cre;Rosa::RFP* control NCCs, with genome-wide H3K4me2 and H3K27me3 distribution (Figures 5A,B). Our analysis revealed that the genes highly up-regulated in the *Ezh2* mutant, were those enriched both in H3K27me3 and H3K4me2 in the control sample. The presence of active and repressive epigenetic marks at the level of the same promoter regions is reminiscent of the situation described for important developmental genes in ES cells (Azuara et al., 2006; Bernstein et al., 2006), which need to be primed for expression although transcriptionally silent (bivalent promoters). The genes decorated only with H3K27me3 in the control also resulted to be up-regulated in the mutant, albeit at a minor extent compared to the "bivalent" ones. The genes that where only enriched in H3K4me2 or that did not show any specific enrichment in the control remained almost unchanged in the *Ezh2* mutant (Figure 5B). These results indicate that the up-regulated genes were prevalently those under direct Polycomb-mediated repression.

To better understand the outcome of *Ezh2* conditional inactivation in NCCs, we performed a Gene Ontology (GO) analysis of the differentially regulated transcripts. We focused our analysis on the Md sub-population, which normally gives rise to the lower jaw. In addition to the *Hox* genes, which are scored in specific classes such as "embryonic skeletal system morphogenesis" and "anterior/posterior pattern specification", we found significant enrichments of genes involved in "neurogenesis and neuronal differentiation", such as for instance *Pou4f1* (a marker for differentiating sensory neurons). This indicates that Ezh2 represses the neurogenic potential of cranial NCCs normally fated to mesenchymal (i.e. chondro/skeletogenic) differentiation (Figure 5A). Although in E10.5 *Wnt1::Cre;Ezh2$^{flox/flox}$;Rosa::RFP* mutant embryos the expression of chondrogenic markers such as *Sox5*, *Sox6*, *Sox9*, or *Col2a1* is only slightly decreased, the GO analysis suggest a consistent trend towards down-regulation as a gene group ensemble, which prefigures

their significant spatial down-regulation in E13.5 embryos , as assessed by in situ hybridisation (Figure 6; and data not shown). These results underscore the role of Ezh2 in the maintenance of mesenchymal fate through repression of alternative neurogenic fate. In the absence of Ezh2 function, NCCs normally migrate to their final destination, begin a chondrogenic differentiation program but they are not able to properly pursue it.

3.5 Discussion and perspectives

The cranial neural crest cell system represents one of the most interesting models in developmental biology to address the problem of self-renewal and differentiation potential *in vivo* of cells that show *bona fide* stem cell properties. Previous studies demonstrated that the fate of NCCs is not irreversibly committed at the progenitor stage in the neural primordium and rather depends upon the environment encountered by NCC during migration and at sites of arrest (Dupin et al., 2010). Paracrine factors like BMP2/4, Wnt and TGF-β signalling pathways as well as Delta family ligands have been shown to modulate the differentiation potential of these cells (De Bellard et al., 2002; Goldstein et al., 2005; Lee et al., 2004; Shah et al., 1996). Studies conducted in the avian embryo demonstrated the existence of cranial neural crest cell progenitors endowed with a different combination of both mesenchymal (osteogenic/chondrogenic) and neurogenic-melanogenic potential (Calloni et al., 2007) which respond differently to Shh signalling.

At the molecular level, the differentiation program undertaken by these cells rely on the instructive role of non-cell autonomous information as well as transcriptional networks already established in pre-migratory cells which reflect their rostro-caudal origin along the neuraxis (e.g. Otx2, Hox – Kimura et al., 1997; Minoux et al., 2009). *Hox* genes for example, are repressed in the anterior part of the embryo (*Hox*-negative domain) and expressed in a rostrocaudally nested manner from the rhombencephalon to the spinal cord (*Hox*-positive domain), reflecting their relative genomic positions within the clusters (spatial collinearity). The importance to maintain a *Hox*-negative domain in the anterior part of the embryo is underscored by gain-of-function experiments in which anterior cranial NCCs are forced to ectopically overexpress *Hox* genes, leading to severe impairment of craniofacial

development (Creuzet et al., 2002). Recently, the transcriptional availability/silencing of *Hox* genes has been proposed to be influenced by regulatory effects played by the chromatin configuration of the clusters (Soshnikova and Duboule, 2009). In particular, maintenance of *Hox* transcriptional states correlates with distinct sub-nuclear domains of active or repressed genes (Bantignies et al., 2011; Noordermeer et al., 2011).

Previous reports (Takihara et al., 1997) indicated that *Phc1* disruption (the mouse homologue of the *Drosophila polyhomeotic* gene) leads to altered antero-posterior patterning and neural crest defects. Furthermore, Phc2 and Phc1 have been shown to act synergistically to mediate repression of *Hox* genes (Isono et al, 2005). This work supports a role of the PRC1 complex in the maintenance of transcriptional repression of *Hox* genes during antero-posterior patterning. Moreover, a large majority of Polycomb targets are co-occupied by PRC2 and PCR1 complexes in ES cells, though a substantial portion of target genes show non-overlapping characteristics (Boyer et al., 2006; Ku et al., 2008). Finally, due to the early lethality of mutant mice a comprehensive analysis of Polycomb loss of function in NCCs and resulting craniofacial defects was missing.

In this study, we addressed the role of Ezh2 in the maintenance of mesenchymal fate of cranial NCCs in the mouse. Our analysis takes advantage from genetically labelled cells to isolate nearly pure populations of NCCs according to their rostrocaudal origin along the developing embryo. In particular, we micro-dissected three sub-populations corresponding to the *Hox*-negative Maxillary (Mx) and Mandibular (Md) prominences of the first pharyngeal arch as well as the *Hox*-positive Hyoid (Hy) NCCs of the second pharyngeal arch. This approach allowed to perform a genome-wide correlation *in vivo* of transcriptome and epigenome from each of these sub-populations and between them, and to use the craniofacial system as readout of the phenotypic effects caused by the *Ezh2* mutation.

Because of the strong evidence pointing at the importance of maintaining *Hox* genes repressed in the embryonic head, we decided to start our analysis by conditionally inactivating Ezh2 in NCCs and investigating its effects on the transcriptional regulation of these important developmental regulators. In control animals, *Hox* clusters in the three NCC sub-populations are highly enriched and decorated with the Polycomb-mediated H3K27me3 repressive mark, irrespectively of the sub-population analysed. However, in the

Hy component, the *Hoxa2* and *Hoxb2* loci are H3K27me3-depleted with a concomitant selective enrichment in H3K4me2 and H3K27ac, correlating with their selective expression in this sub-population. Intriguingly, the bodies of Hox PG1 genes (i.e. *Hoxa1* and *Hoxb1*) are heavily decorated with the H3K27me3 mark in E10.5 Hy NCCs. As *Hoxa1* and *Hoxb1* are expressed in pre-migratory rhombomere 4 (r4)-derived cranial NCCs (Gavalas et al., 1998; Makki and Capecchi, 2010; Murphy et al., 1991; Zhang et al., 1994) it is plausible to assume that Hox PG1 genes were devoid of H3K27me3 decoration in r4-derived NCC progenitors. Consequently, an active process took place in order to modify the collinear expression and change the epigenetic landscape of these genes in migratory and post-migratory NCCs. If the distribution of active and repressive epigenetic marks represents the distribution of *Hox* genes within respective chromatin compartments, we can speculate that, in migratory and post-migratory r4-derived NCCs, Hox PG1 genes colocalize with the rest of the repressed cluster, whereas Hox PG2 would occupy a different active compartment of the nucleus (**Figure 3.1**). In order to validate this model, on-going activities in our laboratory are devoted to study the epigenetic marks associated with Hox PG1 genes in r4 pre-migratory neural crest cells. In parallel, Chromosome Conformation Capture (4C) assays will be used to determine the spatial distribution of *Hox* genes within active and silenced chromatin compartments.

To assess the functional role of Polycomb in the maintenance of the repressive state of *Hox* genes in cranial neural crest cells we took advantage from an *Ezh2* conditional deletion in pre-migratory neural crest cells. The *Ezh2* mutation causes the complete loss of the H3K27me3 mark in all four Hox clusters and, in parallel, results in a general de-repression of their transcriptional state. Phenotypically, the mutation impairs the correct formation of facial and pharyngeal bones and cartilages, in keeping with the previous observation that the ectopic expression of *Hox* genes is incompatible with normal craniofacial development (Creuzet et al., 2002; Couly et al., 1998 and Minoux et al., 2013 submitted).

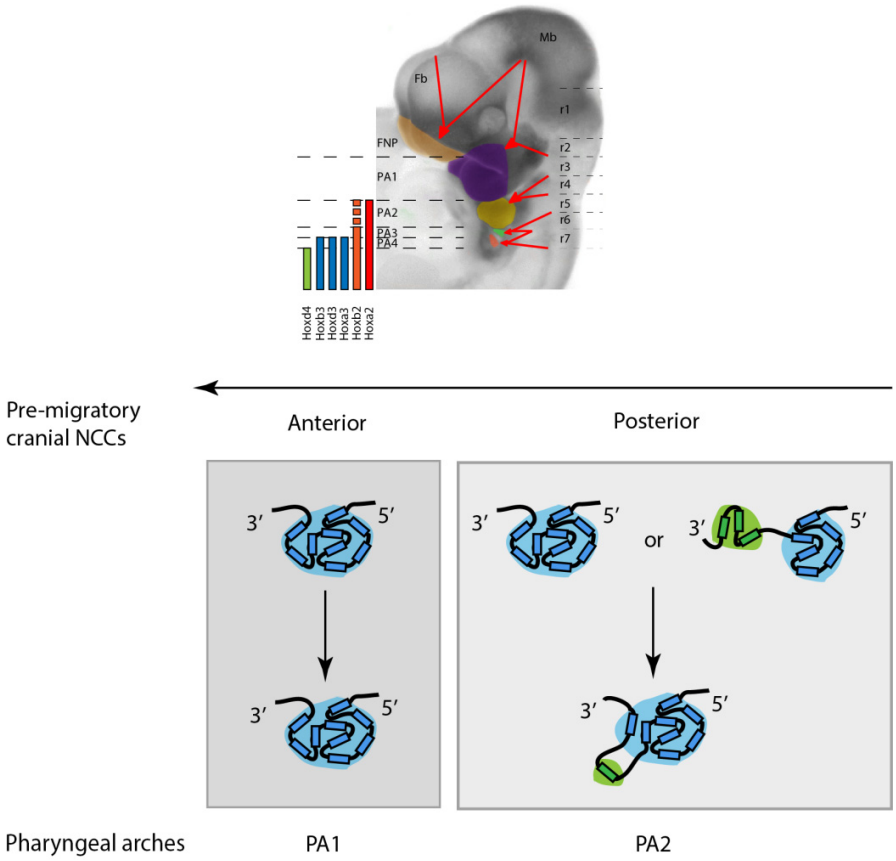

Figure 3.1. Working model. In pre-migratory cranial NCCs a linear distribution of *Hox* transcriptional units between active (green) and repressed (blue) chromatin compartments reflects the silent state in the anterior embryonic domain and the collinear expression of 3' genes in r4-originating cells. In migratory and post-migratory cranial NCCs a switch in the chromatin state would modify the initial collinear configuration and bring Hox PG1 genes back into the repressive domain (modified from Pindyurin and van Steensel, 2012).

More broadly, Ezh2 activity is important for the maintenance of the positional identity of cranial NCC sub-populations. Our transcriptomic and epigenomic data on control Mx, Md and Hy samples reveal a high degree of correlation, at genome-wide scale, amongst

all three cell populations. Only a small subset of loci show specific enrichment/depletion of the epigenetic marks analysed. Importantly, the epigenetically regulated target genes are known to play a crucial role in the rostrocaudal and dorsoventral identity of cranial NCCs (e.g. *Hoxa2, Hoxb2, Hand1/2*), thus indicating that during NCC migration and settling Ezh2 plays an important role *in vivo* in the cell-specific maintenance of the repressed state of key patterning genes.

Previous loss- and gain-of-function experiments, aimed at decipher the role of *Hox* genes in the differentiation of pharyngeal arch derivatives, suggested the presence of a PA1-like skeletogenic ground state shared by all the cranial NCCs populating the pharyngeal region (Minoux et al., 2009). Our study extends the analysis to different sub-populations within the first pharyngeal arch and identifies a shared molecular signature belonging to Md and Hy samples, which probably reflects the common rhombencephalic origin of these two populations. This similarity is more evident in *Ezh2* mutants, where, at genome-wide scale, the two populations lose their molecular identity. In this scenario, Ezh2 would play an important role in maintaining the positional identity of neural crest cells originating from the same rostrocaudal brain region. In fact, the Mx sample, which derives from the mesencephalic region, does not show such a high degree of correlation as between Md and Hy NCCs (both subpopulations are derived from the rhombencephalon), neither in the control nor in the *Ezh2* mutant background. If this interpretation is correct, we would expect to find an even more diverged outlier by analysing a further anteriorly originated sub-population of cNCCs, like those populating the fronto-nasal process (FNP) that derives from the diencephalic region. This hypothesis is currently subject of further investigation in our laboratory. Overall, these findings reveal a somewhat unexpected intrinsic heterogeneity of cranial NCC subpopulations contributing to craniofacial development.

The *Ezh2* mutation leads to the up-regulation of 9.3% of the entire genome. The large majority of those genes show bivalent promoters (i.e. enriched in H3K4me2 and H3K27me3) or decorated only with H3K27me3, indicating that they are under direct control of PRC2. Furthermore, although preliminary, our GO analysis suggests that *Ezh2* plays a role in the maintenance of the mesenchymal (chondro/skeletogenic) fate of migratory and post-migratory cranial NCCs by repressing their neurogenic potential and *Hox* genes, which have been proposed to be major antagonist of the craniofacial program

carried by cranial NCCs (Couly et al., 1998). Interestingly, previous studies demonstrated that the chondrogenic potential of cranial NCCs decreases according to the rostrocaudal distribution of their progenitors (Calloni et al., 2007), which also correlates with an increase of *Hox* expression. To consolidate this observation, we plan to perform *in situ* hybridization as well as immunohistochemisty assays on control and *Wnt1::Cre;Ezh2*$^{flox/flox}$*;Rosa::RFP* embryos to assess quantitatively and qualitatively the change in the expression of neural and chondro/osteogenic markers. The comparison between the transcriptome at E10.5 and our *in situ* hybridisation analysis on the marker *Col2a1* reveals a significant decrease of its expression in E13.5 *Ezh2* conditional mutant fetuses, indicating a loss of chondrogenic potential of mesenchymal NCCs through development. Furthermore, we will also investigate if the de-repression of such an inappropriate program in cNCCs would consequently induce their apoptosis, a change in their proliferative properties, or a stable switch in their fate.

Taken together our data indicate the pleiotropic effects of cell-autonomous *Ezh2* mutation in the maintenance of positional identity and mesenchymal fate of rostrocaudally defiend cranial neural crest cell sub-populations.

3.6 Figure legends

Figure 1 – Method outline. Transgenic embryos expressing the RFP protein in the *Wnt1* domain allow the isolation of fluorescently labeled NCCs. Maxillary, Mandibular and Hyoid pharyngeal arches (A) are dissected at E10.5, dissociated and FACS-sorted (B). The fluorescent signal is detected over the baseline level of a *Wnt1::Cre* negative littermate. The red rectangles indicate the sorted singlets used for the further analysis. For ChIP assay, cells are formaldehyde-fixed before sorting to preserve the "native" chromatin interactions captured at moment of the dissection. Three epigenetic modifications have been used for the analysis (H3K27ac, H3K4me2 and H3K27me3) in combination with RNA profiling. (C) UCSC genome browser snapshot. RNA-seq (black tracks) and ChIP-seq results (grey track= input; blue tracks= H3K27ac, green tracks= H3K4me2; red tracks= H3K27me) are aligned to the reference genome to identify regulatory mechanisms underlying rostro-caudal NCC diversity. Highlighted is the *Hoxa2* genomic locus.

Figure2 – Phenotypic effects of *Ezh2* conditional mutation in NCCs. External view of Control (A) and *Wnt1::Cre;Ezh2*$^{flox/flox}$ mutant fetuses (B). Skeletal preparation of Control (C) and *Wnt1::Cre;Ezh2*$^{flox/flox}$ mutant (D) showing dramatic impairment of jaws and frontal bone formation.

Figure3 – Molecular characterization of *Wnt1::Cre;Ezh2*$^{flox/flox}$ mutant embryos. (A) Bar chart indicating the percentage of genes down-regulated, unchanged and up-regulated in mutant samples. (B) Volcano plot showing the genes differentially expressed in control versus *Ezh2* conditional mutant Md samples (red dots= *Hox* cluster genes). *Hoxa3* in situ hybridization on control (C) and *Ezh2* conditional mutant (D) in E10.5 embryos, a substantial up-regulation is observed in PA2. (E) UCSC genome browser snapshot of *Hoxa* cluster expression in E10.5 *Ezh2* conditional mutant samples. H3K27me3 modification is completely lost and RNA-seq data reveal extensive dysregulation of *Hox* expression. The de-repression pattern appears similar in all the populations analyzed, except for the 3' end of the clusters in the Hy population where the active *Hoxa2* locus affects the expression of nearby 5' genomic region (*Hoxa3*).

Figure 4 - Genome-wide analysis of control and *Ezh2* mutant NCCs. H3K27me3 (A) and H3K27ac (B) enrichments on Mx, Md and Hy samples are represented as heatmaps, lateral red lines indicate *Hox* gene clusters. (C) Pairwise scatter correlation of H3K27ac between Mx, Md and Hy samples, red dots represent promoters differentially enriched. (D) Scatter plot representing the distribution of H3K27ac of Hy versus Mx samples using Md as reference (red dots= Hy genes specifically enriched in H3K27ac; blue dots= Md genes specifically enriched in H3K27ac). (E) Pairwise correlations of RNA-seq data reflecting high similarity within control and mutan Md/Hy samples. (F) Multi-dimensional analysis of RNA-seq data showing loss of cellular identity in Md and Hy mutant samples, solid boxes represent control samples, empty boxes represent *Ezh2* samples.

Figure 5 – Genome-wide correlation of RNA-seq/ChIP-seq data and GO analysis. (A) Scatter plot correlating histone modification enrichment at promoter regions (*x*-axis= H3K27me3, *y*-axis=H3K4me2) and RNA levels (color coded) in control Md samples. In the next panel same analysis performed on *Ezh2* mutant samples, color-coded is indicated the delta-RNA FC of mutant versus control samples. The distribution of red dots in the second panel indicates that the majority of up-regulated genes were bivalent or enriched in H3K27me3 in control samples. (B) Box-and-whisker categorizing the upregulated genes in *Ezh2* mutant Md samples according to H3K27me3/H3K4me2 enrichment. (C) GO analysis comparing *Ezh2* mutant and control Md sampes, listed are cellular functions significantly expected to be modulated in *Ezh2* mutants.

Figure 6 – *Col2a1* expression in control versus *Wnt1::Cre;Ezh2$^{flox/flox}$* mutant fetuses. Normal expression of the chondrogenic marker *Col2a1* in normal E11.5 embryos (A,B) and E13.5 (C-F) fetuses. Respective expression pattern in conditional E11.5 (G,H) and E13.5 (I-L) Ezh2 mutants. A significant decrease of *Col2a1* expression is observed at E13.5 in mutant fetuses indicating a progressive loss of chondrogenic potential.

Figure 1

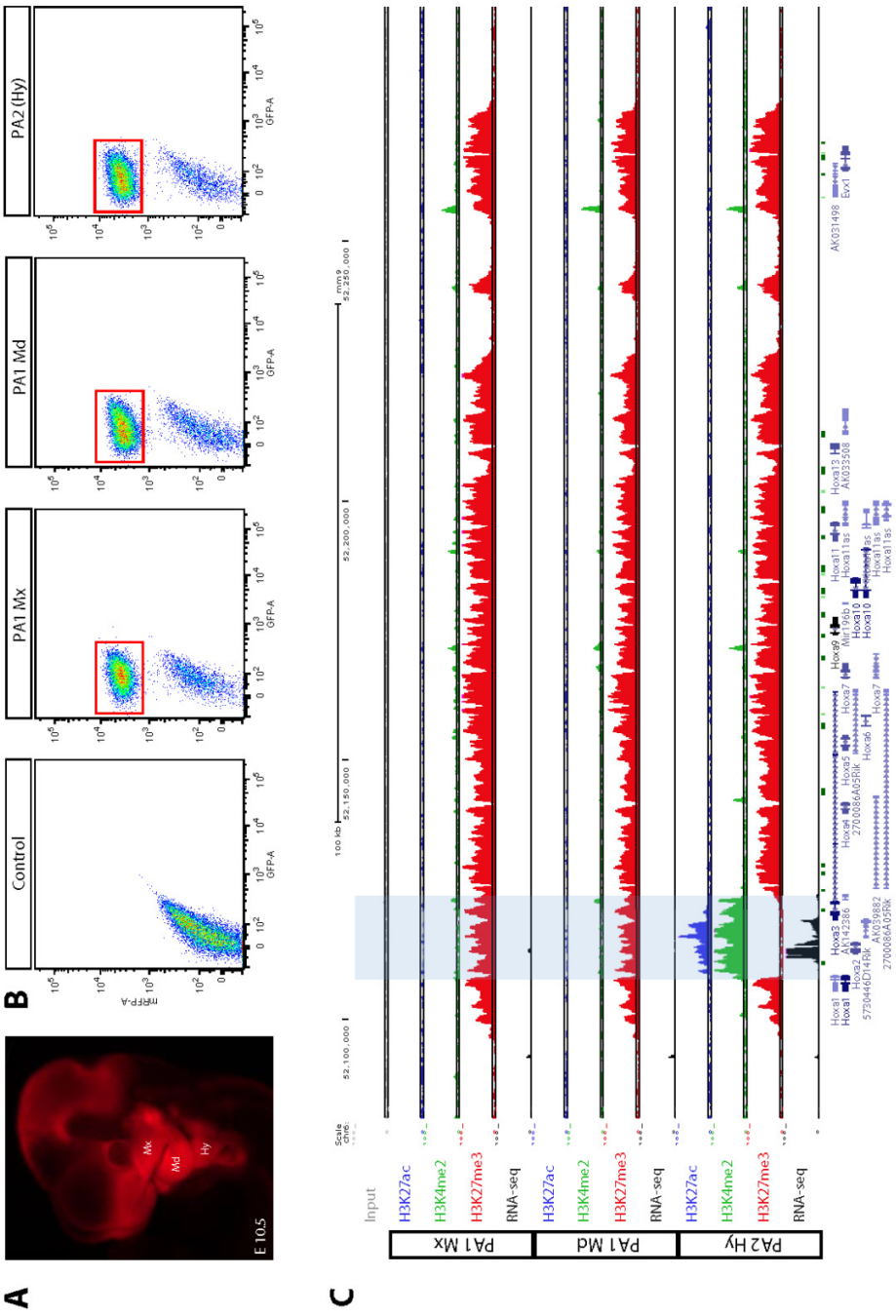
A
B
C
Control
PA1 Mx
PA1 Md
PA2 (Hy)
E 10.5
Mx
Md
Hy
mRFP-A
GFP-A
Input
H3K27ac
H3K4me2
H3K27me3
RNA-seq
PA1 Mx
PA1 Md
PA2 Hy

Figure 2

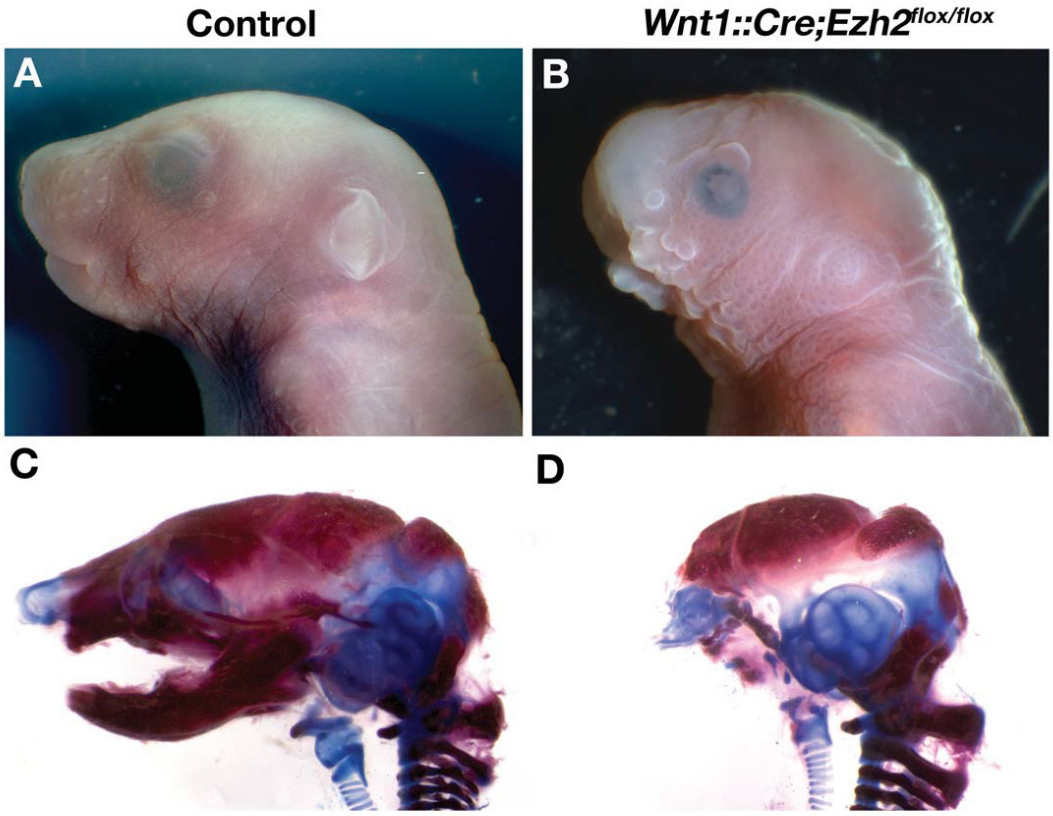

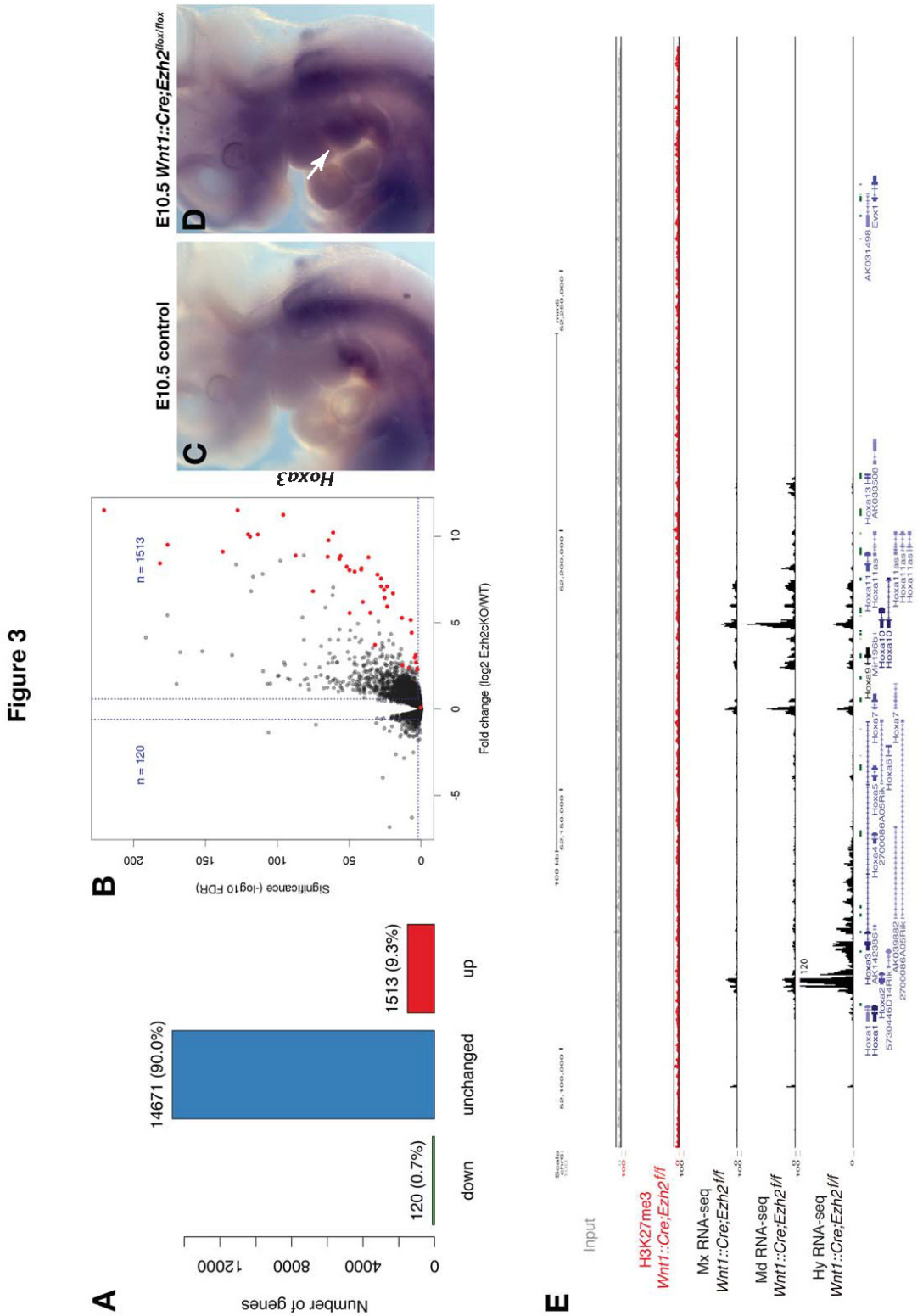
Figure 3
A
Number of genes
0
4000
8000
12000
120 (0.7%)
14671 (90.0%)
1513 (9.3%)
down
unchanged
up
B
Significance (-log10 FDR)
0
50
100
150
200
n = 120
n = 1513
-5
0
5
10
Fold change (log2 Ezh2cKO/WT)
Hoxa3
C
E10.5 control
D
E10.5 Wnt1::Cre;Ezh2flox/flox
E
Input
H3K27me3
Wnt1::Cre;Ezh2f/f
Mx RNA-seq
Wnt1::Cre;Ezh2f/f
Md RNA-seq
Wnt1::Cre;Ezh2f/f
Hy RNA-seq
Wnt1::Cre;Ezh2f/f

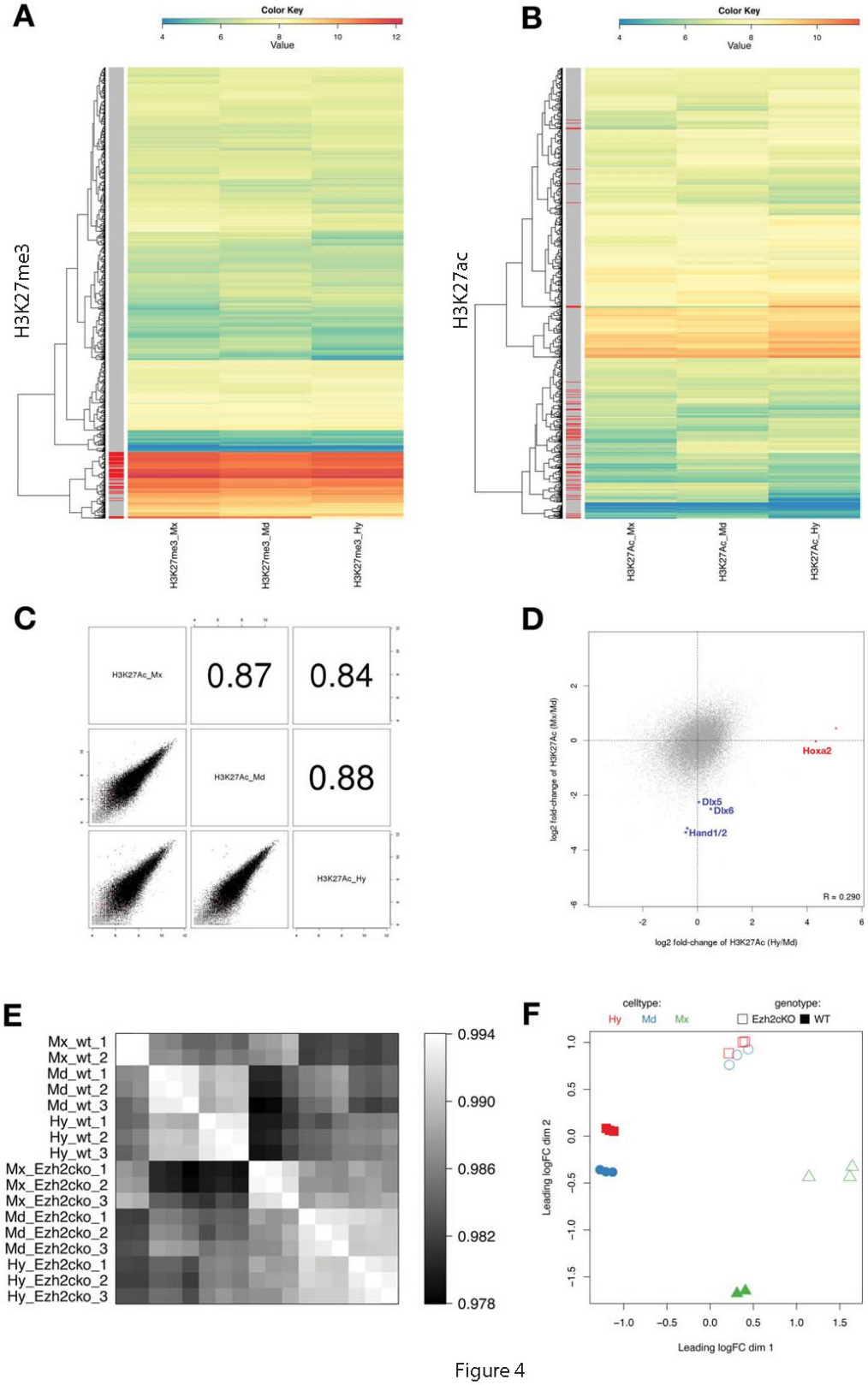
A
Color Key
Value
H3K27me3
H3K27me3_Mx
H3K27me3_Md
H3K27me3_Hy
B
Color Key
Value
H3K27ac
H3K27Ac_Mx
H3K27Ac_Md
H3K27Ac_Hy
C
H3K27Ac_Mx
0.87
0.84
H3K27Ac_Md
0.88
H3K27Ac_Hy
D
log2 fold-change of H3K27Ac (Mx/Md)
log2 fold-change of H3K27Ac (Hy/Md)
Hoxa2
Dlx5
Dlx6
Hand1/2
R = 0.290
E
Mx_wt_1
Mx_wt_2
Md_wt_1
Md_wt_2
Md_wt_3
Hy_wt_1
Hy_wt_2
Hy_wt_3
Mx_Ezh2cko_1
Mx_Ezh2cko_2
Mx_Ezh2cko_3
Md_Ezh2cko_1
Md_Ezh2cko_2
Md_Ezh2cko_3
Hy_Ezh2cko_1
Hy_Ezh2cko_2
Hy_Ezh2cko_3
0.994
0.990
0.986
0.982
0.978
F
celltype:
Hy
Md
Mx
genotype:
Ezh2cKO
WT
Leading logFC dim 2
Leading logFC dim 1

Figure 4

Figure 5

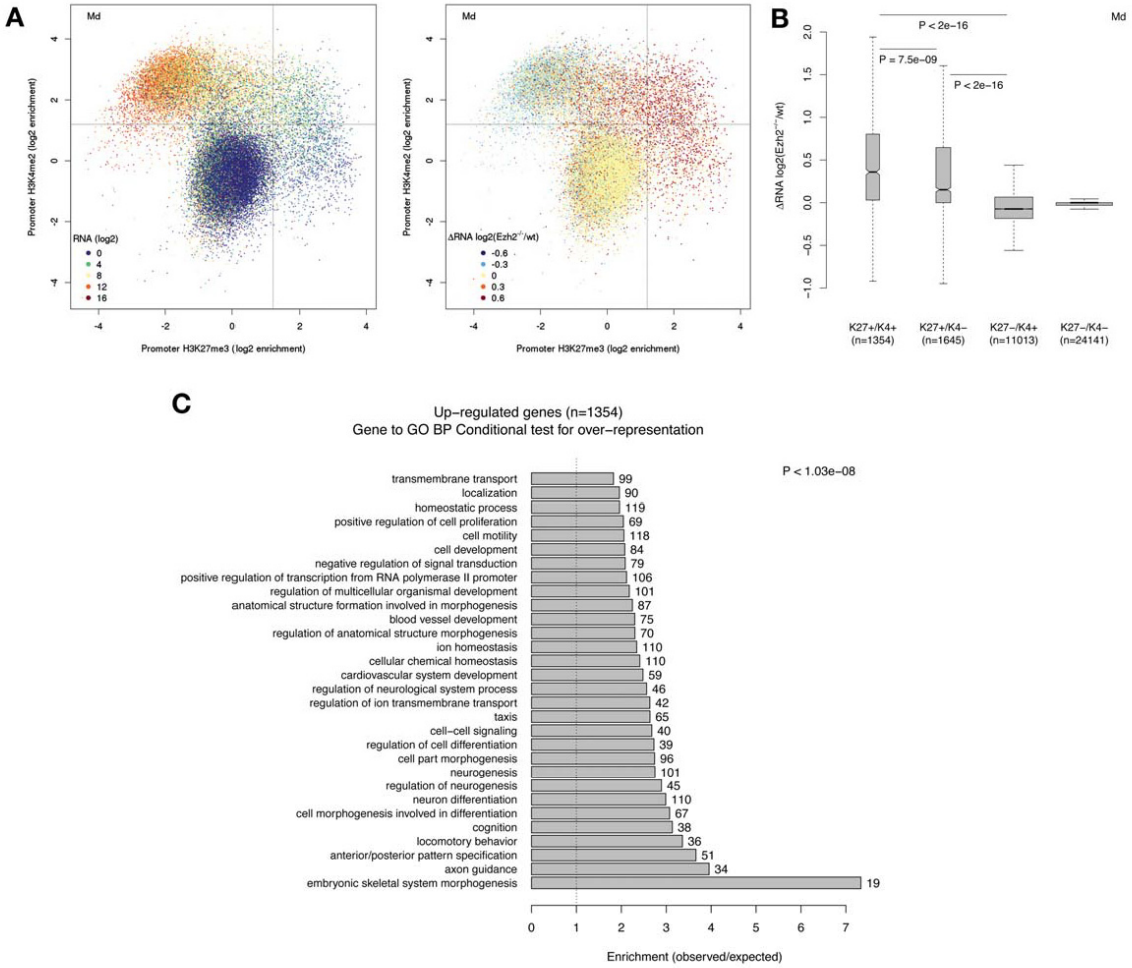
A
Md
Promoter H3K4me2 (log2 enrichment)
Promoter H3K27me3 (log2 enrichment)
RNA (log2)
0
4
8
12
16
ΔRNA log2(Ezh2−/−/wt)
-0.6
-0.3
0
0.3
0.6
B
Md
P < 2e−16
P = 7.5e−09
P < 2e−16
ΔRNA log2(Ezh2−/−/wt)
K27+/K4+ (n=1354)
K27+/K4− (n=1645)
K27−/K4+ (n=11013)
K27−/K4− (n=24141)
C
Up−regulated genes (n=1354)
Gene to GO BP Conditional test for over−representation
P < 1.03e−08
transmembrane transport 99
localization 90
homeostatic process 119
positive regulation of cell proliferation 69
cell motility 118
cell development 84
negative regulation of signal transduction 79
positive regulation of transcription from RNA polymerase II promoter 106
regulation of multicellular organismal development 101
anatomical structure formation involved in morphogenesis 87
blood vessel development 75
regulation of anatomical structure morphogenesis 70
ion homeostasis 110
cellular chemical homeostasis 110
cardiovascular system development 59
regulation of neurological system process 46
regulation of ion transmembrane transport 42
taxis 65
cell−cell signaling 40
regulation of cell differentiation 39
cell part morphogenesis 96
neurogenesis 101
regulation of neurogenesis 45
neuron differentiation 110
cell morphogenesis involved in differentiation 67
cognition 38
locomotory behavior 36
anterior/posterior pattern specification 51
axon guidance 34
embryonic skeletal system morphogenesis 19
Enrichment (observed/expected)

Figure 6

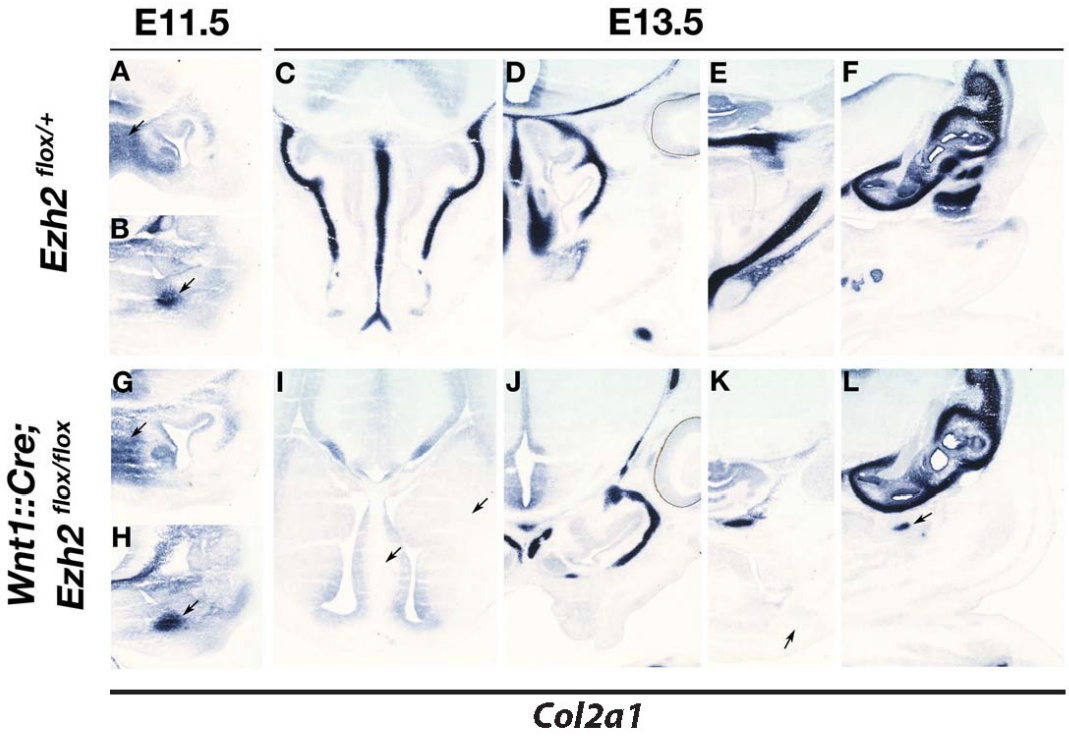
E11.5
E13.5
A
B
C
D
E
F
G
H
I
J
K
L
Ezh2 flox/+
Wnt1::Cre;
Ezh2 flox/flox
Col2a1

3.7 Supplemental Figures

Figure S1 – UCSC Genome Browser snapshots of RNA-seq and ChIP-seq data of control NCCs at Hoxa, Hoxb, Hoxc and Hoxd clusters (1Mb scale). Gray track= input, red track=H3K27me3, black trak= RNA, green boxes= CGI, blue boxes= ref genes, red box= *Hox* gene cluster.

Figure S2 – UCSC Genome Browser snapshots of RNA-seq and ChIP-seq data of control NCCs at Hoxb, Hoxc and Hoxd clusters in Mx, Md and Hy samples. Highlighted is the *Hoxb2* genomic locus. Gray track= input; blue tracks= H3K27ac, green tracks= H3K4me2; red tracks= H3K27me; black track= RNA

Figure S3 – Phenotypic effects of *Hoxa5* conditional overexpression in NCCs. External view of Control (A) and *Wnt1::Cre;Hoxa5-IRES-GFP* E18.5 overexpressing fetuses (B). Respective skeletal preparation of Control (C) and *Wnt1::Cre;Hoxa5-IRES-GFP* overexpressing fetuses (D) showing severe impairment of jaws and frontal bone formation.

Figure S4 - UCSC Genome Browser snapshots of RNA-seq and ChIP-seq data of *Ezh2* mutant NCCs at Hoxb, Hoxc and Hoxd clusters in Mx, Md and Hy samples. Gray track= input; red tracks= H3K27me; black track= RNA

Figure S5 – *Crabp1 in situ* Hybridizations on E10.5 embryos. Semilateral (A) and dorsal view (C) of control embryos. Semilateral (B) and dorsal view (D) of *Wnt1::Cre; Ezh2$^{f/f}$* embryos. Unaltered pattern of migration of different antero-posterior migrating cranial NCC streams is observed.

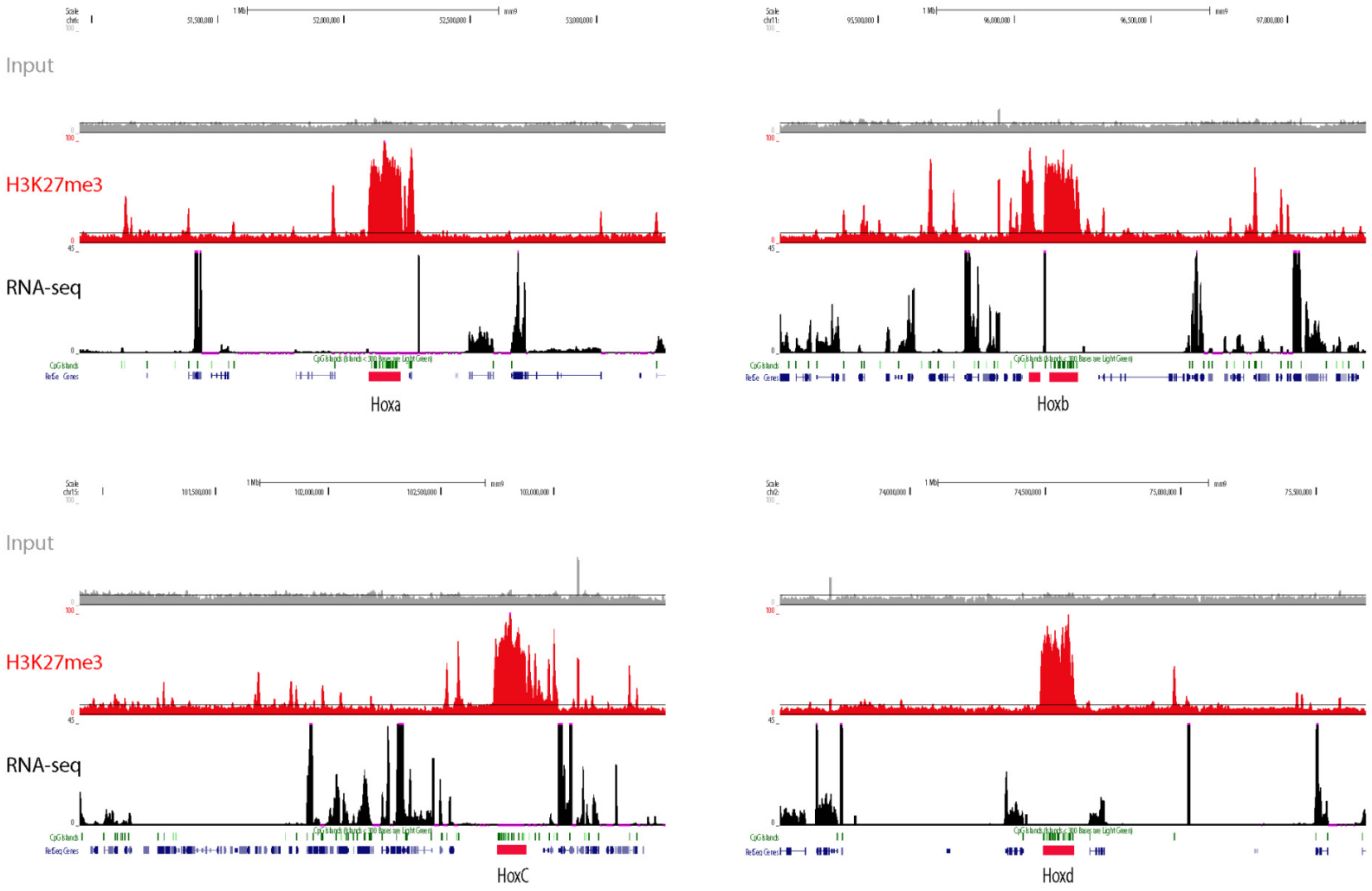
Input
H3K27me3
RNA-seq
Hoxa
Hoxb
Input
H3K27me3
RNA-seq
HoxC
Hoxd

Figure S1

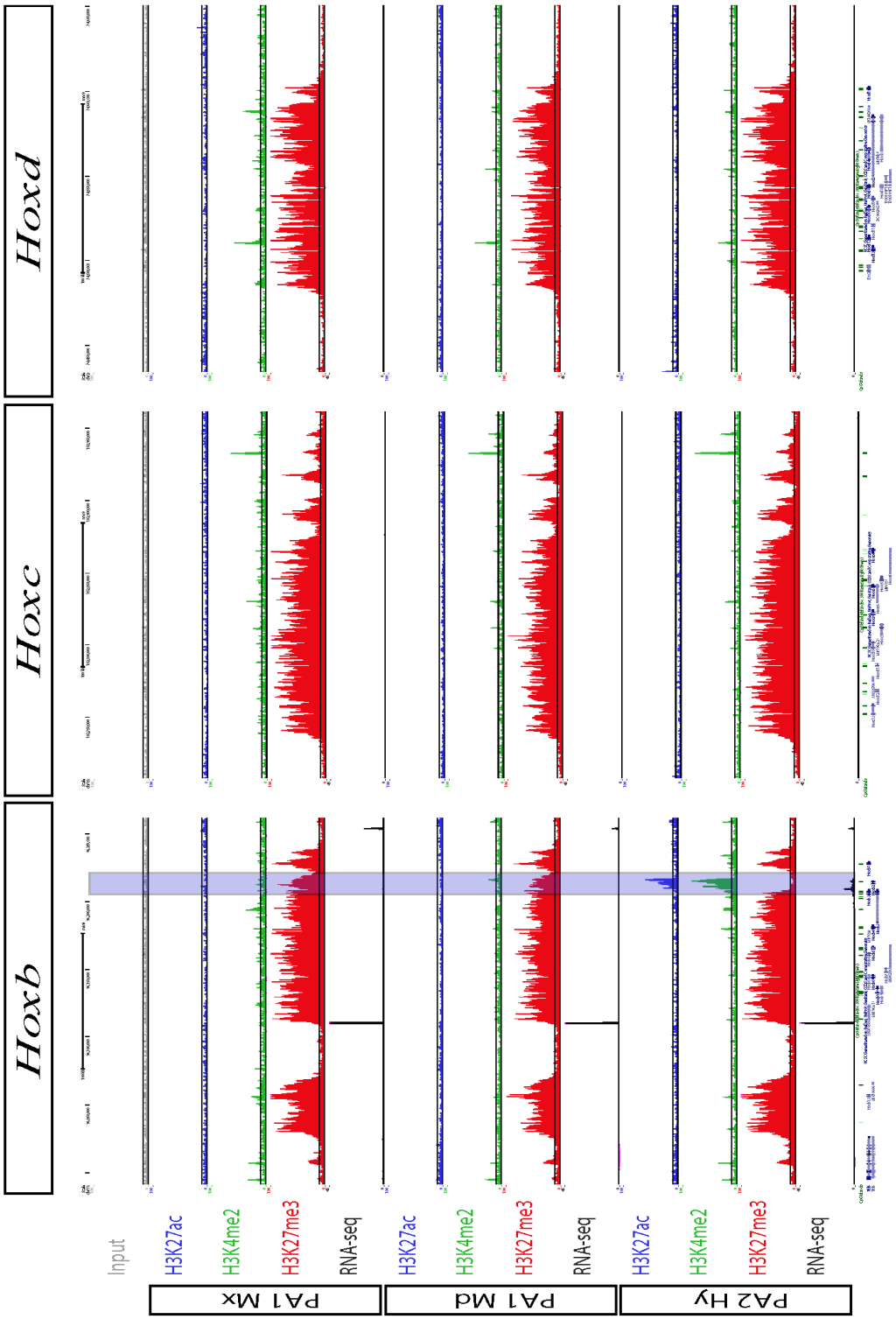
Hoxb
Hoxc
Hoxd
Input
H3K27ac
H3K4me2
H3K27me3
RNA-seq
H3K27ac
H3K4me2
H3K27me3
RNA-seq
H3K27ac
H3K4me2
H3K27me3
RNA-seq
PA1 Mx
PA1 Md
PA2 Hy

Figure S2

Figure S3

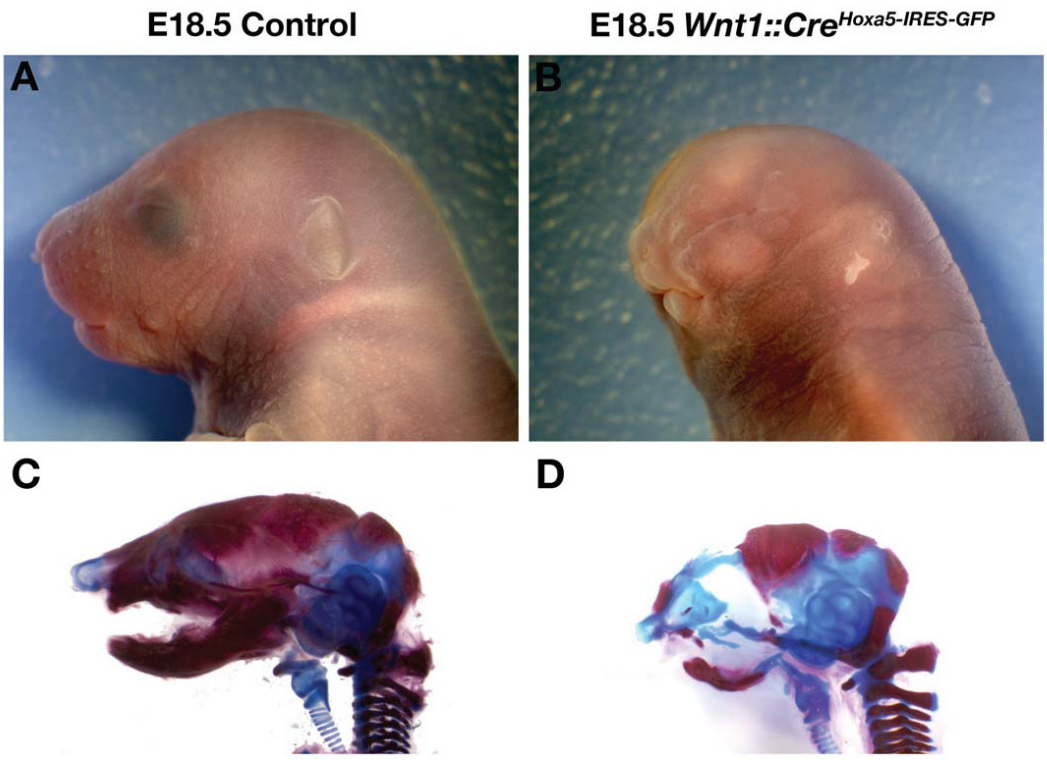

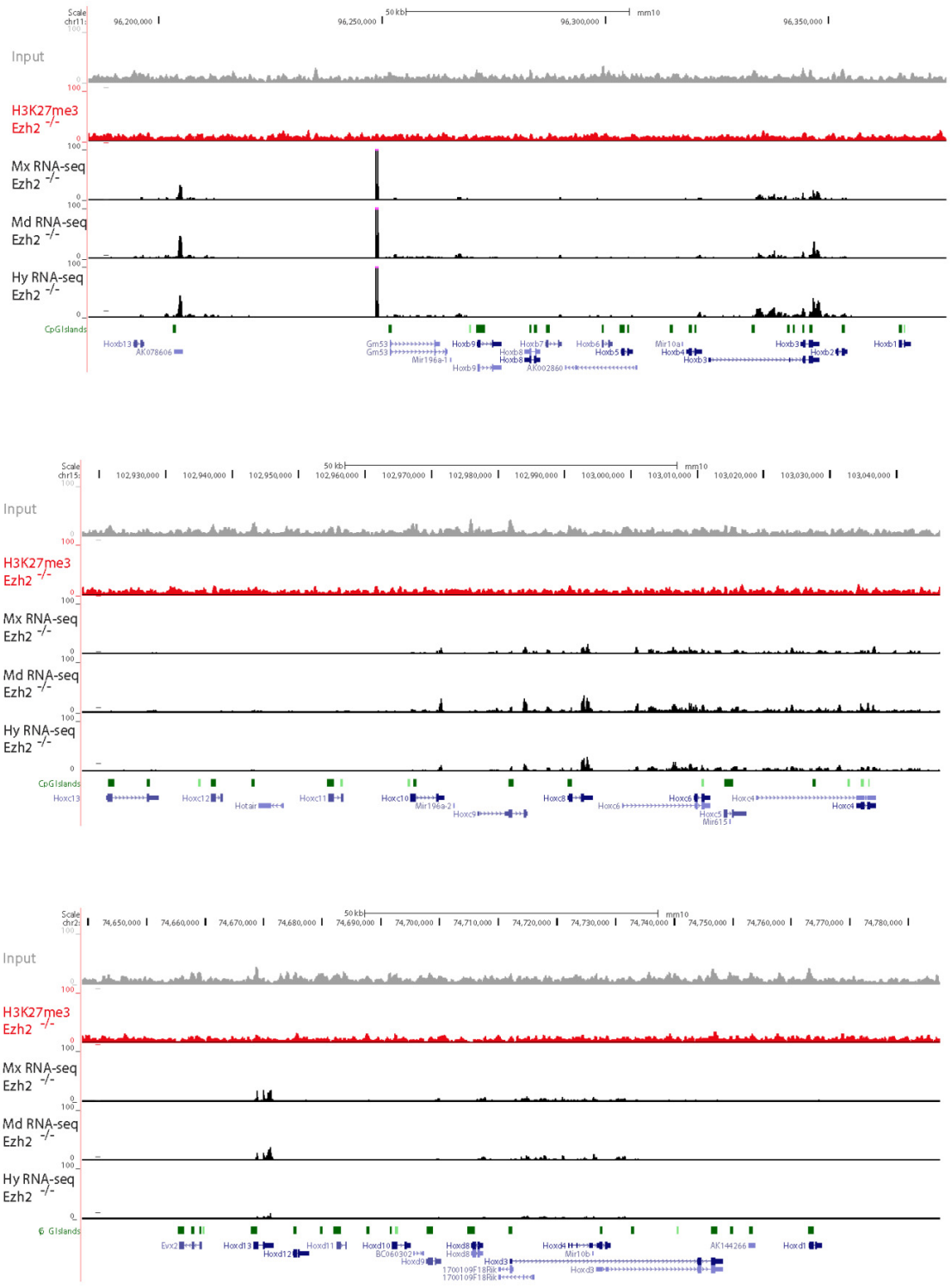
Input
H3K27me3 Ezh2 -/-
Mx RNA-seq Ezh2 -/-
Md RNA-seq Ezh2 -/-
Hy RNA-seq Ezh2 -/-
CpG Islands
Input
H3K27me3 Ezh2 -/-
Mx RNA-seq Ezh2 -/-
Md RNA-seq Ezh2 -/-
Hy RNA-seq Ezh2 -/-
CpG Islands
Input
H3K27me3 Ezh2 -/-
Mx RNA-seq Ezh2 -/-
Md RNA-seq Ezh2 -/-
Hy RNA-seq Ezh2 -/-
CpG Islands

Figure S4

Figure S5

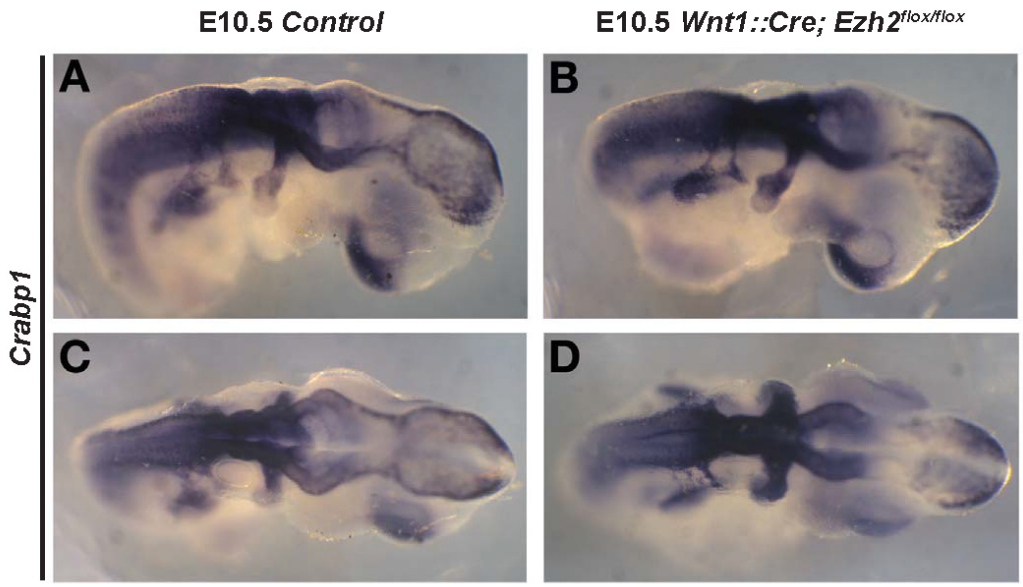

3.8 REFERENCES

Azuara V., Perry, P., Sauer, S., Spivakov, M., Jørgensen, H.F., John, R.M., Gouti, M., Casanova, M., Warnes, G., Merkenschlager, M., Fisher, A.G. 2006. Chromatin signatures of pluripotent cell lines. Nat Cell Biol., May;8(5):532-8.

Baltzinger, M., Ori, M., Pasqualetti, M., Nardi, I., Rijli, F.M., 2005. Hoxa2 knockdown in Xenopus results in hyoid to mandibular homeosis. Dev Dyn 234, 858-867.

Bantignies, F., Roure, V., Comet, I., Leblanc, B., Schuettengruber, B., Bonnet, J., Tixier, V., Mas, A., Cavalli, G., 2011. Polycomb-dependent regulatory contacts between distant Hox loci in Drosophila. Cell, Jan 21;144(2):214-26

Bernstein, B.E., Mikkelsen, T.S., Xie, X., Kamal, M., Huebert, D.J., Cuff, J., Fry, B., Meissner, A., Wernig, M., Plath, K., Jaenisch, R., Wagschal, A., Feil, R., Schreiber, S.L., Lander, E.S. 2006. A bivalent chromatin structure marks key developmental genes in embryonic stem cells.Cell., Apr 21;125(2):315-26.

Beverdam, A., Merlo, G. R., Paleari, L., Mantero, S., Genova, F., Barbieri, O., Janvier, P., Levi, G. (2002). Jaw transformation with gain of symmetry after Dlx5/Dlx6 inactivation: mirror of the past? Genesis 34, 221-227

Boyer, L.A., Plath, K., Zeitlinger, J., Brambrink, T., Medeiros, L.A., Lee, T.I., Levine, S.S., Wernig, M., Tajonar, A., Ray, M.K., Bell, G.W., Otte, A.P., Vidal, M., Gifford, D.K., Young, R.A., Jaenisch, R., 2006. Polycomb complexes repress developmental regulators in murine embryonic stem cells. *Nature* 441: 349–353.

Calloni, G.W., Glavieux-Pardanaud, C., Le Douarin, N.M., Dupin, E. 2007. Sonic Hedgehog promotes the development of multipotent neural crest progenitors endowed with both mesenchymal and neural potentials. Proc Natl Acad Sci U S A. 2007 Dec 11;104(50):19879-84

Couly, G., Grapin-Botton, A., Coltey, P., Ruhin, B., Le Douarin, N.M., 1998. Determination of the identity of the derivatives of the cephalic neural crest: incompatibility between Hox gene expression and lower jaw development. Development (Cambridge, England) 125, 3445-3459.

Creuzet, S., Couly, G., Vincent, C., Le Douarin, N.M., 2002. Negative effect of Hox gene expression on the development of the neural crest-derived facial skeleton. Development (Cambridge, England) 129, 4301-4313.

Danielian, P.S., Muccino, D., Rowitch, D.H., Michael, S.K., McMahon, A.P., 1998. Modification of gene activity in mouse embryos in utero by a tamoxifen-inducible form of Cre recombinase. Curr Biol 8, 1323-1326.

De Bellard, M.E., Ching, W., Gossler, A., Bronner-Fraser, M., 2002. Disruption of segmental neural crest migration and ephrin expression in delta-1 null mice. Dev Biol., Sep 1;249(1):121-30.

Depew, M. J., Lufkin, T., Rubenstein, J.L. (2002). Specification of jaw subdivisions by Dlx genes. *Science* 298, 381-385.

Dupin, E., Calloni, G.W., Le Douarin, N.M., 2010. The cephalic neural crest of amniote vertebrates is composed of a large majority of precursors endowed with neural, melanocytic, chondrogenic and osteogenic potentialities. Cell Cycle., Jan 15;9(2):238-49.

Dupin, E., Sommer, L., 2012. Neural crest progenitors and stem cells: from early development to adulthood. Developmental biology 366, 83-95.

Gavalas, A., Studer, M., Lumsden, A., Rijli, F.M., Krumlauf, R., Chambon, P., 1998. Hoxa1 and Hoxb1 synergize in patterning the hindbrain, cranial nerves and second pharyngeal arch. Development, 125, pp. 1123–1136

Gendron-Maguire, M., Mallo, M., Zhang, M., Gridley, T., 1993. Hoxa-2 mutant mice exhibit homeotic transformation of skeletal elements derived from cranial neural crest. Cell 75, 1317-1331.

Goldstein, A.M., Brewer, K.C., Doyle, A.M., Nagy, N., Roberts, D.J., 2005. BMP signaling is necessary for neural crest cell migration and ganglion formation in the enteric nervous system. Mech Dev., Jun;122(6):821-33.

Grammatopoulos, G.A., Bell, E., Toole, L., Lumsden, A., Tucker, A.S., 2000. Homeotic transformation of branchial arch identity after Hoxa2 overexpression. Development (Cambridge, England) 127, 5355-5365.

Hawkins, R.D., Hon, G.C., Lee, L.K., Ngo, Q., Lister, R., Pelizzola, M., Edsall, L.E., Kuan, S., Luu, Y., Klugman, S., Antosiewicz-Bourget, J., Ye, Z., Espinoza, C., Agarwahl, S., Shen, L., Ruotti, V., Wang, W., Stewart, R., Thomson, J.A., Ecker, J.R., Ren, B., 2010. Distinct epigenomic landscapes of pluripotent and lineage-committed human cells. Cell stem cell 6, 479-491.

Hunter, M.P., Prince, V.E., 2002. Zebrafish hox paralogue group 2 genes function redundantly as selector genes to pattern the second pharyngeal arch. Developmental biology 247, 367-389.

Isono, K., Fujimura, Y., Shinga, J., Yamaki, M., J, O.W., Takihara, Y., Murahashi, Y., Takada, Y., Mizutani-Koseki, Y., Koseki, H., 2005. Mammalian polyhomeotic homologues Phc2 and Phc1 act in synergy to mediate polycomb repression of Hox genes. Molecular and cellular biology 25, 6694-6706.

Kimura, C., Takeda, N., Suzuki, M., Oshimura, M., Aizawa, S., Matsuo, I., 1997. Cis-acting elements conserved between mouse and pufferfish Otx2 genes govern the expression in mesencephalic neural crest cells. Development., Oct;124(20):3929-41.

Kontges, G., Lumsden, A., 1996. Rhombencephalic neural crest segmentation is preserved throughout craniofacial ontogeny. Development (Cambridge, England) 122, 3229-3242.

Ku, M., Koche, R.P., Rheinbay, E., Mendenhall, E.M., Endoh, M., Mikkelsen, T.S., Presser, A., Nusbaum, C., Xie, X., Chi, A.S., Adli, M., Kasif, S., Ptaszek, L.M., Cowan, C.A., Lander, E.S., Koseki, H., Bernstein, B.E., 2008. Genomewide analysis of PRC1 and PRC2 occupancy identifies two classes of bivalent domains. PLoS Genet 4: e1000242.

Lee, H.Y., Kleber, M., Hari, L., Brault, V., Suter, U., Taketo, M.M., Kemler, R., Sommer, L., 2004. Instructive role of Wnt/beta-catenin in sensory fate specification in neural crest stem cells. Science; 303:1020-3.

Makki, N., Capecchi, M.R., 2010. Hoxa1 lineage tracing indicates a direct role for Hoxa1 in the development of the inner ear, the heart, and the third rhombomere. Developmental biology 341, 499-509.

Margueron, R., Reinberg, D., 2011. The Polycomb complex PRC2 and its mark in life. Nature 469, 343-349.

Minoux, M., Antonarakis, G.S., Kmita, M., Duboule, D., Rijli, F.M., 2009. Rostral and caudal pharyngeal arches share a common neural crest ground pattern. Development (Cambridge, England) 136, 637-645.

Minoux, M., Rijli, F.M., 2010. Molecular mechanisms of cranial neural crest cell migration and patterning in craniofacial development. Development (Cambridge, England) 137, 2605-2621.

Murphy, P., Hill, R.E., 1991. Expression of the mouse labial-like homeobox-containing genes, Hox 2.9 and Hox 1.6, during segmentation of the hindbrain. Development (Cambridge, England) 111, 61-74.

Noordermeer, D., Leleu, M., Splinter, E., Rougemont, J., De Laat, W., Duboule, D., 2011. The dynamic architecture of Hox gene clusters. Science. Oct 14; 334 (6053):222-5

Pasqualetti, M., Ori, M., Nardi, I., Rijli, F.M., 2000. Ectopic Hoxa2 induction after neural crest migration results in homeosis of jaw elements in Xenopus. Development (Cambridge, England) 127, 5367-5378.

Peters, H., Wilm, B., Sakai, N., Imai, K., Maas, R., Balling, R., 1999. Pax1 and Pax9 synergistically regulate vertebral column development. Development (Cambridge, England) 126, 5399-5408.

Pindyurin, A.V., van Steensel, B., 2012. Hox in space: gene cluster regulation linked to folding of chromatin. Nucleus.; Mar 1;3(2):118-22.

Rijli, F.M., Mark, M., Lakkaraju, S., Dierich, A., Dolle, P., Chambon, P., 1993. A homeotic transformation is generated in the rostral branchial region of the head by disruption of Hoxa-2, which acts as a selector gene. Cell 75, 1333-1349.

Santagati, F., Minoux, M., Ren, S.Y., Rijli, F.M., 2005. Temporal requirement of Hoxa2 in cranial neural crest skeletal morphogenesis. Development (Cambridge, England) 132, 4927-4936.

Santagati, F., Rijli, F.M., 2003. Cranial neural crest and the building of the vertebrate head. Nat Rev Neurosci 4, 806-818.

Sato, T., Kurihara, Y., Asai, R., Kawamura, Y., Tonami, K., Uchijima, Y., Heude, E., Ekker, M., Levi, G., Kurihara, H. (2008). *An* endothelin-1 switch specifies maxillomandibular identity*. Proc. Natl. Acad. Sci. USA* 105*,* 18806-18811*.*

Shah, N.M., Groves, A.K., Anderson, D.J. 1996. Alternativeneural crest cell fates are instructively promoted by TGFbeta superfamily members. Cell; 85:331-43.

Shen X, Liu Y, Hsu YJ, Fujiwara Y, Kim J, Mao X, Yuan GC, Orkin SH. (2008). EZH1 mediates methylation on histone H3 lysine 27 and complements EZH2 in maintaining stem cell identity and executing pluripotency.Mol Cell., Nov 21;32(4):491-502

Soshnikova, N., Duboule, D., 2009. Epigenetic temporal control of mouse Hox genes in vivo. Science 324, 1320-1323.

Takihara, Y., Tomotsune, D., Shirai, M., Katoh-Fukui, Y., Nishii, K., Motaleb, M.A., Nomura, M., Tsuchiya, R., Fujita, Y., Shibata, Y., Higashinakagawa, T., Shimada, K., 1997. Targeted disruption of the mouse homologue of the Drosophila polyhomeotic gene leads to altered anteroposterior patterning and neural crest defects. Development (Cambridge, England) 124, 3673-3682.

Tomotsune, D., Shirai, M., Takihara, Y., Shimada, K., 2000. Regulation of Hoxb3 expression in the hindbrain and pharyngeal arches by rae28, a member of the mammalian Polycomb group of genes. Mechanisms of development 98, 165-169.

Trainor, P.A., Krumlauf, R., 2001. Hox genes, neural crest cells and branchial arch patterning. Curr Opin Cell Biol 13, 698-705.

Zhang, M., Kim, H.J., Marshall, H., Gendron-Maguire, M., Lucas, D.A., Baron, A., Gudas, L.J., Gridley, T., Krumlauf, R., Grippo, J.F., 1994. Ectopic Hoxa-1 induces rhombomere

transformation in mouse hindbrain. Development (Cambridge, England) 120, 2431-2442.

Chapter 4: Research Article

4.1 "Ezh2 Orchestrates Topographic Migration and Connectivity of Mouse Precerebellar Neurons"

Abstract

We investigated the role of histone methyltransferase Ezh2 in tangential migration of mouse precerebellar pontine nuclei, the main relay between neocortex and cerebellum. By counteracting the sonic hedgehog pathway, Ezh2 represses Netrin1 in dorsal hindbrain, which allows normal pontine neuron migration. In Ezh2 mutants, ectopic Netrin1 derepression results in abnormal migration and supernumerary nuclei integrating in brain circuitry. Moreover, intrinsic topographic organization of pontine nuclei according to rostrocaudal progenitor origin is maintained throughout migration and correlates with patterned cortical input. Ezh2 maintains spatially restricted Hox expression, which, in turn, regulates differential expression of the repulsive receptor Unc5b in migrating neurons; together, they generate subsets with distinct responsiveness to environmental Netrin1. Thus, Ezh2-dependent epigenetic regulation of intrinsic and extrinsic transcriptional programs controls topographic neuronal guidance and connectivity in the cortico-ponto-cerebellar pathway.

Author contribution statement: Experimentally, I participated to the collection and isolation of biological material for chromatin analysis and performed part of these assays. I contributed to the study analysis and interpretation of the relative results.

21. S. E. McGuire, M. Deshazer, R. L. Davis, *Prog. Neurobiol.* **76**, 328 (2005).
22. A. M. Dacks, J. B. Dacks, T. A. Christensen, A. J. Nighorn, *Insect Biochem. Mol. Biol.* **36**, 741 (2006).

Acknowledgments: The authors thank C. Reisenman, R. Alarcón, A. Dacks, G. Davidowitz, and J. Bronstein for advice and assistance; C. Hedgcock and F. van Breugal for images of flowers and moths; and M. Dickinson and H. Bradshaw for manuscript comments. This work was supported by NSF grants IOS 0822709 to J.A.R. and CHE 0216226 to L.A., and NIH grant R01-DC-02751 to J.G.H.

Supplementary Materials
www.sciencemag.org/cgi/content/full/science.1225483/DC1
Materials and Methods
Figs. S1 to S7
Tables S1 to S5
References (*23*–*36*)

1 June 2012; accepted 9 November 2012
Published online 6 December 2012;
10.1126/science.1225483

Ezh2 Orchestrates Topographic Migration and Connectivity of Mouse Precerebellar Neurons

Thomas Di Meglio,[1*] Claudius F. Kratochwil,[1,2*] Nathalie Vilain,[1] Alberto Loche,[1,2] Antonio Vitobello,[1,2] Keisuke Yonehara,[1] Steven M. Hrycaj,[3] Botond Roska,[1,2] Antoine H. F. M. Peters,[1,2] Anne Eichmann,[3,4] Deneen Wellik,[5] Sebastien Ducret,[1] Filippo M. Rijli[1,2]†

We investigated the role of histone methyltransferase *Ezh2* in tangential migration of mouse precerebellar pontine nuclei, the main relay between neocortex and cerebellum. By counteracting the sonic hedgehog pathway, *Ezh2* represses *Netrin1* in dorsal hindbrain, which allows normal pontine neuron migration. In *Ezh2* mutants, ectopic *Netrin1* derepression results in abnormal migration and supernumerary nuclei integrating in brain circuitry. Moreover, intrinsic topographic organization of pontine nuclei according to rostrocaudal progenitor origin is maintained throughout migration and correlates with patterned cortical input. *Ezh2* maintains spatially restricted *Hox* expression, which, in turn, regulates differential expression of the repulsive receptor *Unc5b* in migrating neurons; together, they generate subsets with distinct responsiveness to environmental *Netrin1*. Thus, *Ezh2*-dependent epigenetic regulation of intrinsic and extrinsic transcriptional programs controls topographic neuronal guidance and connectivity in the cortico-ponto-cerebellar pathway.

In mammals, cortical motor and sensory information is mostly relayed to the cerebellum via the hindbrain precerebellar pontine nuclei (PNs), which include pontine gray and reticulotegmental nuclei. The developing hindbrain is rostrocaudally segregated into progenitor compartments, or rhombomeres (r1 to r8) (*1*), genetically defined by nested *Hox* gene expression (*2*). Mouse PN neurons are generated from r6 to r8 lower rhombic lip progenitors (*3*), undergo a long-distance caudorostral tangential migration via the anterior extramural stream (AES), and settle beside the ventral midline (Fig. 1, A and B) (*4*, *5*). Intrinsic expression of transcription factors and guidance receptors and extrinsic distribution of ligands are important for AES migration (*6*-*8*). However, little is known about the epigenetic regulation of these transcriptional programs. Here, we addressed the role of *Ezh2*, which is member of the Polycomb repressive complex 2 and trimethylates histone H3 at lysine 27 (H3K27me3) (*9*).

Ezh2 transcripts are maintained through late stages in lower rhombic lip progenitors, migratory stream, and PN neurons (fig. S1), whereas H3K27m3 is detected throughout the hindbrain (fig. S2). To conditionally inactivate *Ezh2*, we generated transgenic lines in which *Cre* is driven by rhombomere-specific enhancers in spatially restricted regions tiling the caudal hindbrain (*10*) (figs. S3 and S4). To assess cell-autonomous and/or region-specific non–cell autonomous *Ezh2* function in pontine neuron migration, we first crossed *Krox20::Cre* (*10*) to an $Ezh2^{fl/fl}$ allele (*10*) (*Krox20::Cre;*$Ezh2^{fl/fl}$). Inactivation in r3

[1]Friedrich Miescher Institute for Biomedical Research, Maulbeerstrasse 66, 4058 Basel, Switzerland. [2]University of Basel, 4056 Basel, Switzerland. [3]Yale Cardiovascular Research Center, Department of Internal Medicine, Yale University School of Medicine, New Haven, CT 06511–6664, USA. [4]CIRB (Centre Interdisciplinaire de Recherche en Biologie), Inserm U1050, 11 Place Marcelin Berthelot 75005 Paris, France. [5]Department of Cell and Developmental Biology, University of Michigan, Ann Arbor, MI 48109–2200, USA.

*These authors contributed equally to this work.
†To whom correspondence should be addressed. E-mail: filippo.rijli@fmi.ch

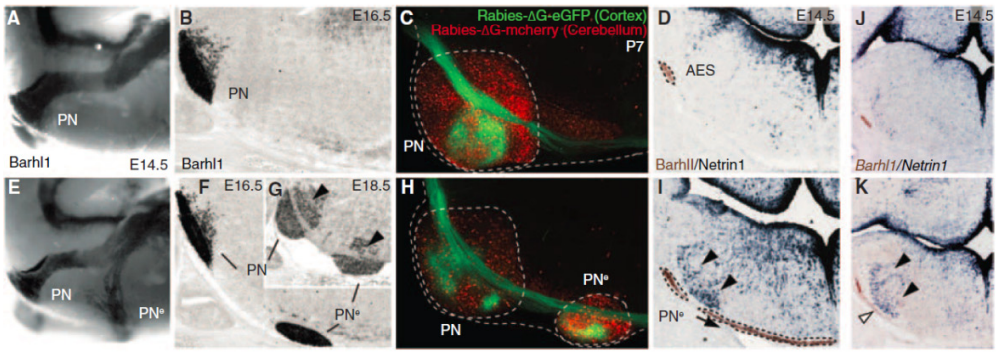

Fig. 1. *Ezh2* non–cell autonomous role in pontine neuron tangential migration. (**A**, **B**, **E**, **F**, and **G**) Migratory phenotypes in control (A) and (B) and *r5-6::Cre;*$Ezh2^{fl/fl}$ mutants (E) to (G). *Barhl1* in situ hybridization in E14.5 whole-mount (A) and (E), E16.5 (B) and (F), and E18.5 (G) sagittal sections. Pontine gray and reticulotegmental [arrowheads (G)] nuclei (PNs) are duplicated (PN^es). (**C** and **H**) Tracings from P7 cortex (rabies-ΔG-eGFP) and cerebellum (rabies-ΔG-mCherry) in controls (C) and *r5-6::Cre;*$Ezh2^{fl/fl}$ mutants (H). PNs and PN^es are connected to cortex and cerebellum. (**D**, **I**, **J**, and **K**) *Barlh1/Netrin1* expression in E14.5 control (D), *r5-6::Cre;*$Ezh2^{fl/fl}$ (I), *r5post::Cre;*$Ezh2^{fl/fl}$*;*$Shh^{fl/+}$ (K), and *r5post::Cre;*$Ezh2^{fl/fl}$*;*$Shh^{fl/fl}$ (J) coronal sections. Ectopic *Ntn1* [arrowheads: (I) and (K)] and PN^e ectopic migration [arrow and white arrowhead, respectively: (I) and (K)] are partially rescued (J).

and r5, which do not contribute to the pontine migratory stream (*3*), resulted in small ectopic PNs in posterior r5 (PN^es) (fig. S5), which supports an *Ezh2* non–cell autonomous role. Deletion in r5 and r6 (*r5-6::Cre;Ezh2*$^{fl/fl}$) resulted in a more prominent phenotype. A neuronal subset split from the migratory stream, turned ventrally, and generated an ectopic duplication of PNs (PN^es) (Fig. 1, E to G). PN^e neurons were nonrecombined *Ezh2*$^{+/+}$ H3K27me3$^+$ located within the r5- and r6-derived territory mostly devoid of H3K27me3 (fig. S2), which confirmed *Ezh2*'s non–cell autonomous function.

To assess whether PN^es integrated corticocerebellar connectivity, we carried out cortex-to-PN and cerebellum-to-PN tracings. We injected viral constructs expressing green fluorescent protein (GFP) (rabies-ΔG-GFP) and/or mCherry (rabies-ΔG-mCherry) in postnatal day 2 (P2) wild type and *r5-6::Cre;Ezh2*$^{fl/fl}$ and *Krox20::Cre;Ezh2*$^{fl/fl}$ mutants. At P7, PNs and PN^es triggered collateralization of corticospinal axons and innervated the cerebellum (Fig. 1, C and H, and fig. S6).

To evaluate *Ezh2* cell-autonomous function, we used the *Wnt1::Cre* deleter (*10*). *Ezh2* transcripts and H3K27me3 were selectively deleted from lower rhombic lip and migratory stream in *Wnt1::Cre;Ezh2*$^{fl/fl}$ mutants (figs. S2 and S7). Nonetheless, the mutation was not sufficient to induce ectopic posterior pontine neuron migration (Fig. 2, J and M, and figs. S5 and S7). The most severe phenotype was observed in *Hoxa2::Cre;Ezh2*$^{fl/fl}$ mutants, where *Ezh2* was inactivated in both AES neurons and their migratory environment, i.e., throughout r3- to r6- and dorsal r7- to r8-derived structures including the lower rhombic lip (figs. S2 and S3). The whole AES did not migrate anterior to r6 and settled into a single posterior ectopic nucleus (PN^e) (fig. S5). Thus, *Ezh2* has a non–cell autonomous role in AES migration, which is enhanced by a cell-autonomous function in progenitors and migrating neurons.

Netrin1 (Ntn1) and Slit1-3 are attractive or repulsive secreted cues that influence pontine neuron migration (*6, 7*). *Slit1-3* expression was not altered in embryonic day 14.5 (E14.5) *r5-6::Cre;Ezh2*$^{fl/fl}$ mutants (fig. S8). In contrast, *Ntn1*, normally expressed in floor-plate and ventral ventricular progenitors (Fig. 1D and fig. S5) (*11*), was ectopically expressed in dorsal progenitors and the mantle layer medially to the AES in *r5-6::Cre;Ezh2*$^{fl/fl}$, *Krox20::Cre;Ezh2*$^{fl/fl}$, *Hoxa2::Cre;Ezh2*$^{fl/fl}$, and *r5post::Cre;Ezh2*$^{fl/fl}$ mutants (Fig. 1I and fig. S5). Additional deletion of *Shh* was sufficient to prevent strong ectopic *Ntn1* activation in dorsal progenitors of E12.5 *r5post::Cre;Ezh2*$^{fl/fl}$*;Shh*$^{fl/fl}$ conditional mutants (fig. S5). At E14.5, ectopic *Ntn1* was almost undetectable and the Ezh2 knockout was partially rescued (Fig. 1, J and K, and fig. S5). Therefore, *Ezh2* is required to restrict *Ntn1* expression to ventral progenitors by silencing *Ntn1* in the dorsal neural tube. However, *Ezh2* deletion is not sufficient to ectopically induce *Ntn1*, which additionally requires Shh signaling from the floor plate. Thus, in the dorsal neural tube, *Ezh2*-mediated epigenetic repression of *Ntn1* may normally counteract Shh-mediated activation.

Ectopic and/or increased environmental Ntn1 levels may trigger premature migration toward the midline. In E14.5 *r5-6::Cre;Ezh2*$^{fl/fl}$ mutants, only a subset of pontine neurons split from the stream and entered the alternative ventral migratory pathway at the level of the ectopic *Ntn1*$^+$ domain (Fig. 1I and fig. S5), which suggested that AES neurons may display intrinsic differential responsiveness to Ntn1 signaling. To map the contributions of r6 (*r6RL*^{p}) or r7 and r8 (*r7-8RL*^{p}) lower rhombic lip–derived neuronal progenies into the pontine stream and nuclei (Fig. 2, B, C and H, and fig. S3), we crossed floxed reporter lines to *r5-6::Cre* or *r7post::Cre* (*Cre* is expressed up to the r6-r7 boundary) (fig. S3H) in which *Cre* is down-regulated before AES migration (fig. S4). *r6RL*^{p} mapping was confirmed by the tamoxifen-inducible *MafB::CreERT2* transgenic line, whose reporter expression pattern is restricted to r5 and r6, similar to that in *r5-6::Cre* (*10*) (fig. S3). To trace the whole precerebellar lower rhombic lip progeny (*r6-8RL*^{p}), we used *r5post::Cre* (figs. S3A and S4).

r6-8RL^p contributed to the whole PNs (fig. S3), whereas *r6RL*^{p} mapped to the most anterior (arrow in Fig. 2H and fig. S3), and *r7-8RL*^{p} filled the remaining posterior portions of PNs (fig. S3). This topographic organization of pontine neuronal subsets directly correlated with their relative position within the migratory stream. Namely, *r6RL*^{p} mapped to the dorsalmost AES, whereas *r7-8RL*^{p} contributed to the remaining portion ventrally to *r6RL*^{p} (Fig. 2, B and C). Thus, the precerebellar lower rhombic lip is rostrocaudally mapped onto the AES dorsoventral axis (Fig. 3E and fig. S1J) and, in turn, onto the PN rostrocaudal axis (fig. S1K), with neuronal subsets maintaining their relative position throughout migration and settling.

Next, we investigated molecular correlates of this intrinsic cellular regionalization and asked whether *Hox* paralog groups (PG) 2 to 5 maintain their spatially restricted progenitor expression patterns in pontine migratory stream and nuclei (Fig. 2). Indeed, *Hox* PG2 (*Hoxa2*/*Hoxb2*) and PG3 (*Hoxa3*/*Hoxb3*), expressed in the whole precerebellar rhombic lip, were correspondingly maintained throughout the pontine migratory stream and nuclei (*6*) (fig. S1). *Hoxb4* is normally expressed up to the r6-r7 boundary, whereas the *Hox PG5* rostral expression limit is posterior to *PG4* genes (*2*). In the AES and PNs, Hoxb4$^+$ neurons extended just ventrally and posteriorly, respectively, to *r6RL*^{p} (Fig. 2, C and D, and fig. S1L), whereas *Hoxa5* and *Hoxb5* transcripts and Hoxa5 protein mapped to the ventralmost migratory stream and posteriormost PNs, respectively (Fig. 2, A, F, H and I, and figs. S1 and S2). Simultaneous detection of Hoxa5 and ZsGreen in *r5-6::Cre;R26R*^{ZsGreen} specimens demonstrated rostrocaudal segregation of *r6RL*^{p} and Hoxa5$^+$ neurons within the PNs (Fig. 2H). To permanently label *Hoxa5*-expressing neurons, we generated a transgenic line in which *Cre* was inserted in-frame at the *Hoxa5* locus (*Hoxa5::Cre*) (*10*) (fig. S3). *Hoxa5::Cre*-expressing neurons segregated to the ventralmost AES and posteriormost PNs, faithfully overlapping endogenous Hoxa5 distribution (Fig. 2, D, E, F and G, and figs. S1F, S3, and S4). Thus, pontine neuron subsets of distinct rostrocaudal origin maintain their relative topographic positions and *Hox* codes throughout migration and settling within the target nucleus (Fig. 4A and fig. S1).

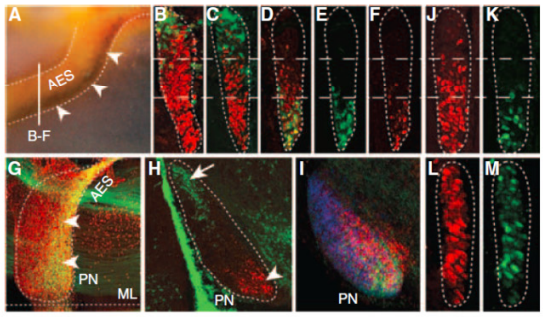

Fig. 2. Intrinsic topography of pontine migratory stream and PNs and *Ezh2*-dependent *Hox* regulation. (**A**) *Hoxb5/Barhl1* in situ hybridization on E15.5 whole-mount brain (lateral view). Arrowheads show Hoxb5$^+$ neuron ventral restriction in AES. (**B** and **C**) E15.5 *r5-6::Cre;R26R*^{ZsGreen} AES coronal sections costained with ZsGreen and Pax6 (red) (B) or ZsGreen and Hoxb4 (red) (C) showing complementary dorsal ZsGreen$^+$ and ventral Hoxb4$^+$ cell distributions [bar in (A) shows section level]. (**D** to **F**) E15.5 *Hoxa5::Cre;R26R*^{ZsGreen} AES sections showing partially overlapping ZsGreen and Hoxb4 (red) costainings with offset dorsal limits (D); ZsGreen$^+$ (E) and Hoxa5$^+$ (F) neurons display similar ventral restriction. (**G** and **H**) E15.5 whole-mount *Hoxa5::Cre;R26R*^{ZsGreen} (G) or *r5-6::Cre;R26R*^{ZsGreen} (H) sagittal sections costained with ZsGreen and Pax6 (red) or ZsGreen and Hoxa5 (red), respectively, illustrating posterior PN restriction of Hoxa5$^+$ neurons [arrowheads: (G) and (H)], and anterior restriction of r6-derived neurons [arrow (H)]. ML, ventral midline. (**I**) *Hoxb3/Hoxb4/Hoxb5* nested in situ expression patterns on PN sagittal section (**J** to **M**) Hoxb4 (red) and Hoxa5 (green) immunostaining of E15.5 *Wnt1::Cre;Ezh2*$^{fl/+}$ control (J) and (K) and *Wnt1::Cre;Ezh2*$^{fl/fl}$ mutant (L) and (M) AES. In (L) and (M), Hoxb4 and Hoxa5 lose their spatial restriction and are ectopically derepressed up to the dorsal edge of the AES.

Is *Ezh2* required to maintain *Hox* nested expression in migrating pontine neurons and PNs? In E14.5 *Wnt1::Cre;Ezh2*$^{fl/fl}$ and *Hoxa2::Cre;Ezh2*$^{fl/fl}$ mutants, Hoxb4, Hoxa5, and *Hoxb5* were ectopically expressed within the anterior lower rhombic lip and spread ventrodorsally throughout the pontine migratory stream (Fig. 2, L and M, and figs. S2 and S7). Thus, by preventing *Hox PG4* and *PG5* expression in anterior precerebellar rhombic lip and migrating neuronal progeny, *Ezh2*-mediated repression contributes to the maintenance of molecular heterogeneity in the migratory stream. This, in turn, may underlie intrinsic differential response of migrating neuron subsets to environmental Ntn1.

Netrin-mediated attraction is counteracted by Unc5 repulsive receptors (*12*), and *Unc5c* inactivation results in variable ectopic migration of AES

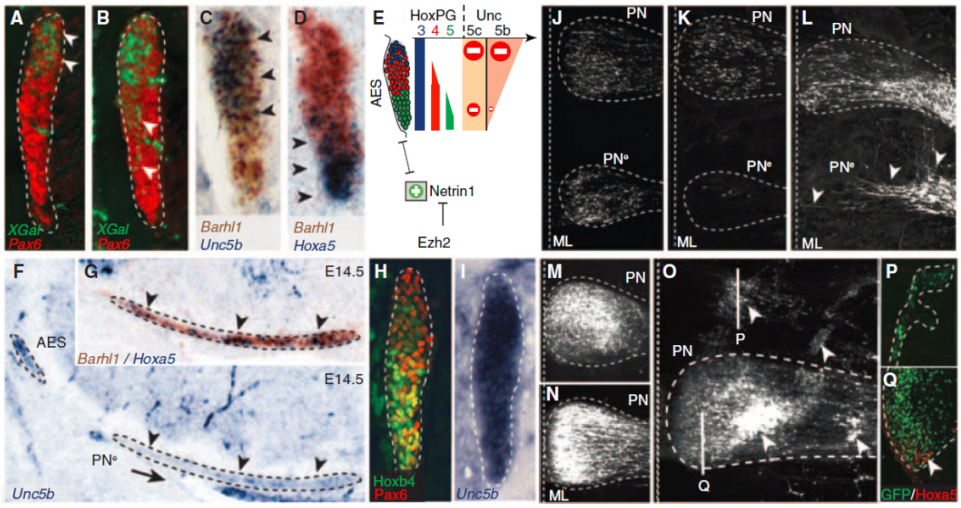

Fig. 3. *Ezh2*- and *Hox*-dependent regulation of *Unc5b* in pontine neuron migration. (**A** and **B**) X-gal (green) and Pax6 (red) costainings of E14.5 *Unc5b*$^{bGal/+}$ heterozygotes (A) and *Unc5b*$^{bGal/bGal}$ homozygotes (B) showing X-gal–stained cell distribution in AES (arrowheads). (**C** to **E**) *Unc5b*/*Barhl1* (C) and *Hoxa5*/*Barhl1* (D) in situ hybridization in E14.5 AES showing complementary dorsoventral expression of *Unc5b* and *Hoxa5* (arrowheads) and summary (E). (**F** and **G**) In *r5-6::Cre;Ezh2*$^{fl/fl}$ mutants, PN^{e} migrating neurons are *Unc5b*-negative (F) and *Hoxa5*$^{+}$/*Barhl1*$^{+}$ (G) (arrowheads). (**H** and **I**) In E14.5 *Hoxa5*$^{-/-}$/*Hoxb5*$^{-/-}$/*Hoxc5*$^{-/-}$ AES, *Unc5b* is up-regulated ventrally (I), whereas Hoxb4 and Pax6 are normally expressed (H). (**J** and **K**) In utero EP in E14.5 *r5-6::Cre;Ezh2*$^{fl/fl}$ mutants of Unc5b/Unc5c/eGFP strongly reduces at E18.5 ectopically migrating PN^{e} neurons (K), as compared with EP of eGFP (J), and partially rescues the phenotype. ML, ventral midline. (**L** to **Q**) In E13.5 wild type, EP of *Ntn1* results in posterior ectopic pontine neuron migration at E17.5, phenocopying *r5-6::Cre;Ezh2*$^{fl/fl}$ mutants [arrowheads (L)]. Although EP at E13.5 of *eGFP* (M) or *Unc5c/eGFP* constructs has no apparent effect on migration at E18.5 (N), EP of *Unc5b/eGFP* results in anterior ectopic migration and/or dorsal-lateral arrest [arrowheads (O)]. Immunostaining on sagittal sections shows that anterior ectopic GFP+/Unc5b^{+} electroporated cells are Hoxa5-negative (P); Hoxa5^{+} cells are normally restricted in posterior PN (Q).

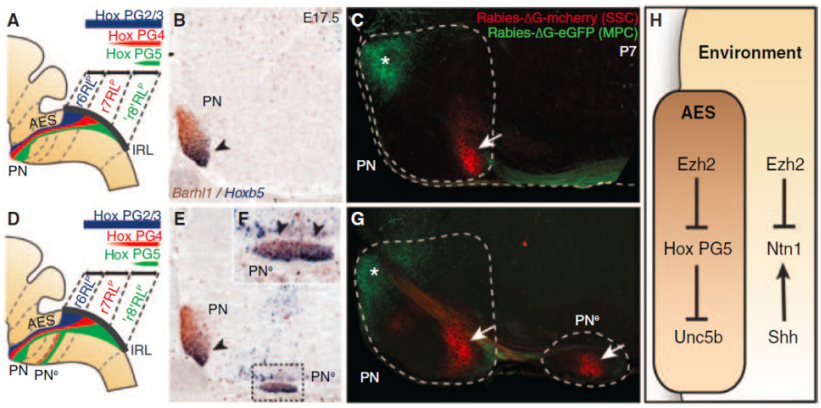

Fig. 4. PN regionalization and patterned cortical input. (**A**, **B**, **D**, **E**, and **F**), *Hox* expression summary in migrating pontine neurons of control (A) and *r5-6::Cre;Ezh2*$^{fl/fl}$ mutants (D). *Barhl1*/*Hoxb5* in situ hybridization on E17.5 sagittal sections (B), (E), and (F). In *r5-6::Cre;Ezh2*$^{fl/fl}$ mutants (E) and (F), Hoxb5^{+} neurons spread throughout the rostrocaudal extent of the ectopic nuclei (PN^{e}s) [arrowheads (F)], whereas, in PNs, they are normally posteriorly restricted as in control [arrowheads: (B) and (E)]. (**C** and **G**) Rabies-ΔG viruses injected in control visual/mediposterior cortex (MPC) and SSC anterogradely trace fibers into anterior (green,*) and posterior (red, arrow) PNs (C), respectively. In *r5-6::Cre;Ezh2*$^{fl/fl}$ mutants (G), PN^{e} lacks innervation by MPC, whereas it is innervated by SSC (arrow). (**H**) *Ezh2*- and *Hox*-dependent genetic circuitry of intrinsic and extrinsic Unc5b/Ntn1 regulation.

neurons (*13*). *Unc5c* is expressed in lower rhombic lip progenitors, down-regulated in migrating neurons, and reactivated upon approaching the midline (fig. S9) (*13*). Thus, *Unc5c* is unlikely to confer a dorsoventrally biased response of the AES to Ntn1. *Unc5b* has been involved in vascular development (*14*), though a role in neuronal development was not explored. We found a dorsoventral high-to-low density of cells expressing *Unc5b* (Fig. 3C and fig. S9) and β-galactosidase activity in $Unc5b^{bGal/+}$ fetuses (Fig. 3A). *Unc5b* expression was, in turn, down-regulated when the migratory stream turned toward the midline (fig. S9C). Dorsoventral *Unc5b* transcript distribution in the migratory stream anti-correlated with *Hox PG5* expression (Fig. 3, C and D). In E14.5 $Hoxa5^{-/-};Hoxb5^{-/-};Hoxc5^{-/-}$ compound mutants, *Unc5b* was up-regulated in ventral $Hoxb4^{+}$/$Pax6^{+}$ AES neurons (Fig. 3, H and I). Thus, Hox PG5 normally represses *Unc5b* in ventral AES neurons originating from posterior precerebellar lower rhombic lip.

In E14.5 $Unc5b^{bGal/bGal}$ null mutants, β-galactosidase^{+} cells partially lost their normal dorsal restriction and spread into ventral AES (Fig. 3B). Thus, *Unc5b* contributes to maintaining topographical organization of dorsal AES subsets. In E16.5 $Unc5c^{-/-}$ fetuses, dorsal *Unc5b*-expressing AES neurons maintained their normal migratory path, whereas ectopic neurons were *Hox* $PG5^{+}$ and mainly *Unc5b*-negative (fig. S9). Therefore, in the absence of *Unc5c*, ventral *Unc5b*-negative AES neurons become more sensitive to Ntn1-mediated attraction than dorsal *Unc5b*-expressing neurons. Similarly, in $r5\text{-}6::Cre;Ezh2^{fl/fl}$ mutants, *Unc5b*-expressing neurons remain dorsal and pursue their normal migration, whereas *Hox* $PG5^{+}$/*Unc5b*-negative neurons are preferentially influenced by Ntn1 up-regulation and ectopically attracted to the midline (Fig. 3, F and G, and fig. S2). Moreover, in $Hoxa2::Cre;Ezh2^{fl/fl}$ mutants, in which all pontine neurons are $Ezh2^{-/-}$/H3K27me3^{-} and migrate through an environment ectopically expressing *Ntn1* (fig. S5), all migrating neurons are prematurely attracted to an ectopic posterior midline position, are *Hox* $PG5^{+}$, and down-regulate *Unc5b* (figs. S2 and S7).

Next, *Unc5b/5c* overexpression by in utero electroporation (EP) of E14.5 lower rhombic lip progenitors was sufficient to cell-autonomously rescue the PN^{e} phenotype in $r5\text{-}6::Cre;Ezh2^{fl/fl}$ mutants [enhanced GFP–positive (eGFP^{+}) neuron quantification in PN^{e}s compared with PNs: eGFP ($n = 5$) 33.79% ± 0.1060; eGFP/Unc5b/5c ($n = 5$) 0.64% ± 0.0044; $P = 0.00011$] (Fig. 3, J and K), which demonstrated that elevating Unc5 receptor levels counteracts increased Ntn1-mediated attraction. Ntn1 overexpression by EP in E13.5 wild-type fetuses induced ectopic posterior migration of AES neurons (Fig. 3L), partially phenocopying the $r5\text{-}6::Cre;Ezh2^{fl/fl}$ mutant phenotype and showing that increasing Ntn1 is sufficient to cause ectopic ventral migration of neuronal subsets.

Furthermore, although overexpression of *Unc5c* in E13.5 wild-type fetuses had no apparent effect on AES migration (Fig. 3, M and N), *Unc5b* EP triggered ectopic anterior migration and/or a block in dorsal position of Hoxa5-negative pontine neuron subsets (Fig. 3, O to Q). Therefore, maintaining constitutively high Unc5b levels in migrating neurons prevents or delays turning toward the midline; the latter results in ectopic anterior migration. Conditional *Hoxa2* overexpression in rhombic lip derivatives by mating *Wnt1::Cre* with a *ROSA26::(lox-STOP-lox)Hoxa2*-internal ribosome entry site (*IRES*)-*eGFP* ($Wnt1::Cre;R26R^{Hoxa2}$) allele (*10*) also resulted in anterior ectopic migration generating rostrally elongated PNs, which maintained high *Unc5b* expression, unlike in control mice (fig. S9). Therefore, although *Hox PG5* are involved in negatively regulating *Unc5b* in the ventral migratory stream, *Unc5b* expression in dorsal AES may be under *Hox PG2*-positive regulation and generates differential responses to environmental Ntn1.

Finally, we investigated whether the PN and PN^{e} patterning differences in $r5\text{-}6::Cre;Ezh2^{fl/fl}$ mutants result in distinct cortical inputs. In P7 $Pcp2::Cre;R26R^{tdTomato}$ animals (*10*) expressing *Cre* in medioposterior (including visual) cortex (MPC), *tdTomato*$^{+}$ axons projected onto the rostral PN, in agreement with (*15*), including the *r6RL*^{p} neuron subset (fig. S6). Coinjection of rabies-ΔG-GFP and rabies-ΔG-mCherry into visual and/or MPC and medial somatosensory cortex (SSC) resulted in rostral GFP^{+} and caudal mCherry^{+} axonal inputs onto the PNs, respectively (Fig. 4C). In $r5\text{-}6::Cre;Ezh2^{fl/fl}$ mutants, PN was targeted both by visual or MPC-derived GFP^{+} (rostrally) and SSC-derived mCherry^{+} (caudally) axons, whereas PN^{e} was innervated by SSC-derived though not visual/MPC-derived axons (Fig. 4G), correlating with their posterior *Hox* $PG5^{+}$ profile (Fig. 4, A, B, and D to F).

During radial migration, correlation to rostrocaudal position of origin is maintained through interaction with glial progenitors (*16*). How long-range tangentially migrating neurons (*17*) maintain information about their origin is less well understood. We show that the topographic migratory program of r6- to r8-derived pontine neurons is largely established in progenitor pools according to rostrocaudal origin and maintained in migrating neurons. We found similar organizational principles during lateral reticular nucleus migration (fig. S10). Moreover, the r2 to r5 rhombic lip also gives rise to neurons that migrate tangentially along a short dorsoventral extramural path and populate distinct brainstem cochlear nuclei with a rostrocaudal topography (*3*). On its caudorostral route, the precerebellar stream migrates ventrally to the cochlear stream (*3*), although they do not mix despite close cellular proximity, which suggests that rhombomere-specific programs may control appropriate precerebellar neuron position during tangential migration. Indeed, we show that the topography of r6 versus r7 versus r8 origin is preserved throughout migration, mapped along the dorsoventral axis of the pontine stream, and eventually within rostrocaudal subregions of the PNs, correlating with patterned cortical input. The transcriptional regulation of this tangential migratory program is epigenetically maintained (Fig. 4H). *Ezh2*-mediated repression maintains dorsoventrally restricted environmental distribution of attractive and/or repulsive cues, such as *Ntn1*, and an intrinsically heterogeneous *Hox* transcriptional program in the migratory stream that, in turn, provides neuronal subsets with distinct Unc5b-dependent responses to environmental Ntn1, and thus contributes to maintaining the neuronal position during migration.

References and Notes

1. A. Lumsden, R. Krumlauf, *Science* **274**, 1109 (1996).
2. S. Tümpel, L. M. Wiedemann, R. Krumlauf, *Curr. Top. Dev. Biol.* **88**, 103 (2009).
3. A. F. Farago, R. B. Awatramani, S. M. Dymecki, *Neuron* **50**, 205 (2006).
4. J. Altman, S. A. Bayer, *J. Comp. Neurol.* **257**, 529 (1987).
5. C. I. Rodriguez, S. M. Dymecki, *Neuron* **27**, 475 (2000).
6. M. J. Geisen *et al.*, *PLoS Biol.* **6**, e142 (2008).
7. K. T. Yee, H. H. Simon, M. Tessier-Lavigne, D. M. O'Leary, *Neuron* **24**, 607 (1999).
8. S. Nóbrega-Pereira, O. Marín, *Cereb. Cortex* **19** (Suppl. 1), i107 (2009).
9. R. Margueron, D. Reinberg, *Nature* **469**, 343 (2011).
10. Materials and methods are available as supplementary materials on *Science* Online.
11. E. Bloch-Gallego, F. Ezan, M. Tessier-Lavigne, C. Sotelo, *J. Neurosci.* **19**, 4407 (1999).
12. K. Hong *et al.*, *Cell* **97**, 927 (1999).
13. D. Kim, S. L. Ackerman, *J. Neurosci.* **31**, 2167 (2011).
14. X. Lu *et al.*, *Nature* **432**, 179 (2004).
15. T. B. Leergaard, J. G. Bjaalie, *Front. Neurosci.* **1**, 211 (2007).
16. P. Rakic, *Science* **241**, 170 (1988).
17. M. E. Hatten, *Annu. Rev. Neurosci.* **22**, 511 (1999).

Acknowledgments: We thank K. Balint, F. Boukhtouche, Y.-Y. Lee, C.-Y. Liang, D. Kraus, T. Mathivet, F. Santagati, J. F. Spetz, and A. Yallowitz for technical support and discussion. We are grateful to M. Tessier-Lavigne, S. H. Orkin, E. Callaway, V. Castellani, P. Mehlen, O. Nyabi, and J. Haigh for gifts of mouse lines, probes, or reagents. The mouse transgenic lines *r5-6::Cre*, *Hoxa2::Cre*, *r5post::Cre*, *r7post::Cre*, *Mafb::CreERT2*, *Hoxa5::Cre*, *ROSA26::(lox-STOPlox) Hoxa2-IRES-EGFP* generated in this research and their respective DNA constructs are available from F.M.R. under a material transfer agreement with the Friedrich Miescher Institute for Biomedical Research, Basel, Switzerland. The SAD G-eGFP and SAD G-mCherry G–deleted rabies viruses used in this research are available from E. M. Callaway under a material transfer agreement with Salk Institute for Biological Studies, La Jolla, CA, USA. T.D. is the recipient of a European Molecular Biology Organization Long-Term Fellowship. Work in F.M.R.'s laboratory is supported by the Swiss National Science Foundation (Sinergia CRSI33_127440), Association pour la Recherche sur la Sclérose en Plaques, and the Novartis Research Foundation.

Supplementary Materials

www.sciencemag.org/cgi/content/full/339/6116/204/DC1
Materials and Methods
Figs. S1 to S10
References (*18*–*37*)

27 August 2012; accepted 7 November 2012
10.1126/science.1229326

Supplementary Materials for

Ezh2 orchestrates topographic tangential migration and connectivity of mouse precerebellar neurons

Thomas Di Meglio*, Claudius F. Kratochwil*, Nathalie Vilain, Alberto Loche, Antonio Vitobello, Keisuke Yonehara, Steven M. Hrycaj, Botond Roska, Antoine H.F.M. Peters, Anne Eichmann, Deneen Wellik, Sebastien Ducret, and Filippo M. Rijli†.

* These authors contributed equally to this work
† To whom correspondence should be addressed: filippo.rijli@fmi.ch

This PDF file includes:

Materials and Methods

Generation of Hoxa5::Cre BAC line

The BAC clone RP23-20F21 (BACPAC Resources Center at Children's Hospital Oakland Research Institute, Oakland, Calif., USA) containing the entire *Hoxa* cluster was used as a template for bacterial recombination as described previously (*18*). The plasmid pN21-Cre was used to amplify a Cre-SV40polyA-Frt-Kanamycin-Frt cassette with 70-mer primers containing 50 nucleotides of homology (indicated as caps) surrounding the coding sequence of the *Hoxa5* first exon, such that *Cre* is inserted in-frame with the *Hoxa5* ATG codon. Forward primer: 5'ACGCACAAACGACCGCGAGCCACAAATCAAGCACACATATCAAAAAACAA atgtccaatttactgaccgt3'; reverse primer:, 5'CAAGACCCGCGCCCCCACGGACGCGTGGATCAGAAAACGGCTGGCTTTACt attccagaagtagtgagga3'. To obtain the *Hoxa5::Cre* BAC construct, EL250 bacteria containing the BAC RP23-20F21 were induced for recombination at 42°C and then electroporated with the Cre-SV40polyA-Frt-Kanamycin-Frt cassette. Bacteria were subsequently arabinose-induced for *Flpe* expression in order to remove the kanamycin cassette. Correct recombination and removal of the resistance gene in the *Hoxa5::Cre* BAC were tested by PCR, restriction enzyme digestion and sequencing. Before microinjection, the modified BAC was linearized by PI-SceI digestion. One founder was obtained that displayed the expected *Cre* expression pattern.

Generation of the MafB::CreERT2 line and tamoxifen treatment

The same approach as above was taken using the BAC clone BAC clone RP23-33A18 (BACPAC Resources Center at Children's Hospital Oakland Research Institute, Oakland, CA). The plasmid pN21-CreERT2 was used to amplify a CreERT2-SV40polyA-Frt-Kanamycin-Frt cassette by using 70-mer primers containing 50 nucleotides of homology (indicated as caps) surrounding the coding sequence of the *MafB* gene, such that the Cre is inserted in-frame with the *MafB* ATG codon.

Forward primer:

5'GGCCGCAAAGTTTTCCCCGCGGCAGCGGCGGCTGAGCCTCGCTTTTAGCGA TGtccaatttactgaccgt3';

reverse primer:

5'GAATAGGGAGTCTGGGCCAGGGCAAGGGCGGGGGCCGGACCCGCCAGGAC ctattccagaagtagtgagga3'.

Tamoxifen was dissolved in corn oil and administered by oral gavage at E7.5 (1mg; 100µl of 10mg/ml stock solution).

Generation of r5post::Cre, r5-6::Cre and r7post::Cre lines

We generated transgenic mice in which *Cre* is driven by rhombomere-specific enhancers of *Hoxb3* (*19*) (*r5-post::Cre*), *Hoxa3* (*20*) (*r5-6::Cre*), or *Hoxb4* (*21*) (*r7post::Cre*) (figs. S3 and S4), which were mated to Gt(ROSA)26Sor ($R26R)^{lacZ}$ (*22*), $R26R^{tdTomato}$ (*23*), or $R26R^{ZsGreen}$ (*23*) reporter lines.

The mouse lines were created by replacing the LacZ gene of the pKS-ß-globin-lacZ vector (BGZ40) (*24*) with a Cre cassette (Clontech) using homologous recombination. Enhancers for *Hoxb3* (*19*) (*r5-post::Cre*, 483 bp), *Hoxa3* (*20*) (*r5-6::Cre*, 629 bp) and

Hoxb4 (*21*) (*r7-post::Cre*, 400 bp) were amplified by PCR from genomic DNA using the following primers: *r5-post::Cre:* forward, 5`ATATCCGCGGGATCGGAGAGGAGAGGGCAA; reverse, 5` CGCGACTAGTGATCTCCAAGGTCCCCTTTCA. *r5-6::Cre:* forward, 5`ATATCCGCGGCAACTTGAAAGGGAAGAGCC; reverse, 5` CGCGACTAGTGATATCAAATAGCAGCGAATCTTC. *r7-post::Cre:* forward, 5`ATATCCGCGGTCCTTGGAAGGTATGAATAG; reverse, 5` CGCGACTAGTTGTTACCTCTGAGCCTCTTG. The PCR bands were purified and inserted 5` of the ß-globin promoter using restriction sites FslI and XhoI (*r5-6::Cre*) and BglI and PvuII (*r5-post::Cre, r7-post::Cre*), thus generating constructs consisting of an enhancer, a ß-globin minimal promoter and Cre recombinase encoding sequence. The constructs were linearized, purified and microinjected into the pronuclei of blastocyst embryos. Founders were identified by PCR and screened at P0 after crossing with $R26R^{lacZ}$ animals. 72 animals were genotyped (19 for *r5post::Cre*; 38 for *r5-6::Cre*; 15 for *r7post::Cre*). 19 were positive for Cre (8 for *r5post::Cre*; 8 for *r5-6::Cre*; 3 for *r7post::Cre*). 3/8 showed the expected recombination pattern at P0 for *r5post::Cre*; 2/8 for *r5-6::Cre* and 1/3 for *r7post::Cre*, while the other founders showed no, ubiquitous or ectopic patterns of recombination.

Generation of Hoxa2::Cre line

For the generation of the *Hoxa2::Cre* transgenic line a 3.5kb EcoRI fragment upstream to the *Hoxa2* promoter (from -3585 to -1) was obtained from the plasmid p314R (*25*) and subcloned in a native orientation upstream to a β-globin minimal promoter, the Cre gene and a SV40 polyA signal. The transgene fragment was excised by digestion with SalI and

NotI, and purified before microinjection.

Generation of the ROSA::(lox-STOP-lox)Hoxa2-IRES-EGFP mouse line

The conditional Hoxa2 overexpression mouse line was generated by using the Gateway-compatible *ROSA26* locus targeting vector as previously described (*26*). LR reactions were performed between the plasmid pENTR-FLAG-Hoxa2 (containing the Hoxa2 cDNA coding sequence with a 5'FLAG tag) and the destination vector pROSA26-DV1 to obtain the targeting vector pROSA26-FLAG-Hoxa2-IRES-EGFP. This vector was linearized with PvuI and electroporated into the E14 ES cell line. The positive ES cell clones, selected by G418 resistance and screened by PCR, were aggregated with morula-stage embryos obtained from inbred (C57BL/6 x DBA/2) F1 mice. Germline transmission of the *ROSA26::(lox-STOP-lox)Hoxa2-IRES-EGFP* allele was obtained. Heterozygous and homozygous mice were viable and fertile.

Other mouse lines used in the study

Wnt1::Cre (*27*), $R26R^{lacZ}$ (*22*), $Ezh2^{fl/fl}$ (kind gift from S.H. Orkin) (*28*), *Hoxa5, Hoxb5, Hoxc5* knockout mice (*29*), $Unc5b^{bGal/bGal}$ knockout mice (kind gift from M. Tessier-Lavigne) (*14*) and $Unc5c^{rcm}$ (embryos kindly obtained from V. Castellani) (*30*) were as described. *Pcp2::Cre* (*31*), $R26R^{tdTomato}$, $R26R^{ZsGreen}$ (*23*) and Shh^{tm2Amc} (Shh^{fl}) mice (*32*) were obtained from Jackson Laboratory.

Circuit tracing

G-deleted rabies virus vectors encoding mCherry (SADΔG-mCherry) or eGFP (SADΔG-eGFP) were harvested from BHK-B19G cells (kind gift from E. Callaway) and centrifuged as described previously (*33*). Stereotaxic injections of viruses to different

areas of neocortex or cerebellum were performed via pulled-glass pipettes using a microinjector (Narishige, IM-9B). Pups were anesthetized by hypothermia, injected at P2 and perfused at P7.

In utero electroporation

In utero electroporation was performed on embryos at E13.5 or E14.5 as described previously (*34*) using different combinations of *eGFP* (pCX-eGFP (*35*)), *Unc5b* (pcDNA- *ratUnc5b* (*36*)), *Unc5c* (pcDNA 3.1-*mouseUnc5c*; kind gift from P. Mehlen) and *Netrin1* (pcDNA 3.1-*humanNetrin1*; kind gift from P. Mehlen) expressing vectors diluted to 1 mg/ml in 1x phosphate buffer (PBS1x). Electroporated brains between E16.5 and P0 were fixed for 30 min in paraformaldehyde (PFA, Merck) 4%/ PBS1x. For rescue experiments on *r5-6::Cre;Ezh2*$^{fl/fl}$ embryos, the proportions of ectopic neurons were quantified by Imaris (Bitplane). A Student's t-test was used for statistical analysis.

Histological analysis, immunostaining, and *in situ* hybridization

Prenatal or postnatal brains, dissected when necessary, were fixed in 4% PFA diluted in phosphate buffer (PBS 1x) from 30 minutes to overnight. For cryostat sections, tissues were cryoprotected in 10% sucrose (Fluka) / PBS1x and embedded in gelatine 7.5% (Sigma) / 10% sucrose / PBS1x before being frozen at -80°C. Cryostat sections (20 µm and 30 µm) were cut (Microm HM560) in coronal and sagittal orientations, respectively. Vibratome sections (80 µm or 35 µm for reconstruction) were prepared from postnatal brains after embedding in 4% agarose (Promega)/0.1 M phosphate buffer (pH 7.4). Immunohistochemistry was performed as described in (*6*, *29*) using rabbit anti-mouse

Pax6 (Millipore; AB2237; 1/1000^{em}), anti-Hoxa5 antibody (Sigma; HPA029319; 1/200^{em}), rat anti-mouse Hoxb4 (developed by A. Gould and R. Krumlauf; obtained from the Developmental Studies Hybridoma Bank developed under the auspices of the NICHD and maintained by The University of Iowa, Department of Biology, Iowa City, IA 52242; 1/100^{em}) or rabbit anti-mouse trimethyl-histone H3 Lys27 (07-449; Millipore; 1/250^{em}), followed by species-specific fluorochrome-coupled secondary antibody staining, including donkey anti-rabbit A546 (Invitrogen; 1/1000^{em}) and the donkey anti-rat A488 (Invitrogen; 1/1000^{em}) diluted in solutions containing DAPI (Invitrogen). Simple and double *in situ* hybridizations were performed as described previously(*6*). The following probes were used: *Barhl1; Hoxa2; Hoxb3; Hoxb4; Hoxb5*, *Hoxa5* (*6*, *29*), *Ntn1* (*6*, *11*), *Unc5b and Unc5c* (*37*). X-galactosidase staining on whole embryos, whole brains or cryostat sections was performed as described in (*6*).

Imaging and Picture Processing

Imaging of fluorescent signals was performed using an Axio imager Z2 upright microscope coupled to a LSM700 Zeiss laser scanning confocal 5x lens (NA 0.25), 10x lens (NA 0.45) or oil/glycerol/water immersion lens 25x (NA 0.8). Stitching of whole-mounts (electroporated brains) was performed using Zen Software at postnatal stages, and using Xuvtools (http://www.xuvtools.org) at prenatal stages. Chromogenic staining was examined by classical wide-field or binocular microscopy (Nikon). Fig. 2I is an inverted artificial superposition of chromogenic signals from adjacent sections. In Fig. 3A, B inverted X-Gal signal is artificially projected onto Pax6 immunohistochemistry.

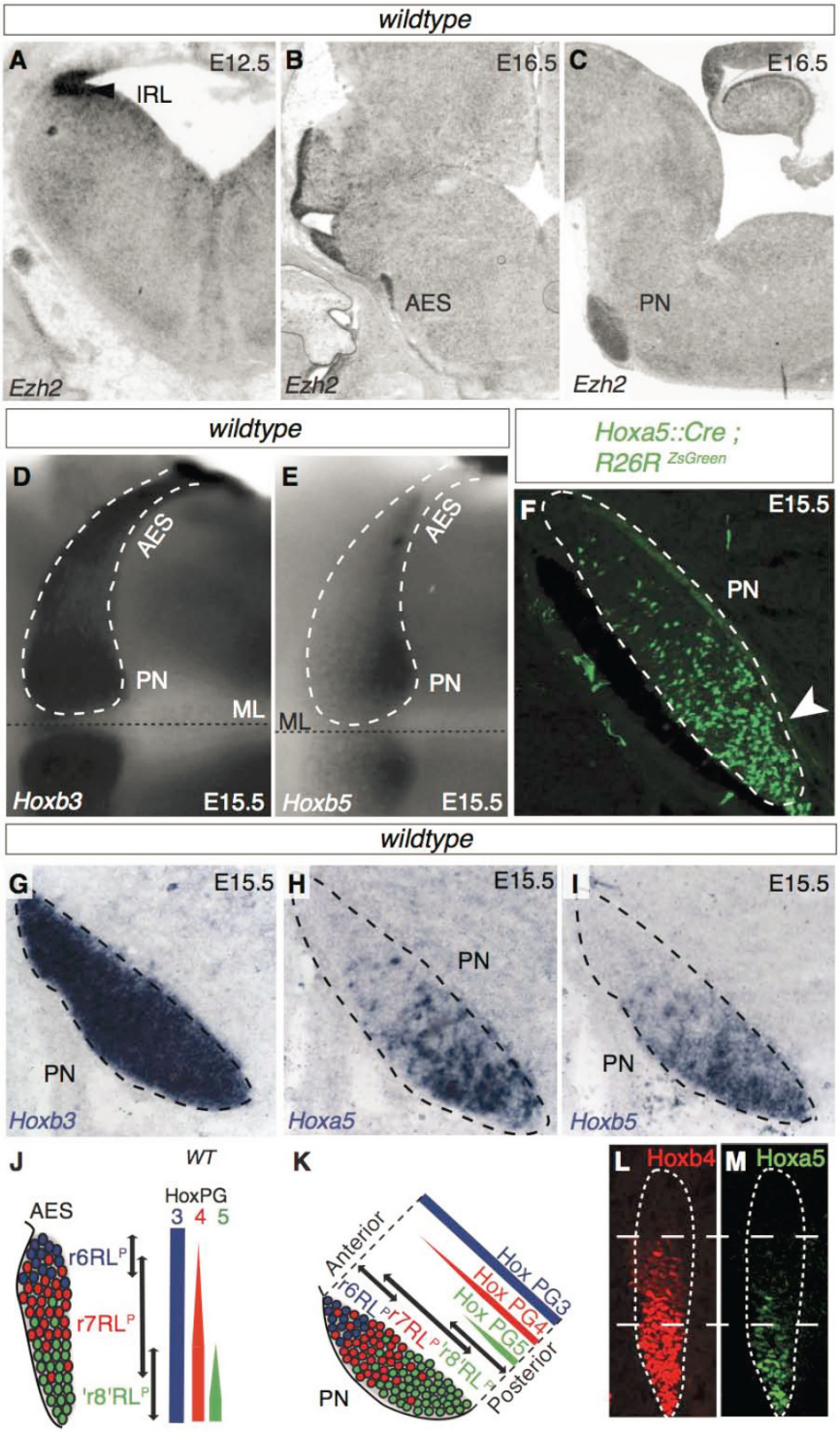
wildtype
A
E12.5
IRL
Ezh2
B
E16.5
AES
Ezh2
C
E16.5
PN
Ezh2
wildtype
Hoxa5::Cre ;
R26R ZsGreen
D
AES
PN
ML
Hoxb3
E15.5
E
AES
PN
ML
Hoxb5
E15.5
F
E15.5
PN
wildtype
G
E15.5
PN
Hoxb3
H
E15.5
PN
Hoxa5
I
E15.5
PN
Hoxb5
J
WT
AES
HoxPG
3 4 5
r6RL^P
r7RL^P
'r8'RL^P
K
Anterior
Hox PG3
Hox PG4
Hox PG5
r6RL^P
r7RL^P
'r8'RL^P
Posterior
PN
L
Hoxb4
M
Hoxa5

Fig. S1. *Ezh2* and *Hox* gene expression in precerebellar rhombic lip derivatives. (A to **C**) *Ezh2 in situ* hybridization on coronal (A, B) and sagittal sections (C). At E12.5 *Ezh2* is expressed in lower rhombic lip (lRL, A) and maintained in E16.5 anterior extramural stream (AES, B) and pontine nuclei (PN, C). (**D** to **E)** E15.5 whole-mount hindbrains show *Hoxb3* expression in all pontine neurons (D) and *Hoxb5* restriction to the posterior PN (E). (**F**) Sagittal section of E15.5 *Hoxa5::Cre;R26R*^{ZsGreen} specimen revealing the localization of ZsGreen^{+} neurons to the posterior PN (arrowhead). **(G** to **I)** E15.5 PN sagittal sections show *Hoxb3* expression in all pontine neurons (G) and restriction of *Hoxa5*$^{+}$ (H) and *Hoxb5*$^{+}$ (I) cells to the posterior PN. (**J** to **K**) Summaries of Fig. 2A-I and fig. S1D-I. (**L** to **M**) Hoxb4 (L) and Hoxa5 (M) immunostaining on a coronal section of a E14.5 wildtype embryo. ML: ventral midline.

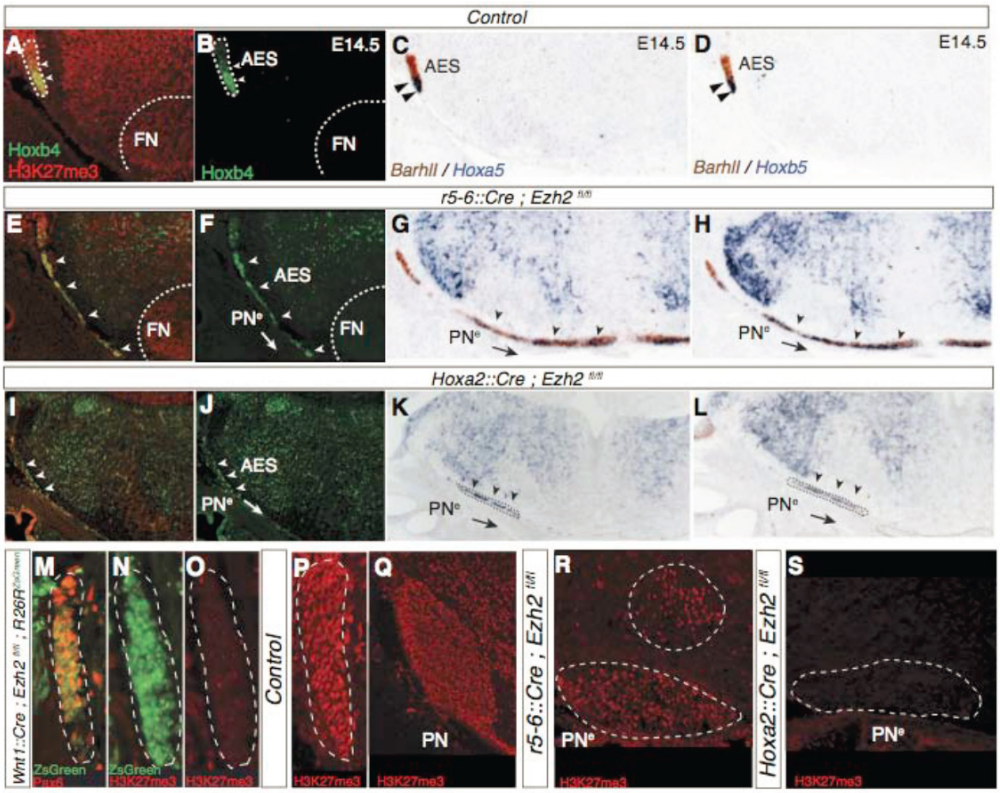

Fig. S2. Hox gene expression in migrating pontine neurons of *Ezh2* conditional mutants. (**A** to **L**) H3K27me3/Hoxb4 immunostaining (A,B,E,F,I,J), *Hoxa5*/*Barhl1* (C,G,K) and *Hoxb5*/*Barhl1* (D,H,L) *in situ* hybridization on coronal sections at r5-r6 level in control (A-D), *r5-6::Cre;Ezh2*$^{fl/fl}$ (E-H) and *Hoxa2::Cre;Ezh2*$^{fl/fl}$ (I-L) E14.5 fetuses. Strong reduction of H3K27me3 in the r5-r6 environment of *Ezh2* conditional knockouts (E,F,I,J). In control (A-D), arrowheads show restricted ventral expression of Hoxb4 (A,B), *Hoxa5* (C) and *Hoxb5* (D) in the anterior extramural stream (AES). In *r5-6::Cre;Ezh2*$^{fl/fl}$ embryos, Hoxb4^{+} pontine neurons migrate to ectopic pontine nuclei (PN^{e}), are Ezh2$^{+/+}$ (co-labeled by H3K27me3/Hoxb4 double immunostaining (arrowheads, E,F)), and express both *Hoxa5* and *Hoxb5* (arrowheads, G,H). In *Hoxa2::Cre;Ezh2*$^{fl/fl}$ embryos, Hoxb4^{+} pontine neurons migrate ectopically to PN^{e} are *Ezh2*$^{-/-}$ as shown by the lack of H3K27me3 (arrowheads, I,J), and express both *Hoxa5* and *Hoxb5* (arrowheads, K,L). The neurons of the facial nucleus (FN), a r4 derivative, still carry the H3K27me3 mark in *r5-6::Cre;Ezh2*$^{fl/fl}$ embryos, showing the specificity of the knockout (E). (**M** to **P**) Pax6 (M) and H3K27me3 (N,O,P) immunohistochemistry of *Wnt1::Cre;Ezh2*$^{fl/fl}$*;R26R*^{ZsGreen} (M-O) and control AES (P) on coronal sections. In the conditional knockout, ZsGreen^{+} pontine neurons express Pax6 (M), but lack the H3K27me3 mark (N,O) in contrast to controls (P). (**Q to S**) H3K27me3 immunohistochemistry on sagittal sections at E18.5 showing loss of the H3K27me3 mark in environment only (R, *r5-6::Cre;Ezh2*$^{fl/fl}$) or environment and PN^{e} (S, *Hoxa2::Cre;Ezh2*$^{fl/fl}$) unlike in controls (Q).

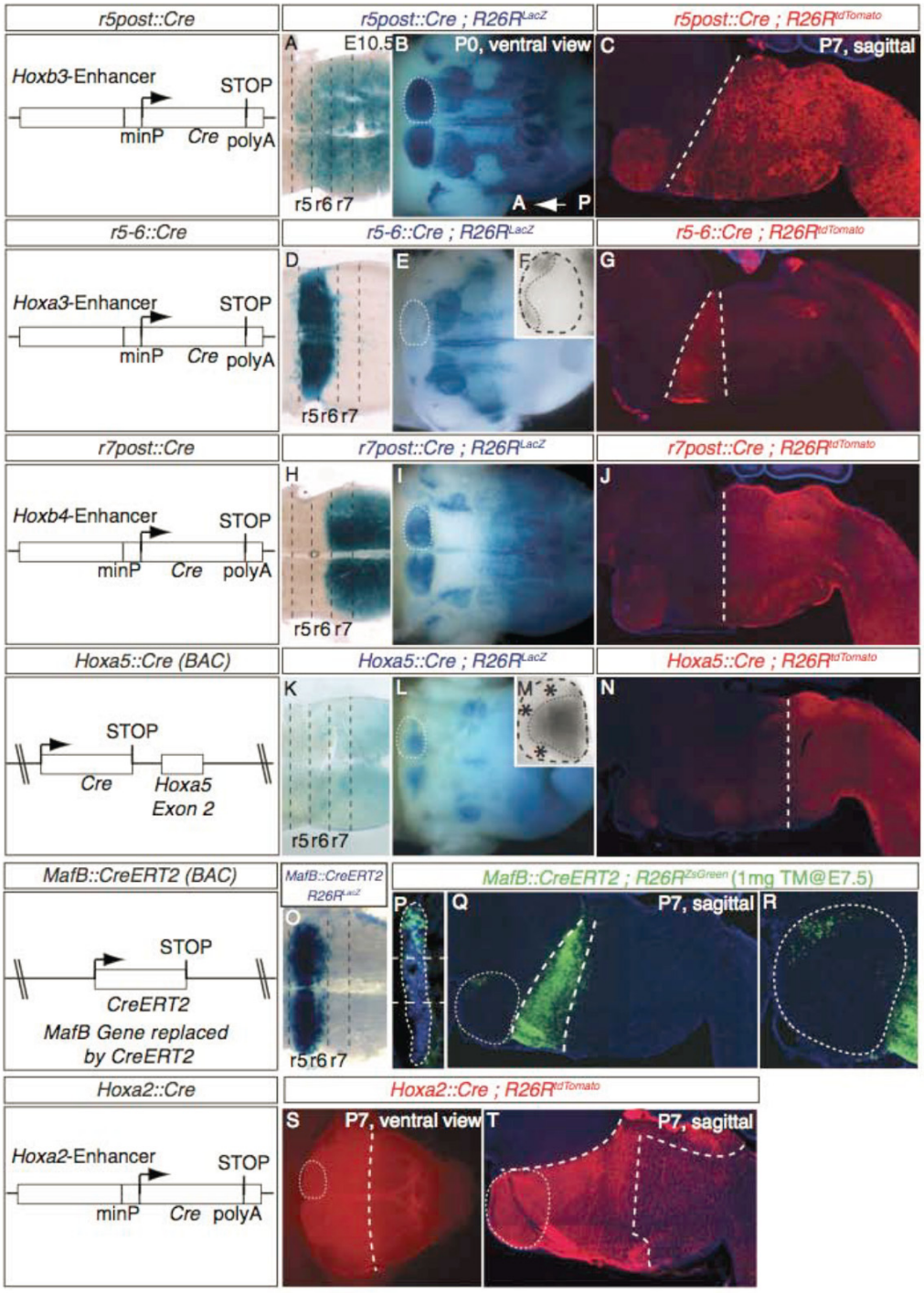

Fig. S3. Generation and characterization of posterior hindbrain Cre-expressing lines. (**A,D,H,K,O**) Embryos carrying *r5post::Cre* (A), *r5-6::Cre* (D), *r7post::Cre* (H)

and *MafB::CreERT2 (*1mg Tamoxifen@E7.5*)* (O) transgenes crossed to the *R26R*^{lacZ} floxed reporter and expressing *ß-galactosidase* (*ßGal*) at E10.5 in a rhombomere-specific manner, with *r5post::Cre* expression spanning r5 to spinal cord (A), *r5-6::Cre* and *MafB::CreERT2* spanning r5 and r6 (D, O), and *r7post::Cre* spanning r7 to spinal cord (H). *Hoxa5::Cre* is not expressed in the hindbrain before E10.5 (K). (**B,E,I,L,S**) Detection of the *ßGal* on whole-mount hindbrains (ventral views) at P0 show the spatially-restricted progeny of these rhombomeres traced after recombination of the *R26R*^{LacZ} locus in each of these Cre or CreERT2 expressing lines (B,E,I,L) or in (S) using the *R26R* ^{tdTomato} reporter line at P7 for *Hoxa2::Cre*. (**F,M**) High magnifications show the segregation of r6 (*r5-6::Cre,* (F)) (rostrally) and *Hoxa5* (i.e. 'r8') (caudally) progenies (M) in the pontine nuclei. (**C,G,J,N,T**) Sagittal sections at P7 show recombined, *tdTomato*$^{+}$ rhombomere progenies of indicated genotypes; segregation of rhombomere-derived territories persists up to postnatal stages. (**P** to **R**) Coronal (P, E15.5) and sagittal sections (Q,R, P7) of *Mafb::CreERT2; R26R*^{ZsGreen} show the dorsal restriction of r5-6 progeny in the anterior extramural stream (P) and the restriction of ZsGreen^{+} cells to the anterior pontine nuclei (R). r: rhombomere; minP: minimal promoter.

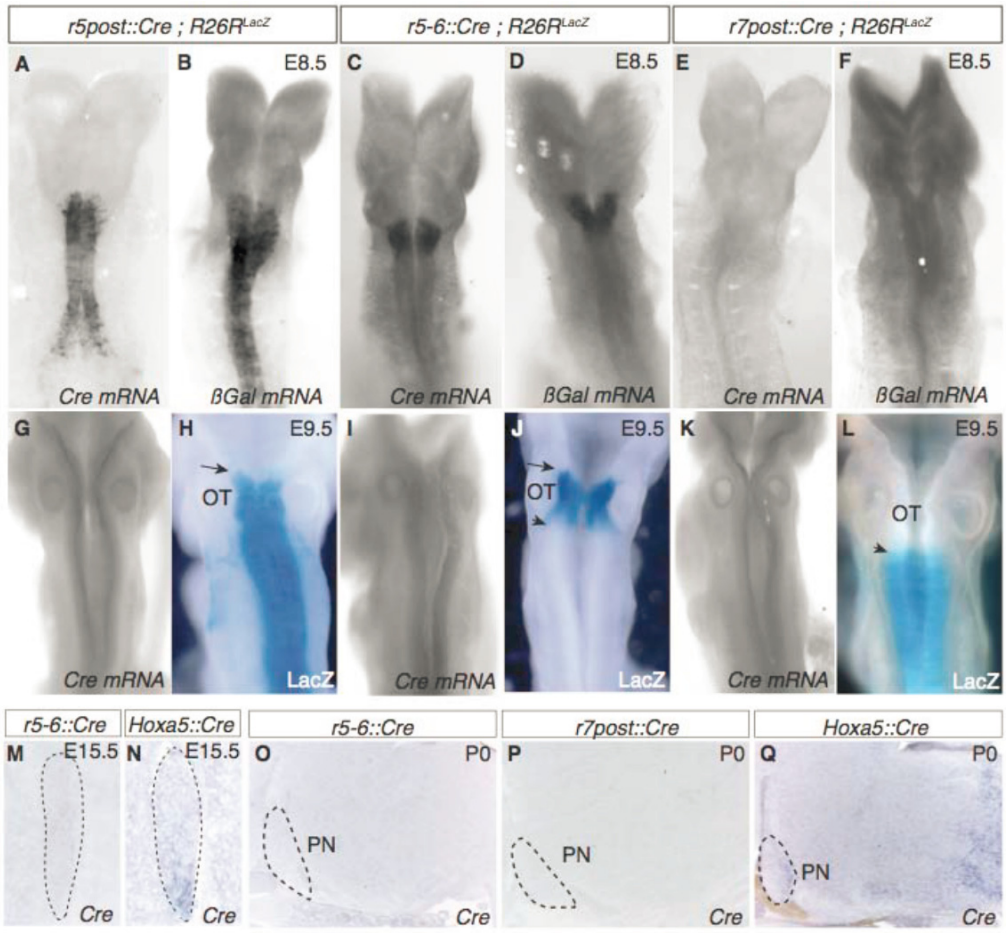

Fig. S4. *Cre* expression patterns in transgenic lines. (**A** to **D**) At E8.5, *Cre* (A,C) and *ß-galactosidase* (*ßGal*) (B,D) are expressed in *r5post::Cre* (A,B) and *r5-6::Cre* (C,D) whole-mount embryos. (**E** to **F**) In *r7post::Cre*, neither *Cre* nor *ß-Gal* are expressed at E8.5. (**G, I, K**) At E9.5, *Cre* transcripts were not detectable in any of the *Cre* transgenics. **(H, J, L**) LacZ signals reveal that the *R26R*^{LacZ} locus has recombined in all three *Cre* transgenics at E9.5. *r5post::Cre* (H) and *r5-6::Cre* (J) share the same *ßGal* anterior boundary (arrow), while *r5-6::Cre* (J) and *r7post::Cre* (L) have their posterior and anterior expression boundaries, respectively, at the r6/r7 border with no overlap (arrowhead). Note that *r7post::Cre;R26R*^{lacZ} show LacZ restricted activity at E9.5 (L), although *Cre* and *ßGal* transcript levels are below *in situ* hybridization detection at E8.5 and E9.5 (E,F,K). (**M** to **N**) *In situ* hybridizations on coronal sections of E15.5 AES show no expression of *Cre* in *r5-6::Cre* (M), while in *Hoxa5::Cre* embryos *Cre* expression faithfully recapitulates endogenous *Hoxa5* expression (N). (**O** to **Q**) On P0 sagittal sections, *Cre* transcripts are not present at detectable levels in *r5-6::Cre* (O) and *r7post::Cre* (P), while *Hoxa5::Cre* newborns show *Cre* expression in posterior hindbrain and posterior PN (Q). OT: otic capsule; PN: pontine nuclei.

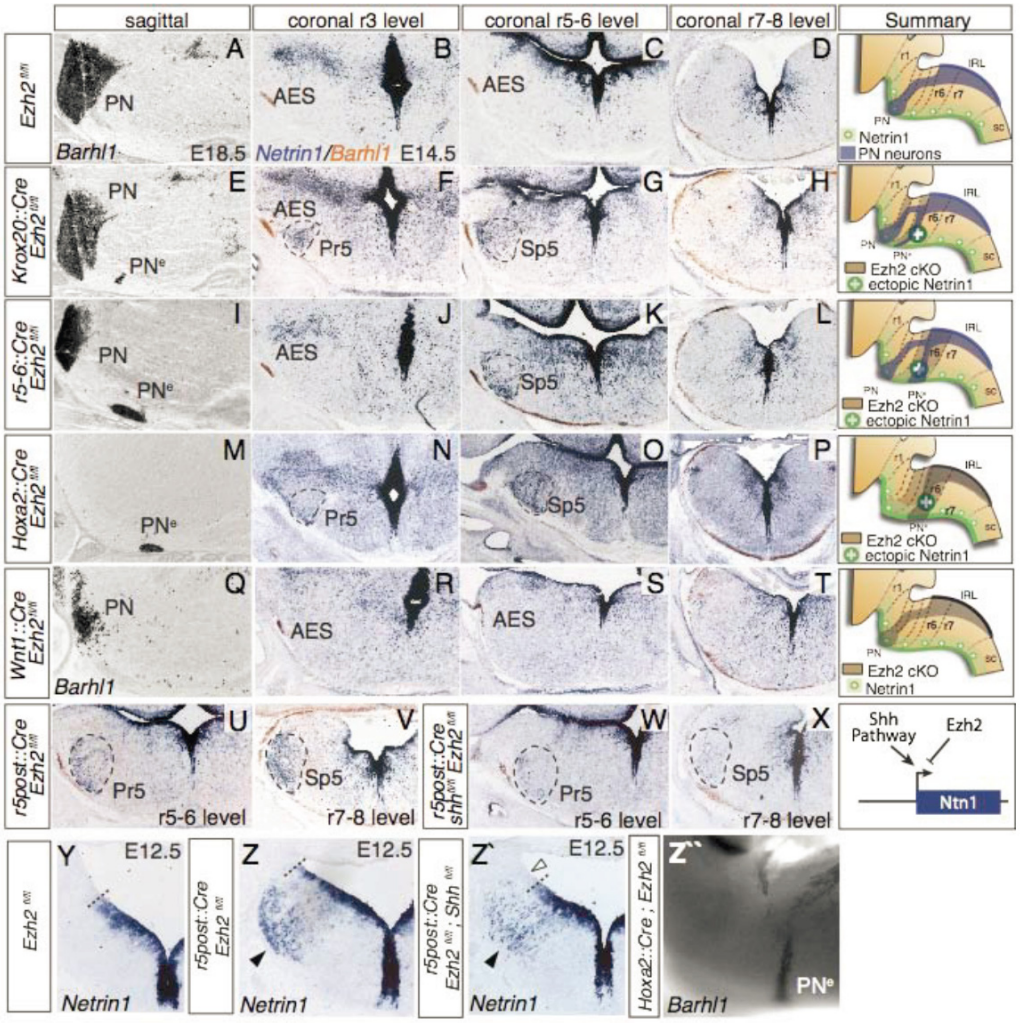

Fig. S5. Analysis of pontine neuron migratory phenotypes in *Ezh2* conditional mutants. (**A** to **T**), PN migratory phenotype in control *Ezh2*$^{fl/fl}$ (A-D), *Krox20::Cre;Ezh2*$^{fl/fl}$ (E-H), *r5-6::Cre;Ezh2*$^{fl/fl}$ (I-L), *Hoxa2::Cre;Ezh2*$^{fl/fl}$ (M-P) and *Wnt1::Cre;Ezh2*$^{fl/fl}$ (Q-T) fetuses. *In situ* hybridization on sagittal sections show rostrocaudal distribution of normal (PN) and ectopic (PN^{e}) *Barhl1*$^{+}$ pontine neurons at E18.5 in the different genotypes (A,E,I,M,Q). Co-detection of *Netrin1* and *Barhl1* transcripts on serial coronal sections taken at the r3, r5/r6 and r7/r8 levels show ectopic expression of *Netrin1* in *Krox20::Cre;Ezh2*$^{fl/fl}$, *r5-6::Cre;Ezh2*$^{fl/fl}$ and *Hoxa2::Cre;Ezh2*$^{fl/fl}$ (dashed lines, F,G,K,N,O) but not in *Wnt1::Cre;Ezh2*$^{fl/fl}$ and *Ezh2*$^{fl/fl}$ embryos at E14.5. (**U** to **X**) Expression of *Netrin1* and *Barhl1* in *r5post::Cre;Ezh2*$^{fl/fl}$ (U, V) and *r5post::Cre;Ezh2*$^{fl/fl}$*;Shh*$^{fl/fl}$ (W,X) at r5/r6 (U, W) and r7/r8 (V, X) levels at E14.5. Ectopic *Netrin1* expression is strongly reduced in *Shh/Ezh2* double cKO (W,X) partially rescuing the *Ezh2* cKO phenotype (U,V). (**Y** to **Z`**) At E12.5, ectopic *Netrin1* expression (black arrowheads) observed in *r5post::Cre;Ezh2*$^{fl/fl}$ mutants (Z) is absent in controls

Ezh2$^{fl/fl}$ (Y) and partially rescued in *r5post::Cre;Ezh2*$^{fl/fl}$*;Shh*$^{fl/fl}$ compound mutants (white and black arrowheads, Z`). (**Z``**) Migratory phenotypes in *Hoxa2::Cre;Ezh2*$^{fl/fl}$ shown by *Barhl1 in situ* hybridization on E14.5 whole-mount. Summaries show the migratory pathways of wildtype and mutants as well as the proposed genetic interaction between Shh, Ezh2 and Netrin1 in the last column. AES: anterior extramural stream; lRl: lower rhombic lip; r: rhombomere; sc: spinal cord; Pr5: principal trigeminal nucleus; Sp5: spinal trigeminal nucleus; cKO: conditional knockout.

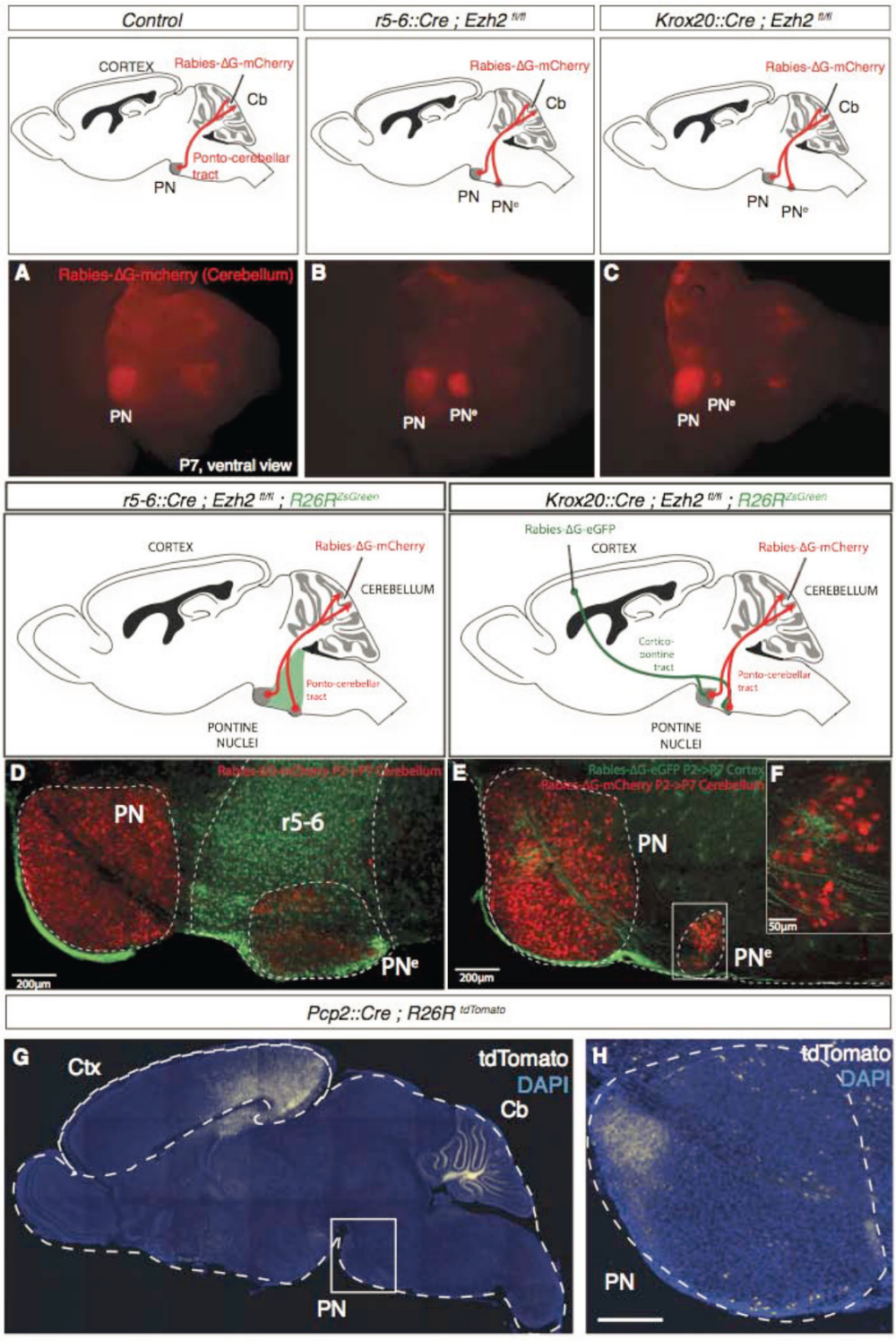
Control
r5-6::Cre ; Ezh2 fl/fl
Krox20::Cre ; Ezh2 fl/fl
CORTEX
Rabies-ΔG-mCherry
Cb
Ponto-cerebellar tract
PN
PNe
A
Rabies-ΔG-mcherry (Cerebellum)
P7, ventral view
B
C
r5-6::Cre ; Ezh2 fl/fl ; R26RZsGreen
Krox20::Cre ; Ezh2 fl/fl ; R26RZsGreen
Rabies-ΔG-eGFP
CEREBELLUM
Cortico-pontine tract
PONTINE NUCLEI
D
E
F
r5-6
200µm
50µm
Pcp2::Cre ; R26R tdTomato
G
Ctx
tdTomato
DAPI
H

Fig. S6. Cortico-ponto-cerebellar connectivity in *Ezh2* conditional mutants. (**A** to **C**) Ventral views of P7 whole-mount hindbrains after retrograde tracing with rabies-ΔG-mCherry from cerebellum (Cb) show that Cb is innervated by normal pontine nuclei (PN) in control (A) and both PN and ectopic pontine nuclei (PN^e) in *Krox20::Cre;Ezh2$^{fl/fl}$* (B) and *r5-6::Cre;Ezh2$^{fl/fl}$* (C) mutants. (**D**) Retrograde injections in P7 *r5-6::Cre;Ezh2$^{fl/fl}$;R26R^{ZsGreen}* animals show that PN^e is included within the ZsGreen$^+$ domain demonstrating PN^e localization in posterior r5/r6 as well as the duplication of both parts of the PN, i.e. reticulotegmental nucleus (inner nucleus) and pontine gray nucleus (outer nucleus). (**E** to **F**) Cortical injections of rabies-ΔG-GFP combined with retrograde cerebellar tracing (rabies-ΔG-mCherry) illustrate that in P7 *Krox20::Cre;Ezh2$^{fl/fl}$* pups, PN^e (F) is also integrated into cortico-ponto-cerebellar connectivity. Injections were carried out at P2 and analyzed at P7. (**G** to **H**) Restricted *tdTomato$^+$* cells in posterior/visual cortex (Ctx) in P7 *Pcp2::Cre;R26R^{tdTomato}* pups (G) and *tdTomato$^+$* axon projection to anterior PN in sagittal sections (H).

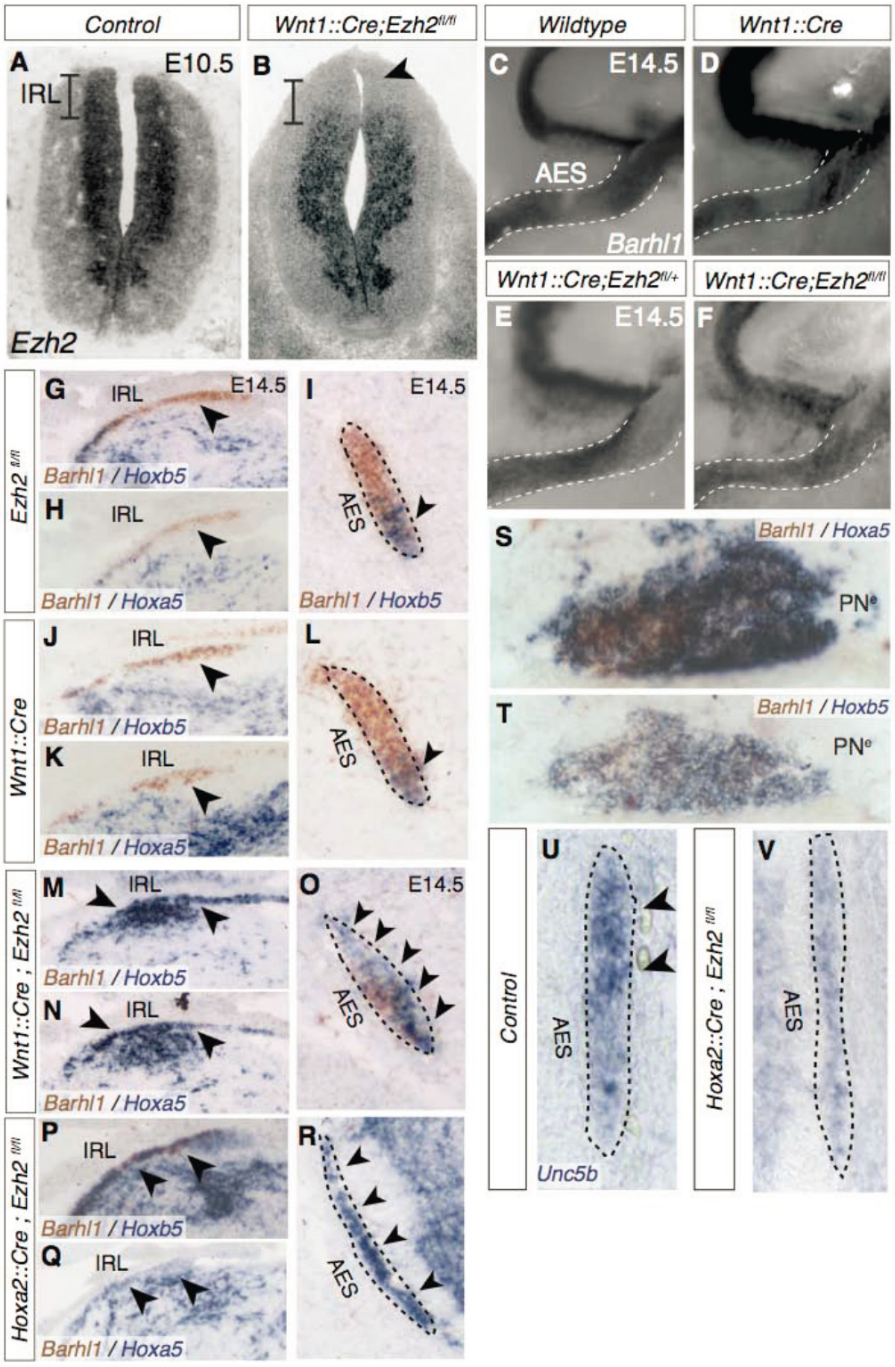

Fig. S7. *Ezh2* cell-autonomous role in rhombic lip and pontine neurons. **(A** to **B)** *Ezh2* is downregulated in the lower rhombic lip (lRL) of *Wnt1::Cre Ezh2*$^{fl/fl}$ embryos at E10.5 (B, arrowhead) compared to controls (A). **(C** to **F)** Lateral views of *Barhl1*$^{+}$

anterior extramural stream (AES) in E14.5 wild type (C), *Wnt1::Cre* (D), *Wnt1::Cre*;*Ezh2*$^{fl/+}$ (E), and *Wnt1::Cre*;*Ezh2*$^{fl/fl}$ (F) conditional mutant whole-mount hindbrains. (**G** to **R**) Co-detection of *Hoxb5* and *Barhl1* (G,I,J,L,M,O,P,R) and *Hoxa5* and *Barhl1* (H,K,N,Q) expression on coronal sections from E14.5 embryos (G-I, *Ezh2fl/fl*; J-L, *Wnt1::Cre*), *Wnt1::Cre:Ezh2*$^{fl/fl}$ (M-O) and *Hoxa2::Cre:Ezh2*$^{fl/fl}$ (P-R) at anterior precerebellar lRL (G,H,J,K,M,N,P,Q) and AES levels (I,L,O,R). In controls *Hoxa5* and *Hoxb5* transcript is absent from the anterior precerebellar lRL (arrowheads, G,H,J,K) and restricted to the ventral AES (I,L). In both *Wnt1::Cre:Ezh2*$^{fl/fl}$ and *Hoxa2::Cre:Ezh2*$^{fl/fl}$ conditional knockouts, *Hoxa5* and *Hoxb5* are expressed ectopically in the anterior precerebellar lRL (arrowheads, M,N,P,Q) and throughout the AES (arrowheads, O,R), while expression is regionalized in controls (arrowheads, H,J). (**S** to **T**) Co-detection of *Hoxa5 (S), Hoxb5 (T)* and *Barhl1 (S,T)* transcripts in E18.5 *Hoxa2::Cre:Ezh2*$^{fl/fl}$ ectopic pontine nuclei (PN^{e}) on sagittal sections. (**U** to **V**) Dorsal *Unc5b* expression at E14.5 in coronal control AES (U), as compared to *Hoxa2::Cre Ezh2*$^{fl/fl}$ AES (V) showing *Unc5b* downregulation. PN: pontine nuclei.

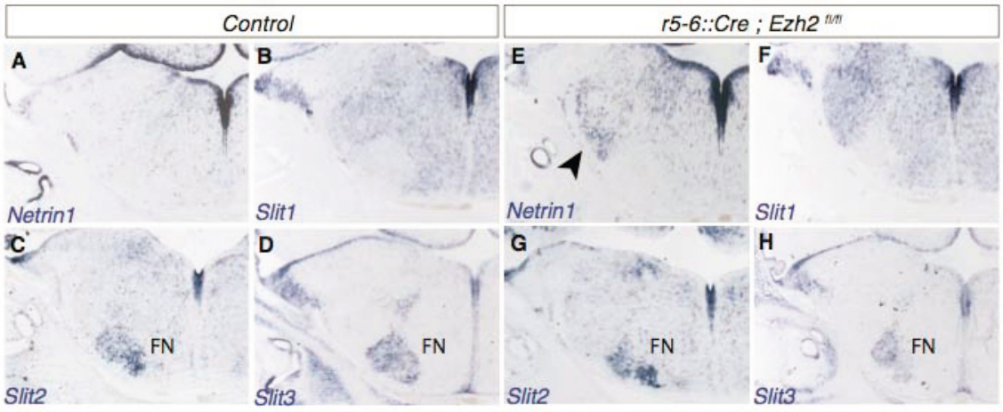

Fig. S8. *Slit1-3* expression patterns in conditional *Ezh2* mutants. (**A** to **H**) *In situ* hybridization for *Netrin1* (A,E), *Slit1* (B,F), *Slit2* (C,G) and *Slit3* (D,H) on adjacent coronal sections at r5-r6 level in E14.5 control (A-D) and *r5-6::Cre;Ezh2*$^{fl/fl}$ (E-H). *Netrin1* is ectopically expressed in *r5-6::Cre;Ezh2*$^{fl/fl}$ (arrowhead, E). FN: facial motor nucleus

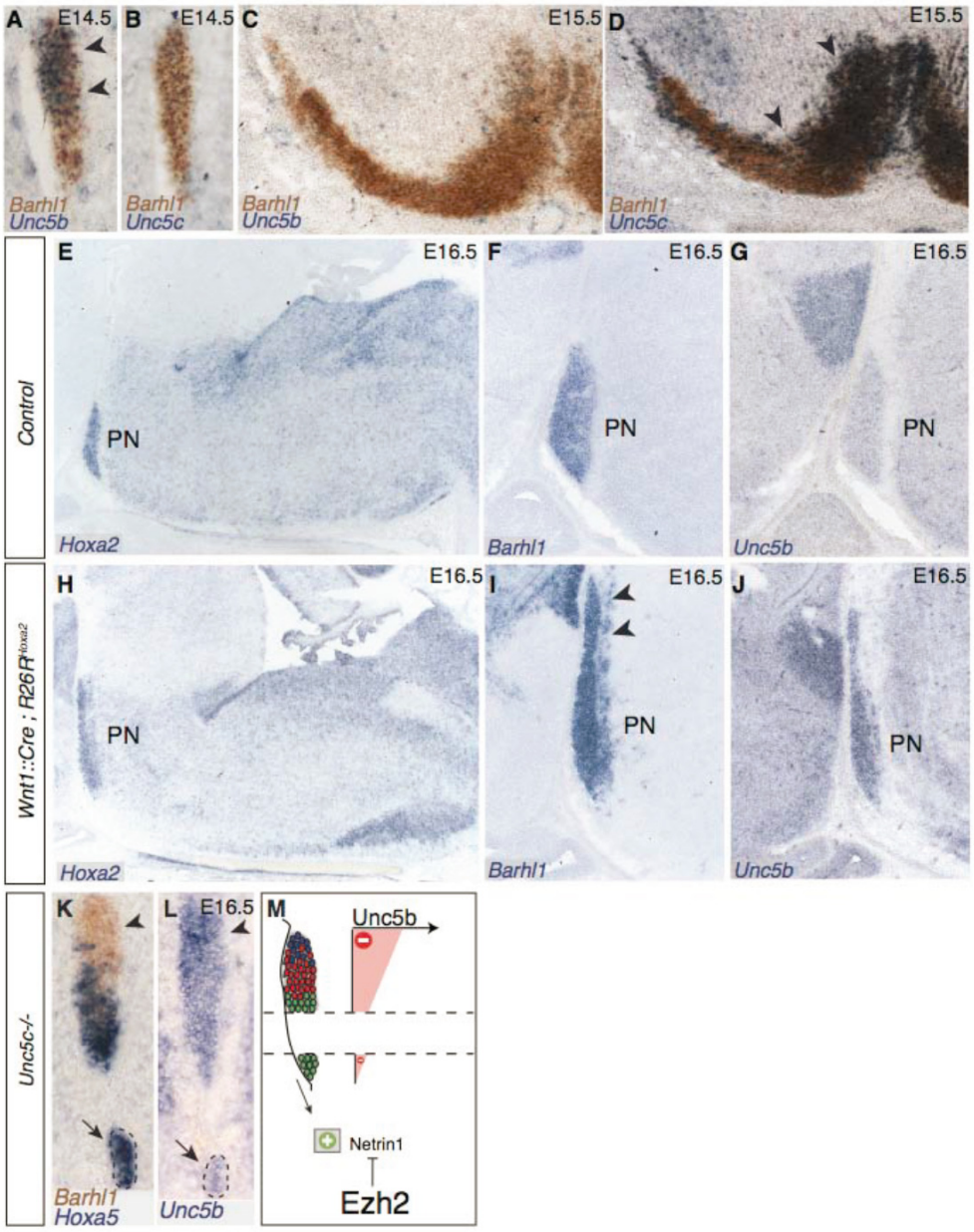

Fig. S9. *Unc5b* and *Unc5c* expression during normal pontine neuron migration and in *Wnt1::Cre;R26R*^{Hoxa2} mutants. (**A** to **D**) Double *in situ* hybridizations for *Barhl1/Unc5b* (A,C) and *Barhl1/Unc5c* (B,D) on coronal sections at E14.5 (A,B) and E15.5 (C,D). *Unc5b* transcripts are detected in the dorsal part of the anterior extramural stream (AES) (arrowheads, A) and become undetectable in *Barhl1*$^{+}$ neurons reaching the ventral midline (C). On the contrary, *Unc5c* transcript expression is undetectable in AES neurons (B) while is reactivated during the second phase of ventral migration

(arrowheads, D). (**E** to **J**) *In situ* hybridization for *Hoxa2* (E,H), *Barhl1* (F,I) and *Unc5b* (G,J) on E16.5 sagittal sections in controls (E-G) and *Wnt1::Cre;R26R*^{Hoxa2} embryos (H-J). In the latter, pontine nuclei (PN) are anteriorly extended (arrow, I) and overexpress *Unc5b* (J), which is undetectable in control E16.5 PN (G). (**K** to **M**) *Hoxa5/Barhl1* (K) and *Unc5b* (L) expression in E16.5 *Unc5c*$^{-/-}$ AES. Ectopically migrating neurons (arrows) strongly express *Hoxa5* while do not express *Unc5b*, as summarized in (M).

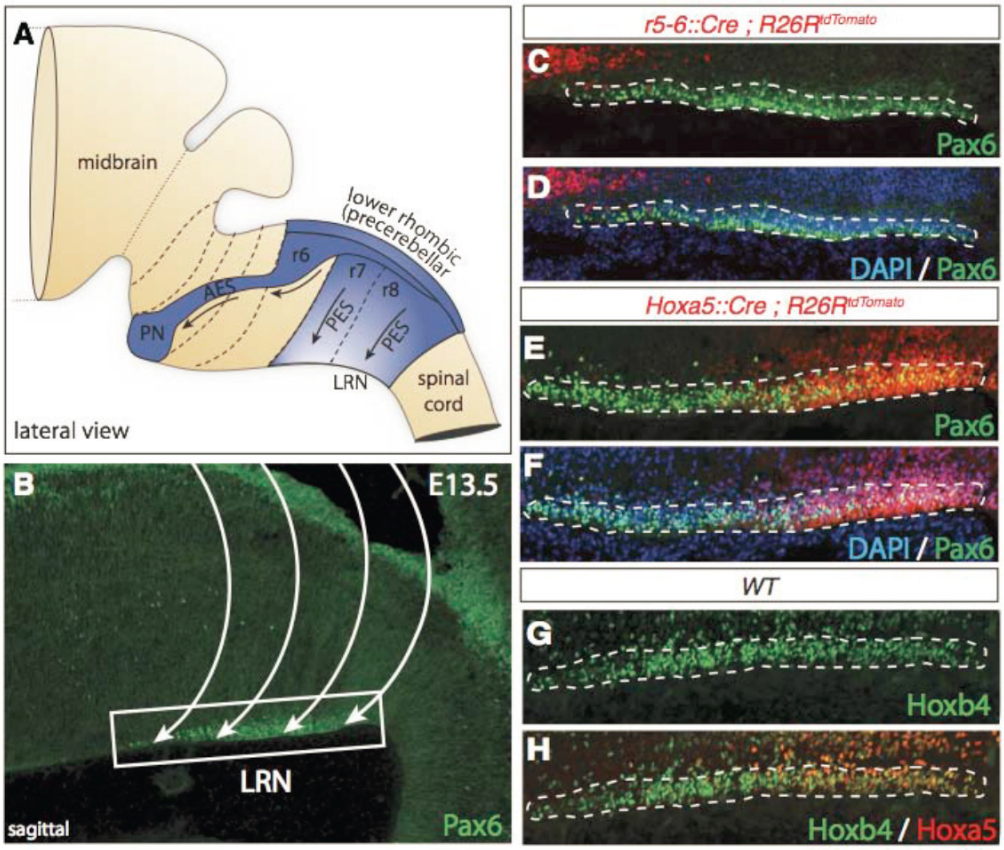

Fig. S10. Topographic organization of migrating lateral reticular nucleus. (**A** to **B**) Lateral reticular nucleus (LRN) neurons originate as the pontine nuclei (PN) from the lower rhombic lip (A) and migrate extramurally to the contralateral side. The migratory stream can be visualized by Pax6 immunostaining on E13.5 sagittal sections (B). (**C** to **D**) Pax6/DAPI double immunohistochemistry on sagittal sections of *r5-6::Cre;R26R*^{tdtomato} embryos at E13.5 showing that LRN neurons lack r5-6 derived progeny. (**E** to **F**) Pax6/DAPI double immunohistochemistry on sagittal sections of *Hoxa5::Cre;R26R*^{tdtomato} embryos at E13.5 showing that posterior LRN neurons are contributed by *Hoxa5::Cre;R26R*^{tdtomato} positive cells. (**G** to **H**) Immunohistochemistry for Hoxb4 (G) and Hoxa5 (H) in migrating LRN neurons on sagittal sections show the posterior restriction of Hoxa5 (H) positive cells. PES: posterior extramural stream; AES: anterior extramural stream.

References

1. A. Lumsden, R. Krumlauf, Patterning the vertebrate neuraxis. *Science* **274**, 1109 (1996).

2. S. Tümpel, L. M. Wiedemann, R. Krumlauf, *Hox* genes and segmentation of the vertebrate hindbrain. *Curr. Top. Dev. Biol.* **88**, 103 (2009).

3. A. F. Farago, R. B. Awatramani, S. M. Dymecki, Assembly of the brainstem cochlear nuclear complex is revealed by intersectional and subtractive genetic fate maps. *Neuron* **50**, 205 (2006).

4. J. Altman, S. A. Bayer, Development of the precerebellar nuclei in the rat: IV. The anterior precerebellar extramural migratory stream and the nucleus reticularis tegmenti pontis and the basal pontine gray. *J. Comp. Neurol.* **257**, 529 (1987).

5. C. I. Rodriguez, S. M. Dymecki, Origin of the precerebellar system. *Neuron* **27**, 475 (2000).

6. M. J. Geisen *et al*., *Hox* paralog group 2 genes control the migration of mouse pontine neurons through slit-robo signaling. *PLoS Biol.* **6**, e142 (2008).

7. K. T. Yee, H. H. Simon, M. Tessier-Lavigne, D. M. O'Leary, Extension of long leading processes and neuronal migration in the mammalian brain directed by the chemoattractant netrin-1. *Neuron* **24**, 607 (1999).

8. S. Nóbrega-Pereira, O. Marín, Transcriptional control of neuronal migration in the developing mouse brain. *Cereb. Cortex* **19**(Suppl. 1), i107 (2009).

9. R. Margueron, D. Reinberg, The Polycomb complex PRC2 and its mark in life. *Nature* **469**, 343 (2011).

<foot>10. Materials and methods are available as supplementary materials on *Science* Online.</foot>

11. E. Bloch-Gallego, F. Ezan, M. Tessier-Lavigne, C. Sotelo, Floor plate and netrin-1 are involved in the migration and survival of inferior olivary neurons. *J. Neurosci.* **19**, 4407 (1999).

12. K. Hong *et al*., A ligand-gated association between cytoplasmic domains of UNC5 and DCC family receptors converts netrin-induced growth cone attraction to repulsion. *Cell* **97**, 927 (1999).

13. D. Kim, S. L. Ackerman, The UNC5C netrin receptor regulates dorsal guidance of mouse hindbrain axons. *J. Neurosci.* **31**, 2167 (2011).

14. X. Lu *et al*., The netrin receptor UNC5B mediates guidance events controlling morphogenesis of the vascular system. *Nature* **432**, 179 (2004).

15. T. B. Leergaard, J. G. Bjaalie, Topography of the complete corticopontine projection: From experiments to principal maps. *Front. Neurosci.* **1**, 211 (2007).

16. P. Rakic, Specification of cerebral cortical areas. *Science* **241**, 170 (1988).

17. M. E. Hatten, Central nervous system neuronal migration. *Annu. Rev. Neurosci.* **22**, 511 (1999).

18. E. C. Lee *et al.*, A highly efficient *Escherichia coli*-based chromosome engineering system adapted for recombinogenic targeting and subcloning of BAC DNA. *Genomics* **73**, 56 (2001).

19. T. O. Yau *et al.*, Auto/cross-regulation of *Hoxb3* expression in posterior hindbrain and spinal cord. *Dev. Biol.* **252**, 287 (2002).

20. M. Manzanares *et al.*, Conserved and distinct roles of *kreisler* in regulation of the paralogous *Hoxa3* and *Hoxb3* genes. *Development* **126**, 759 (1999).

21. A. Gould, N. Itasaki, R. Krumlauf, Initiation of rhombomeric *Hoxb4* expression requires induction by somites and a retinoid pathway. *Neuron* **21**, 39 (1998).

22. P. Soriano, Generalized lacZ expression with the ROSA26 Cre reporter strain. *Nat. Genet.* **21**, 70 (1999).

23. L. Madisen *et al.*, A robust and high-throughput Cre reporting and characterization system for the whole mouse brain. *Nat. Neurosci.* **13**, 133 (2010).

24. M. Studer, A. Lumsden, L. Ariza-McNaughton, A. Bradley, R. Krumlauf, Altered segmental identity and abnormal migration of motor neurons in mice lacking *Hoxb-1*. *Nature* **384**, 630 (1996).

25. F. M. Rijli *et al.*, A homeotic transformation is generated in the rostral branchial region of the head by disruption of *Hoxa-2*, which acts as a selector gene. *Cell* **75**, 1333 (1993).

26. O. Nyabi *et al.*, Efficient mouse transgenesis using Gateway-compatible ROSA26 locus targeting vectors and F1 hybrid ES cells. *Nucleic Acids Res.* **37**, e55 (2009).

27. P. S. Danielian, D. Muccino, D. H. Rowitch, S. K. Michael, A. P. McMahon, Modification of gene activity in mouse embryos in utero by a tamoxifen-inducible form of Cre recombinase. *Curr. Biol.* **8**, 1323 (1998).

28. M. Puschendorf *et al.*, PRC1 and Suv39h specify parental asymmetry at constitutive heterochromatin in early mouse embryos. *Nat. Genet.* **40**, 411 (2008).

29. D. C. McIntyre *et al.*, Hox patterning of the vertebrate rib cage. *Development* **134**, 2981 (2007).

30. S. L. Ackerman *et al.*, The mouse rostral cerebellar malformation gene encodes an UNC-5-like protein. *Nature* **386**, 838 (1997).

31. P. M. Lewis, A. Gritli-Linde, R. Smeyne, A. Kottmann, A. P. McMahon, Sonic hedgehog signaling is required for expansion of granule neuron precursors and patterning of the mouse cerebellum. *Dev. Biol.* **270**, 393 (2004).

32. P. M. Lewis *et al.*, Cholesterol modification of sonic hedgehog is required for long-range signaling activity and effective modulation of signaling by Ptc1. *Cell* **105**, 599 (2001).

33. K. Yonehara *et al.*, Spatially asymmetric reorganization of inhibition establishes a motion-sensitive circuit. *Nature* **469**, 407 (2011).

34. H. Taniguchi, D. Kawauchi, K. Nishida, F. Murakami, Classic cadherins regulate tangential migration of precerebellar neurons in the caudal hindbrain. *Development* **133**, 1923 (2006).

35. T. Okada, K. Keino-Masu, M. Masu, Migration and nucleogenesis of mouse precerebellar neurons visualized by in utero electroporation of a green fluorescent protein gene. *Neurosci. Res.* **57**, 40 (2007).

36. F. Llambi *et al*., The dependence receptor UNC5H2 mediates apoptosis through DAP-kinase. *EMBO J.* **24**, 1192 (2005).

37. E. D. Leonardo *et al*., Vertebrate homologues of *C. elegans* UNC-5 are candidate netrin receptors. *Nature* **386**, 833 (1997).

Chapter 5: Research Article

5.1 "Human Teneurin-1 is a direct target of the homeobox transcription factor EMX2 at a novel alternate promoter"

Abstract

Background: Teneurin-1 is a member of a family of type II transmembrane proteins conserved from C.elegans to vertebrates. Teneurin expression in vertebrates is best studied in mouse and chicken, where the four members teneurin-1 to -4 are predominantly expressed in the developing nervous system in area specific patterns. Based on their distinct, complementary expression a possible function in the establishment of proper connectivity in the brain was postulated. However, the transcription factors contributing to these distinctive expression patterns are largely unknown. Emx2 is a homeobox transcription factor, known to be important for area specification in the developing cortex. A study of Emx2 knock-out mice suggested a role of Emx2 in regulating patterned teneurin expression.

Results: 5'RACE of human teneurin-1 revealed new alternative untranslated exons that are conserved in mouse and chicken. Closer analysis of the conserved region around the newly identified transcription start revealed promoter activity that was induced by EMX2. Mutation of a predicted homeobox binding site decreased the promoter activity in different reporter assays in vitro and in vivo in electroporated chick embryos. We show direct in vivo binding of EMX2 to the newly identified promoter element and finally confirm that the endogenous alternate transcript is specifically upregulated by EMX2.

Conclusions: We found that human teneurin-1 is directly regulated by EMX2 at a newly identified and conserved promoter region upstream of the published transcription start site, establishing teneurin-1 as the first human EMX2 target gene. We identify and characterize the EMX2 dependent promoter element of human teneurin-1.

Author contribution statement: I performed the *in ovo* electroporations, β-galactosidase staining, the chromatin immunoprecipitation assay and the *in situ* hybridizations on mouse brains. I contributed to the study design, analysis and interpretation of the results, preparation of figures.

Beckmann *et al. BMC Developmental Biology* 2011, **11**:35
http://www.biomedcentral.com/1471-213X/11/35

BMC Developmental Biology

RESEARCH ARTICLE Open Access

Human teneurin-1 is a direct target of the homeobox transcription factor EMX2 at a novel alternate promoter

Jan Beckmann[1,2†], Antonio Vitobello[1,2†], Jacqueline Ferralli[1], Daniela Kenzelmann Brož[3], Filippo M Rijli[1,2] and Ruth Chiquet-Ehrismann[1,2*]

Abstract

Background: Teneurin-1 is a member of a family of type II transmembrane proteins conserved from *C.elegans* to vertebrates. Teneurin expression in vertebrates is best studied in mouse and chicken, where the four members teneurin-1 to -4 are predominantly expressed in the developing nervous system in area specific patterns. Based on their distinct, complementary expression a possible function in the establishment of proper connectivity in the brain was postulated. However, the transcription factors contributing to these distinctive expression patterns are largely unknown. Emx2 is a homeobox transcription factor, known to be important for area specification in the developing cortex. A study of Emx2 knock-out mice suggested a role of Emx2 in regulating patterned teneurin expression.

Results: 5'RACE of human teneurin-1 revealed new alternative untranslated exons that are conserved in mouse and chicken. Closer analysis of the conserved region around the newly identified transcription start revealed promoter activity that was induced by EMX2. Mutation of a predicted homeobox binding site decreased the promoter activity in different reporter assays *in vitro* and *in vivo* in electroporated chick embryos. We show direct *in vivo* binding of EMX2 to the newly identified promoter element and finally confirm that the endogenous alternate transcript is specifically upregulated by EMX2.

Conclusions: We found that human teneurin-1 is directly regulated by EMX2 at a newly identified and conserved promoter region upstream of the published transcription start site, establishing teneurin-1 as the first human EMX2 target gene. We identify and characterize the EMX2 dependent promoter element of human teneurin-1.

Background

Many transmembrane proteins mediate cell-cell interactions and thereby regulate key developmental processes. Teneurins are a unique family of type II transmembrane proteins conserved from *Drosophila melanogaster* and *Caenorhabditis elegans* to vertebrates, where four paralogues exist called teneurin 1-4 [1]. This protein class was discovered in a screen for the *Drosophila* homologue of the extracellular matrix protein tenascin-C [2]. Structure and domain architecture are highly conserved across phyla. All proteins of the teneurin family share a large extracellular domain with eight tenascin-type EGF-like repeats followed by a region of conserved cysteines and YD repeats [3]. Recently, several publications suggested that the C-terminal parts of the teneurin proteins contain peptides with similarities to corticotrophin-releasing factor (CRF) and might have a function in modulating CRF-mediated behavior [4]. All vertebrate teneurins have an N-terminal intracellular domain with two polyproline motifs, EF-hand-like metal ion binding sites and several putative phosphorylation sites. This intracellular domain was shown to be cleaved from the membrane and translocates into the nucleus where it can interact with transcription factors and alter gene expression [5-7].

In *C. elegans*, RNAi knockdown and deletion of its single teneurin gene (Ten-1) results in a broad range of phenotypes, including defects in axon guidance and neuronal

* Correspondence: ruth.chiquet@fmi.ch
† Contributed equally
[1]Friedrich Miescher Institute for Biomedical Research, Novartis Research Foundation, Maulbeerstrasse 66, CH-4058 Basel, Switzerland
Full list of author information is available at the end of the article

Beckmann *et al. BMC Developmental Biology* 2011, **11**:35
http://www.biomedcentral.com/1471-213X/11/35

pathfinding, as well as gonadal disintegration and protrusion of the vulva [8-10]. *Drosophila* harbors two teneurin genes, Ten-a [2] and Ten-m/Odz [11,12]. Mutations in either of these genes result in embryonic lethality and Ten-a mutants enhance the segmentation phenotype of weak alleles of Ten-m/Odz [13]. It was also shown that teneurin expression is required for the proliferation and cellular identity in the *Drosophila* eye [14]. Extensive localization studies in mouse [15-17] and chicken [5,18-20] embryos, as well as in rat [21] and zebrafish [22] revealed that the different members of the teneurin protein family are expressed with overlapping patterns by distinct subpopulations of neurons. Experiments *in vitro* and *in vivo* showed that the different members of the teneurin family form disulfide-linked dimers [16,23] and promote homophilic cell-cell adhesions and neurite outgrowth [18,24]. These functions of the protein are believed to mediate correct pathfinding and area recognition of neurons. This was shown in the teneurin-3 knockdown mouse, which exhibits dramatic changes in the mapping of ipsilateral retinal inputs causing mismatches in binocular mapping. This is associated with major deficits in the performance of visually mediated behavioral tasks [25].

Recent findings suggest an important role for the teneurin protein family in establishing cortical arealization and patterning in the developing embryo. Teneurin-2 was found to be expressed in developing limbs, somites and craniofacial mesenchyme in a pattern strikingly similar to that of fibroblast growth factor 8 (Fgf8) and Fgf8 coated beads implanted into chicken limb buds induced ectopic teneurin-2 expression *in situ* [20]. Furthermore, teneurin-4 transcripts are down regulated, and the expression patterns of teneurins are shifted in the cortices of mice deficient in Emx2 [26]. These findings link the regulation of teneurin expression to Fgf8 and Emx2, two proteins that are part of a complex network of growth and transcription factors regulating arealization of the developing brain, a crucial event regulating sensory perception, the control of our movements and behavior (reviewed in [27]). The best studied protein in this network is Emx2. Emx2 is the vertebrate homologue of the *Drosophila* empty spiracles (*ems*) protein, which is involved in the development of the fly head [28]. This protein is a homeobox-containing transcription factor implicated in mouse cerebral cortex development [29]. It is expressed in a graded manner from rostral (low) to caudal (high) [30-33]. Knock-out and overexpression studies of Emx2 showed the function of this transcription factor in establishing the correct size and positioning of cortical areas [reviewed in 34]. Comparing expression analyses of different embryonic stages to the adult for both Emx2 [32,33] and teneurins [5,7,35] showed that areas of Emx2 expression (e.g., the cortical plate, dentate gyrus and the olfactory bulb) strongly correlate with areas of teneurin expression, suggesting a possible role of teneurins in mediating arealization.

The human teneurin-1 gene resides on the × chromosome at position Xq25, a locus with low gene density [reviewed in 36]. Beside severe mental retardation, patients suffering from a syndrome mapped to this locus also suffer from motor sensory neuropathy, deafness and severely impaired vision [37-41]. Given the predominant expression in the developing brain and its function in establishing proper connectivity in the brain, teneurin-1 is a potential target gene for causing XLMR.

In order to provide the basis for an investigation of possible deletions and mutations in teneurin-1 of XLMR patients, we decided to delineate the gene locus and determined the transcription start site(s) of human teneurin-1. We identified a novel promoter upstream of the published transcription start, which is conserved in chicken and mice. We show that EMX2 directly binds to and regulates human teneurin-1 expression at this alternate promoter.

Results

Identification of alternate transcription start sites of the teneurin-1 gene

Whereas the expression and localization of the different members of the teneurin protein family are well characterized, promoter regions regulating teneurin gene expression in vertebrates have not yet been studied. To find the transcription start point of human, mouse and chicken teneurin-1 (gene name is ODZ1), we performed 5'-RACE on brain cDNAs of the respective species. We used gene-specific primers derived from the first coding exon and in each case identified two classes of products (Figure 1 and Table 1). The first class ended with the 5'UTR of the published first exon containing the translation start site (as depicted in the genome browser as ODZ1), and the second class included additional non-coding exons. Two additional exons were found in human, three in mouse, and one in chicken teneurin-1. All of these exons were between 80 kb and over 200 kb distant from the first coding exon. CpG islands were found surrounding the newly identified alternate first exon suggesting promoter activity in this region. Using 4 kb of sequence surrounding the newly identified first exon of human teneurin-1 to BLAST the mouse genome revealed that this entire region was conserved between species with an overall sequence identity of 58%, and included local sequence identities of over 90%. Based on these findings, we considered that teneurin-1 expression is regulated by two different promoters that are used to differentially regulate teneurin-1 expression.

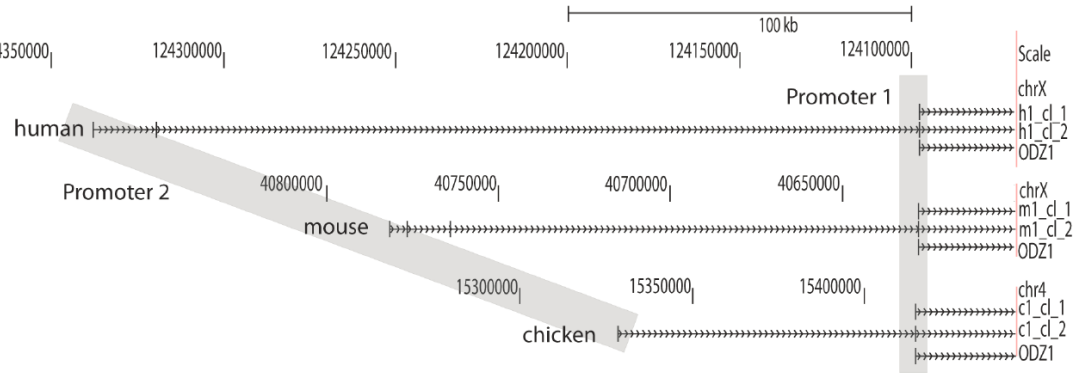

Figure 1 Determination of teneurin-1 transcription start sites. BLAT alignments to the corresponding RefSeq sequences of 2 representative clones per species obtained by 5' rapid amplification of cDNA ends are shown. The sequences of the clones are given in Table 1. The human clone h1_cl_1, the mouse clone m1_cl_1 and the chicken clone c1_cl_1 start with the annotated first exon containing the ATG translation start, whereas clones h1_cl_2, m1_cl_2 and c1_cl_2 contain up to three further non-coding exons. Based on the presence of two different transcription start sites, two alternate promoters (grey shaded areas) are postulated to control the expression of the two types of transcripts. Promoter 1 resides upstream of the first coding exon, whereas Promoter 2 is located about 100-200 kb upstream depending on the species analyzed.

EMX2 transactivates teneurin-1 promoter reporter constructs in cell culture

To test whether human teneurin-1 is a direct target gene of EMX2, we set up a reporter gene assay. We obtained a myc-flag-tagged EMX2 expression plasmid to transfect NIH3T3 cells. Recombinant EMX2 could be detected in cell extracts as a 37kD protein band on Western blots with a FLAG antibody (Figure 2a) and the protein accumulated in the nuclei of the cells as shown by immunostaining (Figure 2b). In order to do promoter reporter assays, we cloned a 4 kb fragment of highly conserved genomic sequence around the published transcription start site, as well as around the newly determined upstream transcription start site of human teneurin-1 into a pSEAP2-basic reporter vector. These promoter reporter constructs were co-transfected with the EMX2 plasmid into HEK293 cells and reporter gene activity was measured (Figure 2c). Interestingly, EMX2 was able to strongly induce reporter gene activity from the newly identified upstream promoter 2, but not from promoter 1, which remained unchanged compared to the empty vector control. Previously it was shown that EMX2 binds to a homeobox binding motif in the Wnt-1 promoter [42]. Upon sequence analysis of the promoter 2 construct we found one conserved site with a high score for EMX2 binding, while the promoter 1 construct possessed several high scoring binding sites. This indicates that the mere presence of core sequences of homeobox binding elements is not sufficient *per se* for the induction by EMX2, but the context may matter as well. To examine whether the homeobox binding motif in the promoter 2 construct contributes to the reporter gene activation upon EMX2 co-transfection, we mutated this motif and measured secreted embryonic alkaline phosphatase (SEAP) reporter gene activity. Indeed, the SEAP activity dropped significantly to 50% compared to the wild-type construct (Figure 2c).

EMX2 transactivates a teneurin-1 promoter construct in chick embryos electroporated *in ovo*

To further prove the promoter activity of the upstream sequence, as well as its dependence on EMX2 expression, we carried out an *in ovo* reporter gene assay in chick embryos. Upon co-electroporation of the promoter 2-lacZ construct with the EMX2 expression vector in the chick embryo neural tube, lacZ staining was strongly detected in the electroporated area (Figure 3b), whereas no staining was visible with the empty lacZ vector control (data not shown) or upon electroporation with the promoter 2-lacZ construct alone (Figure 3b). A GFP-expressing construct was always co-electroporated as well and used as a control for the efficiency of electroporation (Figure 3a).

To confirm the influence of the putative EMX2 binding motif on reporter gene activation *in vivo*, we co-electroporated the mutant promoter 2-lacZ construct with EMX2 and compared the staining with that of embryos co-electroporated with the wild-type promoter 2-lacZ construct and EMX2. Similar to the cell culture based reporter gene assay (Figure 2), reporter gene activity was also strongly reduced *in vivo*. Indeed, the vast majority of the embryos co-electroporated with EMX2 and the mutated promoter 2-lacZ construct showed a much fainter lacZ staining than those co-electroporated with

Beckmann *et al. BMC Developmental Biology* 2011, **11**:35
http://www.biomedcentral.com/1471-213X/11/35

Table 1 Sequences obtained in 5'RACE (Translation start site in bold and underlined)

clone name	sequence
h1_cl_1	TTTTTTTTTTTTTTTGAACTGAGCTTGCTTAATCAGAG**ATG**GAGCAAACTGACTGCAAACCCTACCA GCCTCTACCAAAAGTCAAGCATGAAATGGATCTAGCTTACACCAGTTCTTCTGATGAGAGTGAAG ATGGAAGAAAACCAAGACAGTCATACAACTCCAGGGAGACCCTGCACGAGTATAACCAGGAGCT GAGGATGAATTACAATAGCCAGAGTAGAAAGAGGAAAGAAGTAGAAAAATCTACTCAAGAGAT GGAATTCTGTGAAACCTCTCACACTCTGTGCTCTGGCTACCAAACAGACATGCACAGCGTTTCTCG GCATGGCTACCATCTAGA
h1_cl_2	TTTTTTTTTTTTTTTTGGCGGGGGANCAGCACCTGGGGACGCCGCCGAAACTTGCGCTTGGAATA GGAATTACAAGGGTGACCTTTATTCCGCTGTCTCCTTTTTGATTCCCATAACTTCTGGACCTATCAA GGACTGCTTGCATTAAAGGACTTCCTCATCCTTTTTTTTCATGAAACTGAGCTTGCTTAATCAGAG**A** **TG**GAGCAAACTGACTGCAAACCCTACCAGCCTCTACCAAAAGTCAAGCATGAAATGGATCTAGCT TACACCAGTTCTTCTGATGAGAGTGAAGATGGAAGAAAACCAAGACAGTCATACAACTCCAGGG AGACCCTGCACGAGTATAACCAGGAGCTGAGGATGAATTACAATAGCCAGAGTAGAAAGAGGA AAGAAGTAGAAAAATCTACTCAAGAGATGGAATTCTGTGAAACCTCTCACACTCTGTGCTCTGGC TACCAAACAGACATGCACAGCGTTTCTCGGCATGGCTACCATCTAGA
m1_cl_1	TTTTTTCCACCGCCACCTCCTCCACATGCCTGCACCTGTGCCAGGAAGCCACCTCCTACAGTGGAC TCTCTACAAAGAAGATCAATGACTACCCGCAGCCAGCCCAGCCCAGCTGCTCCTGCTCCTCCAACC AGCACACAGGATTCGGTTCATCTGCATAACAGCTGGGTCTTGAACAGTAACATACCGCTGGAGAC CAGGTACATTTTATGATTGACCATTTCAGCAAAGACTGTTTTCATTAAAGAACTTCCTTATCCTTTT TTCATGAAACTCAGCTTGCTTAATCAGAG**ATG**GAGCAAACAGACTGCAAACCTTATCAGCCTCTG TCCAAAGTCAAGCATGTCTAGA
m1_cl_2	TTTTTTCCCGCAGGAACCAGCAAAGACGCCCTAAGTCCAGCGCACTTACAGCACACCAGCAGAGC TGAGTACCTGGCAAGGAGGCGGGGGACCGCACCTGAGGACATCACTGAAACTTGCGCCTGGACT AGTCCTTCTACTGCCATGGAAACTAGATGGCACAGACAGCGGAGAGTCACTCATTCAGAACAGG GGCCCCCTTTTTAATTTCATGTCAGCCTGTTGGTCCCTGAAAGTAACTGAAAAGGAATTACAAGA GCGACTTTTATTCTGTGTAACTTCTCTTCTGGATCTAACAAGGTACATTTTATGATTGACCATTTCA GCAAAGACTGTTTTCATTAAAGAACTTCCTTATCCTTTTTTCATGAAACTCAGCTTGCTTAATCAGA G**ATG**GAGCAAACAGACTGCAAACCTTATCAGCCTCTGTCCAAAGTCAAGCATGTCTAGA
c1_cl_1	TTTTTTTCCTCATTCCTTAAGGAATTCCAGTTGCTTGTTTTCATGATTTTGAGCCTATTCAGCCAGA G**ATG**GAGCAGATGGACTGCAAACCCTACCAGCCACTGTCAAAAGTTAAACATGAAGTGGATCTA ACNTTACACAAGTTCTTCAGATGAAAGTGAAGATGGCAGAAAGCAAAGGCAATCTTATGACTCA AGAGAAACTCTGAATGAATATAGCCAAGAGCTAAGACTGAACTACAACAGTCAAGGCAGAAAAA GAAAAAATACTGACCAATCCACACAAGACATGGAATTCTGTGAGACACCCCACATTCTGTGCTCT GGCTACCAAACAGATTTACATGGTGTGTCGGAGCACAGCTACCCACTAGAGGTGGGCTCAGATG TTGATACTGAAACCGAAGGTGGCGCATCACCAGATCATGCCCTGAGGATGTGGATGAGGGGGAT GAAGTCAGAACACAGCTCCTGTCCGTCAAGCCGGGCAAACTCAGCGTTGTCCCTGACTGACACTG ACCATGAGAGGAAGTCTGATGGGGAGAATGACATGCCGGGGAGCCCACACAACCAGTTCACGTT TCTAGA
c1_cl_2	TTTTTTTCGCCGAGCCTAGAGGCGATGGGAGCTGCCGAGCCGGGGCGCTGCTGAAAGTTCAGCC GGTGGCCGCGCAGCGCGGACTCATCCTTAAGGAATTCCAGTTGCTTGTTTTCATGATTTTGAGCC CATTCAGCCAGAG**ATG**GAGCAGATGGACTGCAAACCCTACCAGCCACTGTCAAAAGTTAAACAT GAAGTGGATCTAACTTACACAAGTTCTTCAGATGAAAGTGAAGATGGCAGAAAGCAAAGGCAAT CTTATGACTCAAGAGAAACTCTGAATGAATATAGCCAAGAGCTAAGACTGAACTACAACAGTCAA AGCAGAAAAAGAAAAAATACTGACCAATCCACACAAGACATGGAATTCTGTGAGACACCCCACA TTCTGTGCTCTGGCTACCAAACAGATTTACATGGTGTGTCGGAGCACAGATACTCTAGA

EMX2 and the wild type promoter 2-lacZ construct (Figure 3b). These findings show that EMX2 is able to induce reporter gene activity at the alternate teneurin-1 promoter and that this activation is greatly dependent on an intact homeobox binding motif.

EMX2 binds a homeobox core element in the alternate teneurin-1 promoter

To prove that the activation of the construct is due to the direct binding of EMX2 to the homeobox binding motif in the novel upstream promoter, we performed an electrophoretic mobility shift assay (EMSA). Nuclear extracts of HEK293 cells transfected with the EMX2 construct showed a shift of the labeled probe containing the putative homeobox binding site of the upstream promoter, whereas no shift was observed in nuclear extracts of untransfected HEK293 cells or with a mutated labeled probe (Figure 4a, lanes 1-3). To show the specificity of the binding, the effect of wild-type or mutated unlabeled oligo-nucleotide on the protein/DNA interaction was analyzed. Whereas no shift of the oligo-probe was visible when competing with the unlabeled wildtype oligo-nucleotide, the shift was still detected in the presence of excess mutant unlabeled oligo-nucleotide (compare lanes 4 and 5). The complex was super-shifted with a c-myc antibody against the tagged EMX2, and indeed the shifted band disappeared (lane 6). This indicates a direct binding of EMX2 to the probe, but due to a high unspecific background the super-shifted band could not be resolved.

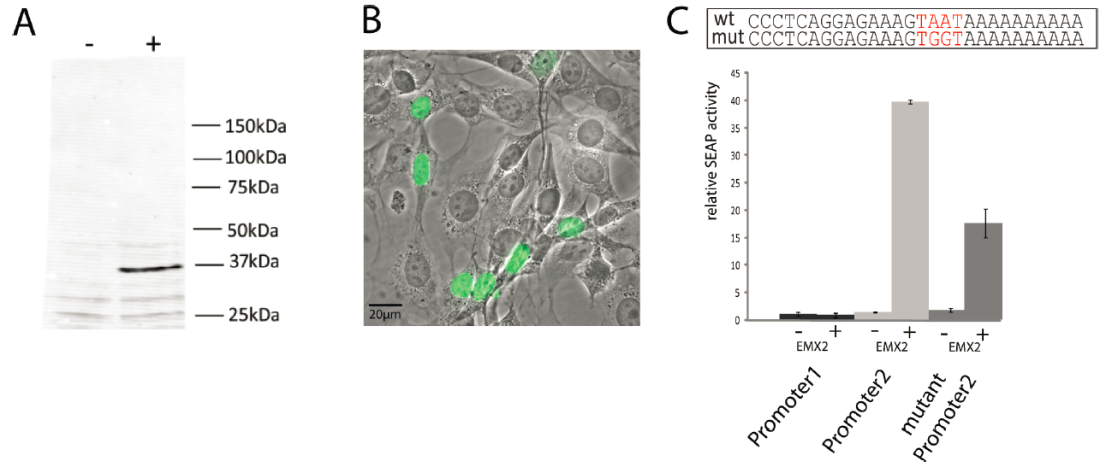

Figure 2 Transcriptional activation of teneurin-1 promoter reporter constructs by EMX2. (A) NIH3T3 cells were transfected with a flag-myc-tagged EMX2 construct or an empty vector and tested for expression by Western blot of whole cell extract with anti-Flag. (B) Immunostaining of the cells with anti-Flag reveals the nuclear accumulation of the EMX2 protein in the nuclei of the cells. (C) HEK293 cells were transfected with EMX2 or empty vector control and co-transfected with different promotor constructs as indicated. The graph shows relative SEAP values for one representative experiment performed in triplicates (n = 5). The activity obtained with the Promotor 1 construct is arbitrarily set to 1. Error bars display standard deviation of the mean. The sequences of the region harboring the putative binding site and the mutation used (mut Promoter 2) are shown in the box above the bar graph.

To reduce the unspecific background obtained with the nuclear extract, we tested EMX2 produced by *in vitro* transcription and translation in the gel shift assay. Whereas no shift of the labeled probe was detected with mock extracts, the same shifted band as with the nuclear extract could be detected with *in vitro* transcribed and translated EMX2 (Figure 4b, lanes 1 and 2), while unspecific background was greatly reduced. The binding of the protein to the probe was successfully competed with an excess of unlabeled wildtype oligo-nucleotides (Figure 4b, lane 3), whereas no competition was detected for unlabeled mutated oligo-nucleotides (Figure 4b, lane 4). Adding c-myc antibody to the binding reaction resulted in a super-shifted band (Figure 4b, lane 5), indicating a direct binding of EMX2 to the homeobox motif in the alternate teneurin-1 promoter.

To test whether an interaction between EMX2 and the binding site in the teneurin-1 promoter can also occur *in vivo* without overexpression of the EMX2 protein, we tested nuclear extracts of brains from E12.5 embryos known to express high EMX2 levels in the EMSA assay (Figure 4c). We were able to detect a shift of the band with the embryo extract, which runs lower than the complex of the overexpressed tagged protein in the control (compare Figure 4c, lanes 1, 2). We were able to compete the binding to the probe with wildtype unlabeled oligo-nucleotides, whereas no competition was detected using the unlabeled mutated oligo-nucleotide (Figure 4c, lanes 3-4). As a final proof of direct binding of EMX2 to the endogenous teneurin-1 promoter at the homeobox binding site *in vivo*, we performed chromatin immunoprecipitation (ChIP) in chicken embryos electroporated with the FLAG-myc-tagged EMX2 construct. Electroporations were performed in developing telencephalic regions in order to test the ability of Flag-myc-tagged EMX2 to bind the target region in its physiological cell context. Indeed, we detected specific enrichment of the target region containing the homeobox binding site after ChIP with the anti-FLAG antibody, recognizing the electroporated tagged EMX2 protein compared to a negative control region, which was not the case in control embryos (Figure 4d).

Teneurin-1 expression pattern correlates with that of *EMX2* in E14.5 embryos

To test whether the endogenous teneurin-1 expression pattern overlaps with sites of EMX2 expression in the developing brain, we performed *in situ* hybridizations with a probe for EMX2, a probe for total teneurin-1 and an additional probe specific for the alternate transcript of teneurin-1 on adjacent sagittal brain sections (Figure 5). The staining for teneurin-1 transcripts showed expression at sites that are in accordance with those reported before for E15.5 embryos [26]. Interestingly, staining with a probe specific for the alternate transcript revealed the same staining pattern as the probe for total teneurin-1, indicating that the long transcripts are indeed expressed at these stages of embryogenesis. We detected a correlation

Beckmann *et al. BMC Developmental Biology* 2011, **11**:35
http://www.biomedcentral.com/1471-213X/11/35

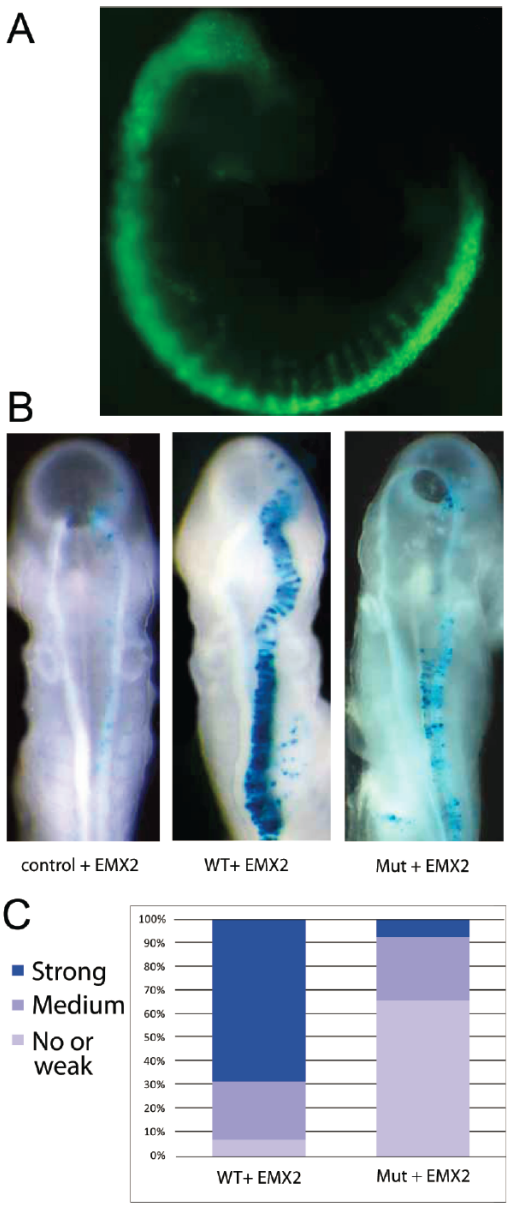

Figure 3 Chicken Embryo Electroporation. (A) Embryos were electroporated at Hamburger and Hamilton stage 10 and collected 24 h later. A CMV-GFP plasmid was always used as positive control of the electroporation and only embryos showing an expression pattern as shown were kept. Embryos electroporated with beta-globin_LacZ (BGZ40) plasmid alone or in combination with EMX2 in pCMV6-Entry (CMV-EMX2) were used as negative controls (not shown). (B) A 4 kb genomic fragment of the teneurin-1 promoter was cloned into the reporter plasmid beta-globin-LacZ (ten-1BGZ40) and electroporated alone (WT control) or in combination with CMV-EMX2 plasmid (WT + EMX2). A mutated version of ten-1BGZ40 lacking a potential EMX2 binding site (mut ten-1BGZ40) was electroporated alone (data not shown) or in combination with CMV-EMX2 (Mut + EMX2). (C) Electroporation results are summarized in stacked columns. Data are represented as percentile of the total number of electroporated embryos (n = 16 for the WT construct and n = 26 for the mutated construct) and are classified according to three levels of reporter expression: strong staining, medium staining and no or weak staining.

between the teneurin-1 signals and the EMX2 signal in a caudal high to rostral low gradient. We find teneurin-1 being expressed in the marginal, but not in the ventricular zone of the cortex. Especially good correlations were found in the caudal cortex, olfactory bulb (ob) and hippocampus (hi) (Figure 5).

EMX2 specifically induces the transcription of the alternate transcript

To test whether EMX2 is able to induce the endogenous teneurin-1 gene from the alternate promoter, we set up a real-time Q-PCR assay. We compared the mRNA expression level for total teneurin-1, as well as for the presence of the exons specific for the alternate transcript in parental HEK293-ECR cells with HEK293-ECR cells stably expressing myc-flag-tagged EMX2 (Figure 6). Indeed, the EMX2 expressing cells showed significantly ($p < 0.01$) elevated transcript levels of total teneurin-1. Although we generally observed a low expression level for the alternate transcript in our cells, it showed a much higher fold induction upon EMX2 expression than the total mRNA. This is further support for our reporter gene studies on the level of the endogenous gene and represents an independent confirmation that EMX2 specifically acts on the alternate promoter of teneurin-1.

Discussion

In this work, we characterized the teneurin-1 gene locus and found novel upstream exons which are conserved between species. These new exons expand the size of the Odz1 locus to more than 800 kb, harboring one intron which is more than 200 kb in size. Genes with large introns have been reported before [43]. A continuous transcription of the entire gene, given a polymerization rate of 3800 nucleotides per minute by RNA polymerase II, would take 3.5 h [44]. This might add another level of regulation of the defined expression in time and space. Here we show that there are at least two promoters regulating teneurin-1 expression with one alternate promoter upstream of the published transcription start. Only this alternate promoter was inducible by EMX2 in reporter gene assays and cells stably overexpressing EMX2 exhibited an increase of the resulting alternate transcript. A single homeobox binding site seems to be critical for the

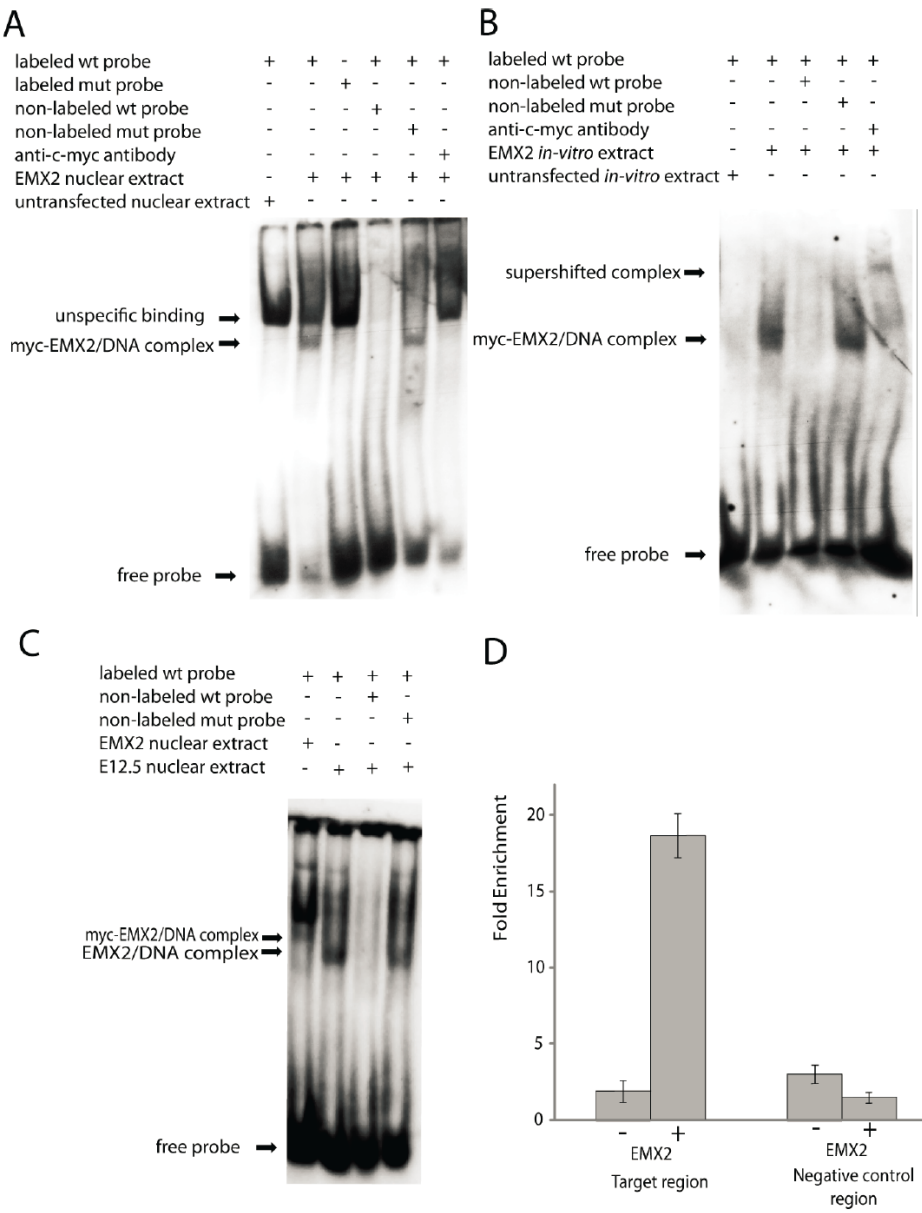

Figure 4 Direct binding of EMX2 to teneurin-1 promoter oligo-nucleotide probes. (A) Electrophoretic Mobility Shift Assays (EMSA) using EMX2 containing nuclear extract or control nuclear extract were performed in the presence or absence of Dig-labeled probe, unlabeled probe for competition, mutated probes and anti-myc antibody as indicated above the lanes. A specific myc-EMX2/DNA complex could be detected as indicated by an arrow. (B) EMSA with in vitro transcribed and translated EMX2 protein or control extracts were analyzed using Dig-labeled wildtype and mutated probes as indicated. Binding to the probe resulted in a myc-EMX2/DNA complex as indicated by an arrow that was competed by unlabeled probe and resulted in a supershifted complex after addition of anti-myc-antibody as indicated. (C) EMSAs with nuclear extracts of E12.5 embryos and nuclear extract of myc-EMX2 overexpressing cells as a control were performed using Dig-labeled wildtype probe. Binding to the probe resulting in a myc-EMX2/DNA complex and an EMX2/DNA complex is indicated by arrows. (D) ChIP of chicken embryos electroporated with flag-myc-tagged EMX2 (+) and control chicken embryos (-). Fold enrichment of the target region, containing the homeobox binding site versus a negative control region from the coding region of the same gene after anti-flag precipitation is shown. Error bars display standard deviation of the mean.

Beckmann *et al. BMC Developmental Biology* 2011, **11**:35
http://www.biomedcentral.com/1471-213X/11/35

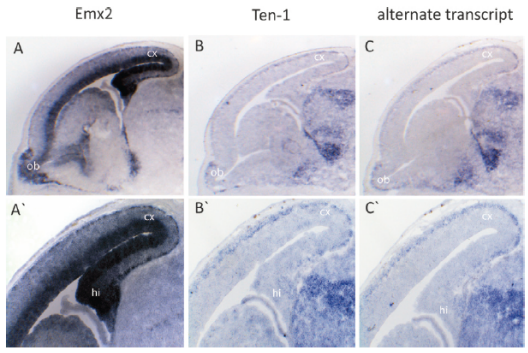

Figure 5 *In-situ* hybridizations for Teneurin-1 and EMX2 expression on sagittal sections at E14.5 mouse embryos. (A; A') Expression of EMX2 in the cortex at higher magnification in A'. (B; B') Expression of total teneurin-1 in an adjacent section. (C; C') Expression of the alternate transcript of teneurin-1 in an adjacent section. Ob, olfactory bulb; hi, hippocampus

promoter activity and is bound directly by EMX2, as shown by gel shift assay and ChIP in chicken embryos. Although one has to take into account that the teneurin-1 expression, especially in later developmental stages, opposes the expression pattern of EMX2, a direct regulation of teneurin-1 expression by EMX2 is likely to occur at earlier stages. First, we and others [26] showed that

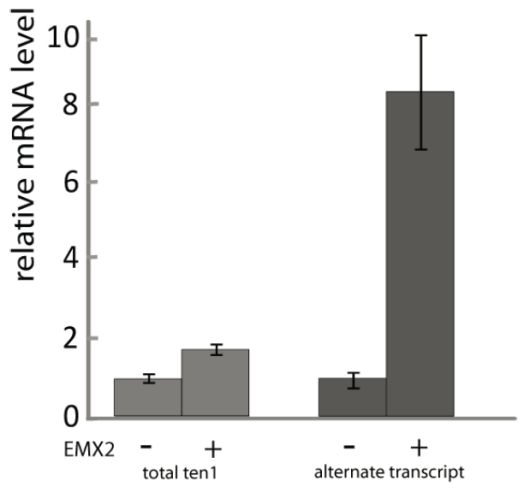

Figure 6 Activation of the alternate transcript by EMX2. RNA was isolated from parental HEK293 cells (-) and HEK293 cells stably expressing EMX2 (+). Teneurin-1 mRNA levels of 3 independent preparations were measured by real-time PCR. The graph shows total teneurin-1 mRNA (total ten1) and mRNA levels under control of the alternate promoter (alternate transcript) relative to GAPDH mRNA values. Values of the parental cells were arbitrarily set to 1. Error bars display standard error of the mean.

total teneurin-1 expression, as well as the expression of the alternate transcript, correlates well with EMX2 expression at E14.5. Secondly, the expression of teneurin-1 is highly dynamic and its patterned expression and the overall expression level collapses in EMX2-deficient mice [26]. Notably, we found teneurin-1 being expressed in the marginal, but not in the ventricular zone of the cortex. This suggests a possible function of EMX2 in post-mitotic neurons via the control of teneurin-1. Based on these findings, it is conceivable that the promoter at the published transcription start is responsible for the basal expression of teneurin-1, whereas the novel promoter is responsible for the graded expression dependent on EMX2. This finding suggests that this promoter region of the teneurin-1 gene is essential in establishing correct patterning of teneurin-1 expression. Although the transcription factors involved in correct patterning and arealization are well known, and their expression patterns are well characterized, very little is known about the downstream mechanisms contributing in establishing proper arealization and pathfinding [reviewed in 45]. A number of reports describe screens to find genes which are differentially expressed within the cortex [24,46,47] or which are potential target genes of differentially expressed transcription factors [11,26,48-50]. Interestingly, in both types of approaches members of the teneurin protein family were revealed as differentially expressed genes, supporting the evidence for a role of teneurin in arealization. Lists of potential target genes of the transcription factors involved in arealization, like Emx2 or Pax6, have also been described in knock-out gene expression studies [26,31,48], but indirect effects on transcription cannot be ruled out and interesting targets need to be validated. In this study, we validated teneurin-1 as the first direct target gene of EMX2 in human. As a transmembrane protein, teneurin-1 is well-suited to convey nuclear signals to the level of cell-cell interactions. However, the molecular mechanisms of how teneurins mediate their proposed function in brain development and patterning of the cortex remain to be elucidated.

Many cases of XLMR have been mapped to Xq25, the locus of the teneurin-1 gene [37-41]. Interestingly, many of these individuals suffer from motor sensory neuropathy [37], and teneurin-1 is predominantly expressed in patterns that relate to anterior sensorimotor areas [26]. Taking into account the regulation of teneurin-1 by EMX2 at the novel promoter, setting up proper arealization of the developing cortex, and the well established functions of teneurins in correct pathfinding and neurite growth, we consider teneurin-1 as a potential target gene for XLMR. When analyzing patient samples, attention should be given to the newly established promoter region, as mutations or deletions in this area could lead to a shift in expression of teneurin-1 early in the developing brain

leading to improper connectivity and consequently to XLMR.

Conclusion

In this work, we show that teneurin-1 expression is regulated by EMX2 at a novel and conserved upstream promoter. We present teneurin-1 as the first direct target gene in humans and characterize the binding site in the newly identified promoter region.

Methods

Rapid amplification of 5' complementary DNA ends (5' RACE)

Total RNA of mouse and chicken brain tissue was purified with QiaShredder and RNA Easy kit (Qiagen, Hombrechtikon, CH) according to manufacturer's instructions. Using these RNA extracts and total human adult normal brain RNA (ams Biotechnology, Oxon, UK) 5'RACEs were performed with the 2nd generation 5'/3'RACE kit (Roche Diagnostic, Mannheim, Germany) according to manufacturer's instructions. Nested PCRs with the primer sequences shown in Table 2 were performed. The bands obtained were purified and cloned into vector pKS$^+$ and sequenced. The sequences were analyzed using the BLAT algorithm on human genome assembly GRCh37, mouse assembly July 2007 and chicken assembly May 2006 (http://genome.ucsc.edu) [51].

Promoter studies

The promoter constructs for human teneurin 1 were amplified from human genomic DNA using the Expand High Fidelity system (Roche) with primer hten1 promoter 1 **XhoI** fw (all primer sequences are given in Table 2) and hten1 promoter 1 **HindIII** rev using the highlighted restriction sites for directional cloning into vector pSEAP2-Basic (Clontech, Mountain View, CA, USA) of the promoter 1 construct. For the hten1 promoter 2 construct, we used hten1 promoter 2 **NheI** fw and hten1 promoter 2 **EcoRI** rev using the highlighted restriction sites for directional cloning into the same vector. The promoter 1 construct contains a sequence of just over 2 kb from nt124097602 to nt124099666 of chromosome × and the promoter 2 construct around 4 kb from nt124336306 to nt124340205 on chromosome × of assembly GRCh37. Analysis of the promoter sequences for potential binding sites was done using the JASPAR database (http://jaspar.cgb.ki.se[52]) and the *ems* matrix. Mutation of the potential homeobox-binding sequence (nt124338584 to nt124338589 on chromosome X) in the promoter 2 was achieved using overlapping PCR with the primer set for hten1 promoter2 and mutated promoter 2 fw and rev. HEK293-EBNA cells were plated at 1 × 10^5 cells per well in six-well plates 18 h before transfection. Cells were transfected in DMEM containing 0.3% FCS with Fugene 6 Transfection reagent (Roche) using 1 μg promoter construct DNA and co-transfected with either empty 1 μg pcDNA3 or flag- and myc-tagged EMX2 in pCMV-Entry (OriGene, Rockville, MD, USA) as indicated in the Result section. Twenty-Four hours after transfection, the medium was collected and SEAP reporter gene activity was measured and normalized for the co-transfected plasmid pGL3, expressing firefly luciferase (Promega, Madison, WI, USA) as previously described [53].

Table 2 Primer sequences

Primer name	Sequence
human RT-PCR	TTAGTGCATGGTCAGGTGAGG
mouse RT-PCR	TCTCCCATCTTCACTCTCATCAG
chicken RT-PCR	GCTGTGTTCTGACTTCATCC
hten PCR1 rev	GTGTCCACATCAGATCCCATCTC
hten nested **XbaI** rev	TAGT**TCTAGA**GCACAGGTGCAGGCATGAGG
mouse PCR1 rev	CTCCAGCTGGTAGCCATGTCG
mouse nested **XbaI** rev	TAGT**TCTAGA**TCTGTGTGGTAGCCGGAGCAC
chicken PCR1 rev	ATGCGCCACCTTCGGTTTCAG
chicken nested **XbaI** rev	TAGT**TCTAGA**GTAGCTGTGCTCCGACACACC
oligo dT anchor primer	GACCACGCGTATCGATGTCGACTTTTTTTTTTTTTTT
hten1 promotor 1 **XhoI** fw	ACTA**CTCGAG**CAAGACCCATGCTGAAGCT
hten1 promotor 1 **HindIII** rev	ACTA**AAGCTT**CTCTGATTAAGCAAGCTCAGTTTC
hten1 promoter 2 **NheI** fw	ACTA**GCTAGC**CCCCTAGAGTGTTCAGCTCT
hten1 promoter 2 **EcoRI** rev	ACTA**GAATTC**GGGCCACCTCAAAAACACCTCC
mutate promoter 2 fw	CCACCCCTCACCCTCAGGAGAAAGTGGTTAAA
mutate promoter 2 rev	TTTAACCACTTTCTCCTGAGGGTGAGGGGTGG
total ten1 qPCR fw	GCATAGTTCCTGTTTGTCCA
total ten1 qPCR rev	TCTGCACATCTTGAGTAGAC
alt exon qPCR fw	GCTTGGAATAGGAATTACAAGG
alt exon qPCR rev	GAAGTCCTTTAATGCAAGCAG
hGAPDH qPCR fw	GGAGTCAACGGATTTGGTC
hGAPDH qPCR rev	AAACCATGTAGTTGAGGTC
ChIP target region fw	TTCAGCTTCCTCGTTCTTCG
ChIP target region rev	GGTGGTTACAACCGCCTTTT
ChIP negative control fw	AGATTCCTGTGAGCCCTGCT
ChIP negative control rev	TCCAACAACTCATGCAATGG

Real-time Q-PCR

HEK293-ECR cells were transfected as described before with the flag-myc-tagged EMX2 construct in pCMV and cells were selected for stably expressing clones with G418 (Roche) for 2 weeks. Clones were pooled and expression of the construct was tested by Western blot

Beckmann *et al. BMC Developmental Biology* 2011, **11**:35
http://www.biomedcentral.com/1471-213X/11/35

(data not shown). From these cells and untransfected HEK293-ECR cells RNA was isolated with QiaShredder and the RNA Easy kit (Qiagen) following the manufacturer's protocol. From this preparation, cDNA was generated using the Superscript III (Invitrogen) polymerase and random primers following the standard protocol. Real-time Q-PCR was performed on these samples with teneurin-1 specific primers and normalized to GAPDH values (sequences Table 2) using SYBR QPCR Supermix with ROX (Invitrogen) on an AbiPrism 7000 system. Three independent experiments were performed and the averaged results are shown and p-values were calculated using the one-way ANOVA.

In ovo electroporation

For reporter assay experiments, chicken eggs were incubated in a humidified chamber at 38°gC and DNA constructs were injected into the lumen of the neural tube of stage Hamburger Hamilton (HH) 10-12 embryos. Construct concentrations were: 1 μg/μl lacZ reporter construct (BGZ40; [54]), 1 μg/μl EMX2 expression vector, and 0.2 μg/μl co-injected EGFP in pCMV as positive control of electroporated cells. Embryos were harvested 24 hours after electroporation and processed for β-galactosidase staining. For EMX2 overexpression, 1 μg/μl of Myc/FLAG-tagged EMX2 expression vector and 0.2 μg/μl of pCMV-EGFP construct were co-injected into the lumen of forebrain of stage HH 14 embryos. Positive tissues (n = 20 brains) were collected 72 hours after electoporation and immediately processed for chromatin cross-linking. As negative control, the same amount of unelectroporated tissue was collected and processed for ChIP experiments. Electroporations were performed as described previously using a square wave electroporator [54].

Chromatin immunoprecipitation Assay

Brains were chopped and then cross-linked in 1% Formaldehyde (F8775, Sigma) for 10 minutes at room temperature. Cross-linking was stopped in 125 mM Glycine for 5 minutes and the material was washed three times in ice cold PBS containing EDTA-free Protease Inhibitor Cocktail (Complete, 04693132001, Roche). DNA shearing was performed in lysis buffer (50 mMTris-HCl pH8.0, 10 mM EDTA, 1%SDS, 1 × Protease Inhibitor Cocktail) using the following parameters: 20 cycles of 30 seconds ON/30 seconds OFF (Diagenode bioruptor sonicator, high power setting).

Chromatin immunoprecipitation was performed by using Dynabeads protein G (100.04D, Invitrogen) as described elsewhere [55]. The following antibodies were used: Mouse monoclonal anti-FLAG M2 (F1804, Sigma), Mouse control IgG (AB18413, Abcam).

Electrophoretic Mobility Gel Shift Assay (EMSA)

EMX2 binding to the promoter construct was examined by Electrophoretic Mobility Gel Shift Assay (EMSA) using DIG-labeled double-stranded oligo-nucleotides (5'CAGGAGAAAGTAATTAAAAAA3' or with mutated binding site 5'CAGGAGAAAGTGGTTAAAAAA3', putative binding site underlined). For probe preparation, 5 μg of sense and anti-sense oligo-nucleotides were diluted in 90 μl TE buffer, incubated for 10 min at 95°C and cooled down for 30 min at room temperature for annealing. DIG-labeling of the probes was achieved using the DIG Gel Shift Kit, 2nd Generation (Roche) according to the manufacturer's instructions. For the gel shift assay, nuclear extracts from stably EMX2 expressing HEK293 cells, *in-vitro* translated extracts or nuclear extracts of E12.5 embryo brains containing 20 μg of total protein were incubated with 4 μl of 5 × binding buffer of the Gel Shift Kit, 1 μg double-stranded poly (dIdC) and 0.1 μg poly-L-lysine in a 19 μl reaction mix. For the competition assay, unlabeled wild-type or mutant annealed oligo-nucleotide were added with a 150-fold excess. This mix was incubated for 20 min at room temperature. Afterwards, 1 μl of labeled probe was added and the mix was incubated for another 20 min at 30°C. For supershifts, 1 μl of c-myc antibody (Sigma) was added after 10 min incubation with the labeled probe. Following another 10 min of incubation, the reaction mix was loaded onto a precast 6% DNA retardation gel (Invitrogen, Carlsbad, CA, USA), which was pre-run in 0.5 × TBE for 20 min at 80 V and 4°C. The gel was run for 1.5 h at 80 V and 4°C. After separation, the complexes were blotted on a positively charged nylon membrane in 0.5 × TBE for 45 min at 280 mA and DIG detection was performed as described in the manufacturer's instructions.

In-vitro transcription and translation of EMX2

In-vitro transcription and translation of EMX2 was achieved using the TNT® Coupled Reticulocyte Lysate System (Promega). 25 μl of TNT® rabbit reticulocyte lysate, 2 μl TNT® reaction buffer, 1 μl TNT® T7 RNA polymerase, 0.5 μl of each Amino Acid mixture without Leucine and without Methionine and 1 μg of EMX2-pCMV-Entry were mixed in a 50 μl reaction mix and incubated for 90 min at 30°C, quick frozen in dry ice/ethanol and stored at -80°C until used in EMSA.

In-situ hybridization

In-situ hybridizations on sections were performed as previously described [56]. The following RNA probes were used: For EMX2 we used the entire CDS of EMX2 (NM_010132.2), for total teneurin-1 we used the probe previously published [26] and for the probe specific for

the alternate transcript we used the sequence described in Table 1 (m1_cl_2) plus the first 100 bp of the CDS of mouse teneurin-1 (NM_011855.3).

Abbreviations

XLMR: X-linked mental retardation; hten1: human teneurin-1; EMSA: Electrophoretic Mobility Shift Assays; RACE: rapid amplification of cDNA ends; CRF: corticotrophin-releasing factor; SEAP: secreted embryonic alkaline phosphatase; ChIP: Chromatin Immunoprecipitation

Acknowledgements

We thank Hans-Rudolf Hotz for the help with the UCSC genome browser, Richard P. Tucker for critical reading of the manuscript and Jean-François Spetz for providing the mouse embryos. This work was supported by the Novartis Research Foundation.

Author details

[1]Friedrich Miescher Institute for Biomedical Research, Novartis Research Foundation, Maulbeerstrasse 66, CH-4058 Basel, Switzerland. [2]University of Basel, Faculty of Science, Basel, Switzerland. [3]Current Address: Department of Radiation Oncology, Division of Radiation and Cancer Biology, Stanford University School of Medicine, Stanford, CA 94305, USA.

Authors' contributions

JB prepared all constructs, participated in the 5'RACE, performed sequence alignments, EMSA and QPCR and prepared the first draft of the manuscript. AV performed the chicken electroporation and the ChIP experiments as well as the mouse *in-situ* hybridization. JF performed the SEAP assay and validated EMX2 expression. DKB performed the 5'RACE in chicken and mouse. FMR participated in the planning and discussion of the experiments. RCE participated in the planning and discussion of the experiments, writing the paper and preparation of the figures. All authors read and approved the final manuscript.

Received: 27 September 2010 Accepted: 8 June 2011
Published: 8 June 2011

References

1. Tucker RP, Kenzelmann D, Trzebiatowska A, Chiquet-Ehrismann R: **Teneurins: Transmembrane proteins with fundamental roles in development.** *The International Journal of Biochemistry & Cell Biology* 2007, **39**:292-297.
2. Baumgartner S, Chiquet-Ehrismann R: **Tena, a *Drosophila* gene related to tenascin, shows selective transcript localization.** *Mechanisms of Development* 1993, 165-176.
3. Minet AD, Chiquet-Ehrismann R: **Phylogenetic analysis of teneurin genes and comparison to the rearrangement hot spot elements of *E. coli*.** *Gene* 2000, **257**:87-97.
4. Lovejoy DA, Rotzinger S, Barsyte-Lovejoy D: **Evolution of Complementary Peptide Systems.** *Annals of the New York Academy of Sciences* 2009, **1163**:215-220.
5. Kenzelmann D, Chiquet-Ehrismann R, Leachman NT, Tucker RP: **Teneurin-1 is expressed in interconnected regions of the developing brain and is processed *in vivo*.** *BMC Developmental Biology* 2008, **8**:30.
6. Nunes SM, Ferralli J, Choi K, Brown-Luedi M, Minet AD, Chiquet-Ehrismann R: **The intracellular domain of teneurin-1 interacts with MBD1 and CAP/ponsin resulting in subcellular codistribution and translocation to the nuclear matrix.** *Experimental Cell Research* 2005, **305**:122-32.
7. Bagutti C, Forro G, Ferralli J, Rubin B, Chiquet-Ehrismann R: **The intracellular domain of teneurin-2 has a nuclear function and represses zic-1-mediated transcription.** *Journal of Cell Science* 2003, **116**:2957-66.
8. Drabikowski K, Trzebiatowska A, Chiquet-Ehrismann R: **ten-1, an essential gene for germ cell development, epidermal morphogenesis, gonad migration, and neuronal pathfinding in *Caenorhabditis elegans*.** *Developmental Biology* 2005, **282**:27-38.
9. Trzebiatowska A, Topf U, Sauder U, Drabikowski K, Chiquet-Ehrismann R: ***Caenorhabditis elegans* teneurin, ten-1, is required for gonadal and pharyngeal basement membrane integrity and acts redundantly with integrin ina-1 and dystroglycan dgn-1.** *Molecular Biology of the Cell* 2008, **19**:3898-908.
10. Mörck C, Vivekanand V, Jafari G, Pilon M: ***C. elegans* ten-1 is synthetic lethal with mutations in cytoskeleton regulators, and enhances many axon guidance defective mutants.** *BMC Developmental Biology* 2010, **10**:55.
11. Baumgartner S, Martin D, Hagios C, Chiquet-Ehrismann R: **Ten(m), a *Drosophila* gene related to Tenascin, is a new pair-rule gene.** *EMBO Journal* 1994, **13**:3728-3740.
12. Levine A, Bashan-Ahrend A, Budai-Hadrian O, Gartenberg D, Menasherow S, Wides R: ***odd Oz*: A novel Drosophila pair rule gene.** *Cell* 1994, **77**:587-598.
13. Rakovitsky N, Buganim Y, Swissa T, Kinel-Tahan Y, Brenner S, Cohen MA, Levine A, Wides R: ***Drosophila* Ten-a is a maternal pair-rule and patterning gene.** *Mechanisms of Development* 2007, **124**:911-924.
14. Kinel-Tahan Y, Weiss H, Dgany O, Levine A, Wides R: ***Drosophila* odz gene is required for multiple cell types in the compound retina.** *Developmental Dynamics* 2007, **236**:2541-2554.
15. Ben-Zur T, Feige E, Motro B, Wides R: **The Mammalian Odz Gene Family: Homologs of a *Drosophila* Pair-Rule Gene with Expression Implying Distinct yet Overlapping Developmental Roles.** *Developmental Biology* 2000, **217**:107-120.
16. Oohashi T, Zhou X-H, Feng K, Richter B, Morgelin M, Perez MT, Su W-D, Chiquet-Ehrismann R, Rauch U, Fassler R: **Mouse Ten-m/Odz Is a New Family of Dimeric Type II Transmembrane Proteins Expressed in Many Tissues.** *Journal of Cell Biology* 1999, **145**:563-577.
17. Zhou X-H, Brandau O, Feng K, Oohashi T, Ninomiya Y, Rauch U, Fässler R: **The murine Ten-m/Odz genes show distinct but overlapping expression patterns during development and in adult brain.** *Gene Expression Patterns* 2003, **3**:397-405.
18. Rubin BP, Tucker RP, Brown-Luedi M, Martin D, Chiquet-Ehrismann R: **Teneurin 2 is expressed by the neurons of the thalamofugal visual system *in situ* and promotes homophilic cell-cell adhesion *in vitro*.** *Development* 2002, **129**:4697-705.
19. Tucker RP, Martin D, Kos R, Chiquet-Ehrismann R: **The expression of teneurin-4 in the avian embryo.** *Mechanisms of Development* 2000, **98**:187-91.
20. Tucker RP, Chiquet-Ehrismann R, Chevron MP, Martin D, Hall RJ, Rubin BP: **Teneurin-2 is expressed in tissues that regulate limb and somite pattern formation and is induced *in vitro* and *in situ* by FGF8.** *Developmental Dynamics* 2001, **220**:27-39.
21. Otaki JM, Firestein S: **Neurestin: Putative Transmembrane Molecule Implicated in Neuronal Development.** *Developmental Biology* 1999, **212**:165-181.
22. Mieda M, Kikuchi Y, Hirate Y, Aoki M, Okamoto H: **Compartmentalized expression of zebrafish ten-m3 and ten-m4, homologues of the Drosophila tenm/odd Oz gene, in the central nervous system.** *Mechanisms of Development* 1999, **87**:223-227.
23. Feng K, Zhou X-H, Oohashi T, Märgelin M, Lustig A, Hirakawa S, Ninomiya Y, Engel Jr, Rauch U, Fässler R: **All Four Members of the Ten-m/Odz Family of Transmembrane Proteins Form Dimers.** *Journal of Biological Chemistry* 2002, **277**:26128-26135.
24. Leamey CA, Glendining KA, Kreiman G, Kang N-D, Wang KH, Fassler R, Sawatari A, Tonegawa S, Sur M: **Differential Gene Expression between Sensory Neocortical Areas: Potential Roles for Ten_m3 and Bcl6 in Patterning Visual and Somatosensory Pathways.** *Cerebral Cortex* 2008, **18**:53-66.
25. Leamey CA, Merlin S, Lattouf P, Sawatari A, Zhou X, Demel N, Glendining KA, Oohashi T, Sur M, Fässler R: **Ten_m3 Regulates Eye-Specific Patterning in the Mammalian Visual Pathway and Is Required for Binocular Vision.** *PLoS Biology* 2007, **5**:e241.
26. Li H, Bishop KM, O'Leary DD: **Potential target genes of EMX2 include Odz/Ten-M and other gene families with implications for cortical patterning.** *Molecular and Cellular Neuroscience* 2006, **33**:136-49.
27. Sansom SN, Livesey FJ: **Gradients in the brain: the control of the development of form and function in the cerebral cortex.** *Cold Spring Harb Perspect Biol* 2009, **1**:a002519.
28. Dalton D, Chadwick R, McGinnis W: **Expression and embryonic function of empty spiracles: a *Drosophila* homeo box gene with two patterning functions on the anterior-posterior axis of the embryo.** *Genes & Development* 1989, **3**:1940-1956.
29. Simeone A, Gulisano M, Acampora D, Stornaiuolo A, Rambaldi M, Boncinelli E: **Two vertebrate homeobox genes related to the *Drosophila***

empty spiracles gene are expressed in the embryonic cerebral cortex. *EMBO Journal* 1992, **11**:2541-2550.
30. Fukuchi-Shimogori T, Grove EA: **Emx2 patterns the neocortex by regulating FGF positional signaling.** *Nature Neuroscience* 2003, **6**:825-831.
31. Bishop KM, Goudreau G, O'Leary DDM: **Regulation of Area Identity in the Mammalian Neocortex by Emx2 and Pax6.** *Science* 2000, **288**:344-349.
32. Gulisano M, Broccoli V, Pardini C, Boncinelli E: **Emx1 and Emx2 show different patterns of expression during proliferation and differentiation of the developing cerebral cortex in the mouse.** *European Journal of Neuroscience* 1996, **8**:1037-1050.
33. Mallamaci A, Iannone R, Briata P, Pintonello L, Mercurio S, Boncinelli E, Corte G: **EMX2 protein in the developing mouse brain and olfactory area.** *Mechanisms of Development* 1998, **77**:165-172.
34. O'Leary DDM, Chou S-J, Sahara S: **Area Patterning of the Mammalian Cortex.** *Neuron* 2007, **56**:252-269.
35. Otaki JM, Firestein S: **Segregated expression of neurestin in the developing olfactory bulb.** *Neuroreport* 1999, **10**:2677-2680.
36. Minet AD, Rubin BP, Tucker RP, Baumgartner S, Chiquet-Ehrismann R: **Teneurin-1, a vertebrate homologue of the *Drosophila* pair-rule gene ten-m, is a neuronal protein with a novel type of heparin-binding domain.** *Journal of Cell Science* 1999, **112(Pt 12)**:2019-32.
37. Malmgren H, Sundvall M, Dahl N, Gustavson KH, Anneren G, Wadelius C, Steenbondeson ML, Pettersson U: **Linkage maping of a severe X-linked mental-retardation syndrome.** *American Journal of Human Genetics* 1993, **52**:1046-1052.
38. Gustavson KH, Anneren G, Malmgren H, Dahl N, Ljunggren CG, Backman H: **New X-linked syndrome with severe mental retardation, severely impaired vision, severe hearing defect, epileptic seizures, spasticity, restricted joint mobility and early death.** *American Journal of Medical Genetics* 1993, **45**:654-658.
39. Cabezas DA, Slaugh R, Abidi F, Arena JF, Stevenson RE, Schwartz CE, Lubs HA: **A new X linked mental retardation (XLMR) syndrome with short stature, small testes, muscle wasting, and tremor localises to Xq24-q25.** *Journal of Medical Genetics* 2000, **37**:663-668.
40. Martínez F, Martínez-Garay I, Oltra S, Moltó MD, Orellana C, Monfort S, Prieto F, Tejada I: **Localization of MRX82: A new nonsyndromic X-linked mental retardation locus to Xq24-q25 in a Basque family.** *American Journal of Medical Genetics* 2004, , **131A**: 174-178.
41. Vitale E, Specchia C, Devoto M, Angius A, Rong S, Rocchi M, Schwalb M, Demelas L, Paglietti D, Manca S, *et al*: **Novel X-linked mental retardation syndrome with short stature maps to Xq24.** *American Journal of Medical Genetics* 2001, **103**:1-8.
42. Iler N, Rowitch DH, Echelard Y, McMahon AP, Abate-Shen C: **A single homeodomain binding site restricts spatial expression of Wnt-1 in the developing brain.** *Mechanisms of Development* 1995, **53**:87-96.
43. Shepard S, McCreary M, Fedorov A: **The Peculiarities of Large Intron Splicing in Animals.** *PLoS ONE* 2009, **4**:e7853.
44. Singh J, Padgett RA: **Rates of in situ transcription and splicing in large human genes.** *Nat Struct Mol Biol* 2009, **16**:1128-1133.
45. O'Leary DDM, Sahara S: **Genetic regulation of arealization of the neocortex.** *Current Opinion in Neurobiology* 2008, **18**:90-100.
46. Funatsu N, Inoue T, Nakamura S: **Gene Expression Analysis of the Late Embryonic Mouse Cerebral Cortex Using DNA Microarray: Identification of Several Region- and Layer-specific Genes.** *Cereb Cortex* 2004, **14**:1031-1044.
47. Mühlfriedel S, Kirsch F, Gruss P, Chowdhury K, Stoykova A: **Novel genes differentially expressed in cortical regions during late neurogenesis.** *European Journal of Neuroscience* 2007, **26**:33-50.
48. Gangemi RMR, Daga A, Muzio L, Marubbi D, Cocozza S, Perera M, Verardo S, Bordo D, Griffero F, Capra MC, *et al*: **Effects of Emx2 inactivation on the gene expression profile of neural precursors.** *European Journal of Neuroscience* 2006, **23**:325-334.
49. Holm PC, Mader MT, Haubst N, Wizenmann A, Sigvardsson M, Götz M: **Loss- and gain-of-function analyses reveal targets of Pax6 in the developing mouse telencephalon.** *Molecular and Cellular Neuroscience* 2007, **34**:99-119.
50. Numayama-Tsuruta K, Arai Y, Takahashi M, Sasaki-Hoshino M, Funatsu N, Nakamura S, Osumi N: **Downstream genes of Pax6 revealed by comprehensive transcriptome profiling in the developing rat hindbrain.** *BMC Developmental Biology* 2005, **10**:6.
51. Kent WJ: **BLAT - The BLAST-Like Alignment Tool.** *Genome Research* 2002, **12**:656-664.
52. Bryne JC, Valen E, Tang M-HE, Marstrand T, Winther O, Piedade I da, Krogh A, Lenhard B, Sandelin A: **JASPAR, the open access database of transcription factor-binding profiles: new content and tools in the 2008 update.** *Nucl Acids Res* 2008, **36**:D102-106.
53. Degen M, Goulet S, Ferralli J, Roth M, Tamm M, Chiquet-Ehrismann R: **Opposite effect of fluticasone and salmeterol on fibronectin and tenascin-C expression in primary human lung fibroblasts.** *Clinical & Experimental Allergy* 2009, **39**:688-699.
54. Itasaki N, Bel-Vialar S, Krumlauf R: **'Shocking' developments in chick embryology: electroporation and *in ovo* gene expression.** *Nature Cell Biology* 1999, **1**:E203-E207.
55. Vitobello A, Ferretti E, Lampe X, Vilain N, Ducret S, Ori M, Spetz J-F, Selleri L, Rijli M Filippo: **Hox and Pbx Factors Control Retinoic Acid Synthesis during Hindbrain Segmentation.** *Developmental Cell* **20**:469-482.
56. Minoux M, Antonarakis GS, Kmita M, Duboule D, Rijli FM: **Rostral and caudal pharyngeal arches share a common neural crest ground pattern.** *Development* 2009, **136**:637-645.

doi:10.1186/1471-213X-11-35
Cite this article as: Beckmann *et al.*: **Human teneurin-1 is a direct target of the homeobox transcription factor EMX2 at a novel alternate promoter.** *BMC Developmental Biology* 2011 **11**:35.

Discussion and outlook

During this PhD work we have investigated the counteracting effects of active (RA signaling) and repressive (Polycomb-mediated repression) mechanisms able to modulate the transcriptional state of *Hox* genes, which, in turn, play an important role in the embryonic body patterning.

Although the *Hox* positional system has been conserved during the evolution, there are important differences between flies and vertebrates with regard to the molecular events that lead to their activation along the rostro-caudal embryonic axis. In flies, the transcription of homeotic selector genes is determined by the hierarchical control exerted by maternal effect genes as well as zygotic *gap* and *pair-rule* genes. In mouse, the anterior expression boundaries of *Hoxa1* and *Hoxb1* in the hindbrain are set by their responsiveness to RA signaling (Dupé et al. 1997; Marshall et al., 1994; Studer et al., 1998). Previous works underlined the crucial function of Hox transcription factors during hindbrain development (Gavalas et al. 1997, 1998; Studer et al., 1998; Rossel and Capecchi, 1999). In particular, *Hoxa1* mutation leads to a dramatic reorganization of the rhombomeric (r) identities causing a posterior expansion of r3 and affecting the development of r4 and r5 (Dollé et al., 1993; Carpenter et al., 1993). This reorganization results in the absence of the abducens (VI cranial nerve), reduction of the facial (VII), absence of the spiral and vestibular ganglia (VIII) as well as reduction of glossopharyngeal (IX) and vagus (X) nerves (Mark et al., 1993). Furthermore, Pbx is a well-characterized Hox cofactor and participate to the auto- and cross-regulatory loops responsible for the maintenance of rhombomere-specific Hox transcriptional states (Ferretti et al., 2005; Maconochie et al., 1997; Pöpperl et al., 1995).

How during the evolution Hox genes became under the control of RA signaling is ill characterized. Furthermore, the molecular mechanisms leading to proper expression of RA synthesizing enzymes during embryonic development are still elusive. Raldh2 is the earliest RA synthesizing enzyme expressed during embryonic development and its mutation causes pleiotropic developmental abnormalities such as altered turning, shortened bodies, abnormal development of forebrain and limb buds, a dilated heart, hypoplastic posterior branchial arches, and somite/vertebral patterning defects (Niederreither et al., 1999). In

order gain insight into the transcriptional control of *Raldh2* we started from the observation that Pbx1/Pbx2 double mutants show most of the developmental defects exhibited by *Raldh2* mutant animals (Capellini et al., 2008; Selleri et al., 2001; Stankunas et al., 2008). Furtermore, given the known functional interaction between Hox and Pbx we hypothesized a potential involvement of Hox transcription factors in *Raldh2* regulation. In the first work we demonstrate the presence of non-cell-autonomous effects mediated by Hox and Pbx mutations on hindbrain segmentation in the mouse. We show that Hox and Pbx play a crucial role in the maintenance of Raldh2 expression in the mesoderm. Compound *Pbx1*$^{-/-}$*/Pbx2*$^{-/-}$ and *Hoxa1*$^{-/-}$*/Pbx1*$^{-/-}$ mouse embryos fail to maintain proper levels of *Raldh2* expression over time and exhibit lower RA reporter activity. Moreover, *Hoxa1*$^{-/-}$*/Pbx1*$^{-/-}$ compound mutants show hindbrain segmentation defects that can be partially rescued by exogenous RA complementation. Mesoderm-specific *Hoxa1* and *Pbx1b* knockdowns in *Xenopus* embryos also result in *Raldh2* downregulation and hindbrain defects similar to mouse mutants. Mechanistically, Hox-Pbx and Meis factors form tri-molecular complexes able to bind directly a specific regulatory element, located within the first intron of *Raldh2* locus, which is required to maintain normal *Raldh2* expression levels *in vivo*. Taken together, our data reveal a RA-mediated feed-forward regulatory loop that puts in register the spatial collinear expression of *Hox* genes in the paraxial mesoderm with their expression in the neural tube. These findings show how retinoic signaling pathway could have been evolutionary co-opted for vertebrate patterning and integrated into the *Hox* positional system.

These results underline the role of Hox and Pbx transcription factors in the maintenance of Raldh2 expression. In the future, would be interesting to investigate the transcriptional network responsible for its initiation. We speculate that the same mechanism discovered by our research might play a role, but such hypothesis would be difficult to demonstrate in the mouse because of the presence of several Hox and Pbx paralog genes. Interestingly, *Hoxd1* is not expressed in the neuroephitelium at this stage, although it is cyclically transcribed in the newly formed somites and in the posterior presomitic mesoderm (Pitera et al., 2001). Furthermore, other reports describe dramatic hindbrain reorganization to a rhombomere 1-like identity upon *Hox* PG1 gene knockdown in Xenopus (McNulty et al., 2005) or Pbx loss-of-function in Zebrafish (Waskiewicz et al.,

2002). These observations strengthen the hypothesis that, at the early gastrula stage, Hox PG1 and Pbx might play a role also in the onset of the RA signaling.

After the initial expression of *Hox* PG1 genes, the activation of the following paralog groups reflects their position along the clusters from 3' to 5'. This phenomenon called temporal collinearity (Izpisúa-Belmonte et al., 1991) indicates a sequential acquirement of the transcriptional competency of these genes. Although not completely deciphered, this mechanism relies on the presence of regulatory elements located in the nearby gene-desert regions surrounding of the *Hox* clusters (Tschopp et al., 2009). Recently, the transcriptional availability/silencing of *Hox* genes has been revisited in terms of chromatin configuration of the clusters (Soshnikova and Duboule, 2009). In particular, maintenance of *Hox* transcriptional states correlates with distinct sub-nuclear domains of active or repressed genes (Bantignies et al., 2011; Noordermeer et al., 2011). According to this model, in rostral-most embryonic regions, where *Hox* genes are completely silent, each *Hox* cluster is organized as a single repressive domain, while in posterior regions, a progressive number of *Hox* genes become expressed and relocated to an active chromatin compartment, following their distribution from 3' to 5' along the clusters (spatial collinearity).

To date, the molecular signals responsible for the maintenance of repressive state or the absence of de-repression of *Hox* genes in rostral embryonic domains have been not totally elucidated. Signaling pathways such as FGF, produced by the midbrain/hindbrain boundary could play a role (Trainor et al., 2002) or the expression of RA degrading enzymes (Uehara et al., 2007) can individually, or in combination, lead to the establishment of this configuration. However, previous reports suggested a role of the PRC1 complex in the maintenance of transcriptional repression of *Hox* genes during antero-posterior patterning (Isono et al, 2005), but due to the early lethality of mutant mice a comprehensive analysis of Polycomb loss of function was missing.

In the second part of this manuscript, using the cranial nural crest cells (cNCCs) as model for our study, we investigated the role of Ezh2, the catalytic component of the Polycomb repressive complex 2 (PRC2), in the maintenance of the repressive state of *Hox* genes and deployed the craniofacial system as readout of the phenotypic effects caused by the *Ezh2* mutation. cNCCs are *bona fide* stem cells that, differently from their posterior

counterparts, are endowed with a different combination of both mesenchymal (osteogenic/chondrogenic) and neurogenic-melanogenic potential (Calloni et al., 2007). This transient population of cells originates from the dorsal neural tube, undergo epithelial-to-mesenchymal transition and populate the frontonasal and pharyngeal regions where they contribute to the formation of most of the cartilages and bones of the skull, facial and pharyngeal skeletons (Santagati and Rijli, 2003; Minoux and Rijli, 2010).

Differently from posterior NCCs, *Hox* genes are not active in the most anterior cranial NCC populations and their ectopic expression in this system leads to severe impairment of craniofacial development (Creuzet et al., 2002). This situation underscore the importance to maintain *Hox* genes repressed in order to achieve proper development of the anterior part of the embryo. Taking advantage from genetically labeled NCCs, we performed genome-wide transcriptional and epigenetic analysis on nearly pure populations of FACS-sorted cNCCs isolated from different rostrocaudal origins along the developing E10.5 embryo, namely the *Hox*-negative Maxillary (Mx) and Mandibular (Md) prominences of the first pharyngeal arch as well as the *Hox*-positive Hyoid (Hy) NCCs of the second pharyngeal arch. In control samples and independently on their rostrocaudal origins, the epigenomic profile revealed the presence of high enrichment of H3K27me3 at the level of the four *Hox* clusters, the epigenetic mark catalyzed by Ezh2 and associated with transcriptional repression (Margueron and Reinberg, 2011). However, in the Hy population, *Hoxa2* and *Hoxb2* loci were depleted of H3K27me3 and enriched in H3K4me2 and H3K27ac, epigenetic marks associate with positively regulated promoters and enhancers. This epigenetic landscape not only reflects the transcriptional state of Hox genes in the three cNCC sub-populations analyzed, but is also reminiscent of the collinear activation of 3' *Hox* genes in pre-migratory progenitors. Intriguingly, an important observation was done in regard to the epigenetic configuration of 3' *Hox* PG1 genes (i.e. *Hoxa1* and *Hoxb1*). While in rhombomere 4 (R4)-derived pre-migratory cNCCs PG1 genes are active (Gavalas et al., 1998; Makki and Capecchi, 2010; Murphy et al., 1991; Zhang et al., 1994), suggesting an absence of H3K27me3 decoration, in migratory and post-migratory cells high enrichment of this mark was found at the level of these loci, indicating that an active deposition of the Ezh2-mediated modification took place. This result emphasizes the idea that migrating NCCs are still plastic and not irreversibly committed (Dupin et al., 2010).

To address the functional role of Ezh2 in the cNCC system we induced its conditional mutation in pre-migratory progenitors. In *Ezh2* mutant cNCCs, the H3K27me3 mark is completely lost from all four clusters and a consequent de-repression of *Hox* genes is observed. Phenotypically, the mutation impairs the correct formation of facial and pharyngeal bones and cartilages. This result is in line with the previous data demonstrating that the ectopic expression of *Hox* genes is incompatible with normal craniofacial development (Creuzet et al., 2002; Couly et al., 1998 and Minoux et al., 2013 submitted).

More broadly, Ezh2 activity is important for the maintenance of the positional identity of cranial NCC sub-populations. Previous studies suggested the presence of a PA1-like skeletogenic ground state shared by all the cranial NCCs populating the pharyngeal region (Minoux et al., 2009). In keeping with this hypothesis, our genome-wide analysis identified high degree of correlation between Md and Hy samples. This similarity is more evident in *Ezh2* mutants, where, at genome-wide scale, the two populations lose their molecular identity. We speculate that this situation reflects their common rhombencephalic origin. This interpretation is corroborated by the fact that the Mx sub-population, deriving mostly from the mesencephalic region, never shows such high degree of correlation with the other two samples, neither in the Ezh2 mutation background.

Finally, our analysis reveals that most of the effects mediated by the *Ezh2* mutation are due to the de-repression of its direct targets, i.e. genes whose promoters showed bivalent or H3K27me3 enrichment in the control samples. Although preliminary, our GO analysis suggests that *Ezh2* plays a role in the maintenance of the mesenchymal (chondro/skeletogenic) fate of migratory and post-migratory cranial NCCs by repressing their neurogenic potential. Taken together our data strongly indicate the role of Ezh2 in the maintenance of the mesenchymal potential and positional identity of cranial neural crest cells during mouse craniofacial development.

At the moment, our laboratory is consolidating some of the hypotheses derived from the analysis of the epigenetic configuration of the clusters. In particular, it will be of particular importance to assess the epigenetic configuration of *Hox* PG1 genes in r4-derived pre-migratory progenitors in order to prove the existence of a *de novo* deposition of H3K27me3 on migrating and post-migratory cNCCs. Furthermore, according to the recent

publication correlating the presence of active and repressive chromatin domains with the distribution of H3K4me3 and H3K27me3 modifications (Noordermeer et al., 2011) we would expect to observe that, in migratory and post-migratory r4-derived NCCs, Hox PG1 genes colocalize with the rest of the repressed cluster, whereas *Hox* PG2 would occupy a different active compartment of the nucleus. To address this question Chromosome Conformation Capture (4C) assays will be used to determine the spatial distribution of *Hox* genes within active and silenced chromatin compartments.

In this study we did not include the anterior-most population of cNCCs originating from the diencephalic region and colonizing the frontonasal process (FNP), but an analysis of their transcriptome will be important to link the loss of positional identity observed in the Md and Hy samples to their common rhombencephalic origin. In fact, if our interpretation is correct, we would expect to observe maintenance of distinct expression profiles among Ezh2 mutant populations originating from different regions.

Finally, our laboratory is now investigating the cell identity of *Ezh2* mutant cNCCs. In keeping with the observation that the mutation causes a de-repression of the neural fate at the expenses of the chondro/osteogenic potential, we are performing a characterization of the neural versus mesenchymal markers expressed by mutant cells. Furthermore, we will also investigate if the de-repression of such an inappropriate program in cNCCs would consequently induce their apoptosis, a change in their proliferative properties, or a stable switch in their fate.

Bibliography

Abu-Abed S., Dolle P., Metzger D., Beckett B., Chambon P., Petkovich M. (2001). The retinoic acid-metabolizing enzyme, CYP26A1, is essential for normal hindbrain patterning, vertebral identity, and development of posterior structures. Genes Dev., 15, pp. 226–240

Akam M., Dawson I., Tear G. (1988). Homeotic genes and the control of segment diversity. *Development, 104:123-133*

Baltzinger M., Ori M., Pasqualetti M., Nardi I., Rijli F.M. (2005). Hoxa2 knockdown in Xenopus results in hyoid to mandibular homeosis. Dev Dyn 234, 858-867.

Bantignies F., Roure V., Comet I., Leblanc B., Schuettengruber B., Bonnet J., Tixier V., Mas A., Cavalli G. (2011). Polycomb-dependent regulatory contacts between distant Hox loci in Drosophila. Cell, Jan 21;144(2):214-26

Barrow J.R., Capecchi M.R. (1996). Targeted disruption of the Hoxb-2 locus in mice interferes with expression of Hoxb-1 and Hoxb-4. Development (Cambridge, England) 122, 3817-3828.

Birgbauer E., Sechrist J., Bronner-Fraser M., Fraser S. (1995). Rhombomeric origin and rostrocaudal reassortment of neural crest cells revealed by intravital microscopy. Development 121, 935-945.

Boyer L.A., Plath K., Zeitlinger J., Brambrink T., Medeiros L.A., Lee T.I., Levine S.S., Wernig M., Tajonar A., Ray M.K., et al. (2006). Polycomb complexes repress developmental regulators in murine embryonic stem cells. *Nature* 441*:* 349–353.

Capellini TD, Di Giacomo G, Salsi V, Brendolan A, Ferretti E, Srivastava D, Zappavigna V, Selleri L. (2006). Pbx1/Pbx2 requirement for distal limb patterning is mediated by the hierarchical control of Hox gene spatial distribution and Shh expression. *Development*, *133*: *2263*–2273

Capellini TD, Zewdu R, Di Giacomo G, Asciutti S, Kugler JE, Di Gregorio A, Selleri L. (2008). Pbx1/Pbx2 govern axial skeletal development by controlling Polycomb and Hox in mesoderm and Pax1/Pax9 in sclerotome. Dev Biol., Sep 15;321(2):500-14.

Carpenter EM, Goddard JM, Chisaka O, Manley NR, Capecchi MR. (1993). Loss of Hox-A1 (Hox-1.6) funtion results in the reorganization of the murine hindbrain. Development. Aug; 118(4):1063-75

Chen S., Ma J., Wu F., Xiong L.J., Ma H., Xu W., Lv R., Li X., Villen J., Gygi S.P., et al. (2012). The histone H3 Lys 27 demethylase JMJD3 regulates gene expression by impacting transcriptional elongation. Genes Dev. *26,* 1364–1375.

Cheutin T., Cavalli G. (2012). Progressive polycomb assembly on H3K27me3 compartments generates polycomb bodies with developmentally regulated motion. PLoS Genet., Jan;8(1):e1002465

Chopra V.S., Hendrix D.A., Core L.J., Tsui C., Lis J.T., Levine M. (2011). The polycomb group mutant esc leads to augmented levels of paused Pol II in the Drosophila embryo. Mol. Cell *42,* 837–844.

Cotterell J., Sharpea J. (2010). An atlas of gene regulatory networks reveals multiple three-gene mechanisms for interpreting morphogen gradients. Mol Syst Biol., 6: 425.

Couly G. F., Coltey P. M., Le Douarin N. M. (1993). The triple origin of skull in higher vertebrates: a study in quail-chick chimeras. Development 117, 409- 429.

Couly G, Grapin-Botton A, Coltey P, Ruhin B, Le Douarin NM (1998) Determination of the identity of the derivatives of the cephalic neural crest: incompatibility between Hox gene expression and lower jaw development. Development 125: 3445–3459

Creuzet S., Couly G., Vincent C, Le Douarin N.M. (2002). Negative effect of Hox gene expression on the development of the neural crest-derived facial skeleton. Development, Sep;129(18):4301-13.

Davenne M., Maconochie M.K., Neun R., Pattyn A., Chambon P., Krumlauf R., Rijli F.M. (1999). Hoxa2 and Hoxb2 control dorsoventral patterns of neuronal development in the rostral hindbrain. Neuron 22, 677-691.

Dietzel S., Niemann H., Brückner B., Maurange C., Paro R. (1999). The nuclear distribution of Polycomb during Drosophila melanogaster development shown with a GFP fusion protein. Chromosoma, May;108(2):83-94.

Dollé P., Izpisúa-Belmonte J.C., Falkenstein H., Renucci A., Duboule D. (1989). Coordinate expression of the murine Hox-5 complex homoeobox-containing genes during limb pattern formation. Nature, 342; pp. 767–772

Dollé P, Lufkin T, Krumlauf R, Mark M, Duboule D, Chambon P. (1993). Local alterations of Krox-20 and Hox gene expression in the hindbrain suggest lack of rhombomere 4 and 5 in homozygote null Hoxa-1 (Hox1.6) mutant embryos. Proc Natl Acad Sci U S A., Aug 15; 90(16):7666-70.

Dupé V., Davenne M., Brocard J., Dollé P., Mark M., Dierich A., Chambon P. Rijli F.M. (1997). In vivo functional analysis of the Hoxa-1 3' retinoic acid response element (3'RARE). Development, Jan;124(2):399-410.

Durston AJ, Timmermans JP, Hage WJ, Hendriks HF, de Vries NJ, Heideveld M, Nieuwkoop PD. (1989). Retinoic acid causes an anteroposterior transforma- tion in the developing central nervous system. Nature 340:140–144.

Ferretti E, Cambronero F, Tümpel S, Longobardi E, Wiedemann LM, Blasi F, Krumlauf R. (2005). Hoxb1 enhancer and control of rhombomere 4 expression: complex interplay between PREP1-PBX1-HOXb1 binding sites. Mol Cell Biol. Oct;25(19):8541-52.

Folberg A, Kovács EN, Featherstone MS. (1997). Characterization and retinoic acid responsiveness of the murine Hoxd4 transcription unit. J Biol Chem. Nov 14;272(46):29151-7.

Forlani S., Lawson K.A., Deschamps J. (2003). Acquisition of Hox codes during gastrulation and axial elongation in the mouse embryo. Development, Aug;130(16):3807-19.

Francis N.J., Kingston R.E., Woodcock C.L. (2004). Chromatin compaction by a polycomb group protein complex. Science *306,* 1574–1577.

Frasch M., Chen X., Lufkin T. (1995). Evolutionary-conserved enhancers direct region-specific expression of the murine Hoxa-1 and Hoxa-2 loci in both mice and Drosophila. Development, Apr;121(4):957-74

Fujii H., Sato T., Kaneko S., Gotoh O., Fujii-Kuriyama Y., Osawa K., Kato S., Hamada H. (1997). Metabolic inactivation of retinoic acid by a novel P450 differentially expressed in developing mouse embryos. EMBO J 16:4163–4173.

Gale E, Zile M, Maden M. (1999). Hindbrain respecification in the retinoid-deficient quail. Mech Dev 89:43–54.

Gammill L. S., Bronner-Fraser M. (2003). Neural crest specification: migrating into genomics. Nat. Rev. Neurosci. 4, 795-805.

Gao Z., Zhang J., Bonasio R., Strino F., Sawai A., Parisi F., Kluger Y., Reinberg D. (2012). PCGF homologs, CBX proteins, and RYBP define functionally distinct PRC1 family complexes. Mol Cell., Feb 10;45(3):344-56.

Gavalas A, Davenne M, Lumsden A, Chambon P, Rijli FM. (1997). Role of Hoxa-2 in axon pathfinding and rostral hindbrain patterning. Development. Oct;124(19):3693-702.

Gavalas A., Studer M., Lumsden A., Rijli F.M., Krumlauf R., Chambon P. (1998). Hoxa1 and Hoxb1 synergize in patterning the hindbrain, cranial nerves and second pharyngeal arch. Development, 125, pp. 1123–1136

Gavalas A., Trainor P., Ariza-McNaughton L., Krumlauf R. (2001) Synergy between Hoxa1 and Hoxb1: the relationship between arch patterning and the generation of cranial neural crest Development, 128, pp. 3017–3027

Gavalas A. (2002). ArRAnging the hindbrain. Trends in Neurosciences vol 25 no.2 February

Gavalas A., Ruhrberg C., Livet J., Henderson C.E., Krumlauf R. (2003) Neuronal defects in the hindbrain of Hoxa1, Hoxb1 and Hoxb2 mutants reflect regulatory interactions among these Hox genes. Development Dec;130(23):5663-79.

Gendron-Maguire M., Mallo M., Zhang M., Gridley, T. (1993). Hoxa-2 mutant mice exhibit homeotic transformation of skeletal elements derived from cranial neural crest. *Cell* 75, 1317-1331.

Godsave SF, Koster CH, Getahun A, Mathu M, Hooiveld M, van der Wees J, Hendriks J, Durston AJ. (1998). Graded retinoid responses in the developing hindbrain. Dev Dyn 213:39–49.

Gould A., Morrison A., Spoat G., White R.A., Krumlauf R. (1997). Positive cross-regulation and enhancer sharing: two mechanisms for specifying overlapping Hox expression patterns. Genes Dev. Apr 1;11(7):900-13.

Gould A, Itasaki N, Krumlauf R. (1998). Initiation of rhombomeric Hoxb4 expression requires induction by somites and a retinoid pathway. Neuron, Jul;21(1):39-51.

Grammatopoulos G.A., Bell E., Toole L., Lumsden A., Tucker A.S. (2000). Homeotic transformation of branchial arch identity after *Hoxa2* overexpression. *Development* 127, 5355–5365.

Gross, J. B. and Hanken, J. (2008). Review of fate-mapping studies of osteogenic cranial neural crest in vertebrates. Dev. Biol. 317, 389-400.

Hernandez R.E., Putzke A.P., Myers J.P., Margaretha L., Moens C.B. (2007). Cyp26 enzymes generate the retinoic acid response pattern necessary for hindbrain development. Development Jan;134(1):177-87.

Hollemann T., Chen Y., Grunz H., Pieler T. (1998). Regionalized metabolic activity establishes boundaries of retinoic acid signalling. EMBO J 17:7361–7372.

Hunt P., Wilkinson D., Krumlauf R., (1991). Patterning the vertebrate head: murine Hox 2 genes mark distinct subpopulations of premigratory and migrating cranial neural crest. Development (Cambridge, England) 112, 43-50.

Hunter M.P., Prince V.E. (2002). Zebrafish hox paralogue group 2 genes function redundantly as selector genes to pattern the second pharyngeal arch. *Dev. Biol.* 247, 367–389.

Iimura T, Pourquié O. (2006). Collinear activation of Hoxb genes during gastrulation is linked to mesoderm cell ingression. Nature, Aug 3;442(7102):568-71

Iimura T, Denans N, Pourquié O. (2009). Establishment of Hoxvertebral identities in the embryonic spine precursors.Curr Top Dev Biol.,88:201-34.

Ingham P.W. (1985). A clonal analysis of the requirement for the trithorax gene in the diversification of segments in Drosophila. J Embryol Exp Morphol. 1985 Oct;89:349-65.

Irving C, Nieto M.A., DasGupta R., Charnay P., Wilkinson D.G. (1996). Progressive spatial restriction of Sek-1 and Krox-20 gene expression during hindbrain segmentation. Dev Biol, Jan 10;173(1):26-38.

Izpisúa-Belmonte JC, Falkenstein H, Dollé P, Renucci A, Duboule D. (1991). Murine genes related to the Drosophila AbdB homeotic genes are sequentially expressed during development of the posterior part of the body. EMBO J.,Aug;10(8):2279-89.

Jurgens, G. (1985). A group of genes controlling the spatial expression of the Bithorax complex in Drosophila. Nature, 316: 153-155.

Kicheva A., Cohen M., Briscoe J. (2012). Developmental Pattern Formation: Insights from Physics and Biology. Science, Oct, Vol. 338 no. 6104 pp. 210-212.

Kiecker C., Lumsden A. (2005). Compartments and their boundaries in vertebrate brain development. Nat Rev Neurosci. Jul;6(7):553-64. Review.

Kim J., Lo L., Dormand, E., Anderson D.J. (2003). SOX10 maintains multipotency and inhibits neuronal differentiation of neural crest stem cells. *Neuron* **38,** 17–31

Köntges G. and Lumsden A. (1996). Rhombencephalic neural crest segmentation is preserved throughout craniofacial ontogeny. Development 122, 3229-3242.

Krumlauf R. (1993). Hox genes and pattern formation in the branchial region of the vertebrate head. Trends Genet. 9, 106-112.

Ku M., Koche R.P., Rheinbay E., Mendenhall E.M., Endoh M., Mikkelsen T.S., Presser A., Nusbaum C., Xie X., Chi A.S., et al. (2008). Genomewide analysis of PRC1 and PRC2 occupancy identifies two classes of bivalent domains. PLoS Genet 4: e1000242.

Kulesa P. M. and Fraser S. E. (2000). In ovo time-lapse analysis of chick hindbrain neural crest cell migration shows cell interactions during migration to the branchial arches. Development 127, 1161-1172.

Kuratani S., Matsuo I., Aizawa S. (1997). Developmental patterning and evolution of the mammalian viscerocranium: genetic insights into comparative morphology. Dev Dyn 209, 139-155.

Langston A.W., Gudas L.J. (1992). Identification of a retinoic acid responsive enhancer 3' of the murine homeobox gene Hox-1.6. Mech Dev. Sep;38(3):217-27.

Langston A.W., Thompson J.R., Gudas L.J., (1997). Retinoic acid-responsive enhancers located 3' of the Hox A and Hox B homeobox gene clusters. Functional analysis. J Biol Chem., Jan 24;272(4):2167-75.

Lauberth S.M., Nakayama T., Wu X., Ferris A.L., Tang Z., Hughes S.H., Roeder R.G. (2013). H3K4me3 Interactions with TAF3 Regulate Preinitiation Complex Assembly and Selective Gene Activation. Cell, Volume 152, Issue 5, 28 February 2013, Pages 1021–1036

Le Douarin N. M. and Kalcheim C. (1999). The Neural Crest. Cambridge, UK: Cambridge University Press.

Lee HY, Kléber M, Hari L, Brault V, Suter U, Taketo MM, Kemler R, Sommer L. (2004). Instructive Role of Wnt/b-Catenin in Sensory Fate Specification in Neural Crest Stem Cells. Science Feb 13;303(5660):1020-3.

Lefebvre V., Huang W., Harley V. R., Goodfellow P. N., de Crombrugghe B. (1997). SOX9 is a potent activator of the chondrocyte-specific enhancer of the Proα1(II) collagen gene. *Mol. Cell Biol.* **17,** 2336–2346.

Lewis E.B. (1978). A gene complex controlling segmentation in Drosophila. Nature, Dec 7;276(5688):565-70.

Lumsden A., Sprawson N., Graham A. (1991). Segmental origin and migration of neural crest cells in the hindbrain region of the chick embryo. *Development* **113,** 1281–1291

Maconochie M.K., Nonchev S., Studer M., Chan S.K., Popperl H., Sham M.H., Mann R.S., Krumlauf R. (1997). Cross-regulation in the mouse HoxB complex: the expression of Hoxb2 in rhombomere 4 is regulated by Hoxb1 Genes Dev., 11, pp. 1885–1895

Maconochie M.K., Nonchev S., Manzanares M., Marshall H., Krumlauf R. (2001). Differences

in Krox20-dependent regulation of Hoxa2 and Hoxb2 during hindbrain development. Dev Biol, May 15;233(2):468-81.

Mallo M., Brändlin I., (1997). Segmental identity can change independently in the hindbrain and rhombencephalic neural crest. Dev Dyn, Oct;210(2):146-56.

Makki N., Capecchi M.R. (2010). Hoxa1 lineage tracing indicates a direct role for Hoxa1 in the development of the inner ear, the heart, and the third rhombomere. Dev Biol, May 15;341(2):499-509.

Manley N.R., Selleri L., Brendolan A., Gordon J., Cleary M.L. (2004). Abnormalities of caudal pharyngeal pouch development in Pbx1 knockout mice mimic loss of Hox3 paralogs. Dev Biolo., Dec 15;276(2):301-12.

Manzanares M, Cordes S, Kwan CT, Sham MH, Barsh GS, Krumlauf R. (1997). Segmental regulatio of Hoxb-3 by Kreisler. Nature, May 8;387(6629):191-5.

Manzanares M., Cordes S., Ariza-McNaughton L., Sadl V., Maruthainar K., Barsh G., Krumlauf R. (1999). Conserved and distinct roles of Kreisler in regulation of the paralogous Hoxa3 and Hoxb3 genes. Development. Feb;126(4):759-69

Manzanares M, Bel-Vialar S, Ariza-McNaughton L, Ferretti E, Marshall H, Maconochie MM, Blasi F, Krumlauf R. (2001). Independent regulation of initiation and maintenance phases of Hoxa3 expression in the vertebrate hindbrain involve auto- and cross-regulatory mechanisms. Development Sep;128(18):3595-607.

Mark M, Lufkin T, Vonesch JL, Ruberte E, Olivo JC, Dollé P, Gorry P, Lumsden A, Chambon P. (1993). Two rhombomeres are altered in Hoxa-1 mutant mice. Development. Oct;119(2):319-38

Marshall H, Nonchev S, Sham M.H., Muchamore I., Lumsden A., Krumlauf R. (1992). Retinoic acid alters hindbrain Hox code and induces transformation of rhombomeres 2/3 into a 4/5 identity. Nature, Dec 24-31;360(6406):737-41.

Marshall H., Studer M., Pöpperl H., Aparicio S., Kuroiwa A., Brenner S., Krumlauf R. (1994). A conserved retinoic acid response element required for early expression of the homeobox gene *Hoxb-1*. Nature, 370, pp. 567–571

Matsuo I., Kuratani S., Kimura C., Takeda N. and Aizawa S. (1995). Mouse Otx2 functions in the formation and patterning of rostral head. Genes Dev. 9, 2646-2658.

Maves L., Jackman W., Kimmel C.B. (2002). FGF3 and FGF8 mediate a rhombomere 4 signaling activity in the zebrafish hindbrain. Development, 129, pp. 3825–3837

McBratney-Owen B., Iseki S., Bamforth S. D., Olsen B. R. and Morriss-Kay G. M. (2008). Development and tissue origins of the mammalian cranial base. Dev. Biol. 322, 121-132.

McKay I.J., Muchamore I., Krumlauf R., Maden M., Lumsden A., Lewis J. (1994) The kreisler mouse: a hindbrain segmentation mutant that lacks two rhombomeres. Development Aug;120(8):2199-211.

McNulty C.L., Peres J.N., Bardine N., van den Akker W.M., Durston A.J. (2005). Knockdown of the complete Hox paralogous group 1 leads to dramatic hindbrain and neural crest defects Development, 132, pp. 2861–2871

Minoux M., Antonarakis G.S., Kmita M., Duboule D., Rijli F.M. (2009) Rostral and caudal pharyngeal arches share a common neural crest ground pattern. Development,136, 637-645

Mishra R.K., Yamagishi T., Vasanthi D., Ohtsuka C., Kondo T. (2007). Involvement of polycomb-group genes in establishing HoxD temporal colinearity. Genesis, Sep;45(9):570-6.

Moazed D., O'Farrell P.H. (1992). Maintenance of the engrailed expression pattern by Polycomb group genes in Drosophila. Development, Nov;116(3):805-10.

Moens CB, Selleri L. (2006). Hox cofactor in vertebrate development. Dev Biol. Mar 15;291(2):193-206. Epub 2006 Mar 3. Review.

Morales A. V., Barbas J. A. and Nieto M. A. (2005). How to become neural crest: from segregation to delamination. Semin. Cell Dev. Biol. 16, 655-662.

Morey L., Aloia L., Cozzuto L., Benitah S.A., Di Croce L. (2013). RYBP and Cbx7 define specific biological functions of polycomb complexes in mouse embryonic stem cells. Cell Rep., Jan 31;3(1):60-9.

Mulder G.B., Manley N., Maggio-Price L. (1998). Retinoic acid-induced thymic abnormalities in the mouse are associated with altered pharyngeal morphology, thymocyte maturation defects, and altered expression of Hoxa3 and Pax1. Teratology 58: 263–275

Müller J., Gaunt S., Lawrence P.A. (1995). Function of the Polycomb protein is conserved in mice and flies. Development, Sep;121(9):2847-52.

Narita Y, Rijli FM. (2009). Hox genes in neural patterning and circuit formation in the mouse hindbrain. Curr Top Dev Biol.;88:139-67. Review.

Niederreither K., McCaffery P., Drager U. C., Chambon P., Dollé P. (1997). Restricted expression and retinoic acid-induced downregulation of the retinaldehyde dehydrogenase type 2 (RALDH-2) gene during mouse development. *Mech. Dev.* 62, 67–78

Niederreither K., Subbarayan V., Dollé P., Chambon P. (1999). Embryonic retinoic acid synthesis is essential for early mouse post-implantation development. *Nat. Genet.* 21, 444–448.

Niederreither K., Vermot J., Schuhbaur B., Chambon P., Dollé P. (2000). Retinoic acid synthesis and hindbrain patterning in the mouse embryo. *Development* 127, 75–85

Niederreither K., Vermot J., Messaddeq N., Schuhbaur B., Chambon P., Dollé P. (2001). Embryonic retinoic acid synthesis is essential for heart morphogenesis in the mouse. *Development* 128, 1019–1031.

Noden, D. M. (1983). The role of the neural crest in patterning of avian cranial skeletal, connective, and muscle tissues. Dev. Biol. 96, 144-165.

Noordermeer D., Leleu M., Splinter E., Rougemont J., De Laat W., Duboule D. (2011). The dynamic architecture of Hox gene clusters. Science. Oct 14;334(6053):222-5

Oury F, Murakami Y, Renaud JS, Pasqualetti M, Charnay P, Ren SY, Rijli FM. (2006). Hoxa2-and rhombomere-dependent development of the mouse facial somatosensory map. Science, Sep 8;313(5792):1408-13.

Pearson J.C., Lemons D., McGinnis W. (2005). Modulating Hox gene functions during animal

body patterning. Nat Rev Genet. Dec; 6(12):893-904. Review.

Pasqualetti M., Ori M., Nardi I., Rijli, F. M. (2000) Ectopic Hoxa2 induction after neural crest migration results in homeosis of jaw elements in *Xenopus. Development* 127, 5367–5378.

Peifer M., Karch F., Bender W. (1987). The bithorax complex: Control of segment identity. Genes and Development, 1", 891-898.

Pitera J.E., Milla P.J., Scambler P., Adjaye J. (2001). Cloning of HOXD1 from unfertilised human oocytes and expression analyses during murine oogenesis and embryogenesis. Mech Dev. Dec;109(2):377-81.

Pöpperl H., Bienz M., Studer M., Chan S.K., Aparicio S., Brenner S., Mann R.S., Krumlauf R. (1995). Segmental expression of Hoxb-1 is controlled by a highly conserved autoregulatory loop dependent upon exd/pbx. Cell. Jun 30;81(7):1031-42.

Pöpperl H., Rikhof H., Chang H., Haffter P., Kimmel C.B., Moens C.B. (2000). Lazarus is a novel pbx gene that globally mediates hox gene function in zebrafish. Mol. Cell, 6, pp. 255–267

Potterf S.B., Mollaaghababa R., Hou L., Southard-Smith E.M., Hornyak T.J., Arnheiter H., Pavan W.J. (2001) Analysis of SOX10 function in neural crest-derived melanocyte development: SOX10- dependent transcriptional control of dopachrome tautomerase. *Dev. Biol.* **237,** 245–257.

Prince V. and Lumsden A. (1994). Hoxa-2 expression in normal and transposed rhombomeres: independent regulation in the neural tube and neural crest. Development 120, 911-923.

Rhinn M, Dollé P. (2012). Retinoic acid signaling during development. Development. Mar;139(5):843-58.

Rijli F.M., Mark M., Lakkaraju S., Dierich A., Dolle P., Chambon P. (1993). A homeotic transformation is generated in the rostral branchial region of the head by disruption of Hoxa-2, which acts as a selector gene. *Cell* **75,** 1333- 1349.

Ringrose L., Paro R. (2007). Polycomb/Trithorax response elements and epigenetic memory of cell identity. Development, Jan;134(2):223-32. Review.

Rinn J.L., Kertesz M., Wang J.K., Squazzo S.L., Xu X., Brugmann S.A., Goodnough L.H., Helms J.A., Farnham P.J., Segal E., Chang H.Y. (2007). Functional demarcation of active and silent chromatin domains in human HOX loci by noncoding RNAs. Cell, Jun 29;129(7):1311-23.

Roelen B.A.J., de Graaff W., Forlani S., Deschamps J. (2002). *Hox* cluster polarity in early transcriptional availability: a high order regulatory level of clustered *Hox* genes in the mouse. Mechanisms of Development, Volume 119, Issue 1, Nov, Pages 81–90

Rossel M., Capecchi M.R. (1999).Mice mutant for both Hoxa1 and Hoxb1 show extensive remodeling of the hindbrain and defects in craniofacial development. Development, 126, pp. 5027–5040

Santagati F. and Rijli F. M. (2003). Cranial neural crest and the building of the vertebrate head. Nat. Rev. Neurosci. 4, 806-818.

Santagati F., Minoux M., Ren S.Y., Rijli F.M. (2005). Temporal requirement of Hoxa2 in cranial neural crest skeletal morphogenesis. Development, Nov;132(22):4927-36

Saurin A.J., Shiels C., Williamson J., Satijn D.P., Otte A.P., Sheer D., Freemont P.S. (1998). The human polycomb group complex associates with pericentromeric heterochromatin to form a novel nuclear domain. J Cell Biol., Aug 24;142(4):887-98

Sauka-Spengler T, Bronner-Fraser M. (2008). A gene regulatory network orchestrates neural crest formation. Nat Rev Mol Cell Biol. Jul;9(7):557-68. Review.

Sauvageau M, Sauvageau G. (2010).Polycomb group proteins: multi-faceted regulators of somatic stem cells and cancer.Cell Stem Cell., Sep 3;7(3):299-313

Schuettengruber B., Ganapathi M., Leblanc B., Portoso M., Jaschek R., Tolhuis B., van Lohuizen M., Tanay A., Cavalli G. (2009). Functional anatomy of polycomb and trithorax chromatin landscapes in Drosophila embryos. PLoS Biol., Jan 13;7(1):e13.

Schuettengruber B., Martinez A.M., Iovino N., Cavalli G. (2011). Trithorax group proteins: switching genes on and keeping them active. Nat Rev Mol Cell Biol., Nov 23;12(12):799-814.

Schwartz Y.B., Kahn T.G., Nix D.A., Li X.Y., Bourgon R., Biggin M., Pirrotta V. (2006). Genome-wide analysis of Polycomb targets in Drosophila melanogaster. Nat Genet., Jun;38(6):700-5.

Sechrist J., Serbedzija G. N., Scherson T., Fraser S.E., Bronner-Fraser M. (1993) Segmental migration of the hindbrain neural crest does not arise from its segmental generation. *Development* **118,** 691–703.

Selleri L., Depew M.J., Jacobs Y., Chanda S.K., Tsang K.Y., Cheah K.S., Rubenstein J.L., O'Gorman S., Cleary M.L. (2001). Requirement for Pbx1 in skeletal patterning and programming chondrocyte proliferation and differentiation Development, 128, pp. 3543–3557

Serbedzija G. N., Bronner-Fraser M. and Fraser S. E. (1992). Vital dye analysis of cranial neural crest cell migration in the mouse embryo. Development 116, 297-307

Sham M.H., Vesque C., Nonchev S., Marshall H., Frain M., Gupta R.D., Whiting J., Wilkinson D., Charnay P., Krumlauf R. (1993). The zinc finger gene Krox20 regulates HoxB2 (Hox2.8) during hindbrain segmentation.Cell. Jan 29;72(2):183-96.

Sing A., Pannell D., Karaiskakis A., Sturgeon K., Djabali M., Ellis J., Lipshitz H.D., Cordes S.P. (2009). A vertebrate Polycomb response element governs segmentation of the posterior hindbrain. Cell, Sep 4;138(5):885-97.

Sirbu I.O., Gresh L.,Barra J., Duester G. (2005). Shifting boundaries of retinoic acid activity control hindbrain segmental gene expression. Development 132, 2611-2622

Smith E., Lin C., Shilatifard A. (2011). The super elongation complex (SEC) and MLL in development and disease. Genes Dev. 2011 Apr 1;25(7):661-72.

Soshnikova N., Duboule D. (2009). Epigenetic temporal control of mouse Hox genes in vivo. Science, Jun 5;324(5932):1320-3.

Sparmann A., van Lohuizen M. (2006). Polycomb silencers control cell fate, development and cancer. Nat Rev Cancer., Nov;6(11):846-56. Review.

Spitz F., Furlong E.E. (2012). Transcription factors: from enhancer binding to developmental control. Nat Rev Genet., Sep;13(9):613-26

Stankunas K, Shang C, Twu KY, Kao SC, Jenkins NA, Copeland NG, Sanyal M, Selleri L, Cleary ML, Chang CP. (2008). Pbx/Meis deficiencies demonstrate multigenetic origins of congenital heart disease.Circ Res. Sep 26;103(7):702-9.

Steventon B., Carmona-Fontaine C. and Mayor R. (2005). Genetic network during neural crest induction: from cell specification to cell survival. Semin. Cell Dev. Biol. 16, 647-654.

Stolt C.C., Rehberg S., Aber M., Lommes P., Riethmacher D., Schachner M., Bartsch U., Wegner M. (2002) Terminal differentiation of myelin- forming oligodendrocytes depends on the transcription factor Sox10. *Genes Dev.* 16, 165–170.

Struhl, G. (1981). A gene required for correct initiation of segmentaldetermination in Drosophila. Nature,293, 36-41

Studer M., Pöpperl H, Marshall H., Kuroiwa A., KrumlaufR. (1994). Role of a conserved retinoic acid response element in rhombomere restriction of Hoxb-1. Science, Sep 16;265(5179):1728-32.

Studer M., Gavalas A., Marshall H., Ariza-McNaughton L., Rijli F.M., Chambon P., Krumlauf R.(1998). Genetic interactions between Hoxa1 and Hoxb1 reveal new roles in regulation of early hindbrain patterning Development, 125, pp. 1025–1036.

Swindell E.C., Thaller C., Sockanathan S., Petkovich M., Jessell T.M., Eichele G. (1999). Complementary domains of retinoic acid production and degradation in the early chick embryo. Dev Biol 216: 282–296.

Tavares L., Dimitrova E., Oxley D., Webster J., Poot R., Demmers J., Bezstarosti K., Taylor S., Ura H., Koide H., Wutz A., Vidal M., Elderkin S., Brockdorff N. (2012). RYBP-PRC1 complexes mediate H2A ubiquitylation at polycomb target sites independently of PRC2 and H3K27me3. Cell., Feb 17;148(4):664-78.

1.

Trainor P.A., Ariza-McNaughton L., Krumlauf R. (2002). Role of the isthmus and FGFs in resolving the paradox of neural crest plasticity and prepatterning. Science., Feb 15;295(5558):1288-91.

Tschopp P, Tarchini B, Spitz F, Zakany J, Duboule D. (2009). Uncoupling time and space in the collinear regulation of Hox genes. PLoS Genet., Mar;5(3):e1000398.

Tümpel S., Cambronero F., Sims C., Krumlauf R., Wiedemann L.M. (2008). A regulatory module embedded in the coding region of hoxa2 controls expression in rhombomere 2 Proc Natl Acad Sci U S A., Dec 23;105(51):20077-82.

Uehara M, Yashiro K, Mamiya S, Nishino J, Chambon P, Dolle P, Sakai Y. (2007). CYP26A1 and CYP26C1 cooperatively regulate anterior-posterior patterning of the developing brain and the production of migratory cranial neural crest cells in the mouse. Dev Biol. Feb 15;302(2):399-411. Epub 2006 Sep 30.

Vieux-Rochas M, Coen L, Sato T, Kurihara Y, Gitton Y, Barbieri O, Le Blay K, Merlo G, Ekker M, Kurihara H, Janvier P, Levi G. (2007). Molecular dynamics of retinoic acid-induced craniofacial malformations: implications for the origin of gnathostome jaws. PLoS One, Jun 6;2(6):e510.

Walshe J., Maroon H., McGonnell I.M., Dickson C., Mason I. (2002). Establishment of Hindbrain Segmental Identity Requires Signaling by FGF3 and FGF8. Curr Biol Jul 9;12(13):1117-23.

Wang H, Wang L, Erdjument-Bromage H, Vidal M, Tempst P, Jones RS, Zhang Y. (2004). Role of histone H2A ubiquitination in Polycomb silencing. Nature, Oct 14;431(7010):873-8.

Wang K.C., Yang Y.W., Liu B., Sanyal A., Corces-Zimmerman R., Chen Y., Lajoie B.R., Protacio A., Flynn R.A., Gupta R.A., Wysocka J., Lei M., Dekker J., Helms J.A., Chang H.Y. (2011). A long noncoding RNA maintains active chromatin to coordinate homeotic gene expression. Nature, Apr 7;472(7341):120-4.

Waskiewicz A.J., Rikhof H.A., Moens C.B. (2002) Eliminating zebrafish pbx proteins reveals a hindbrain ground state Dev. Cell, 3, pp. 723–733

Wendling O., Norbert B., Chambon P., Mark M. (2001). Roles of retinoic acid receptors in early embryonic morphogenesis and hindbrain patterning. Development, 128, 2031-2038

White J.C., Highland M., Kaiser M., Clagett-Dame M. (2000). Vitamin A deficiency results in the dose-dependent acquisition of anterior character and shortening of the caudal hindbrain of the rat embryo. Dev Biol 220:263–284.

White J.A., Guo Y.D., Baetz K., Beckett-Jones B., Bonasoro J., Hsu K.E., Dilworth F.J., Jones G., Petkovich M. (1996). Identification of the retinoic acid-inducible all-trans-retinoic acid 4-hydroxylase. J Biol Chem 271:29922–29927.

White R.J., Schilling T.F. (2008). How Degrading: Cyp26s in Hindbrain Development. Developmental Dynamics, 237:2775–2790.

Wilkinson DG, Bhatt S, Chavrier P, Bravo R, Charnay P. (1989). Segment-specific expression of a zinc-finger gene in the developing nervous system of the mouse. Nature. Feb 2;337(6206):461-4.

Whiting J., Marshall H., Cook M., Krumlauf R., Rigby P.W., Stott D., Allemann R.K. (1991). Multiple spatially specific enhancers are required to reconstruct the pattern of Hox-2.6 gene expression. Genes Dev. Nov;5(11):2048-59.

Woo C.J., Kharchenko P.V., Daheron L., Park P.J., Kingston R.E. (2010). A region of the human HOXD cluster that confers polycomb-group responsiveness. Cell, Jan 8;140(1):99-110.

Woo C.J., Kharchenko P.V., Daheron L., Park P.J., Kingston R.E. (2013). Variable Requirements for DNA-Binding Proteins at Polycomb-Dependent Repressive Regions in Human HOX Clusters. Mol Cell Biol., Aug;33(16):3274-85.

Young T, Deschamps J. (2009). Hox, Cdx and anteroposterior patterning in the mouse embryo. Curr Top Dev Biol. 2009;88:235-55. Review.

Acknowledgments

I would like to express my gratitude to my supervisor Prof. Filippo M. Rijli for his valuable mentorship and for giving me the opportunity to grow professionally. Under his supervision I was encouraged to enhance my skills and develop a critical scientific mind.
I also took advantage from the unique enriched environment that the Friedrich Miescher Institute offers; in particular I would like to thank the members of my thesis committee Prof. Antoine Peters and Prof. Silvia Arber who provided me with suggestion and insightful comments during the PhD program.

I would like to thank our collaborators Prof. Licia Selleri and Dr. Elisabetta Ferretti and Dr. Xavier Lampe for scientific debates, exchanges of knowledge and skills, which helped enrich the content of our work.

A special thanks goes to all the members of the laboratory, in particular to Maryline Minoux for the intellectual exchange and generous support received during the preparation of the present manuscript; Nathalie Vilain and Sébastien Ducret for their assistance and the irreplaceable help received during the revision of the Developmental Cell paper. I have greatly benefited from the daily interactions with experienced and promising scientists: Ahmad Bechara, Alberto Loche, Kajari Karmakar, Dominik Kraus, Thomas Di Meglio, Claudius Kratochwil, Christophe Laumonnerie, Yuichi Narita and Liseth Parra.

I also want to acknowledge the extraordinary support brought by members of FMI facilities including Michael Stadler (Computational Biology), Jean-François Spetz (Transgenic Facility), Hubertus Kohler (FACS), Tim Roloff , Sophie Dessus-Badus, Stephane Thiry, Kirsten Jacobeit (Functional Genomics) Birgit Heller, Tamara Ramadan (Animal Facility) and Susan Thomas (Human Resources).

Finally, I would also like to thank my friends and my family for the support they provided me through my entire life and in particular, I must acknowledge my wife and best friend, Sonia and our marvelous kids Noah and Nicole, for their love, patience and encouragement.

My warmest thoughts go out to whom is not with us anymore, we miss you so much and we hope to make you proud of us.